TRANSPORTATION RESEARCH
22 1991
C.2
BOARD LIBRARY

TRANSPORTATION RESEARCH

RECORD

No. 1301

Materials, Construction, and Maintenance

Factors Affecting Properties and Performance of Pavements and Bridges 1991

A peer-reviewed publication of the Transportation Research Board

TRANSPORTATION RESEARCH BOARD
NATIONAL RESEARCH COUNCIL
WASHINGTON, D.C. 1991

Transportation Research Record 1301
Price: $22.00

Subscriber Category
III materials, construction, and maintenance

TRB Publications Staff
Director of Publications: Nancy A. Ackerman
Senior Editor: Naomi C. Kassabian
Associate Editor: Alison G. Tobias
Assistant Editors: Luanne Crayton, Kathleen Solomon, Norman Solomon
Graphics Coordinator: Diane L. Ross
Production Coordinator: Karen S. Waugh
Office Manager: Phyllis D. Barber
Production Assistant: Betty L. Hawkins

Printed in the United States of America

Library of Congress Cataloging-in-Publication Data
National Research Council. Transportation Research Board.

Factors affecting properties and performance of pavements and bridges 1991.
p. cm.—(Transportation research record, ISSN 0361-1981 ; no. 1301)
ISBN 0-309-05105-3
1. Pavements, Concrete—Testing. 2. Concrete—Additives. I. National Research Council (U.S.). Transportation Research Board. II. Series: Transportation research record ; 1301.
TE7.H5 no. 1301
[TE278]
388 s—dc20
[625.8] 91-4953
CIP

Sponsorship of Transportation Research Record 1301

GROUP 2—DESIGN AND CONSTRUCTION OF TRANSPORTATION FACILITIES
Chairman: Raymond A. Forsyth, Sacramento, California

Concrete Section
Chairman: Thomas J. Pasko, Jr., Federal Highway Administration

Committee on Performance of Concrete
Chairman: William P. Chamberlin, Construction Materials Specialist
M. Arockiasamy, Philip D. Cady, James R. Clifton, Philip H. Decabooter, Glenn William De Puy, John W. Figg, Kenneth C. Hover, Donald J. Janssen, Inam Jawed, Joseph F. Lamond, Richard C. Meininger, Roger P. Northwood, John T. Paxton, Steven A. Ragan, V. Ramakrishnan, John Ryell, Charles F. Scholer, David Stark, Richard Edwin Weyers

Committee on Mechanical Properties of Concrete
Chairman: Michael M. Sprinkel, Virginia Transportation Research Council
Archie F. Carter, Jr., J. Harold Deatherage, James T. Dikeou, Wilbur Charles Greer, Jr., Lloyd E. Hackman, Inam Jawed, Kevin Jones, Louis A. Kuhlmann, Joseph F. Lamond, V. M. Malhotra, Richard C. Meininger, Edward G. Nawy, Sandor Popovics, V. Ramakrishnan, Masood Rasoulian, David R. Reidenouer, Gary L. Robson, Robert R. Santoro, Ernest Schrader, Raymond J. Schultz, S. P. Shah, P. Soroushian, Peter C. Tatnall, Dan G. Zollinger

Committee on Chemical Additions and Admixtures for Concrete
Chairman: H. Celik Ozyildirim, Virginia Transportation Research Council, Charlottesville, VA
William F. Boles, Bernard C. Brown, John W. Bugler, Ramon L. Carrasquillo, Henry H. Duval, Jr., Richard D. Gaynor, W. J. Head, Inam Jawed, Daniel P. Johnston, Louis A. Kuhlmann, T. J. Larsen, Michael F. Pistilli, Joseph H. Pound, V. Ramakrishnan, Lawrence R. Roberts, Philip A. Rosskopf, Raymond J. Schutz, Maris A. Sermolins, A. Haleem Tahir, Suneel N. Vanikar, David Whiting

Committee on Basic Research Pertaining to Portland Cement and Concrete
Chairman: J. Francis Young, University of Illinois-Urbana Champaign
Pierre-Claude Aitcin, Jamshid M. Armaghnai, John W. Bugler, James R. Clifton, Sidney Diamond, Ellis M. Gartner, Patrick E. Grattan-Bellew, Jens Holm, Thomas A. Holm, R. D. Hooton, Donald J. Janssen, Inam Jawed, Hamil Jennings, Frederick D. Kinney, Stella L. Marusin, W. C. Ormsby, H. Celik Ozyildirim, Masood Rasoulian, Micheline Regourd, Lawrence R. Roberts, Della M. Roy, Gary L. Vondran, Lillian F. Wakeley, David Whiting

Evaluations, Systems and Procedures Section
Chairman: Terry M. Mitchell, Federal Highway Administration

Committee on Mineral Aggregates
Chairman: Vernon J. Marks, Iowa Department of Transportation
Bernard D. Alkire, David A. Anderson, John S. Baldwin, George M. Banino, Steven Chrismer, Robert J. Collins, Warren B. Diederich, Graham R. Ford, Stephen W. Forster, James G. Gehler, Robert F. Hinshaw, Ian L. Jamieson, Rita B. Leahy, Dah-Yinn Lee, Peter Malphurs, Charles R. Marek, W. R. Meier, Jr., Richard C. Meininger, Charles A. Pryor, Jr., William J. Quinn, Stuart Schwotzer, Barbara J. Smith, Mary Stroup-Gardiner, Lennard J. Wylde

Frederick D. Hejl and G. P. Jayaprakash, Transportation Research Board staff

Sponsorship is indicated by a footnote at the end of each paper. The organizational units, officers, and members are as of December 31, 1990.

Transportation Research Record 1301

Contents

Foreword

This Record contains information on aggregates for use in asphalt concrete (AC), portland cement concrete (PCC), portland cement, and PCC admixtures. The information in this Record is of interest to state and local materials, construction, and maintenance engineers, as well as contractors and materials producers.

Sprinkel and Milliron applied a latex-modified portland cement slag slurry to restore skid resistance to concrete pavements and bridge decks. Soroushian and Tlili investigated the effects of latex modification on the impact resistance, flexural strength, and toughness of plain and steel-fiber-reinforced concretes. They found that latex modification was effective in increasing the impact resistance and flexible strength of plain concrete, but that the combined action of steel fibers and latex polymers produced the best performance characteristics. Walters examined the combined use of silica fume and styrene-butadiene latexes as overlays for bridge and parking-garage decks. The results indicated that the combined use produced mortars and concretes that had properties superior to those using only one of the components. Kuhlmann addressed problems of what were the external and internal sources of cracking in latex-modified concrete overlays, how to prevent the cracks, and what to do about them if they occur. Nawy analyzed the control of cracking in concrete structures and made recommendations for the maximum tolerable flexural crack widths in concrete elements. Soroushian and Tlili investigated the effects of latex modification on microcracking in concrete materials. Naik et al. investigated the performance of structural-grade concrete using high volumes of low-calcium fly ash (Class F). They determined that these fly ash concretes achieved adequate strengths appropriate for structural application even at a 60 percent cement replacement.

Kandhal et al. compared various test methods for evaluating the shape of sand-sized materials using both natural and manufactured sands and identified a new National Aggregate Association test as providing the best classification. Janssen and Almond developed a pressurized water test for predicting the resistance of coarse aggregate for PCC to freeze-thaw deterioration. Rogers et al. found that the micro-Deval test was effective in evaluating fine aggregate used either in AC or PCC. The micro-Deval test was more indicative of the quality of the materials than either the attrition test or the sulfate soundness test. Amirkhanian et al. investigated whether the Los Angeles abrasion test correlated well with aggregate performance in AC mixtures, and found that it did not. Croteau et al. evaluated carbonate rock for potential alkali-carbonate reactivity using three different alkali (sodium hydroxide) levels. Senior and Rogers supported use of the micro-Deval test, unconfined freezing and thawing test, and petrographic examination for predicting aggregate quality. Their research showed this system to be better than the sulfate soundness or Los Angeles abrasion tests for determining quality. Barksdale et al. used computerized image analysis to evaluate shape, surface area, and roughness of fine aggregate. They promoted the use of computers and modern technology for evaluating the physical characteristics of aggregate. Smith and Fager identified the British polishing wheel, used in conjunction with the British pendulum, as an effective method of evaluating an aggregate's long-term frictional properties.

Bishara developed a rapid, yet accurate, method for determining the sulfur trioxide content of hydraulic cement. The method required about 2 hr to run and required no equipment other than a pH meter and ordinary glassware. Ramamurti and Jayaprakash developed a simple and rapid method for determining chloride content in PCC powder. The test used an organic flocculant to separate the insoluble portion from a hot-water suspension, and the clear decant was analyzed for chloride content using a chloride ion-selective electrode. Jang

and Iwasaki developed a visualization technique involving color mapping for the determination of chloride ion distribution and concentration near the steel reinforcement in concrete.

Ghafoori and Chang investigated the use of phosphogypsum as an aggregate in the construction of various roller-compacted concrete (RCC) slabs. From their demonstration projects, they concluded that phosphogypsum-based RCC was suitable for pavement construction application. Snow investigated the influence of the constituents of portland cement, aggregates, and fly ash on alkali-silica reaction in concrete. Vruno et al. related the performance of lignite fly ash concrete after 15 years of field curing and use on a North Dakota Interstate highway to the original laboratory data.

Restoring Skid Resistance to Concrete Pavements and Bridge Decks Using a Latex-Modified Portland Cement Slag Slurry

MICHAEL M. SPRINKEL AND ROBERT MILLIRON

The functional life of concrete pavements and bridge decks is frequently reduced by a loss of skid resistance from traffic rather than from structural deterioration of the concrete. By using the bonding capabilities of latex modification, a thin application of a latex-modified portland cement slag slurry has been used to restore skid resistance to concrete pavements and bridges decks, thus extending their useful life in the absence of other types of distress. Applications of this technique in Virginia are described.

For providing good skid resistance, pavements and bridge decks must have adequate microtexture and macrotexture (ASTM E867-89). A sharp microtexture is required to provide friction between the tire and the surface. A deep macrotexture is required to drain water from the surface so that friction can occur between the tire and the high points of the surface and so that hydroplaning can be avoided.

In Virginia before 1970, one pavement and many bridge decks were constructed with aggregates such as limestone and dolomite that polish rapidly when subjected to traffic (ASTM D3319-83). In the 1970s, new pavements and decks were constructed with polish-resistant aggregates such as siliceous, basalt, and granite; new decks were also constructed with latex-modified concrete overlays (with a minimum thickness of 1.25 in.) that contained polish-resistant aggregates. Older decks, particularly those suffering from corrosion-induced distress, were rehabilitated with similar latex-modified concrete overlays that contained polish-resistant aggregates providing adequate microtexture.

In the late 1970s, it was recognized that new pavements, decks, and overlays should be grooved to provide adequate macrotexture (*1*). Grooves approximately ⅛ in. wide by ⅛ in. deep and spaced at approximately ¾ in. on center were applied to the pavement or deck by dragging a tining device across the surface of the plastic concrete before placing the curing materials (*2*). In 1984, diamond grinding was used to restore the skid resistance of the one pavement constructed with polishing aggregate, but the skid numbers dropped rapidly as the aggregate polished. In 1989, shotblasting was used (as an experiment) to temporarily restore the skid resistance of two 300-ft sections of this pavement.

M. M. Sprinkel, Virginia Transportation Research Council, Box 3817 University Station, Charlottesville, Va. 22903–0817. R. Milliron, Lanford Brothers Co., P.O. Box 7330, Roanoke, Va. 24019.

In the latter part of 1989, because of problems with obtaining a uniform tined texture on decks constructed with concrete mixtures having a low water-to-cement ratio and because the tining operation delayed the application of the curing materials (thereby causing an increase in the incidence of plastic shrinkage cracking), grooves were sawcut into the surface of decks cast full depth and into overlays on decks after the concrete had cured for a minimum of 14 days (*3*).

A latex-modified slag slurry was applied (as an experiment) in Virginia in 1989 and 1990 to increase the skid resistance of the older pavement, and a bridge deck was constructed with polishing limestone aggregate and insufficient macrotexture. The surfaces had lost their microtexture but were not otherwise distressed. The technique was first used in Indiana in September and October of 1980 and later used in San Juan, Puerto Rico, in October and November of 1986 (*4* and C. Pelton, personal communication).

The installation in Indiana may be described as follows (*4*). The applications were placed on SR37 just ahead of a traffic signal at the intersection with SR144 approximately 10 mi south of Indianapolis. Shotblasting, sandblasting, rotomilling, and wet brooming were used to prepare five 350- by 12-ft test sections in each of the two lanes of the concrete pavement. The latex-modified slag slurry was placed on seven sections with a slurry seal applicator modified with oscillating scrub brushes that brushed the slurry into the surface. A water truck and hose were used to wet the pavement ahead of the placement. The slurry was mixed with a mortar mixer of 6-ft^3 capacity that was pulled behind a truck loaded with ingredients. The mixture consisted of 94 lb of portland cement, 244 lb of boiler slag (passed through a 3/16-in. sieve), 38 lb of 48 percent solids latex emulsion, and 22 lb of water. One application was made with expanded shale rather than slag, and no slurry was placed on a rotomilled test section in each lane. The slurry was opened to traffic after 24 to 48 hr of curing.

Skid tests done at 40 mph in October 1980 produced skid numbers in the 50s and 60s for the test sections covered with slag, in the 50s for the sections that were rotomilled but not overlaid, and in the teens for the untreated surfaces. Skid tests done 3 years later, in October 1983, produced skid numbers in the 40s and 50s for the test sections covered with slurry and those that were rotomilled.

The final report on the project recommends the use of shotblasting or sandblasting for surface preparation because

no spalls were noted after 3 years in service. Also, the report recommends the use of boiler slag because it provides the highest skid numbers. (The installations on SR37 had been preceded by the hand application of 14 different materials on a low-volume concrete pavement in the Spring of 1978, which was monitored for 2½ years.) Finally, the report recommends against the use of rotomilling for surface preparation because it damages the concrete surface. The test sections were overlaid with asphalt in 1985 because of complaints from the public about the appearance. The test sections covered with slag were still bonded and providing acceptable skid numbers (K. Kercher, personal communication).

The following description of the installation in Puerto Rico is based on a phone conversation with the contractor (C. Ando, personal communication). The slurry in Puerto Rico was applied in October and November 1986 to approximately 6 lane-miles of two- and four-lane jointed concrete pavement and five bridge decks and approaches that had low skid numbers. The first step of the installation involved grinding the concrete surface to remove ⅛ to ¾ in. of the top surface to clean the surface and to restore the surface profile. A rotomill with a 9-ft-wide triple-head-block carbide-tipped drum was used to grind the surface at a rate of approximately 300 ft^2/min (C. Latham, personal communication). The grinding operation was followed by a cleaning operation in which the surface was blasted with high-pressure water to remove the fine cuttings and the cement paste. Typically, the grinding and cleaning operations preceded the application of the slurry by 2 or 3 days, and traffic was allowed to use the cleaned surface. Just before placing the slurry, the surface was lightly cleaned again with high-pressure water to remove contaminants, particularly in the wheel paths. A vehicle equipped with two mortar mixers and a slurry paving box was used to apply the slurry. The ingredients were added to the mixers by hand as follows: 1 bag of portland cement, 245 lb of slag, 38 lb of latex emulsion, and 22 lb of water. The slag was passed through a No. 8 sieve before being used. A light fog mist was applied to the surface from the front of the vehicle. The slurry was applied at night when the air temperature was typically in the 70s. The slurry was opened to traffic after 24 to 36 hr initially, and as the work progressed, it was opened to traffic in 12 hr with the exception of one section that was opened after only 6 hr of cure.

The following summary of the performance of the installation in Puerto Rico is based on telephone conversations with the contractor and the FHWA representative responsible for the application (C. Pelton and C. Ando, personal communications). Within the first 6 months, approximately 0.5 percent of the slurry had delaminated. After 4 years, approximately 1 percent had delaminated and the base concrete was showing in places in the wheel paths. The wear can be attributed to the high volume of traffic.

According to the contractor, the delaminations in the pavement are confined to the joints between the 20-ft sections and can be attributed to a failure to sawcut the slurry over the joints. The delaminations on the bridge decks can be attributed to the shallow cover over the top mat of rebar that would not allow the grinder to remove much concrete from some surfaces. Plastic shrinkage cracks in the decks have not reflected through the slurry (C. Ando, personal communication).

According to the FHWA representative, the delaminations were caused by incomplete surface preparation, applications that were too thick, and mixtures that were not properly proportioned. These problems were greater than usual because the slurry was placed at night during the rainy season and because the contractor was hastening the application to finish before Thanksgiving holiday traffic arrived. Areas that received a proper application are still performing (C. Pelton, personal communication).

OBJECTIVES

The objectives of this paper are to describe the application and initial performance of a latex-modified slag slurry used in Virginia to increase the skid resistance of a pavement and a bridge deck.

APPLICATION OF LATEX-MODIFIED PORTLAND CEMENT SLAG SLURRY

Air-cooled blast furnace slag having a gradation similar to an ASTM C33 concrete sand (see Table 1) was used in the slurry mixtures. However, the slag used on the bridge deck was first passed through a No. 8 sieve. Material that passed the sieve was used in the mixture (see Table 2), and material that was retained was broadcast onto the freshly placed slurry at the rate of 5 lb/yd^2 to provide additional microtexture and macrotexture. The slag was obtained from Ducan Slag Products Company in Pittsburgh, Pennsylvania. The details of the applications are presented in Table 3.

Before the slurry was placed, the surfaces were shotblasted to remove dirt, oil, weak surface mortar, and materials that could interfere with the bonding or curing of the slurry. Some surfaces were prewet before the slurry was placed, and some were not. The slurry was batched with a concrete mobile and brooms were used to brush the latex-modified slag slurry into the surface (see Figure 1). For the bridge deck applications, the slurry was struck off and pulled forward with gage rakes set to provide a slurry 3/16 to ¼ in. thick. For increased skid resistance, slag retained on the No. 8 sieve was broadcast onto the struck-off surface. A liquid membrane curing material was also applied. Because the gage rakes, broadcast of aggregate, and liquid membrane curing material were not used on the 300-ft pavement application, the surface was uneven, provided a rough ride, and was not pleasing to the eye.

MECHANICAL PROPERTIES OF LATEX-MODIFIED SLAG SLURRY

Compressive Strength

The slurry must cure for at least 24 hr to obtain adequate strength (1,000 psi compressive strength) for traffic (see Table 4). A slag slurry mixture made with a special blended cement of high early strength should be evaluated for use when a short lane closure time is required.

TABLE 1 SIEVE ANALYSIS OF SLAG (PERCENT PASSING INDICATED SIEVE)

Sieve	Slag	ASTM C33
3/8	100	100
4	95	95-100
8	63	80-100
16	39	50-85
30	24	25-60
50	16	10-30
100	9	2-10
200	4	—

TABLE 2 MIXTURE PROPORTIONS FOR LATEX-MODIFIED PORTLAND CEMENT SLAG SLURRY (lb/yd^3)

	Design[a]	Actual[b]
Cement[c]	791	811
Slag[d]	2,062	2193
Latex emulsion	320	328
Water	185	115
W/C	0.44	0.35

[a]Assuming 3% void content.
[b]The slag was assumed to have an 8% moisture content, but was found to have an 11% moisture content. A correction for absorption was not made.
[c]Type III portland.
[d]Specific gravity = 2.34
Mohs scale hardness = 5.5
Sodium Sulfate = 4%
Absorption = 6.89

TABLE 3 LATEX-MODIFIED SLAG SLURRY APPLICATIONS

	Pavement Travel Lane I-81 NBL Botetourt Co.	Deck Passing Lane I-81 NBL over 679 Rockbridge Co. Structure No. 2016	Deck Travel Lane I-81 NBL over 679 Rockbridge Co. Structure No. 2016
Size	300 ft x 12 ft	204 ft x 12 ft	204 ft x 12 ft
Date shotblasted	5/17/89	10/31/89	4/26/90
Date slurry applied	5/17/89	10/31/89	4/26/90
Time slurry applied	3:30 - 4:30 p.m.	—	10:00 - 11:30 a.m.
Weather	Sunny	—	Sunny
Air temperature,°F	82°F	—	86°F
Date opened to traffic	5/19/89	—	4/28/90
Age opened to traffic	42 hrs	4 wks	48 hrs

FIGURE 1 A latex-modified slag slurry overlay is applied to a bridge deck to increase the skid resistance.

Bond Strength

The average tensile rupture strength (American Concrete Institute 503R) of the slurry overlay placed on the passing lane of the bridge was measured on November 13 at an age of 13 days and found to be 260 lb/in.^{2} for the average of six tests (*5*). Because the majority of the failure was in the base concrete, the bond strength could be assumed to be greater than 260 lb/in.^{2}. Although a few small areas have spalled in the concrete pavement, no spalls have occurred on the bridge deck. Also, few cracks have been noted.

Skid Numbers at 40 mph

Skid tests were conducted at 40 mph using a smooth tire (ASTM E524-88). The minimum acceptable skid number in

TABLE 4 COMPRESSIVE STRENGTH (lb/in²) VERSUS AGE FOR OVERLAYS

Age	Latex-Modified Slag Slurry Test Section	
	I-81 NBTL pavement	I-81 NBTL bridge deck
18 hr	370	—
24 hr	—	1,050
40 hr	1,970	—
48 hr	—	1,590
28 day	4,100	2,680

Results based on average of three tests on 2-in field cured mortar cube specimens.

Virginia is 20. New surfaces should have skid numbers much higher than 20 because the numbers decline as the cumulative traffic over the surfaces increases (*6*).

The bridge deck and pavement constructed in the 1960s with polishing limestone aggregate and a screeded surface exhibited skid numbers of 17 and 27, respectively, before the slurry was placed. Several months after the slurry was placed, the average skid numbers were 39 and 65, respectively. A higher skid number was obtained for the pavement because the macrotexture was greater. An adequate skid number was obtained for the bridge deck, and the application to the deck was smoother and more pleasing to the eye.

COST

The cost of the latex-modified slag slurry was $5.90/yd², which was higher than the $2.50/yd² to $3.50/yd² cost of shotblasting, diamond grinding, and rotomilling; it is about the same as the cost of sawcut grooves; and it is very low compared to the $35/yd² cost of a latex-modified concrete overlay (of minimum thickness 1.3 in.).

SERVICE LIFE

The service life cannot be determined at this time; it will likely be a function of the type and volume of traffic. On the basis of the experiences in Indiana and Puerto Rico, a life in excess of 5 years seems likely for high-volume roads.

ADVANTAGES OF LATEX-MODIFIED SLAG SLURRY

The applications in Indiana, Puerto Rico, and Virginia illustrate that a latex-modified slag slurry can be placed on pavements and bridge decks to provide adequate surface texture. One advantage of the slag slurry is increased cover over the top mat of rebar in decks as compared with the sawcutting of grooves, shotblasting, diamond grinding, and rotomilling for skid resistance. Another advantage of the latex-modified slag slurry is that new decks and pavements can be constructed with polishing aggregates, thereby extending the diminishing supplies of aggregates. The slurry can also be applied to provide adequate skid resistance. Tining the plastic concrete and sawcutting grooves in the hardened concrete are not acceptable methods for increasing skid resistance when decks or pavements are constructed with polishing aggregates because the surface does not have adequate microtexture. A final advantage is the high microtexture and adequate macrotexture at a low cost compared with 2-in.-thick portland cement concrete overlays, 1.25-in.-thick latex-modified concrete overlays, and 0.25-in.-thick polymer overlays. However, the latter types of overlays are usually applied to decks constructed with black steel to retard the infiltration of chloride ion.

SPECIAL PROVISION

A Virginia Department of Transportation special provision that was prepared on the basis of the experimental applications follows.

1. Description. This work shall consist of preparing and shotblasting concrete surfaces and furnishing and applying latex portland cement slurry in accordance with this specification and in reasonably close conformity with the lines, grades, and details shown on the plans or established by the engineer.

2. Materials. Latex portland cement slurry shall conform to the requirements of Section 219 of the *Specifications* except that the maximum water per pound of cement shall be 0.45 lb, and the design minimum laboratory compressive strength shall be 3,000 psi. Latex portland cement slurry shall have a mix design similar to:

Ingredient	*Density, lb/yd³*
Type III portland cement	791
Air-cooled blast furnace slag	2,062
Latex emulsion	320
Water	185

The air-cooled blast furnace slag shall have a gradation similar to ASTM C33 and shall be passed through a No. 8 sieve. Blast furnace slag that passes through the sieve shall be used in the latex portland cement slurry. Blast furnace slag retained by the sieve shall be broadcasted on the surface of the latex slurry at a rate of 5 lb/yd².

3. Construction. Section 416.09 of the *Specifications* is completely replaced by the following sequence of operation:

1. Close one lane.
2. Shotblast deck surface in closed lane.
3. Air-blast the deck surface to remove loose material.
4. Apply latex slurry.
5. Broom latex slurry into the surface.
6. Level latex slurry with gage rakes.
7. Broadcast slag onto surface of latex slurry.
8. The slurry shall be protected from drying by prompt

application of wet burlap and polyethylene when the evaporation rate exceeds 0.05 lb/ft²/hr as determined using the chart shown as Figure 1 in the ACI standard practice for curing concrete (ACI 308). The burlap and polyethylene shall be removed after 24 hr of curing.

9. Once proper compressive strength has been attained, open lane to traffic and begin operation in the other lane with Number 1.

One lane of a structure shall be closed at night or early morning; shotblasting shall be completed and latex slurry applied by noon of the same day.

a. Surface Preparation. The contractor shall shotblast the deck to remove material detrimental to the bonding of the latex slurry. The shotblasting equipment shall not be operated at a rate that exceeds 12 yd²/min. The contractor shall verify the results of shotblasting by performing sandpatch tests in accordance with ASTM E965. One test must be conducted on each 100 yd². For areas of less than 400 yd², four tests must be conducted. The macrotexture depth shall be greater than or equal to 0.03 in. for each test. If the required depth is not obtained, the contractor shall shotblast the deck and conduct tests until an adequate macrotexture is obtained.

Deck drains and expansion joints shall be protected from latex slurry's being applied to or passed through. The protective coverings of deck drains and expansion joints shall be removed after latex slurry has cured sufficiently.

At least 1 hr before the application of latex slurry, the deck shall be thoroughly moistened with water. All puddles of water shall be removed in an approved manner so that the deck is in a saturated surface dry condition before the application of latex slurry.

b. Placing and Finishing Latex Slurry. Latex slurry shall be applied in accordance with Section 404 of the *Specifications* and as stated herein.

In addition to the ambient air temperature requirements in Section 404.16, the latex slurry shall not be applied when the surface temperature of the deck exceeds 90°F.

Latex slurry shall be leveled by pulling adjustable gage rakes parallel to the direction of traffic, and the slurry shall be 3/16 to 1/4 in. thick.

Precautions shall be taken to protect freshly placed latex slurry from rain. All placing operations shall stop when it starts to rain. The engineer may order the removal of any material damaged by rainfall.

The lane shall be kept closed until 2-in. mortar cubes cured at the site obtain a compressive strength that exceeds 1,000 psi.

4. Method of Measurement and Basis of Payment. Latex portland cement slurry will be measured in square yards of surface area. Latex portland cement slurry will be paid for at the contract unit price per square yard, which price shall be full compensation for shotblasting the deck; for furnishing, placing, and finishing latex slurry; for disposal of unsound and contaminated concrete, and for all materials, labor, tools, equipment, and incidentials necessary to complete the work.

Payment will be made under the Pay Item latex portland cement slurry with Pay Unit in square yards.

CONCLUSIONS

The application of a latex-modified portland cement slag slurry has potential to be an economical technique for increasing the microtexture and macrotexture of hardened concrete surfaces constructed with polishing aggregates and not otherwise distressed. It can also be used as an alternative to grinding, rotomilling, shotblasting, and sawcutting grooves on hardened concrete surfaces constructed with polish-resistant aggregates. The technique is limited to pavements and bridge decks that can be closed for at least 1 day to allow for proper cure.

REFERENCES

1. D. Mahone, K. H. McGhee, G. McGhee, and J. E. Galloway, Jr. *Texturing New Concrete Pavements*. VTRC 77-R25. Virginia Transportation Research Council, Charlottesville, Va., Nov. 1976, p. 13.
2. *Road and Bridge Specifications*. Virginia Department of Transportation, Richmond, Va., Jan. 1987, p. 433.
3. *Road and Bridge Specifications*. Virginia Department of Transportation, Richmond, Va., Revised 1989.
4. K. J. Kercher. *Evaluation of Thin Concrete Overlay on SR-37*. Indiana Department of Highways, Indianapolis, Ind., Aug. 1984.
5. Field Test for Surface Soundness and Adhesion, Appendix A—Test Methods. *ACI Manual of Concrete Practice, Part 5*, American Concrete Institute, Detroit, Mich., 1982, p. 503R30-31.
6. M. M. Sprinkel. Performance of Multiple-Layer Polymer Concrete Overlays on Bridge Decks, Polymers in Concrete: Advances and Applications SP116-5, American Concrete Institute, Detroit, Mich., 1989, pp. 61-95.

Publication of this paper sponsored by Committee on Mechanical Properties of Concrete.

Latex Modification Effects on the Impact Resistance and Toughness of Plain and Steel-Fiber-Reinforced Concretes

PARVIZ SOROUSHIAN AND ATEF TLILI

The effects of latex modification and steel fiber reinforcement on the impact resistance and flexural strength and toughness of concrete materials were investigated. Two levels of latex content and two different fiber volume fractions were considered. Latex modification was particularly effective in increasing the impact resistance of plain concrete. Flexural strength was also increased in the presence of latex, but the flexural toughness of plain concrete did not receive major benefits from latex modification. Steel fibers were effective in increasing the impact resistance and flexural strength and toughness of concrete. The advantages associated with the joint use of steel fibers and latex polymers in concrete materials are assessed. Specifically, the effects of steel fiber reinforcement and latex modification on the impact resistance, flexural strength, and toughness characteristics of concrete materials are addressed. The hypothesis is that the improved adhesion capacity and ductility of concrete matrices incorporating latex polymers make them more compatible with steel fibers. The combined action of steel fibers and latex polymers produces the best performance characteristics. In the case of impact resistance and flexural toughness, the joint effects of latex and steel fibers are more than additive, indicating a positive interaction between the two. Latex modification seems to make concrete matrices more compatible with steel fibers. The increase in fiber-to-matrix bond in the presence of latex also seems to enhance the reinforcement properties of steel fibers in concrete.

Ordinary concrete suffers from relatively low flexural strength, toughness, and impact resistance. Steel fiber reinforcement and polymer modification each can partly overcome some of these problems.

Steel fibers enhance the ductility and energy absorption capacity, flexural strength, and impact resistance of concrete. Latex modification, on the other hand, improves the impermeability as well as strength and ductility characteristics of concrete.

Latex polymers in the presence of steel fibers provide a better bonding between fibers and the concrete matrix because of the formation of a monolithic polymer film that surrounds the fibers, fills the smaller voids, and links the cementitious environment to the fibers. As a result, the formation of many of the microcracks that tend to take place along the fiber-matrix interface is prevented. In addition, the resistance of fibers against pull-out action is further enhanced, resulting in improved flexural strength, toughness characteristics, and impact resistance.

Civil and Environmental Engineering Department, Michigan State University, East Lansing, Mich. 48824.

BACKGROUND

Impact Resistance

The impact resistance of concrete materials is an important factor in the design of systems such as concrete overlays on industrial floors and airfield pavements.

Latex, because of its film formation action inside the concrete matrix, gives the material some microcrack arresting properties that can potentially lead to improvements in the impact resistance of concrete (*1*). Further test data are needed for verifying the latex modification effects on the impact resistance of concrete.

Steel fiber reinforcement has also been shown in various investigations to significantly improve the impact resistance of concrete. Figure 1 (*2*) shows typical improvements in the impact resistance of concrete obtained through steel fiber reinforcement, which can be attributed to the crack-arresting action of fibers.

Flexural Performance

Latex modification of concrete provides the material with higher flexural strengths (see Figure 2) (*3*). This increase in flexural strength can be attributed to the microcrack-arresting action of polymers in concrete, and also to the bonding they provide between the matrix and aggregates. Improvements of workability through latex modification (which reduces water requirements for achieving similar workability in latex-modified concrete) is another factor contributing to flexural strength in latex-modified concrete.

Previous test results (*4*) have indicated that, at a polymer-cement ratio of 0.20, styrene-butadiene, saran, acrylic, and polyvinyl alcohol latexes provide flexural strengths of the order of 2, 3, 1.4, and 3 times, respectively, that of plain mortar after 28 days of dry curing at 50 percent relative humidity.

Steel fibers have been found to increase the first-crack and ultimate flexural strengths of concrete (*2*). They also make major contributions to the ductility and toughness (represented by the area under the flexural load-deflection curve) of the material. Steel fibers, with their desirable pull-out performance, are especially effective at relatively large deformations and crack widths.

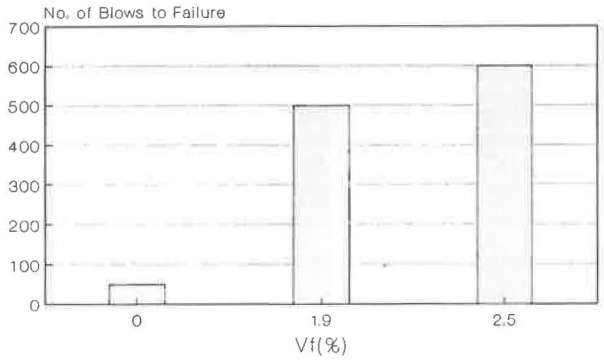

FIGURE 1 Effect of steel fiber reinforcement on the impact resistance of concrete (hooked-end steel fibers, length-to-diameter ratio = 100) (*2*).

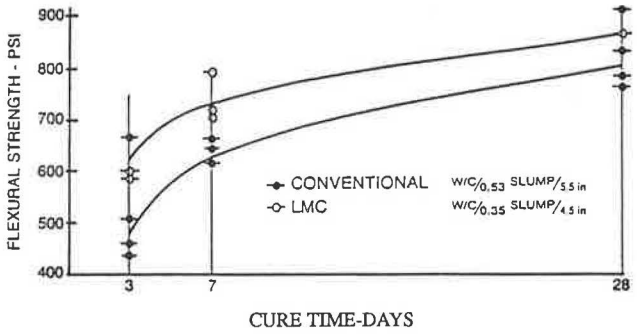

FIGURE 2 Flexural strength of plain concrete and concrete modified by latex (styrene-butadiene) versus cure time (*3*).

TABLE 1 MIX PROPORTIONS FOR EXPERIMENTAL WORK

V_f (%)	Styrenene Butadiene L/c (%)	w/c	Slump mm. (in.)	Vebe Time (sec.)	Air Content (%)
0	0	0.43	152 (6.0)	-----	5.5
0	10	0.32	190 (7.5)	-----	4.5
0.75	0	0.45	127 (5.0)	6.5	6.5
0.75	10	0.34	152 (6.0)	5.0	5.0

--- = no measurement taken
V_f = fiber volume fraction;
L/c= latex-cement ratio, by solids weight;
w/c= water-cement ratio, by weight;
s/c=2.5=sand-cement ratio, by weight; and
st./c=1.5=stone-cement ratio, by weight.

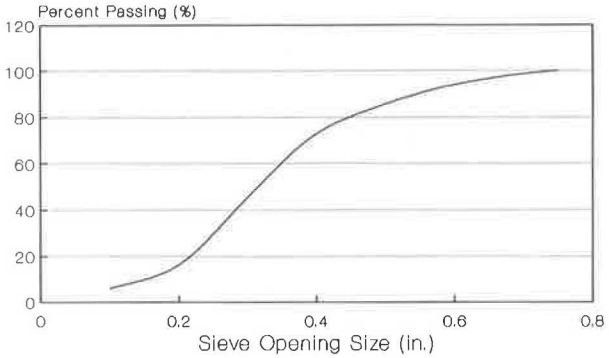

FIGURE 3 Gradation of crushed limestone coarse aggregate.

EXPERIMENTAL PROGRAM

The mix proportions selected for the latex-modified steel-fiber-reinforced concrete (LMSFRC) mixtures with different latex and fiber contents are presented in Table 1. The cement in all these mixes is regular Type I, the coarse aggregate is crushed limestone (see Figure 3 for gradation) with a maximum particle size of 13 mm (½ in.); the fine aggregate is natural sand with gradation satisfying the ASTM C–33 gradation requirements; the latex is BASF Styrofan 1186 styrene-butadiene dispersion (see Table 2 for properties); the steel fibers are hooked-end with a length of 30 mm (1.18 in.) and a diameter of 0.5 mm (0.0197 in.). The air-entraining agent (used only in the unmodified mixtures) was a completely neutralized vinsol resin solution.

Water content was adjusted in different mixtures, depending on the latex and fiber contents, for achieving a desirable level of workability [represented by the British Standard BS 1881 VB time of 7 to 9 sec for fibrous mixes and a slump of 76 to 127 mm (3 to 5 in.) for plain mixes]. The air content was also adjusted by varying the dosage rate of air-entraining agent.

Three cylindrical specimens 152 mm (6 in.) in diameter and 63.5 mm (2.5 in.) in height were prepared for impact tests from each of the four mixes presented in Table 1. They were moist-cured inside their molds under wet burlap coated by a

TABLE 2 PROPERTIES OF STYRENE BUTADIENE LATEX

Typical Properties	
Total solids (wt. %)	47
Specific gravity	1.01
pH (25 C)	10
Surface tension (mN/m)	38
Weight/volume , lb/U.S.gal. (kg/l)	8.3 (1.01)

polyethylene sheet for the first 24 hr and then demolded and cured in air until the test age of 28 days. The impact resistance test is performed by repeatedly dropping a 4.5-kg (10-lb) hammer on a hard steel ball supported on the cylinder from a height of 457 mm (18 in.) (*5*). The number of blows required to cause the first visible crack and the ultimate failure represents the impact resistance of the material. Ultimate failure is assumed to occur when the cracks open so far that the pieces of concrete are touching three of the four positioning lugs on the base plate. Figure 4 (*5*) shows the impact resistance test apparatus.

In addition, for each mix, three 102- × 102- × 356-mm (4- × 4- × 14-in.) prismatic flexural specimens were prepared. They were all moist-cured inside their molds under wet burlap

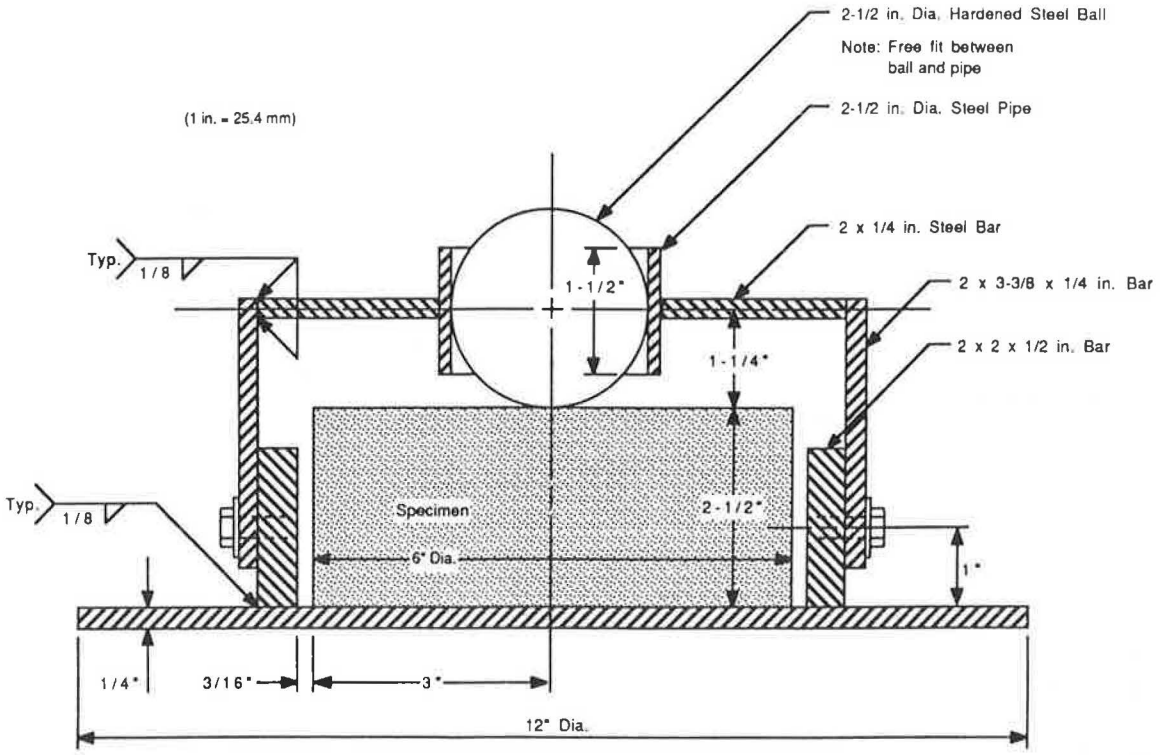

FIGURE 4 Apparatus for impact resistance test (5).

coated by a polyethylene sheet for the first 24 hr and then demolded and cured in air until the test age of 28 days. The flexural specimens were tested following the ASTM C-1018 and the Japanese Concrete Institute procedures (JCI-SF) by four-point loading on a span of 305 mm (12 in.). The flexural test set-up is shown in Figure 5. A computerized data acquisition system was used for load and deflection measurements, and also for the processing of the flexural test results.

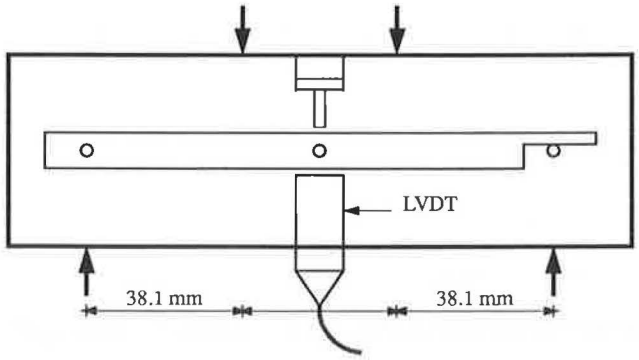

FIGURE 5 Flexural test set-up.

EXPERIMENTAL RESULTS

Impact Resistance

The impact resistance test results obtained for the mixes presented in Table 1 are presented in Table 3 and shown in Figure 6. It can be seen that latex addition increases the impact resistance of plain concrete by an average of 800 percent. Steel fiber reinforcement increases the impact resistance by an average of 370 percent. Combined use of latex polymers and steel fibers leads to major improvements in impact resistance, causing a 1,500 percent increase over plain concrete.

When both steel fibers and latex are added to the plain concrete mix, the improvements in impact resistance are superior. This effect indicates that there is an effective interaction between the steel fibers and the latex, which may result from the improved fiber-to-matrix bonding in the presence of latex polymers, and also from the increased compatibility of steel fibers and the matrix because of the reduced brittleness of the matrix incorporating latex.

When fibers are missing from the matrix, even in the presence of latex, there is only a small difference between the first crack and the failure impact resistance. This indicates that fibers, but not latex, can provide the material with post-cracking integrity.

In order to statistically investigate the effects of latex modification and steel fiber reinforcement on impact resistance, one-way analyses of variances were conducted. A one-way analysis of variance (ANOVA) performed for the cases of unmodified and latex-modified plain concretes [fiber volume fraction (Vf) of 0 percent] indicated that the effects of latex content on the impact resistance of plain concrete are significant with about 15.2 percent chances of error in this statement. A similar one-way ANOVA performed for the cases of unmodified and latex-modified steel-fiber-reinforced concrete (SFRC) (Vf = 0.75 percent) resulted in similar conclusions, with about 15.3 percent chance of error in stating that there is a latex effect on the impact resistance at Vf = 0.75 percent.

TABLE 3 IMPACT RESISTANCE TEST RESULTS FOR MIXES PRESENTED IN TABLE 1

Vf (%)	L/c (%)	Number of Blows to First Crack	Number of Blows to Failure
0	0	29	33
		25	28
		32	35
0	10	232	233
		503	503
		50	53
0.75	0	60	106
		190	247
		154	264
0.75	10	900	1065
		395	530
		148	278

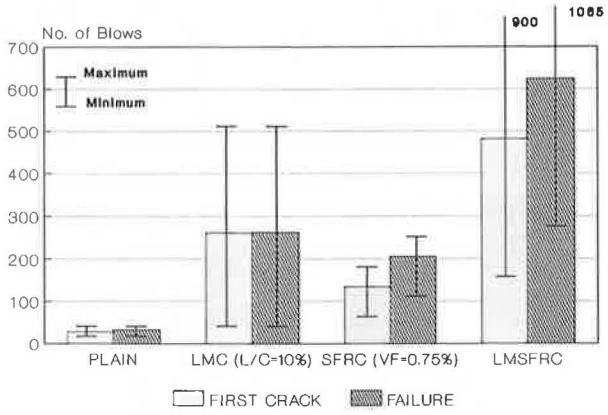

FIGURE 6 Impact resistance test results.

Similar analyses were performed to investigate the effects of steel fiber reinforcement at constant latex content on the impact resistance of the concrete matrix. For the case of unmodified concrete (latex-cement ratio L/c = 0 percent), the one-way ANOVA showed that fiber addition has a significant positive effect on the impact resistance, with only 2.6 percent chance of error in this statement. At a constant L/c of 10 percent, the corresponding one-way ANOVA revealed that there is about 24.6 percent chance of error in stating that there is a fiber effect on impact resistance of concrete at a latex-cement ratio of 10 percent.

The scatter in impact resistance test results is relatively large. This leads to conditions where, in spite of the large differences in average values of impact resistance for different mix proportions, the chance of error in stating that such a difference exists sometimes exceeds 15 percent.

Flexural Performance

The average flexural load-deflection curves for the four mix compositions considered in this investigation are presented in Figure 7. The improvements resulting from latex modification

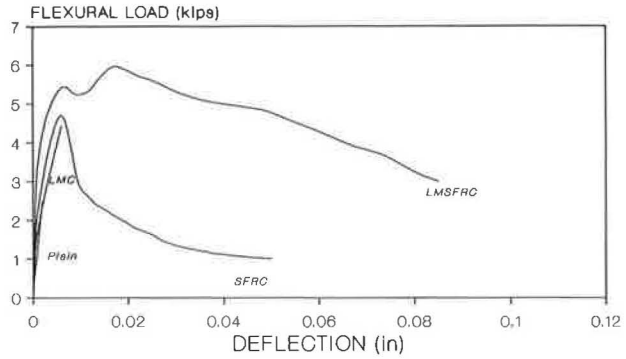

FIGURE 7 Average flexural load versus deflection relationships.

and steel fiber reinforcement, and the desirable joint effects of latex and steel fibers, are obvious in this figure. The flexural strength and toughness (defined as the area underneath the flexural load-deflection curve up to a flexural deflection equal to the span length divided by 150) test results obtained for the mixes of Table 1 are presented in Table 4.

Flexural Strength

From Table 4 and Figure 8, it can be seen that latex addition (L/c = 10 percent) increases the flexural strength of plain concrete by about 87 percent, whereas steel fiber reinforcement (Vf = 0.75 percent) increases it slightly more by about 92 percent. When plain concrete is both modified with latex polymers and reinforced with steel fibers, the improvements in flexural strength are more significant (an increase of about 150 percent over plain concrete).

A factorial analysis of variance performed on these results confirmed the significance of the effects of latex polymers, steel fibers, and their interaction, at the 5 percent level of significance. The relative significance of the effects of fibers, latex, and their interaction on the flexural strength, as indicated by the factorial analysis of variance, is presented in Table 5.

TABLE 4 FLEXURAL STRENGTH AND TOUGHNESS TEST RESULTS

Vf (%)	L/c (%)	Flexural Strength (ksi)	Flexural Toughness (k-in)
0	0	0.420	0.00003
		0.467	0.00005
		0.522	0.00002
0	10	0.880	0.0046
		0.868	0.0058
		0.775	0.0034
0.75	0	0.893	0.254
		0.869	0.207
		0.881	0.231
0.75	10	1.018	0.339
		1.235	0.425
		1.126	0.382

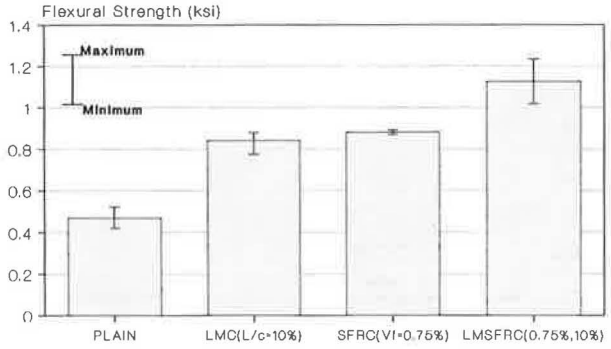

FIGURE 8 Flexural strength test results.

TABLE 5 FACTORIAL ANALYSIS OF VARIANCE OF FLEXURAL STRENGTH TEST RESULTS

Factor	Importance
Steel Fibers	**
Latex	**
Interaction	**

"**" very significant
"*" Significant

Flexural Toughness

Steel fiber reinforcement is indicated in Table 4 and Figure 9 to have positive effects on the flexural toughness of concrete, whereas the improvements in toughness resulting from latex modification are relatively small. Latex modification, however, is highly effective in improving toughness characteristics in the presence of steel fibers.

A factorial analysis of variance confirmed that the effects of latex and steel fibers on flexural toughness, as well as their interaction, are important at the 5 percent level of significance (see Table 6).

The significant improvements in flexural toughness of SFRC resulting from latex modification (noting that latex has relatively small effects on the flexural toughness of plain concrete) can be attributed to the improvements in fiber-to-matrix interfacial bond characteristics by latex polymers. In order to confirm this, microscopic pictures were taken of the steel fibers pulled out of unmodified and latex-modified steel-fiber-reinforced concretes at the fractured surfaces of the flexural specimens. As shown in Figure 10a, the steel fibers pulling

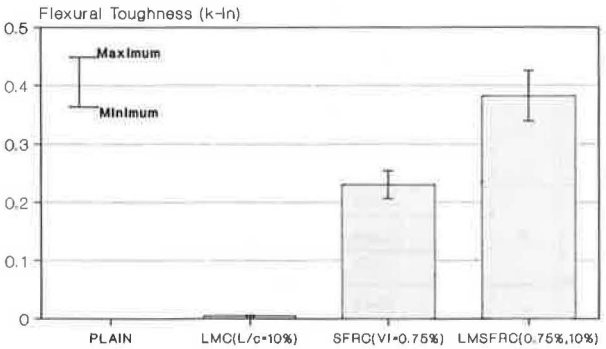

FIGURE 9 Flexural toughness test results.

TABLE 6 FACTORIAL ANALYSIS OF VARIANCE OF FLEXURAL TOUGHNESS TEST RESULTS

Factor	Importance
Steel Fibers	**
Latex	**
Interaction	*

"**" very significant
"*" Significant

(a)

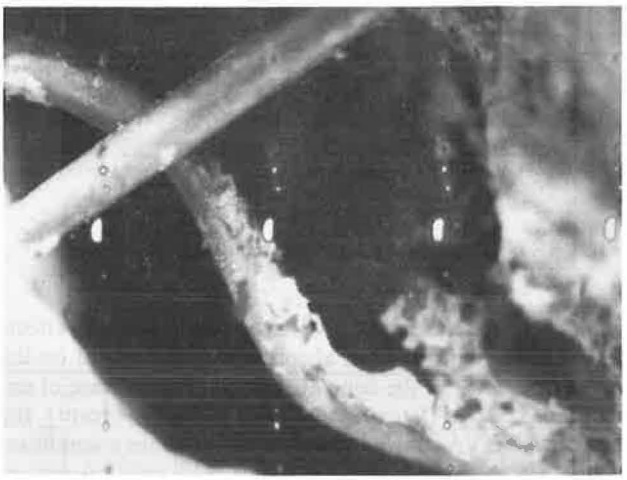

(b)

FIGURE 10 Microscopic pictures of steel fibers pulling out of (a) unmodified concrete, (b) latex-modified concrete.

out of unmodified concrete were clean, indicating an interface shear failure. The steel fibers pulling out of latex-modified concrete (Figure 10b) were partially coated with the polymer-cement comatrix, indicating that the interface shear strength was strong enough to encourage shear failure in the matrix further away from the interface zone.

SUMMARY AND CONCLUSIONS

Experimental results regarding the effects of steel fiber reinforcement and latex modification on the impact resistance

and flexural strength and toughness characteristics of concrete are reported.

From the generated test results, the following conclusions could be drawn:

1. Latex modification of steel fiber reinforcement increases the impact resistance of the concrete matrix, with superior impact strengths obtained when steel fibers and latex polymers are used simultaneously, indicating an effective interaction between latex and steel fibers resulting from the improved bonding between the fibers and the latex-modified mixtures.
2. The separate actions of latex polymers and steel fibers in concrete lead to improved flexural strength of concrete. The combined action of latex modification and steel fiber reinforcement leads to highest flexural strength values.
3. Steel fiber reinforcement is effective in increasing the flexural toughness (area underneath the flexural load-deflection curve) of concrete. Although latex modification has relatively small effects on the flexural toughness of plain concrete, it is capable of significantly improving the toughness characteristics of SFRC. These improvements can be attributed to the positive effects of latex modification on the fiber-to-matrix interfacial bond characteristics and pull-out behavior.

ACKNOWLEDGMENTS

Financial support for the performance of this research was provided by BASF Canada, Inc., and the Research Excellence Fund of the State of Michigan. These contributions are gratefully acknowledged. The authors are also thankful to Kar Lok from BASF Canada, Inc. and Lawrence T. Drzal from the Composite Materials and Structures Center of Michigan State University for their encouragement and technical support.

REFERENCES

1. *Concrete Admixtures Handbook*. Chapter 7, Noyes Publications, 1984, p. 398.
2. P. Soroushian and Z. Bayasi. Mechanical Properties of SFRC. *Proc., Concrete Seminar*, Michigan State University, East Lansing, Feb. 1987.
3. P. Soroushian and F. Aouadi. *Latex-Modified Concrete: State-of-the Art*. Department of Civil and Environmental Engineering, Michigan State University, East Lansing, Aug. 1988.
4. ACI Committee 548. *State of the Art, Polymers in Concrete*. American Concrete Institute, Detroit, Mich., 1977.
5. ACI Committee 544. Measurement of Properties of Fiber Reinforced Concrete. Report ACI 544.2R. *ACI Materials Journal, Proceedings*, Vol. 85, No. 6, Nov.–Dec. 1988, pp. 583–593.

Publication of this paper sponsored by Committee on Mechanical Properties of Concrete.

Silica Fume, Latex-Modified Portland Cement Mortars and Concretes

D. GERRY WALTERS

Portland cement mortars and concretes, modified by the addition of silica fume (SF) or by styrene-butadiene (S–B) latexes, have and are being used as overlays for bridge and parking-garage decks. The overlays are used both in repair of old construction and in new construction. The primary reason for the incorporation of either admixture in overlays is to improve permeability resistance of the mortar or concrete to deicing salts. The latter cause corrosion of reinforcing steel, which in turn leads to deterioration of the deck. SF is widely used to produce high compressive strength concrete. Laboratory work is described that examines the combined use of silica fume and S–B latex. The results indicate that the combined use of SF and S–B latex yields mortars and concretes that have superior properties to those using one or the other of the admixtures. This work also indicates that the two admixtures can be combined into one, which means that current equipment for placing latex-modified mortars or concretes could be used without modification.

S–B latex-modified mortars and concretes (LMCs) have been used since 1959 (*1*) as protective overlays for bridge and parking-garage decks. LMC is now considered a standard-type overlay for providing permeability resistance to deicing salts and satisfactory adhesion or bond to the subdeck of the construction.

SF-modified concrete (SFC) has been used since 1982 (*2*) for similar applications.

Although LMC has low permeability to water-soluble salts, it is significantly higher than that of SFC; also the compressive strength of LMC is significantly lower. Conversely, it is accepted that SFC has lower adhesion and flexural strength values than those of LMC, and the latter does not require extensive moist curing.

SF and S–B latex have been used together in portland cement mixtures (M. MacArthur, unpublished data), but there does not appear to have been any attempt to use the combination for deck overlays.

EXPERIMENTAL

In this work, the following test procedures were used:

- Flow of mortars (ASTM C230), 25 drops;
- Wet densities were determined by measuring the mass in grams required to fill a 400-ml Vicat cup and dividing the value by 400;
- Compressive strength of mortars (ASTM C109);
- Flexural strength (ASTM C78);
- Permeability (AASHTO T277);
- Adhesion-tensile bond method developed by Kuhlmann (*3*); and
- Dry densities were determined by measuring the mass of the various test specimens and dividing by their relative and approximate volume.

The mixture proportioning of all of the mortars used a 3:1 ratio of silica sand to portland cement. Details of the gradation of the silica sand are presented in Table 1.

Except where stated otherwise, the mortars and concretes were cured for 1 day in the mold covered with wet paper toweling and plastic sheeting followed by storage in laboratory air at about 50 percent relative humidity and at 75°F until time of testing.

Four mortars were prepared, one contained no admixtures, the second had a ratio of SF to portland cement of 0.10, the third a ratio of S–B polymer to cement of 0.15, and the fourth used both admixtures with ratios of SF and S–B polymer to cement of 0.10 and 0.15, respectively. The SF (Emsac F-100, Elkem Materials, Inc., Pittsburgh, Pa.) was obtained in an aqueous dispersion with a reported activity of 50 percent. The S–B latex (Tylac 6800 9–00, Reichhold Chemicals, Inc., Dover, Del.), which was carboxylated and had an approximate S–B ratio of 65/35, had a solids or nonvolatile content (NVC) of 47 percent. The nonlatex mortars had ratios of water to cement of 0.50, whereas those containing latex had ratios of 0.34. The unhardened mortars were measured for flow. The hardened mortars were measured for adhesion and for permeability. The nonlatex mortars were cured in saturated lime water for 27 days after demolding (where applicable).

SF is available in several forms (*2*). Two other SFs were obtained from different suppliers, one was an aqueous dispersion (Force 10,000. W. R. Grace Co., Cambridge Mass.) with a reported activity of 60 percent, whereas the second was in powder form (MB–SF, Master Builders, Cleveland, Ohio).

The three SFs were blended with the S–B latex to give a ratio of polymer to SF of 0.67. Viscosities of the blends were measured immediately and periodically over a period of 66 days. The blends were stored in closed plastic containers at about 75°F. Viscosities were measured using an RVF Brookfield viscometer at 20 rpm with a No. 3 spindle.

The three SFs were used at a 10 percent level on portland cement in a mortar with a ratio of S–B polymer to cement of 0.15. The water level was adjusted to yield a flow of 100 to 114 percent. A fourth mortar was included in the series that contained no SF. The mortars were measured for wet density, dry density, adhesion, and permeability, for set times

Emulsion Polymers Division, Reichhold Chemicals, Inc., P.O. Drawer K, Dover, Del. 19903.

TABLE 1 GRADATION OF ESG SAND

SIEVE SIZE	% PASSING	% PASSING CUMULATIVE
3/8 inch	100	0
# 4	99	1
# 8	95	5
# 16	84	16
# 30	29	71
# 50	6	94
#100	2	98

FINENESS MODULUS = 2.85

using Gillmore needles (ASTM C266). Adhesion was measured 9 days after mixing, dry density 21 days after mixing, and permeability 28 days after mixing.

One of the SF dispersions was blended with the S–B latex to give a ratio of polymer to SF of 0.67. This blend was stored in a closed plastic container at about 75°F. At 0, 1, 2, 3, and 4 months after making the blend, samples were taken and used to make portland cement mortars using a ratio of polymer to cement of 0.15, a ratio of SF to cement of 0.10, and a ratio of water to cement of 0.32. The mortars were measured for flow and wet density. A 2-in.-high, 4-in.-diameter cylinder was made with each mortar. Permeability of the specimen was measured 28 days after mixing.

Using one of the SF dispersions and the S–B latex, portland cement mortars were made using ratios of SF to portland cement of 0.00, 0.05, and 0.10. Ratios of S–B polymer to portland cement were 0.00, 0.075, and 0.15. Water levels were adjusted to a flow of 100 to 114 percent. The unhardened mortars were measured for wet density. The mortars not containing latex were cured for 1 day in the relevant mold covered with wet paper toweling and plastic sheeting, followed by storage in saturated lime-water at about 75°F. The hardened mortars were measured for density. Flexural strengths were determined 7 and 28 days after mixing, with samples measuring 5 × 1 × 1 in. Compressive strengths were measured 7 and 28 days after mixing, permeability 28 days after mixing. In all cases, three test specimens were used in measuring each property.

TABLE 2 COMPARISON OF LATEX-MODIFIED CONCRETES

Concrete Proportioning	A-5 parts by weight,	B-5 as received
Portland cement Type I	100	100
ESG Sand	250	250
Pea-Gravel*	200	200
S-B Latex (47% NVC)	32	32
SF dispersion (50%)	0	12
water	19	14
Unhardened Concrete Properties		
Slump, C 143, inches	3.5	4.0
Air Content, C 231, %	6.2	6.4
Density, Lb/cu. ft	141	141
Hardened Concrete Properties		
Compressive Strength, C 39, psi		
3 days	3330	3200
7 days	3860	3830
14 days	4070	5660
28 days	5750	6850
Adhesion, Tensile Bond, psi		
3 days	205	190
7 days	250	250
14 days	300	275
28 days	310	270
Flexural Strength, C 78, psi		
28 days	1010	1100
Permeability, T 277, coulombs		
14 days	1640	590
28 days	1190	250

* the pea-gravel had an approximate diameter of 1/4 inch, all of it passed through a 3/8 inch sieve and none passed through a No. 4 sieve.

November 1, 1990

TABLE 3 COMPARISON OF PORTLAND CEMENT MORTARS

Mortar	A-1	B-1	C-1	D-1
Proportioning	parts by weight, as received			
Portland Cement I	100	100	100	100
ESG Sand	300	300	300	300
SF dispersion (50%)	0	20	0	20
S-B Latex (47% NVC)	0	0	32	32
water	50	40	17	7
Unhardened Mortar Properties				
Flow, C 230, %	111	123	112	115
Type of Cure	Wet	Wet	Dry	Dry
Hardened Mortar Properties				
Adhesion, psi				
7 days	140	155	365	290
Permeability, coulombs				
28 days	8160	900	1980	120

Finally, two latex-modified concretes were prepared. Mixture proportioning is presented in Table 2. One contained SF at a ratio of SF to portland cement of 0.06, whereas the other did not. The unhardened concretes were measured for air content (ASTM C231), slump (ASTM C143), and wet density using a 0.5-ft^3 bucket. The hardened concretes were measured for flexural strength after 28 days using 22- × 6- × 6-in. beams; for compressive strength after 3, 7, 14, and 28 days using 6- × 3-in.-diameter cylinders by ASTM C39; for adhesion after 3, 7, 14, and 28 days; and for permeability after 14 and 28 days. For flexural strength, compressive strength, and adhesion measurements, three specimens were tested at each age. For permeability measurements, four test specimens were tested at each age.

RESULTS AND DISCUSSION

Values for coefficients of variations (COV) were determined for adhesion (tensile bond), permeability, flexural strength, and compressive strength. These values obtained by dividing the standard deviation by the average value and expressing it as a percentage, were as follows:

Parameter	*COV (%)*
Adhesion	7.3
Permeability	11.7
Flexural strength	8.9
Compressive strength	3.2

Table 3 presents the initial comparison of unmodified; SF-modified; latex-modified; and silica fume, latex-modified mortars (SFLMC). As expected, the SFC gave a significantly lower permeability than that of the LMC, which in turn was significantly lower than that of the unmodified mortar. However, the permeability of the SFLMC was significantly lower than that of the SFC. Also as expected, the bond strength of the SFC was similar to that of the unmodified mortar, whereas that of the LMC was higher. The bond strength of the SFLMC was significantly higher than those of either of the unmodified and SF mortars, and the former approached that of the LMC. This study indicated that the combined use of SF and S–B latex could yield a material with outstanding permeability resistance without significant loss of other advantageous properties.

Table 4 presents the viscosity of the blends of the three different types of SF with the S–B latex. The viscosity of the blend using the SF in powder form could not be obtained because an incompatible mixture was obtained. It appeared that the surfactant in the latex was unable to wet out the SF powder. With one of the SF dispersion-latex blends, the viscosity was relatively constant over the storage period of 66 days, whereas the viscosity of the other blend gradually increased. The SF dispersions probably contain water-reducing agents that would account for the various degrees of compatibility of the latex with the three silica fumes.

Table 5 presents the comparison of LMC with SFLMC using the three different sources of SF. The two SFLMC values using the dispersed SF gave virtually identical properties, but the permeability of the SFLMC using the powdered form of SF was significantly higher than that of the other mortars.

The blend of the one SF dispersion and S–B latex gave similar workability and permeability properties in a portland cement mortar despite being stored in the blended form for 4 months. Data are presented in Table 6.

Table 7 presents the data obtained from a series of mortars that contained ratios of SF and S–B latex to cement varying from 0.0 to 0.10 and 0.0 to 0.15, respectively. As expected, compressive strength increases with increasing SF level, as permeability decreases. Also as expected, flexural strength increases with increasing S–B latex level, as permeability decreases. Although the incorporation of the S–B latex causes a decrease in the compressive strength of SFC, the incorporation of SF does not cause any decrease in the flexural strength of LMC. From this work, it was judged that the optimum ratios of S–B latex and SF for overlay applications would be 0.15 and 0.07, respectively.

Table 2 presents the comparison of a standard latex-modified concrete overlay with one modified by the addition of SF at a level to yield a ratio of SF to cement of 0.7. No significant differences were observed in the properties of the unhardened concretes. But the SFLMC gave significantly lower (better) permeability values and higher compressive strengths,

TABLE 4 COMPATIBILITY OF LATEX AND SILICA FUME

Mixture	A-2	B-2	C-2
	parts by weight, as received		
S-B Latex (47% NVC)	100	100	100
SF dispersion (60% active)	52.2	0	0
SF dispersion (50% active)	0	62.5	0
SF powder	0	0	31.5
Viscosity, Brookfield, RVF, 20 rpm			
initial, cps	460	220	ic
7 days, cps	480	500	ic
14 days, cps	500	800	ic
28 days, cps	420	1060	ic
66 days, cps	500	1240	ic

ic = incompatible mixture obtained.

TABLE 5 LATEX-MODIFIED MORTARS WITH DIFFERENT SILICA FUMES

Mortar	A-3	B-3	C-3	D-3
Mixture Proportioning	parts by weight, as received			
Portland Cement, I	100	100	100	100
ESG Sand	300	300	300	300
S-B latex (47% NVC)	32	32	32	32
SF dispersion (60%)	0	16.7	0	0
SF dispersion (50%)	0	0	20	0
SF powder	0	0	0	10
water	15	7.6	4.5	20
Unhardened Mortar Properties				
Flow, C 230, %	112	111	111	111
Set Times, Gillmore				
initial, min	95	80	55	75
final, min	210	140	100	200
Wet Density, g/ml	2.24	2.27	2.27	2.21
Hardened Mortar Properties				
Dry Density, g/ml	2.08	2.12	2.09	2.05
Adhesion, psi	360	310	310	365
Permeability, coulombs	930	140	100	520

TABLE 6 STORAGE OF LATEX AND SILICA FUME BLEND

Time of Storage months	0	1	2	3	4
Flow, %	106	107	106	106	107
Wet Density g/ml	2.26	2.27	2.26	2.28	2.27
Permeability coulombs	130	180	140	140	130

TABLE 7 MORTARS WITH VARYING LEVELS OF LATEX AND SILICA FUME

Mortar Proportioning	A-4	B-4	C-4	D-4	E-4	F-4	G-4	H-4	I-4
	parts by weight as received								
P. Cement I	100	100	100	100	100	100	100	100	100
ESG Sand	300	300	300	300	300	300	300	300	300
SF (50%)	0	10	20	0	10	20	0	10	20
S-B Latex (47%)	0	0	0	16	16	16	32	32	32
water	45	44	35	30	25	20	15	10	8
Unhardened Mortar Properties									
Flow, %	111	113	111	111	111	111	110	111	111
Density, g/ml	2.30	2.30	2.03	2.28	2.21	2.24	2.21	2.22	2.24
Type of Cure	Wet	Wet	Wet	Dry	Dry	Dry	Dry	Dry	Dry
Hardened Mortar Properties									
Density, g/ml	2.12	2.23	2.19	2.12	2.11	2.15	2.12	2.17	2.16
Compressive Strength, psi									
7 days	5180	5970	6710	5320	5520	6380	5410	5770	5540
28 days	6750	8000	8830	6900	7040	8100	6650	6950	6750
Flexural Strength, psi									
7 days	440	560	640	890	930	940	1410	1370	1240
28 days	720	690	800	1330	1520	1410	1800	1830	1820
Permeability, 28 days									
coulombs	6890	2150	610	3590	460	350	2010	270	140

whereas bond and flexural strengths were similar to that of the LMC.

CONCLUSIONS

The combined use of silica fume and S–B latex dispersions can yield a concrete that is suitable for overlay applications. Such a concrete has excellent permeability resistance and acceptable compressive strength, while maintaining the good adhesion and flexural strength properties of latex-modified concrete.

Because acceptable blends of SF and S–B latex can be made and stored for reasonable periods of time, normal equipment and practices used for LMC should also be suitable for SFLMC.

RECOMMENDATIONS

It is recommended that further work be carried out using SF and S–B latex blends, particularly to (a) determine if the blends are cost effective, (b) determine resistance of SFLMC to freezing and thawing, and (c) examine the use of such blends in mobile mixers and in field placements.

ACKNOWLEDGMENT

Acknowledgment is extended to all my colleagues at Reichhold Chemicals, Inc., who helped in the preparation of this paper, especially to Pete Callaway and Lex Miller, who performed all of the experimental work.

REFERENCES

1. L. A. Kuhlmann. Latex-Modified Concrete. In *Applications of Polymer Concrete.* Publication SP-69. American Concrete Institute, Detroit, Mich., 1981, pp. 123–144.
2. M. D. Luther. Silica Fume (Micro Silica) Effects on Concrete Permeability and Steel Corrosion. In *Michigan State University Concrete Technology Seminars—4, Recent Advances in Concrete Technology*, Michigan State University, Feb. 1990, East Lansing, pp. 5-1–5-19.
3. L. A. Kuhlmann. Measuring Bond Strength of latex-Modified Concrete and Mortar. *Materials Journal of the American Concrete Institute*, Vol. 87, No. 4, July–Aug. 1990, pp. 387–394.

Publication of this paper sponsored by Committee on Mechanical Properties of Concrete.

Cracks in Latex-Modified Concrete Overlays—How They Get There, How Serious They Are, and What To Do About Them

L. KUHLMANN

The cause, effect, and prevention of cracks in latex-modified concrete (LMC) overlays were investigated. The types of cracks that occur in concrete, whether the concrete is LMC or conventional, are divided into two categories: internally caused and externally caused. Internally caused cracks are plastic and shrinkage cracks. As in any quality concrete, LMC is subject to both of these if good construction practices are not followed. In addition, because LMC has a low water content, it has little bleed water available to evaporate and thus should be protected during placement if extreme drying conditions exist. Externally caused cracks include cracks caused by physical tearing, and flexural, reflective, and thermal cracks. All of these processes can be minimized or avoided by following proper construction practices. If cracking occurs in an LMC overlay, it is necessary first to determine the extent of the cracking before deciding on the remedy. Cracks that are shallow, ⅛ in. deep or less, do not affect the permeability performance of the overlay. Deeper cracks, however, should be sealed. Laboratory studies of crack-sealing techniques indicate that the low-viscosity sealers are capable of filling most cracks and are recommended when full-depth penetration is required.

Because overlays are designed to provide protective concrete layers on bridge and parking garage decks, it is desirable to produce a concrete layer that has integrity and uniformity, and minimize any condition that will cause cracks, thus compromising the barrier properties of the overlay. Latex-modified concrete (LMC), like any other concrete, will crack when the tensile stresses exerted on it exceed the tensile strength of the material itself. Like any other concrete, these tensile stresses can be produced both by external and internal sources. Typical of these internal sources are plastic and drying shrinkage. Examples of external sources are structural movement, reflective cracks from the deck, thermal expansion, and tearing while finishing.

These cracking influences are addressed—how to attempt to avoid them, and what to do about cracks if they occur. An attempt is made to understand how cracks occur and how to try to prevent them. In addition, factors that are blamed for cracks but in fact have nothing to do with them are also discussed.

Larkin Laboratory, Dow Chemical Company, Midland, Mich. 48640.

CRACKS IN LMC OVERLAYS—HOW DO THEY GET THERE?

Internally Caused Cracks

Plastic Shrinkage

Plastic shrinkage in concrete is caused by water evaporating from the exposed surface faster than it can be replaced by bleed water before the concrete has hardened. As drying occurs, moisture leaves the surface of the concrete and shrinkage stresses develop before the concrete gains sufficient strength to resist them. The solution, of course, is to prevent this evaporation until the concrete gains proper strength.

Like most quality concretes, LMC mixes have a low water-cement ratio (typically less than 0.40) and there is little bleed water available to replenish that which is lost to evaporation. This is particularly critical for thin overlays where there is a high surface area per unit volume of concrete. Reduction of this plastic shrinkage can be accomplished in two ways:

1. Place concrete when the evaporation rate is low, i.e., less than 0.15 (lb/ft²)/hr. This evaporation rate is a function of concrete and air temperature, wind speed, and relative humidity, and can be determined from the chart, shown in Figure 1, published in The American Concrete Institute's *Recommended Practices for Hot Weather Concreting* (*1*).
2. Install the curing cover close behind the finishing operation. The cure cover is typically damp burlap and polyethylene film, and they both should be held down with suitable weights to prevent them from being blown off. (The polyethylene films should be white to minimize solar heat gain and increase in the temperature of the fresh concrete too quickly.)

The effect of bleed water on early plastic shrinkage cracking of these systems was demonstrated on 12- × 12- × 1-in. samples of latex-modified mortars made with two different water-cement ratios. The samples were exposed to a wind of 9 mph at 81°F and 18 percent relative humidity [at an evaporation rate of 0.22 (lb/hr)/ft²] for over 2 hr. The sample with a water-cement ratio of 0.26 cracked; the one with a water-cement ratio of 0.45 did not, indicating that the former had insufficient bleed water to resist initial plastic shrinkage (Table

1). These findings do not imply that the evaporation chart is in error, or that increasing the water content is an answer to cracking. These relatively small samples were made from mortar, so the data may not translate directly to large areas of concrete normally associated with overlays. More testing needs to be done on this subject. However, what the data confirm is that concrete is a complex material and that many factors need to be considered when working with it. It will continue to be important to monitor environmental conditions while placing LMC, and to take precautionary measures during hot, dry, and windy conditions.

Drying Shrinkage

Like any other concrete, the drying shrinkage of LMC is affected by the amount of water in the mix. It is the water-cement interaction that influences the drying shrinkage of the concrete, not the latex. Comparative tests (*2*) have indicated that LMC and conventional concrete with the same water-cement ratio have the same shrinkage characteristics. Whether the concrete is latex-modified or conventional, excess shrinkage will result from excess water in the mix. The key, then, is to make sure that excess water is not added. This precaution is best accomplished by making a trial mix of the proposed ingredients in a laboratory where all the components can be accurately measured, mixed, and tested. This procedure will relate slump to water-cement ratio, so that in the field, slump measurements will be accurate indications of water content.

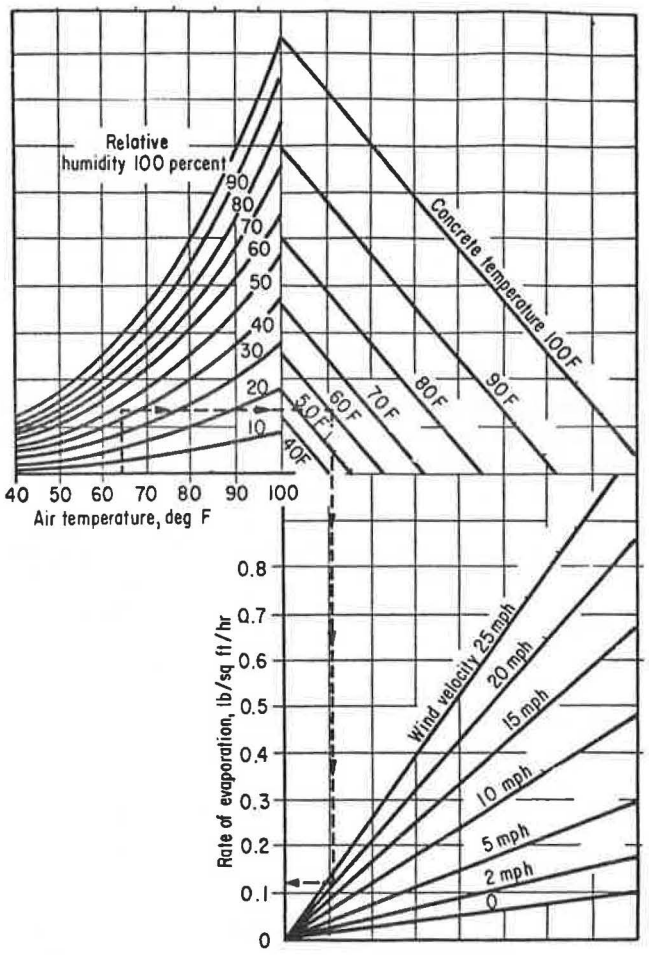

FIGURE 1 Nomograph for determining rate of evaporation (*1*).

TABLE 1 EFFECT OF WATER-CEMENT RATIO ON CRACKING OF LATEX-MODIFIED MORTAR EXPOSED TO WIND

Water-cement Ratio	Appearance of Cracks?
0.26	yes
0.45	no

NOTE: Wind 10 mph, temperature 72°F, relative humidity 50 percent.

By making a trial mix, it is possible to evaluate the various components that are used. Use of the wrong sand, for instance, can result in a concrete mix that requires excess water to achieve a workable slump. In LMC mixes, where the sand content is relatively high, it is particularly important that this component be chosen carefully. Figure 2 (*3*) shows the surface imperfections that are present on many sand particles. These surface imperfections have a detrimental effect on the mix because the macrosurface voids first have to be filled with paste, i.e., cement, water, air, (and latex if appropriate), before the concrete begins to flow. Thus, a sand with many of these macrosurface voids demands extra water before the concrete has a workable slump, thus producing an overwatered concrete with inferior properties. Obviously, if slump alone is used to monitor water content of a field mix, the concrete can easily have extra water added inadvertently.

This surface phenomenon is confirmed by the data in Table 2 where the surface areas of two different sands are shown to be different by a factor of over 4, even though both met ASTM C 33 for gradation. In laboratory tests, the high surface area of the Maryland sand produced a concrete of much lower slump than the control mix, both at the same water-cement ratio. Or put the other way, to achieve the same slump, more water would be required by the concrete made with the Maryland sand so that if slump were the only test conducted, the mix would easily be overwatered and produce low-quality concrete. Permeability results from laboratory tests of LMC made with the sand confirmed these findings.

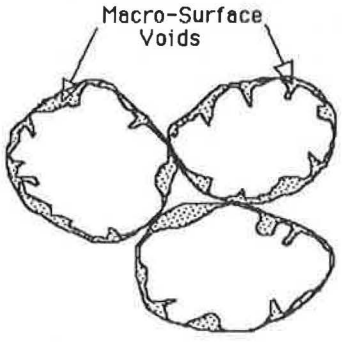

FIGURE 2 Macrosurface voids of sand particles.

TABLE 2 SURFACE AREAS OF TWO DIFFERENT CONCRETE SANDS

Sand Source	Surface Area[a] (m^2/g)
Michigan[b]	0.477
Maryland	2.093

[a]By Nitrogen absorption test.
[b]Control.

Externally Caused Cracks

This process is caused by externally applied stresses on the surface of LMC before it has set but after a crust has formed.

Particular care must be exercised when finishing LMC to avoid tearing the surface and causing cracks. LMC is different from conventional concrete in that a crust, i.e., a relatively firm material caused by the drying of the latex, will form on its surface if exposed too long to the air while in the plastic state. When this crust forms, the working life of the LMC has expired, while underneath, the concrete will be quite plastic until the setting time has expired. The difference between these two could be as much as 2 hr, depending on the drying conditions of the air and the temperature of the LMC. This surface crust can be torn and cause surface cracks if the finishing operation continues. On bridge deck overlays, where a rake is commonly used for applying grooves, these tears will appear as short and shallow (typically ½- × ⅛- in.) cracks oriented 90° to the direction of the grooves. (The effect of this type of crack on the permeability properties of LMC is discussed later.)

Flexural cracks are caused by excessive tensile stress applied to the overlay by flexural movement over negative moment areas. Excess deflection of a bridge deck under traffic can cause cracks to appear in an overlay at the negative moment region. The pattern of such cracks would be transverse, approximately in straight lines, and probably spaced 2 to 4 ft apart. These cracks can occur in any concrete overlay, including LMC. Even though the flexural strength of LMC is greater than conventional concrete, it is not designed to resist these excess tensile stresses.

In new two-course construction, the overlay should be placed after removing the forms from the base concrete, so that stresses caused by the weight of the overlay are borne by the underlying concrete. If placed before the forms are removed, the overlay will have to carry a portion of its own weight and may crack in negative-moment regions.

Reflective cracks are caused by movement of the underlying concrete reflecting through the overlay. Any time there is a crack in a concrete deck that is to be overlaid with a well-bonded, rigid material such as LMC, it is imperative to determine beforehand whether the crack is stable. If the underlying concrete on either side of the crack continues to move after the overlay is applied, whether from load deflection or temperature change, it is certain that the crack will be reflected into and through the overlay. In order to address this problem, a soft joint should be installed in the overlay right over the crack in the deck.

Expansion joints in the deck can cause the same problem. They should not be overlaid at the time of placement of the overlay, with the expectation of cutting them with a saw the following day. Doing so would result in a crack in the overlay over the joint, and possibly some debonding adjacent to the joint. The proper procedure is to form the overlay joint with an expandable material (i.e., plastic foam) and pour the overlay against it. After cure, the material can be removed and replaced with the final joint material.

Temperature-related cracks are caused by temperature differences between the newly-placed overlay and underlying concrete creating excessive differential expansion. Because many overlays are placed during the summer, there is concern about the proper time of day to place the overlay to avoid differential expansion between the deck and the overlay. Both early morning and late evening placements are commonly used to address this problem (as well as to avoid working during midday, when the temperature and wind can aggravate crusting). There are no definitive studies comparing cracking performance with time of placement, but the argument for early morning is persuasive and is presented here for consideration.

Early in the morning, i.e., just before dawn, the deck is cool. As the overlay is placed and the temperature rises, both the deck and the overlay warm and expand together, minimizing differential movement between the two. The heat received by the overlay in the morning hours accelerates cure, producing additional strength to resist subsequent drying shrinkage. (The procedure of prewetting the deck before overlay placement will also help this situation by cooling the deck even more.) Traffic-related cracks are caused by vibration from traffic in adjacent lanes that loosens the finished but not yet hardened LMC. Where the grade of the deck is severe, i.e., greater than 6 percent, and there is vibration from adjacent traffic, freshly placed LMC may move downhill slightly, creating cracks. This process can happen even hours after placement if the temperature of the LMC is low. The best solution is to reroute or reduce traffic. If this can't be done, reducing the slump of the LMC or utilizing Type III cement to accelerate cure, will help the situation.

Other Possible Causes of Cracks

There have been some instances where transverse cracks have appeared in overlays placed while traffic is on adjacent lanes. Because the cracks have some order, i.e., they are relatively straight and in a specific direction, the question has been raised as to whether the traffic vibration has caused cracking by flexing the bridge. Field data on this issue, however, are inconclusive. In any case, because there is the possibility that maintaining traffic during overlay construction may adversely affect the movement of the deck, consideration should be given to placing the overlay when the traffic count is low or when vehicle speed is restricted.

It has been reported (*4*) that screeding and finishing operations—particularly, the rate of movement of the screed—can have an effect on cracking of conventional mixes. Roller finishers are typically used to finish LMC overlays; to date, there has been no research to determine if there is a relation between roller speed and cracking. Clearly, this subject needs more study.

HOW SERIOUS ARE CRACKS IN LMC OVERLAYS?

Although having cracks in LMC overlays is not desirable, when they do occur it is important to understand the impact

that a particular type of crack has on performance of the overlay. The overlay should not be assumed to be a total loss needing replacement. Rather, it is important to know what impact the cracks might have on the performance of the overlay. This can only be determined by examining the cracks in detail, preferably by cores taken from the deck, to determine their width and depth. For instance, a shallow crack (⅛ in. deep) has little effect on the permeability of the overlay, whereas a deeper one (½ in.) has a significant effect. Tests conducted on cores taken from an LMC overlay had both of these types of cracks. The shallow cracks had the appearance of tears that are typically caused by late tining, when the crust has begun to form on the surface, whereas the deep crack appeared to be from plastic shrinkage. Using the rapid permeability test (*15*) (AASHTO T 277-83), chloride permeability was measured on the cores with cracks, and compared to a core without cracks. The results (Table 3) indicate that the core with shallow tears in the surface had the same low permeability (260 coulombs) as the core without cracks, indicating that these shallow tears do not affect the permeability performance of the overlay. The core with the deep crack, however, had a significantly higher permeability (700 coulombs), and thus required sealing. For this particular overlay, the treatment was to seal the deep cracks with a low-viscosity polymer, and treat the shallow tears as cosmetic blemishes by covering them with a latex-cement slurry. These treatments are discussed further later.

WHAT TO DO ABOUT CRACKS

Even with the best of intentions, cracks do occasionally appear in LMC overlays. If the degree of cracking is not severe, where severe refers both to size and frequency, the cracks can be treated so that the overlay is restored to serviceable condition. (The degree of cracking that requires replacement of the overlay rather than crack treatment is not addressed here because it would need to be determined on an individual basis.)

Two studies (*5*,*6*) have reported on the effect of sealers on filling cracks in LMC. Both consisted of slabs of LMC that were intentionally cracked by exposure of the fresh concrete to heat and wind to induce plastic shrinkage cracks. In one case, the sample was 3½ in. thick; in the other it was 1 in. thick. In both cases, cracks of various widths and depths were created.

After the LMC cured, the cracks were sealed with a variety of materials, including epoxy and methacrylate (both of low viscosity), sodium silicate, and latex-cement slurry. Samples were then cut from the slabs and the cross sections examined to determine depth of penetration of the various sealant materials. The results are presented in Table 4.

TABLE 3 PERMEABILITY TEST RESULTS OF CORES FROM AN LMC OVERLAY

Core	Type of Crack	Permeability (Coulombs)
Control	None	260
Sample 1	Tears; ⅛ in. deep	260
Sample 2	Shrinkage; ½ in. deep	700

TABLE 4 EVALUATION OF MATERIALS FOR SEALING CRACKS IN LMC

Sealer	Viscosity	Cracks Penetrated?
Study A—LMC Slab Thickness 1 in. (*6*)		
Methacrylate	10–20 cps	yes
Epoxy	10–20 cps	yes
Latex-cement-sand slurry[a]	"pancake batter"	no[b]
Study B—LMC Slab Thickness 3.5 in. (*7*)		
Methacrylate A	60 cps	yes
Epoxy	175 cps	yes
Epoxy	not reported	yes
Sodium-silicate	not reported	no
Latex-cement-slurry[c]	"pourable"	yes[d]

[a]Cement/sand = 0.33; latex solids/cement = 0.15; water/cement = 0.38.
[b]Slurry was well bonded but only covered the surface of the crack.
[c]Latex solids/cement = 0.15; water/cement = 0.67.
[d]Only at bottom of wide cracks.

These studies indicate that the methacrylate and epoxy sealers were effective in penetrating and filling cracks and should be used for repairing cracked overlays. Two different latex-cement mixes were studied and neither of them appeared to be particularly suitable for filling cracks. The mix in Study A consisted of sand, cement, latex, and water, whereas the other was just cement, latex, and water. The former had the lower water-cement ratio and thus less flow. The slurry used in Study A did not penetrate but tended to bridge the cracks and bond to the top surface of the overlay. The mix used in Study B was of low enough viscosity to flow into the cracks but it did not fill them significantly. In addition, the high water-cement ratio of this mix would make the long-term performance of such a grout suspect. Use of these slurry mixes should be limited to treatment of the shallow tears and cracks. The sodium silicate product that was tested did not indicate any effect on filling the cracks.

HOW TO PREVENT CRACKS IN LMC OVERLAYS

The obvious first step in addressing a problem is to try and prevent it from occurring in the first place. Preventing cracks in LMC overlays can best be accomplished by following proper construction practices for quality concrete. This means having a specification that is appropriate for the project; using high-quality materials and equipment that is in good operating order; employing people who are experienced, quality conscious, and interested in producing good work; and making decisions on the job that will benefit the long-term performance of that job. In particular, for LMC, it means keeping close control of the water in the mix; avoiding placement of LMC when the evaporation rate is above 0.10 (lb/ft^2)/hr; and applying the burlap cover appropriately to avoid plastic shrinkage cracking.

Another possible crack prevention measure is related to the curing schedule. Typically LMC is cured for 1 day damp and the remaining days open to air drying. Under normal conditions, this procedure is good but if temperature and wind conditions are not favorable, 1 day of damp curing may not be long enough to prevent shrinkage cracking during drying. Recent research (*7*) on the effect of curing schedule on shrink-

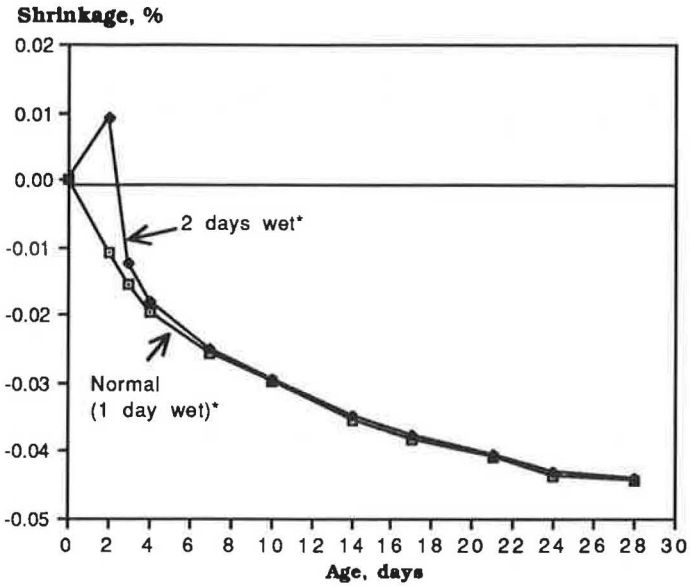

FIGURE 3 Shrinkage of LMC versus initial cure time, *lower curve*, normal (1 day wet), *upper curve*, 2 days wet, remaining days at 72°F, 50 percent relative humidity.

age of LMC indicates that during the initial wet-cure period, slight expansion of the concrete occurs, and that by extending the wet cure beyond 1 day there is potential to offset shrinkage stresses that occur during the dry-cure period.

Results of shrinkage studies with 1 day versus 2 days of damp cure are shown in Figure 3. These data indicate that by extending the damp cure time to 2 days, slight expansion of the LMC will occur, thus putting the overlay into compression and reducing the tendency to create shrinkage cracks. The compressive strength properties were essentially unaffected by this extra day of wet cure.

CONCLUSIONS

1. Cracks in LMC are not always detrimental to the long-term performance of the material. Shallow tears from late-finishing operations need not be sealed. Deep cracks should be sealed, using low-viscosity epoxy or methacrylate sealers.
2. Cracking in LMC can be controlled by proper attention to the quality of the materials used in the mix as well as the construction procedures used to place it.

RECOMMENDATIONS

- Placement of LMC overlays should be limited to conditions for which the evaporation rate is less than 0.10 (lb/ft^2)/hr.
- Two days of wet cure should be considered as a standard curing procedure for LMC.
- Care should be exercised during placement of overlays where the grade exceeds 6 percent and traffic is maintained on adjacent lanes. Traffic should be rerouted or slowed, or Type III cement should be incorporated in the mix design.
- Research should be conducted on the roller finisher to determine if there is a relationship between speed of the roller and cracking.

REFERENCES

1. ACI Committee 305. *Recommended Practice for Hot Weather Concreting.* ACI 305R-77, American Concrete Institute, Detroit, Mich., Revised 1982, 17 pp.
2. Y. Ohama and S. Kan. Effects of Specimen Size on Strength and Drying Shrinkage of Polymer-Modified Concrete. *The International Journal of Cement Composites and Lightweight Concrete*, Vol. 4, No. 4, Nov. 1982.
3. I. Ishai and E. Ton. Concept and Test Method for a Unified Characterization of the Geometric Irregularity of Aggregate Particles. *Journal of Testing and Evaluation*, ASTM, Philadelphia, Pa., Jan. 1977.
4. C. A. Shaeles and K. H. Hover. Influence of Mix Proportions and Construction Operations on Plastic Shrinkage Cracking in Thin Slabs. *ACI Materials Journal.* American Concrete Institute, Detroit, Mich. Nov./Dec. 1988, pp. 495–504.
5. L. A. Kuhlmann, D. Moldovan, and M. Mielke. An Evaluation of Sealers for Cracked Latex Modified Concrete. Dow Chemical Co., Midland, Mich., Sept. 1990.
6. J. R. Landgren and W. F. Perenchio. *Investigation of Potential Sealants for Plastic Shrinkage Cracks in Concrete.* Wiss, Janney, Elstner Assoc., Inc., Northbrook, Ill., 1986.
7. L. A. Kuhlmann. Polymer Modified Concrete and Mortar for Repair and Overlay Applications. *Concrete Technology Seminar*, Michigan State University, Lansing, Mich. Feb. 7, 1990.

Publication of this paper sponsored by Committee on Mechanical Properties of Concrete.

Flexural Cracking in Concrete Structures

EDWARD G. NAWY

The state-of-the-art in the evaluation of the flexural crack width development and crack control of macrocracks is described. It is based on extensive research over the past 50 years in the United States and overseas in the area of macrocracking in reinforced and prestressed concrete beams and two-way-action slabs and plates. Control of cracking has become essential to maintain the integrity and aesthetics of concrete structures. The trends are stronger than ever—toward better use of concrete strength, use of higher-strength concretes including superstrength concretes of over 20,000-psi compressive strength, use of more prestressed concretes, and increased use of limit failure theories—all requiring closer control of serviceability requirements of cracking and deflection behavior. Common expressions are discussed for the control of cracking in reinforced-concrete beams and thick one-way slabs; prestressed, pretensioned, and posttensioned flanged beams; and reinforced-concrete, two-way-action, structural floor slabs and plates. In addition, recommendations are given for the maximum tolerable flexural crack widths in concrete elements.

Presently, the trend is stronger than ever—toward better use of concrete strength, use of higher-strength concretes including superstrength concretes of 20,000-psi (138-MPa) compressive strength and higher, use of high-strength reinforcement, use of more prestressed concretes, and increased use of limit failure theories—all requiring closer control of serviceability requirements in cracking and deflection behavior. Hence, knowledge of the cracking behavior of concrete elements becomes essential.

Concrete cracks early in its loading history. Most cracks are a result of the following actions to which concrete can be subjected:

1. Volumetric change caused by drying shrinkage, creep under sustained load, thermal stresses including elevated temperatures, and chemical incompatibility of concrete components.
2. Direct stress caused by applied loads or reactions or internal stress caused by continuity, reversible fatigue load, long-term deflection, camber in prestressed systems, and environmental effects including differential movement in structural systems.
3. Flexural stress caused by bending.

Although the net result of these three actions is the formation of cracks, the mechanisms of their development cannot be considered to be identical. Volumetric change generates internal microcracking that may develop into full cracking, whereas direct internal or external stress or applied loads and reactions could either generate internal microcracking, such as in the case of fatigue caused by reversible load, or flexural macrocracking leading to fully developed cracking.

Department of Civil and Environmental Engineering, Rutgers University, Piscataway, N.J. 08855.

Although the macrocracking aspects of cracking behavior are emphasized, it is also important to briefly discuss microcracking.

MICROCRACKING

Microcracking can be mainly classified into two categories: (a) bond cracks at the aggregate-mortar interface, and (b) paste cracks within the mortar matrix. Interfacial bond cracks are caused by interfacial shear and tensile stresses caused by early volumetric change without the presence of external load. Volume change caused by hydration and shrinkage could create tensile and bond stresses of sufficient magnitude to cause failure at the aggregate-mortar interface (*1*). As the external load is applied, mortar cracks develop because of increase in compressive stress, propagating continuously through the cement matrix up to failure. A typical schematic stress-strain diagram (Figure 1) shows that the nonlinear relationship developed early in the stress history and started with bond microcracking. Although extensive work exists in the area of volumetric change cracking, the need is apparent for additional work on creep effects on microcracking and also for the development of a universally acceptable fracture theory to interrelate the nonlinear behavioral factors resulting in crack propagation.

It appears that the damage to cement paste seems to play a significant role in controlling the stress-strain relationship in concrete. The coarse aggregate particles act as stress raisers that decrease the strength of the cement paste. As a result, microcracks develop that can only be detected by large magnification. The importance of additional work lies not only in the evaluation of the microcracks, but also in the evaluation of their significance for the development of macrocracks that generate from those microcracked centers of plasticity.

FLEXURAL CRACKING

External load results in direct and bending stresses, causing flexural, bond, and diagonal tension cracks. Immediately after the tensile stress in the concrete exceeds its tensile strength, internal microcracks form. These cracks generate into macrocracks propagating to the external fiber zones of the element.

Immediately after the full development of the first crack in a reinforced-concrete element, the stress in the concrete at the cracking zone is reduced to zero and is assumed by the reinforcement (*2*). The distributions of ultimate bond stress, longitudinal tensile stress in the concrete, and longitudinal tensile stress in the steel are shown in Figure 2.

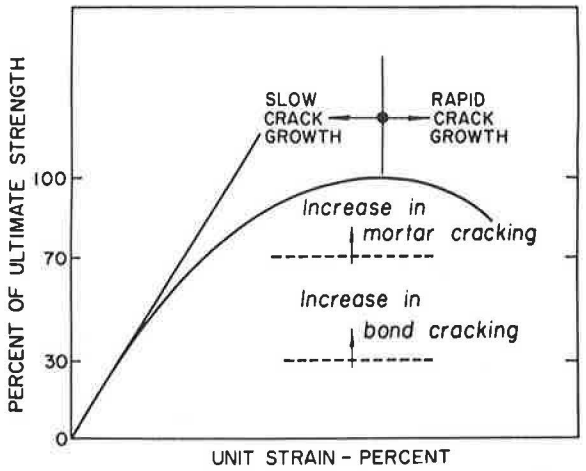

FIGURE 1 Schematic stress-strain diagram of concrete in microcracking.

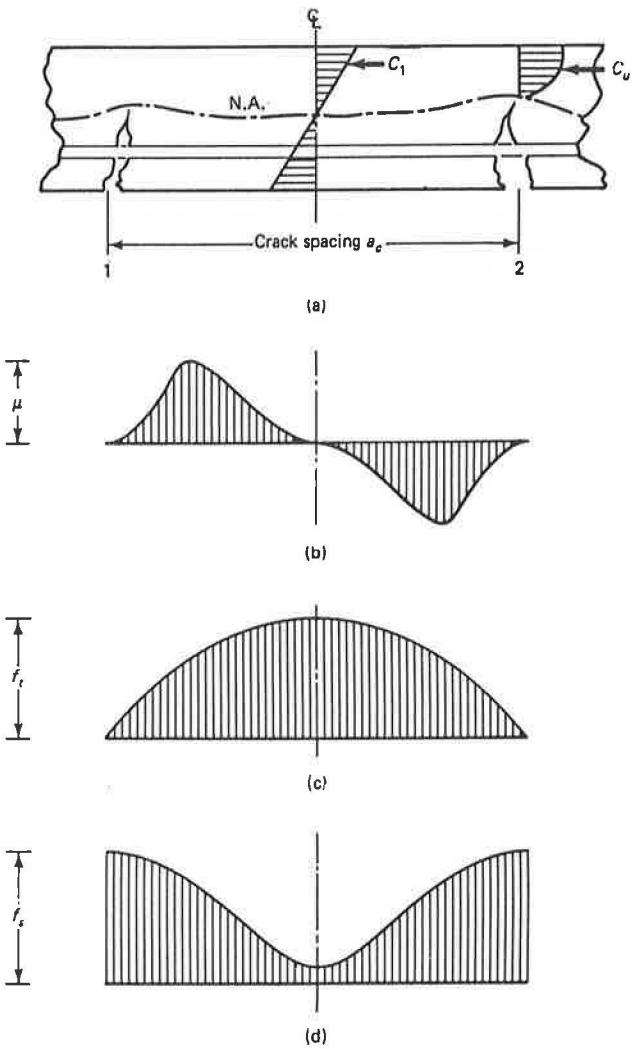

FIGURE 2 Schematic stress distributions (a) between two flexural cracks for (b) ultimate bond stress, (c) longitudinal tensile stress in the concrete, and (d) longitudinal tensile stress in the steel.

In Figure 2, crack width is a primary function of the deformation of reinforcement between adjacent Cracks 1 and 2, if the small concrete strain along the crack interval a_c is neglected. The crack width would hence be a function of the crack spacing, and vice versa, up to the level of stabilization of crack spacing (Figure 3).

The major parameters affecting the development and characteristics of the cracks are percentage of reinforcement, bond characteristics and size of bar, concrete cover, and the concrete stretched area (namely, the concrete area in tension). On this basis, one can propose the following mathematical model:

$$w = \alpha\, a_c^{\beta} \varepsilon_s^{\gamma} \tag{1}$$

where

w = maximum crack width,
α, β, and γ = nonlinearity constants, and
ε_s = strain in the reinforcement induced by external load.

Crack spacing a_c is a function of the factors enumerated previously, being inversely proportional to bond strength and active steel ratio (steel percentage in terms of the concrete area in tension).

The basic mathematical model in Equation 1 with the appropriate experimental values of the constants α, β, and γ can be derived for the particular type of structural member. Such a member can be a one-dimensional element such as a beam, a two-dimensional structure such as a two-way slab, or a three-dimensional member such as a shell or circular tank wall. Hence, it is expected that different forms or expressions apply for the evaluation of the macrocracking behavior of different structural elements consistent with their fundamental structural behavior (*1–10*).

FLEXURAL CRACK CONTROL IN REINFORCED-CONCRETE BEAMS

Requirements for crack control in beams and thick one-way slabs in the American Concrete Institute (ACI) Building Code

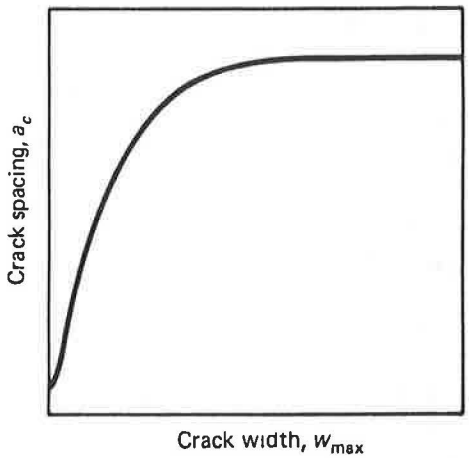

FIGURE 3 Schematic variation of crack width with crack spacing.

(ACI 318) are based on the statistical analysis of maximum crack width data from a number of sources. The following general conclusions were reached:

1. The steel stress is the most important variable;
2. The thickness of the concrete cover is an important variable, but not the only geometric consideration;
3. The area of concrete surrounding each reinforcing bar is also an important geometric variable;
4. The bar diameter is not a major variable; and
5. The size of the bottom crack width is influenced by the amount of strain gradient from the level of the steel to the tension face of the beam.

The simplified expression relating crack width to steel stress is as follows (*4*):

$$w_{max} = 0.076\ \beta\ f_s(d_c A)^{1/3} \times 10^{-3} \quad (2)$$

where

f_s = reinforcing steel stress, kips/in.^{2} (ksi);
A = area of concrete symmetric with reinforcing steel divided by number of bars, in.^{2};
d_c = thickness of concrete cover measured from extreme tension fiber to center of bar or wire closest thereto, in.; and
h_1 = distance from neutral axis to the reinforcing steel, in.;
h_2 = distance from neutral axis to extreme concrete tensile surface, in.; and
$\beta = h_2/h_1$.

A plot relating the reinforcement strength to the ratio of the concrete area in tension to the reinforcement area is shown in Figure 4 for all bar sizes.

In the ACI code, when the design field strength f_y for tension reinforcement exceeds 40,000 psi, cross sections of maximum positive and negative moment have to be so proportioned that the quantity z given by

$$z = f_s\ (d_c A)^{1/3} \quad (3)$$

does not exceed 175 kips/in. for interior exposure and 145 kips/in. for exterior exposure. Calculated stress in the reinforcement at service load f_s (ksi) shall be computed as the moment divided by the product of steel area and internal moment area. In lieu of such computations, it is permitted to take f_s as 60 percent of specified length f_y.

When the strain ε_s in the steel reinforcement is used instead of stress f_s, Equation 3 becomes

$$w = 2.2\ R_i\ \varepsilon_s\ (d_c A)^{1/3} \quad (4)$$

Equation 4 is valid in any system of measurement.

The cracking behavior in thick one-way slabs is similar to that in shallow beams. For one-way slabs having a clear concrete cover in excess of 1 in. (25.4 mm), Equation 4 can be adequately applied if $\beta = 1.25$ to 1.35.

Committeé EuroInternationale du Beton (CEB) Recommendations

Crack control recommendations proposed that the European Model Code for Concrete Structures (*9*) apply to both pre-

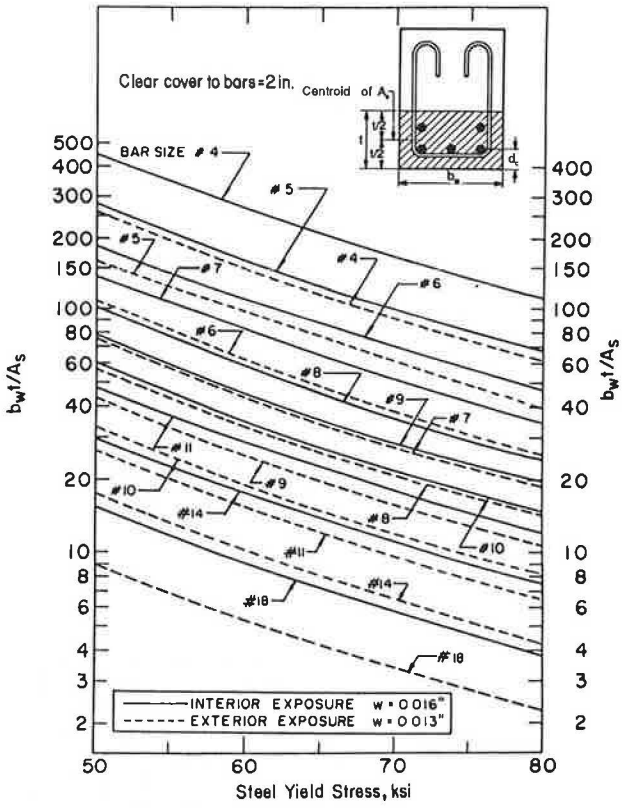

FIGURE 4 Steel reinforcement strength f_y versus ratio of concrete area in tension to reinforcement area for stress level $f_s = 0.6f_y$.

stressed and reinforced concrete can be summarized as follows:

The mean crack width w_m in beams is expressed in terms of the mean crack spacing s_{rm}, such that

$$w_m = \varepsilon_{sm} s_{rm} \quad (5)$$

$$\varepsilon_{sm} = \frac{f_s}{E_s}\left[1 - \chi\left(\frac{f_{sr}}{f_s}\right)^2\right] \leq 0.4\,\frac{f_s}{E_s} \quad (6)$$

where

ε_{sm} = average strain in the steel,
f_s = steel stress at the crack,
f_{sr} = steel stress at the crack caused by cracking forces at the tensile strength of concrete, and
χ = bond coefficient (1.0 for ribbed bars, reflecting influence of load repetitions and load duration).

The mean crack spacing is

$$s_{rm} = 2\left(c - \frac{s}{10}\right) + \chi_2\chi_3\,\frac{d_b}{Q_R} \quad (7)$$

where

c = clear concrete cover;
s = bar spacing, limited to $15d_b$;
χ_2 = coefficient that is 0.4 for ribbed bars;
χ_3 = coefficient that depends on the shape of the stress diagram, 0.125 for bending;

$Q_R = A_s/A_t$; and
A_t = effective area in tension.

Depending on arrangement of bars and type of external forces, A_t is limited by a line $c + 7d_b$ from the tension face for beams (in the case of thick slabs, not more than halfway to the neutral axis).

A simplified formula can be derived for the mean crack width in beams with ribbed bars.

$$w_m = 0.7 \frac{f_s}{E_s} \left(3_c + 0.05 \frac{d_b}{Q_R}\right) \tag{8}$$

A characteristic value of the crack width, presumably equivalent to the probable maximum value, is given by $0.7w_m$.

FLEXURAL CRACK CONTROL IN PRESTRESSED, PRETENSIONED, AND POSTTENSIONED BEAMS

The increased use of partial prestressing, allowing limited tensile stresses in the concrete under service and overload conditions while allowing nonprestressed steel to carry the tensile stresses, is becoming prevalent because of practicality and economy. Consequently, an evaluation of the flexural crack widths and spacing and control of their development become essential. Work in this area is relatively limited because of the various factors affecting crack width development in prestressed concrete. However, experimental investigations support the hypothesis that the major controlling parameter is the reinforcement stress change beyond the decompression stage. Nawy et al. have undertaken extensive research since the 1960s on the cracking behavior of prestressed, pretensioned, and posttensioned beams and slabs because of the great vulnerability of the highly stressed prestressing steel to corrosion and other environmental effects and the resulting premature loss of prestress (*11,12*). Serviceability behavior under service and overload conditions can be controlled by the design engineer through the application of the criteria presented in this section.

Mathematical Model Formulation for Serviceability Evaluation

Crack Spacing

Primary cracks form in the region of maximum bending moment when the external load reaches the cracking load. As loading is increased, additional cracks will form and the number of cracks will be stabilized when the stress in the concrete no longer exceeds its tensile strength at further locations regardless of load increase. This condition is important as it essentially produces the absolute minimum crack spacing that can occur at high steel stresses, to be termed the stabilized minimum crack spacing. The maximum possible crack spacing under this stabilized condition is twice the minimum, to be termed the stabilized maximum crack spacing. Hence, the stabilized mean crack spacing a_{cs} is deduced as the mean value of the two extremes.

The total tensile force T transferred from the steel to the concrete over the stabilized mean crack spacing can be defined as

$$T = \gamma\, a_{cs}\, \mu\, \Sigma o \tag{9a}$$

where

γ = a factor reflecting the distribution of bond stress;
μ = maximum bond stress, which is a function of $f_c'^{1/2}$;
a_{cs} = mean stabilized spacing; and
Σo = sum of reinforcing element circumferences.

The resistance R of the concrete area A_t in tension can be defined as

$$R = A_t f_t' \tag{9b}$$

where f_t' = tensile splitting strength of the concrete. By equating Equations 9a and 9b, the following expression for a_{cs} is obtained:

$$a_{cs} = c \frac{A_t f_t'}{\Sigma o\, (f_c')^{1/2}} \tag{10a}$$

where c is a constant to be developed from the tests. The concrete stretched area, namely the concrete area in tension A_t for both the evenly distributed and nonevenly distributed reinforcing elements, is shown in Figure 5. With a mean value of $f_t'/(f_c')^{1/2} = 7.95$ in this investigation, a regression analysis

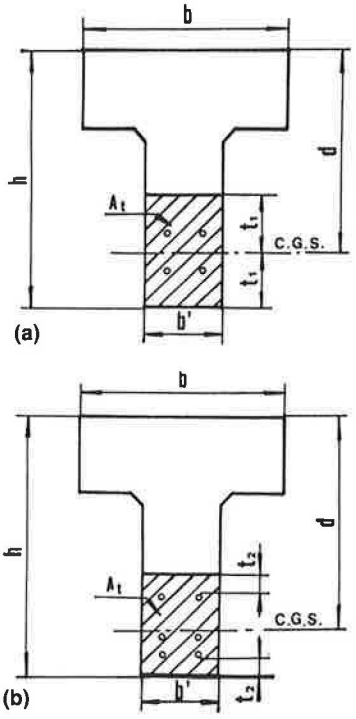

FIGURE 5 Effective concrete area in tension (a) for even distribution of reinforcement in concrete, and (b) for noneven distribution of reinforcement in concrete.

of the test data resulted in the following expression for the mean stabilized crack spacing:

$$a_{cs} = 1.20A_t/\Sigma o \tag{10b}$$

Crack Width

If Δf_s is the net stress in the prestressed tendon or the magnitude of the tensile stress in the normal steel at any crack width load level in which the decompression load (decompression here means $f_c = 0$ at the level of the reinforcing steel) is taken as the reference point, then for the prestressed tendon

$$\Delta f_s = f_{nt} - f_d \tag{11}$$

where

f_{nt} = stress in the prestressing steel at any load beyond the decompression load, and
f_d = stress in the prestressing steel corresponding to the decompression load.

The unit strain $\varepsilon_s = \Delta f_s/E_s$. It is logical to disregard as insignificant the unit strains in the concrete caused by the effects of temperature, shrinkage, and elastic shortening. The maximum crack width as defined in Equation 1 can be taken as

$$w_{max} = ka_{cs}\varepsilon_s^{\alpha} \tag{12a}$$

where k and α are constants to be established by tests, or

$$w_{max} = k'a_{cs}(\Delta f_s)^{\alpha} \tag{12b}$$

where k' is a constant in terms of constant k.

Expressions for Pretensioned Beams

Equation 12a is rewritten in terms of Δf_s so that analysis of the test data of all the simply supported test beams in this work leads to the following expression at the reinforcement level:

$$w_{max} = (1.4 \times 10^{-5})a_{cs}(\Delta f_s)^{1.31} \quad \text{(in.)} \tag{13}$$

Linearizing Equation 13 for easier use by the design engineer leads to the following simplified expression of the maximum crack width at the reinforcing steel level:

$$w_{max} = (5.85 \times 10^{-5})\frac{A_t}{\Sigma o}(\Delta f_s) \tag{14a}$$

and a maximum crack width (in.) at the tensile face of the concrete:

$$w'_{max} = (5.85 \times 10^{-5})R_i\frac{A_t}{\Sigma o}(\Delta f_s) \tag{14b}$$

A plot of the data and the best-fit expression for Equation 14a are shown in Figure 6 with a 40 percent spread (which is reasonable in view of the randomness of crack development and the linearization of the original expression in Equation 13).

Expressions for Posttensioned Beams

The expression developed for the crack width in posttensioned bonded beams that contain mild steel reinforcement is

$$w_{max} = (6.51 \times 10^{-5})\frac{A_t}{\Sigma o}(\Delta f_s) \tag{15a}$$

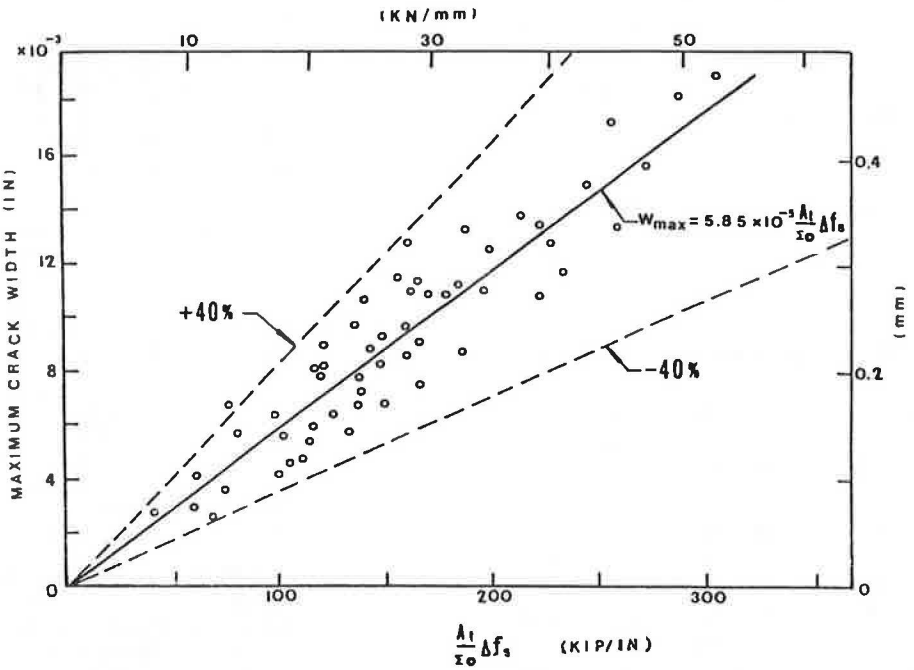

FIGURE 6 Linearized maximum crack width versus $(A_t/\Sigma o)\ \Delta f_s$ for pretensioned beams.

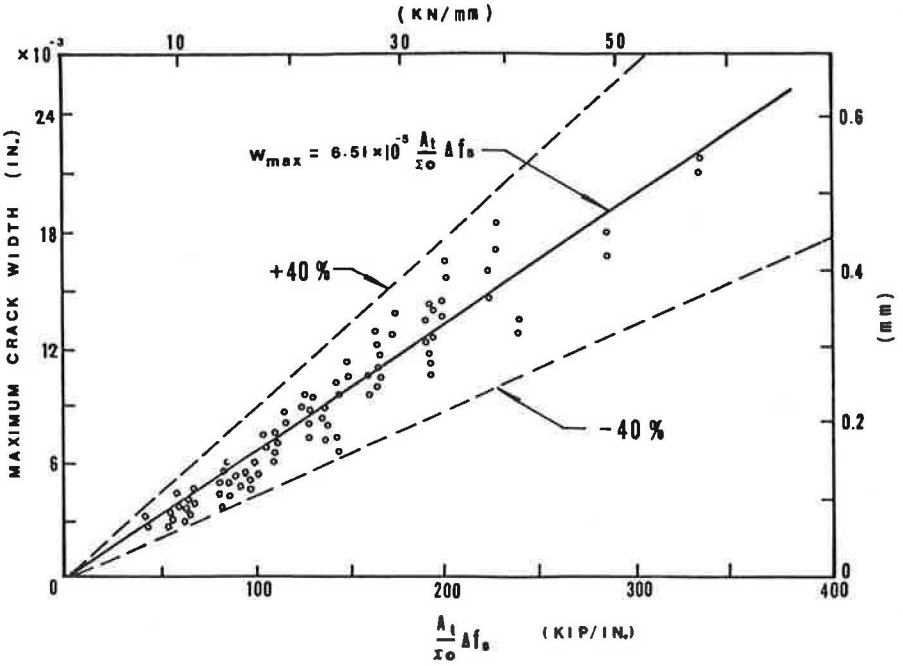

FIGURE 7 Linearized maximum crack width versus $(A_t/\Sigma o)\ \Delta f_s$ for posttensioned beams.

for the width at the reinforcement level closest to the tensile face, and

$$w_{max} = (6.51 \times 10^{-5}) R_i \frac{A_t}{\Sigma o} (\Delta f_s) \qquad (15b)$$

at the tensile face of the concrete lower fibers.

For nonbonded beams, the factor 6.51 in Equations 15a and 15b becomes 6.83.

A plot of the data and the best-fit expression for Equation 15a are shown in Figure 7.

A typical plot of the effect of the various steel percentages on the crack spacing at the various steel levels Δf_s is shown in Figure 8. In this plot, crack spacing stabilizes at a net stress level of 36 ksi.

Other Work on Cracking in Prestressed Concrete

On the basis of the analysis of results of various investigators, Naaman (*8*) produced the following modified expression for partially prestressed pretensioned members

$$(w_{max}) = \left[42 + 5.58 \frac{A_t}{\Sigma o} (\Delta f_s)\right] \times 10^{-5} \quad \text{(in.)} \qquad (16)$$

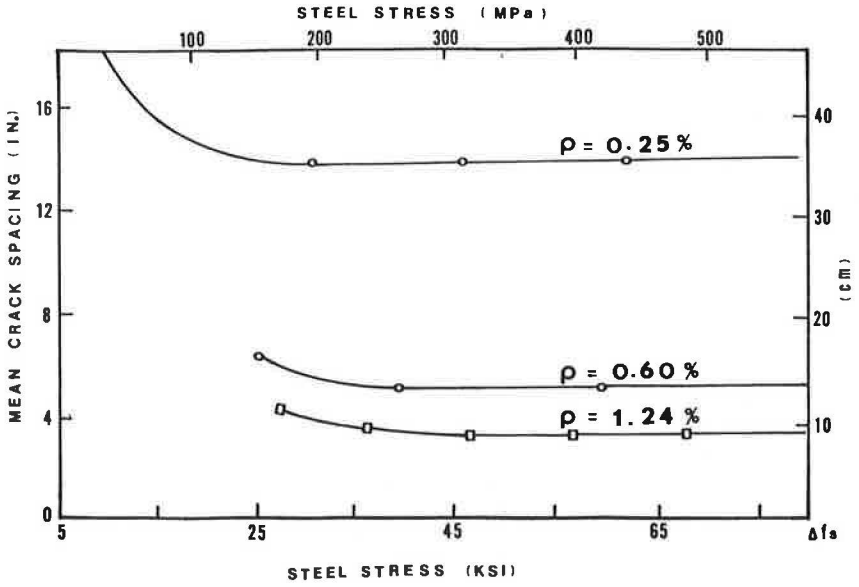

FIGURE 8 Effect of steel percentage on mean crack spacing in prestressed beams.

This regression expression is close to Equation 14. When plotted against the experimental results of the various researchers, it gives a best fit as shown in Figure 9.

The author's equations and the CEB–Fédération Internationale de la Précontrainte (FIP) equations can be compared using similar notations.

$$\text{Nawy:} \quad w_{\max} = \zeta\left(\frac{A_t}{\Sigma o}\right)\Delta\sigma_p$$

$$\text{CEB–FIP:} \quad w_{\max} = \left(k\frac{\phi}{\rho_t} + \alpha_0\right)\frac{\Delta\sigma_p}{E_s}\left[1 - b\left(\frac{\Delta\sigma_{pr}}{\Delta\sigma_p}\right)^2\right]$$

These equations are similar assuming $1/\Sigma o = \lambda(\phi/\rho_t)$, where ϕ is the diameter of the bar, λ is a multiplier, k and b are experimental parameters, and α_0 and $\Delta\sigma_{pr}/\Delta\sigma_p{}^2$ are terms in the CEB–FIP expression not of major significance that are accounted for by using $\zeta = 6.51$ for the posttensioned beams in the author's expressions.

The study by Meier and Gergely (*10*), concentrating on the area of concrete in tension and the nominal strain in the concrete at the tensile face, does not yield a reliable prediction of the crack width. In particular, it does not account for the actual stress in the steel reinforcement and depends on measurements of strain at the concrete surface that are difficult to reliably evaluate.

FLEXURAL CRACK CONTROL IN TWO-WAY-ACTION SLABS AND PLATES

Flexural crack control is essential in structural floors where cracks at service load and overload conditions can be serious, such as in office buildings, schools, parking garages, industrial buildings, and other floors where the design service load levels exceed those in normal-sized apartment building panels and also in all cases of adverse exposure conditions.

Flexural Cracking Mechanism and Fracture Hypothesis

Flexural cracking behavior in concrete structural floors under two-way action is significantly different from that in one-way members. Crack control equations for beams underestimate the crack widths developed in two-way slabs and plates, and do not tell the designer how to space the reinforcement. Cracking in two-way slabs and plates is controlled primarily by the steel stress level and the spacing of the reinforcement in the two perpendicular directions. In addition, the clear concrete cover in two-way slabs and plates is nearly constant [¾ in. (19 mm) for interior exposure], whereas it is a major variable in the crack control equations for beams. The results from extensive tests on slabs and plates by Nawy et al. demonstrate this difference in behavior in a fracture hypothesis on crack development and propagation in two-way plate action. As shown in Figure 10, stress concentration develops initially at the points of intersection of the reinforcement in the reinforcing bars and at the welded joints of the wire mesh, that is, at grid nodal points, thereby dynamically generating fracture lines along the paths of least resistance, namely, along A_1B_1, A_1A_2, A_2B_2, and B_2B_1. The resulting fracture pattern is a total repetitive cracking grid, provided that the spacing of the nodal points A_1, B_1, A_2, and B_2 is close enough to generate this preferred initial fracture grid of orthogonal cracks narrow in width as a preferred fracture mechanism.

If the spacing of the reinforcing grid intersections is too large, the magnitude of stress concentration and the energy absorbed per unit grid is too low to generate cracks along the reinforcing wires or bars. As a result, the principal cracks follow diagonal yield-line cracking in the plain concrete field away from the reinforcing bars early in the loading history. These cracks are wide and few.

This hypothesis also leads to the conclusion that surface deformations of the individual reinforcing elements have little effect in arresting the generation of the cracks or controlling their type or width in a slab or plate of two-way action. In a

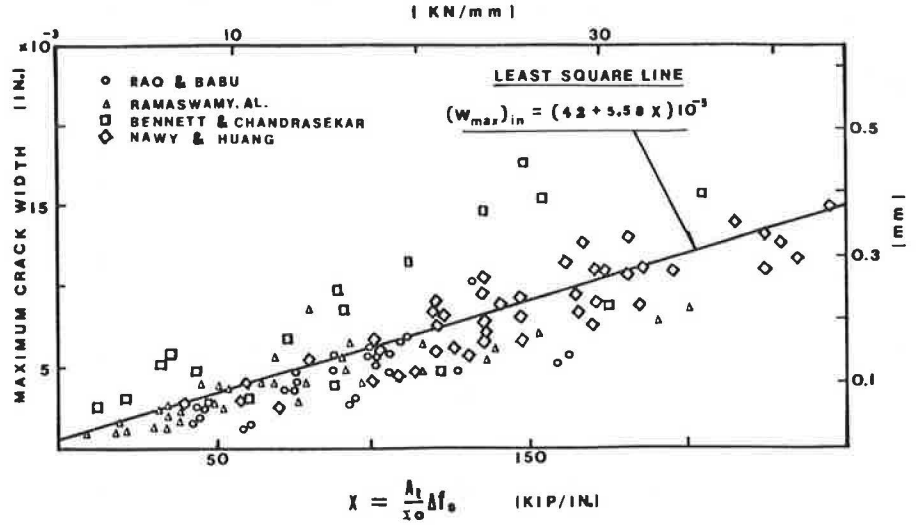

FIGURE 9 Reinforcement stress versus crack width (best-fit data of several investigators).

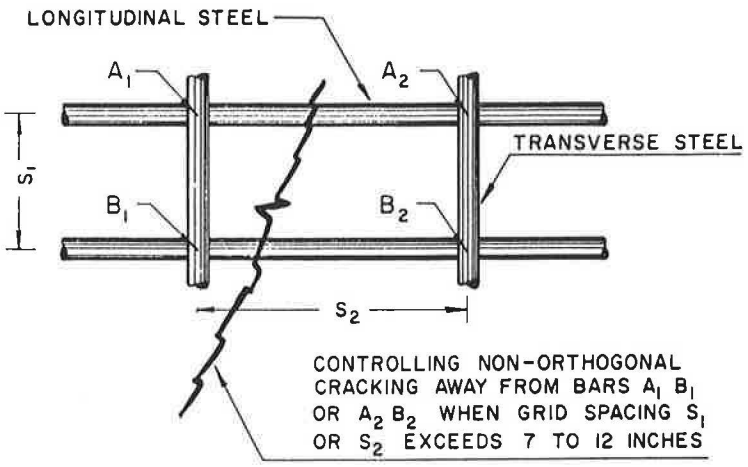

FIGURE 10 Grid unit in two-way-action reinforcement.

similar manner, one may conclude that the scale effect on cracking behavior during two-way action is insignificant, because the cracking grid would be a reflection of the reinforcement grid if the preferred orthogonal narrow cracking widths develop. Therefore, to control cracking in floors with a two-way action, the major parameter to be considered is the reinforcement spacing in two perpendicular directions. Concrete cover has only a minor effect, because it is usually a small constant of value 0.75 in. (19 mm).

For a constant area of steel determined for bending in one direction, that is, for energy absorption per unit slab area, the smaller the spacing of the transverse bars or wires, the smaller should be the diameter of the longitudinal bars. The reason is that less energy has to be absorbed by the individual longitudinal bars. When the magnitude of fracture is determined by the energy imposed per specific volume of reinforcement acting on a finite element of the slab, a proper choice of the reinforcement grid size and bar size can control cracking into preferred orthogonal grids.

This hypothesis is important for serviceability and reasonable overload conditions. In relating orthogonal cracks to yield-line cracks, the failure of a slab ultimately follows the generally accepted rigid-plastic yield-line criteria.

Crack Control Equation

The basic Equation 1 for relating crack width to strain in the reinforcement is

$$\tilde{w} = \alpha a_c^{\beta} \varepsilon_s^{\gamma} \tag{17}$$

where

a_c = crack spacing,
ε_s = unit strain in the reinforcement, and
α, β, γ = constants.

The effect of the tensile strain in the concrete between the cracks is neglected as insignificant.

As a result of the fracture hypothesis, the mathematical model of Equation 17, and the statistical analyses of the data for 90 slabs tested to failure, the following equation for crack control emerged:

$$w = K_{\beta} f_s \left(\frac{d_{b1} s_2}{Q_{i1}}\right)^{1/2} \tag{18}$$

where

w = crack width at concrete face caused by flexural load, in.;
k = fracture coefficient, in.^{2}/lb;
β = ratio of the distance from the neutral axis to the tensile face of the slab to the distance from the neutral axis to the centroid of the reinforcement grid;
f_s = actual average service load stress level, or 40 percent of the design yield strength, ksi;
d_{b1} = diameter of the reinforcement in Direction 1 closest to the concrete outer fibers, in.;
s_2 = spacing of the reinforcement in the perpendicular Direction 2, in.;
A_s = area of steel per foot of width of concrete, in.^{2};
c_1 = clear concrete cover measured from the tensile face of the concrete to the nearest edge of the reinforcing bar in Direction 1, in.; and
Q_{i1} = active steel ratio, given by $A_s/12(d_{b1} + 2c_1)$.

Direction 1 is the direction of the reinforcement closest to the outer concrete fibers; this is the direction for which the crack control check is to be made.

The quantity whose square root is taken is termed the "grid index," and can be transformed as follows:

$$G_I = \frac{d_{b1} s_2}{Q_{i1}} = \frac{s_1 s_2 d_c}{d_{b1}} \frac{8}{\pi} \tag{19}$$

in which s_1 is the spacing of the reinforcement in Direction 1.

For uniformly loaded, restrained, square slabs and plates of two-way action, $k = 2.8 \times 10^{-5}$ in.^{2}/lb. For concentrated loads or reactions, or when the ratio of short span to long span is less than 0.75 but greater than 0.5, $k = 2.1 \times 10^{-5}$ in.^{2}/lb. For a span aspect ratio of less than 0.5, $k = 1.6 \times 10^{-5}$ in.^{2}/lb.

Although β varies in value between 1.20 and 1.35, the intermediate value β = 1.25 was used to simplify the calculations.

Subscripts 1 and 2 generally pertain to the two directions of reinforcement. Detailed values of the fracture coefficients for various boundary conditions are presented in Table 1.

A graphical solution of Equation 18 is shown in Figure 11 for f_y = 60,000 psi (414 MPa) and f_s = 0.4 f_y = 24,000 psi (165.5 MPa) for rapid determination of the reinforcement size and spacing needed for crack control.

Permissible Crack Widths in Concrete Structures

The maximum crack width that a structural element should be permitted to develop depends on the particular function of the element and the environmental conditions to which the structure is liable to be subjected. Table 2 from the ACI Committee 224 report on cracking serves as a reasonable guide on the permissible crack widths in concrete structures under the various environmental conditions that are normally encountered.

The crack control equation and guidelines presented are important not only for the control of corrosion in the reinforcement but also for deflection control. The reduction of the stiffness EI of the two-way slab or plate caused by orthogonal cracking when the limits of permissible crack widths in Table 2 are exceeded, can lead to excessive deflection, both short-term and long-term. Deflection values several times those anticipated in the design, including deflection caused by construction loading, can be reasonably controlled through camber and control of the flexural crack width in the slab or plate. Proper selection of the reinforcement spacings s_1 and s_2 in the perpendicular directions as discussed in this section, and not exceeding 12 in. center to center, can maintain good serviceability performance of a slab system under normal and reasonable overload conditions.

In most cases, the magnitude of crack widths increases in long-term exposure and long-term loading. The increase in crack width can vary considerably in cases of cyclic loading, such as in bridges, but the width increases at a decreasing rate with time. In most cases, a doubling of crack width after several years under sustained loading can be expected.

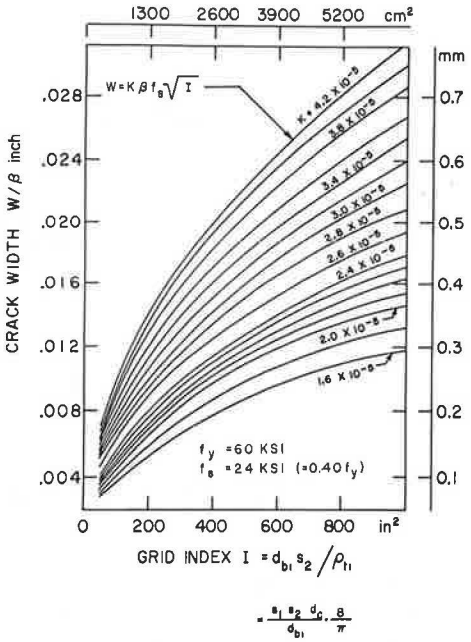

FIGURE 11 Crack control reinforcement distribution in two-way-action slabs and plates for all exposure conditions: f_y = 60,000 psi, f_s = 24,000 psi (= 0.40f_y).

CONCLUSIONS

With the aid of the expressions summarized in the following, the design engineer and the constructor can limit the flexural

TABLE 1 FRACTURE COEFFICIENTS FOR SLABS AND PLATES

Loading type[a]	Slab shape	Boundary condition[b]	Span ratio,[c] S/L	Fracture coefficient 10^{-5} K
A	Square	4 edges r	1.0	2.1
A	Square	4 edges s	1.0	2.1
B	Rectangular	4 edges r	0.5	1.6
B	Rectangular	4 edges r	0.7	2.2
B	Rectangular	3 edges r, 1 edge h	0.7	2.3
B	Rectangular	2 edges r, 2 edges r	0.7	2.7
B	Square	4 edges r	1.0	2.8
B	Square	3 edges r, 1 edge h	1.0	2.9
B	Square	2 edges r, 2 edges h	1.0	4.2

[a]Loading type: A, concentrated; B, uniformly distributed.

[b]Boundary condition: r, restrained; s, simply supported; h, hinges.

[c]Span ratio: S, clear short span; L, clear long span.

TABLE 2 MAXIMUM PERMISSIBLE FLEXURAL CRACK WIDTHS

Exposure condition	Crack width in.	Crack width mm.
Dry air or protective membrane	0.016	0.41
Humidity, moist air, soil	0.012	0.30
De-icing chemicals	0.007	0.18
Seawater and seawater spray; wetting and drying	0.006	0.15
Water-retaining structures (excluding nonpressure pipes)	0.004	0.10

macrocrack width that develops in concrete systems. By limiting the width to within the permissible levels presented in Table 2 in accordance with the prevailing environmental conditions, it would be possible to prevent or considerably minimize long-term corrosion deterioration and also maintain the aesthetic behavior of the various elements of the system.

1. Reinforced-Concrete Beams and Thick One-Way Slabs

$$w_{max} = 0.076\beta f_s (d_c A)^{1/3} \times 10^{-3}$$

or

$$z = f_s (d_c A)^{1/3}$$

where f_s is in ksi and z is not to exceed a value of 145 kip/in. for exterior exposure or 175 kip/in. for interior exposure.

2. Prestressed, Pretensioned Beams
   a. Steel reinforcement level

$$w_{max} = (5.85 \times 10^{-5}) \frac{A_t}{\Sigma o} (\Delta f_s)$$

   b. Tensile face of concrete

$$w'_{max} = (5.85 \times 10^{-5}) R_i \frac{A_t}{\Sigma o} (\Delta f_s)$$

3. Prestressed Post-Tensioned Beams
   a. Steel reinforcement level

$$w_{max} = (6.51 \times 10^{-5}) \frac{A_t}{\Sigma o} (\Delta f_s)$$

   b. Tensile face of concrete

$$w_{max} = (6.51 \times 10^{-5}) R_i \frac{A_t}{\Sigma_o} (\Delta f_s)$$

For nonbonded beams, the factor 6.51 becomes 6.83.

4. Two-way Action Structural Slabs and Plates

$$w_{max} = K\beta f_s (G_1)^{1/2}$$

where

$$G_1 = \frac{s_1 s_2 d_c}{d_{b1}} \frac{8}{\pi}$$

Values of coefficient K are presented in Table 3.

Some useful metric unit equivalents are presented below:

Customary Unit	*Metric Unit*
1 in.	25.4 mm
1 ft	0.305 m
1 in.^{2}	645.16 mm^2
1 in.^{3}	16 387.06 mm^3
1 in.^{4}	416.231 mm^4
1 psi	6.895 Pa
1 ksi	6.895 MPa
1 lb	4.448 N
1 kip	4448 N
1 lb/ft	14.594 N/m
1 kip/ft	14.594 kN/m
1 kip-in	113 N-m
1 $\sqrt{f'_c}$ psi	0.083036 $\sqrt{f'_c}$ MPa

TABLE 3 K VALUES FOR FULLY RESTRAINED SLABS AND PLATES

Slab/Plate Conditions[a]	K
Uniformly loaded, square	2.8×10^{-5}
At concentrated loads and columns	2.1×10^{-5}
$0.5 < l_s/l_l < 0.75$	2.1×10^{-5}
$l_s/l_l < 0.5$	0.6×10^{-5}

[a]For simply supported slabs multiply these values by 1.6. Interpolate K values for intermediate span ratios l_s/l_l or for partial restraints at the boundaries such as cases of end and corner panels of multipanel floor systems. l_s and l_l are the short and long spans of the two-way slab or plate, respectively.

REFERENCES

1. *Building Code Requirements for Reinforced Concrete* (ACI 318-89) and *Commentary* (ACI 318R-89). American Concrete Institute, Detroit, Mich., 1989, 389 pp.
2. E. G. Nawy. *Reinforced Concrete—A Fundamental Approach*, 2nd ed. Prentice-Hall, Englewood Cliffs, N.J., 1990, 738 pp.
3. ACI Committee 224. Control of Cracking in Concrete Strucures. *ACI Journal Proceedings*, Vol. 20, No. 10, Oct. 1980, pp. 35–76.
4. P. Gergely, and L. A. Lutz. Maximum Crack Width in Reinforced Concrete Flexural Members. *Causes, Mechanism, and Control of Cracking in Concrete*, SP-20, American Concrete Institute, Detroit, Mich., 1968, pp. 87–117.
5. E. G. Nawy and K. W. Blair. Further Studies on Flexural Crack Control in Structural Slab Systems. In *Cracking, Deflection, and Ultimate Load of Concrete Slab Systems*, SP-30, American Concrete Institute, Detroit, Mich., 1971, pp. 1–41.

6. E. G. Nawy. Crack Control Through Reinforcement Distribution in Two-Way Acting Slabs and Plates. *ACI Journal Proceedings*, Vol. 69, No. 4, April 1972, pp. 217–219.
7. E. G. Nawy. Crack Control in Beams Reinforced with Bundled Bars. *ACI Journal Proceedings*, Oct. 1972, pp. 637–639.
8. A. E. Naaman and A. Siriaksorn. Serviceability Based Design of Partially Prestressed Beams, Part I—Analysis. *PCI Journal*, Vol. 24, No. 2, March–April 1979, pp. 64–89.
9. CEB-FIP. *Model Code for Concrete Structures*. Paris, 1978, pp. 1–347.
10. S. W. Meier and P. Gergely. Flexural Crack Width in Prestressed Concrete Beams. Technical Note, *ASCE Journal*, ST2, Feb. 1981, pp. 429–433.
11. E. G. Nawy. Flexural Cracking Behavior of Partially Prestressed Pretentioned and Post-Tensioned Beams—State-of-the-Art. In *Cracking in Prestressed Concrete Structures*, American Concrete Institute, Detroit, Mich., 1990, pp. 1–42.
12. E. G. Nawy. *Prestressed Concrete—A Fundamental Approach*. Prentice-Hall, Englewood Cliffs, N.J., 1989, 739 p.

Publication of this paper sponsored by Committee on Mechanical Properties of Concrete.

Latex Modification Effects on the Mechanisms of Microcrack Propagation in Concrete Materials

PARVIZ SOROUSHIAN AND ATEF TLILI

Improvements in the matrix microstructure associated with latex modification of plain and steel-fiber-reinforced concrete materials are assessed. In particular, this study investigates the effects of latex modification of concrete matrix on the microcracking and failure mechanisms. In order to study the process of failure in concrete under increasing stress levels, microscopic investigations were performed on concrete cylinders preloaded to different compressive stress levels. The effects of latex modification of concrete matrix on the microcracking and failure mechanisms were also investigated. Five stress levels were selected. At each stress level, two thin slices, one longitudinal and the other transverse, were prepared and investigated for microcracking characteristics after special surface preparation. Through the use of an image analysis system, three different types of measurements were made: aggregate-interface (bond) crack length per unit area; matrix crack length per unit area; and microcrack orientation defined as the average crack inclinations with respect to the direction of loading. In plain concrete, microcracks were found to be present even before loading, because of factors such as differential shrinkage movements, settlements, and thermal strains between aggregates and cement paste. They appeared dominantly at the coarse aggregate-cement paste interfaces. At higher compressive stress levels, the propagation of microcracks extended from interfaces into the matrix. At peak compressive stress, microcracks had a tendency to interconnect and localize. Latex modification of concrete reduced the microcrack intensities at lower stress levels; this was particularly true for the aggregate-cement paste interface microcracks. Measurements on microcrack orientation revealed that the matrix microcracks were generally oriented less than 20 degrees from the longitudinal axis of the specimen (i.e., the direction of loading). At the aggregate-cement interface, the microcrack orientation was random.

Concrete materials suffer from microcracking at cement-aggregate interfaces, along fiber-matrix interfaces, or around the entrapped air voids, even before loading. Under increased loading, microcracks tend to grow and interconnect to form microcrack channels or get arrested by matrix constituents such as aggregates, steel fibers, and air voids.

Latex polymers in plain and steel-fiber-reinforced concrete (SFRC) reduce the microcracking damage under external loading because of their pore filling and superior interface zone bonding.

BACKGROUND

Under external loading, microcracks occur (or start to grow) at the cement-aggregate interfaces, around the entrapped air voids, or along the fiber-matrix interfaces. With increased loading, some microcracks grow and connect with each other to form large macrocracks, while some others are arrested by aggregates, air voids, or fibers. The propagation of microcracks leads to increased nonlinearity of the material before the peak load is reached.

For air-dried mortar and concrete, shrinkage-induced bond cracks around large aggregate particles appear before any loading (*1*) (see Figure 1). Under load, debonding and multiple cracking around sand grains and air voids are observed frequently (*1*), and this phenomenon seems to be more pronounced between adjacent sand grains than around isolated ones. In normal-weight concrete, the crack changes orientation when it encounters an aggregate by passing around it instead of crossing it (see Figure 2) (*1*). In concrete, the crack

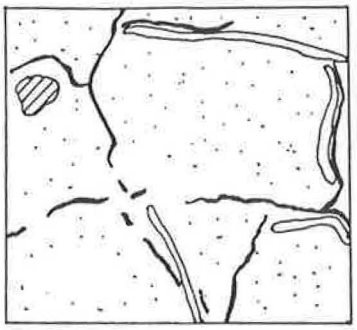

FIGURE 1 Bond crack before loading in air-dried mortar.

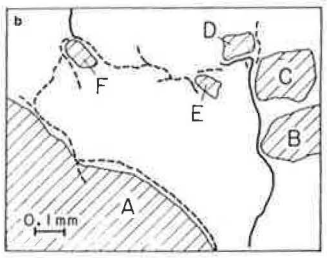

FIGURE 2 Shifting of crack direction after encountering aggregates (*1*).

Department of Civil and Environmental Engineering, Michigan State University, East Lansing, Mich. 48824.

pattern is more tortuous than in mortar (Figure 3) because concrete cracks must propagate around the densely spaced aggregate pieces as well as sand grains. The reorientation, branching, and multiple cracking associated with the interaction of microcracks with the encountered aggregate particles lead to the dissipation of a large amount of energy, which is beneficial to the material behavior under load.

When fibers are present in the matrix, the growth and interconnection of microcracks become a more energy-absorptive process and thus fibers enhance the prepeak behavior and the ultimate tensile strength of fiber-reinforced concrete.

Once a microcrack intersects a fiber at an angle, it generally interacts with the fiber in a manner that makes further propagation more energy absorptive (see Figure 4). The microcrack can advance beyond a steel fiber along its original path as shown in Figure 5a (20 percent of the time), by shifting as shown in Figure 5b (30 percent of the time), or by branching into multiple postfiber cracks as shown in Figure 5c (50 percent of the time). The microcrack encountering a fiber stays continuous, making the lateral shifts around the fibers, as can be clearly seen in the picture of the groove under a steel fiber that intersected microcracks in Figure 6.

Microcrack propagation at the fiber-matrix interface might take place at the interface itself, leading to the separation of matrix from the fiber by debonding (Figure 7a), or it might occur at a small distance (~20 μm) from the fiber and parallel to it by pseudodebonding (Figure 7b) that separates the body of the matrix from a thin layer of interface that remains attached to the fiber.

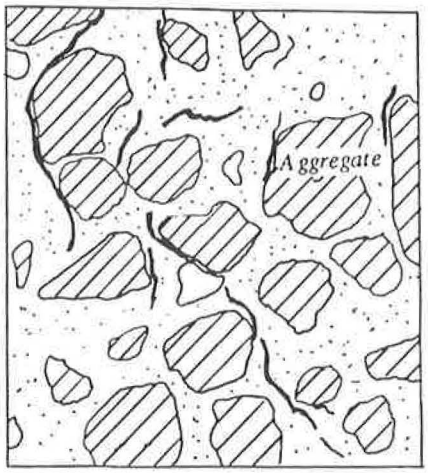

FIGURE 3 Tortuosity of cracking.

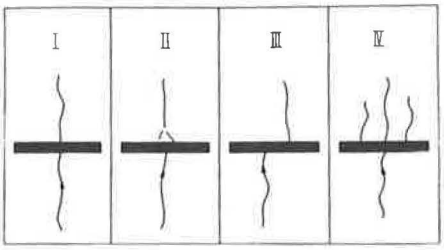

FIGURE 4 Cracking patterns observed at the intersection of a propagating crack and a fiber normal to its path (*1*).

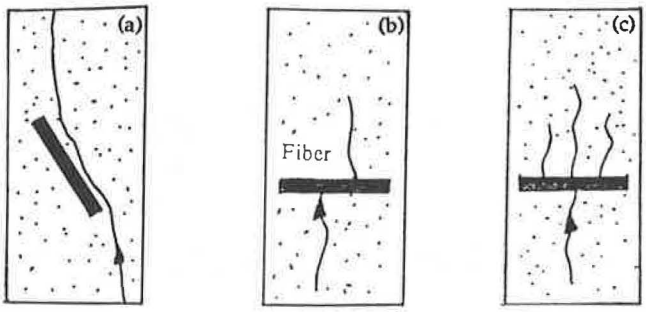

FIGURE 5 Illustrations of crack types (a) parallel running, (b) shifting, and (c) branching.

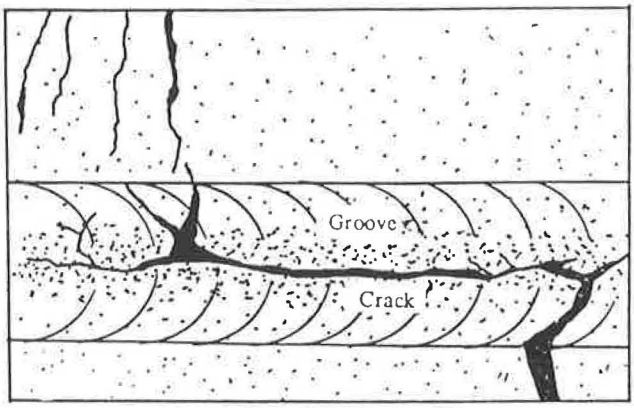

FIGURE 6 Continuous nature of shifted microcracks around a steel fiber.

With their microcrack-arresting action, fibers tend to increase the fracture energy and consequently the tensile strength of concrete. Fiber pull-out or rupture tends to dominate the postcracking progress of failure in SFRC under direct tension.

EXPERIMENTAL PROGRAM

For each one of the mixes presented in Table 1, 15 specimens were cast. The specimens were 75 mm (3 in.) in diameter and 150 mm (6 in.) long. They were moist-cured for 48 hr inside their molds while being covered with a wet burlap and a plastic sheet, and then air-cured until the test age of 28 days. Three specimens out of each group of 15 were tested under compression until failure, with stresses and strains monitored throughout the test. On the basis of the average compressive strength (f'_c) obtained from these three tests for each mix, five stress levels were selected and two specimens of the same mix were loaded to each predetermined stress level and then unloaded. The five stress levels considered in this study were 0.00 f'_c, 0.30 f'_c (prepeak), 0.80 f'_c (prepeak), 1.00 f'_c (peak), and 0.90 f'_c (postpeak).

After each specimen was covered with a thin layer of epoxy, the specimen was encased (i.e., circumscribed) in a fibrous mortar mount 100 mm (4 in.) in diameter. This mount was

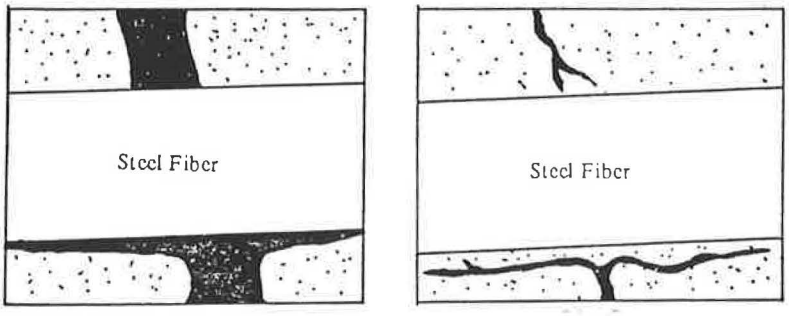

FIGURE 7 Microcrack propagation at the steel fiber–cement interface, (a) debonding, and (b) pseudo-debonding.

necessary to maintain the integrity of specimens (especially those loaded to large strains) during handling and slicing for microstructural investigations. The specimens were then sectioned, one transversely and one longitudinally, to slices 13 mm (0.5 in.) thick that were cut from the center of the specimen using a diamond saw (see Figure 8).

The slices were then washed in a jet of water and allowed to dry in the laboratory for 24 hr. They were then stained with black indian ink, grouped with silicon carbide on rotating laps over a sequence of five grit sizes: #180, #240, #320, #400, and #600. These specimen preparation steps help distinguish the microcracks under the microscope. Figure 9 shows a view of the longitudinal and transverse slices after being prepared for microstructural studies.

The slices were examined for microcracking characteristics using an image analysis system of typical magnification 25×. The cracks at the prepared faces of the slices were visible as black lines. The microstructural studies were conducted after dividing the surface area of the slice to be viewed under the microscope into about thirty 13- × 13-mm (0.5- by 0.5-in.) squares, each to be viewed as a separate field of measurement (see Figure 9).

Once subdivided, the slices were viewed through a microscope connected to the image analysis system. For each field of view on the microscope (which covers a 4- × 3-mm area within each 13- × 13-mm square of the mesh), the following three measurements were performed:

1. The intensity of bond cracks at aggregate- and fiber-cement interfaces (as shown in Figure 10) with intensity defined as the total crack length per unit area;
2. The intensity of matrix cracks (both aggregate interface and matrix cracks are shown in Figure 11); and
3. Microcrack orientations defined as the average inclination of cracks with respect to the direction of loading (performed on the longitudinal slices only).

Measurements on microcrack intensity reveal information on the process of failure in concrete materials under increasing stress levels, as influenced by the presence of steel fibers and latex polymers. Inclinations of microcracks provide indications of the nature of failure mechanism under compression.

EXPERIMENTAL RESULTS

Results of microstructural studies on the process of microcrack propagation and failure under compressive stresses in plain, latex-modified concrete (LMC) and latex-modified steel-

TABLE 1 SELECTED-MIX PROPORTIONS FOR EXPERIMENTAL WORK FOR SAND-CEMENT AND GRAVEL-CEMENT RATIOS OF 2.5 AND 1.5, BY WEIGHT, RESPECTIVELY

V_f (%)	Styrene Butadiene L/c (%)	w/c	Slump mm. (in.)	VB Time (sec.)	Air Content (%)
0	0	0.43	152 (6.0)	-----	5.5
0	10	0.32	190 (7.5)	-----	4.5
0.75	0	0.45	127 (5.0)	6.5	6.5
0.75	10	0.34	152 (6.0)	5.0	5.0

--- = no measurement taken
V_f = fiber volume fraction;
L/c= latex-cement ratio, by solids weight;
w/c= water-cement ratio, by weight;
s/c=2.5=sand-cement ratio, by weight; and
st./c=1.5=stone-cement ratio, by weight.

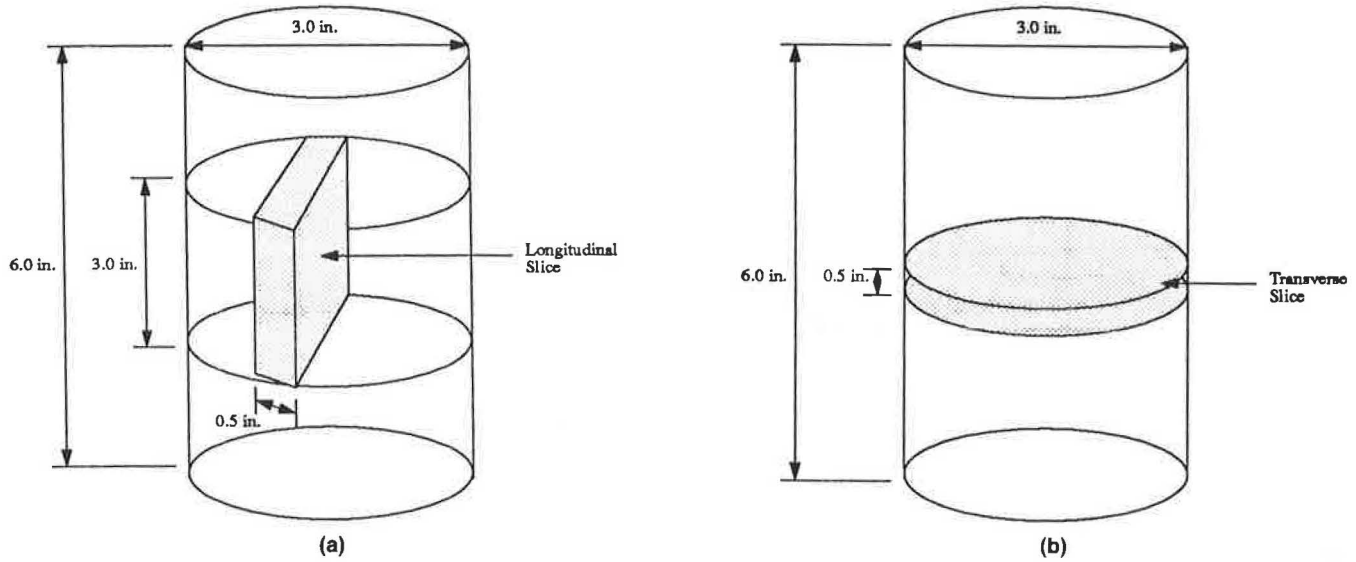

FIGURE 8 Locations of transverse and longitudinal slices, (a) longitudinal slice, and (b) transverse slice.

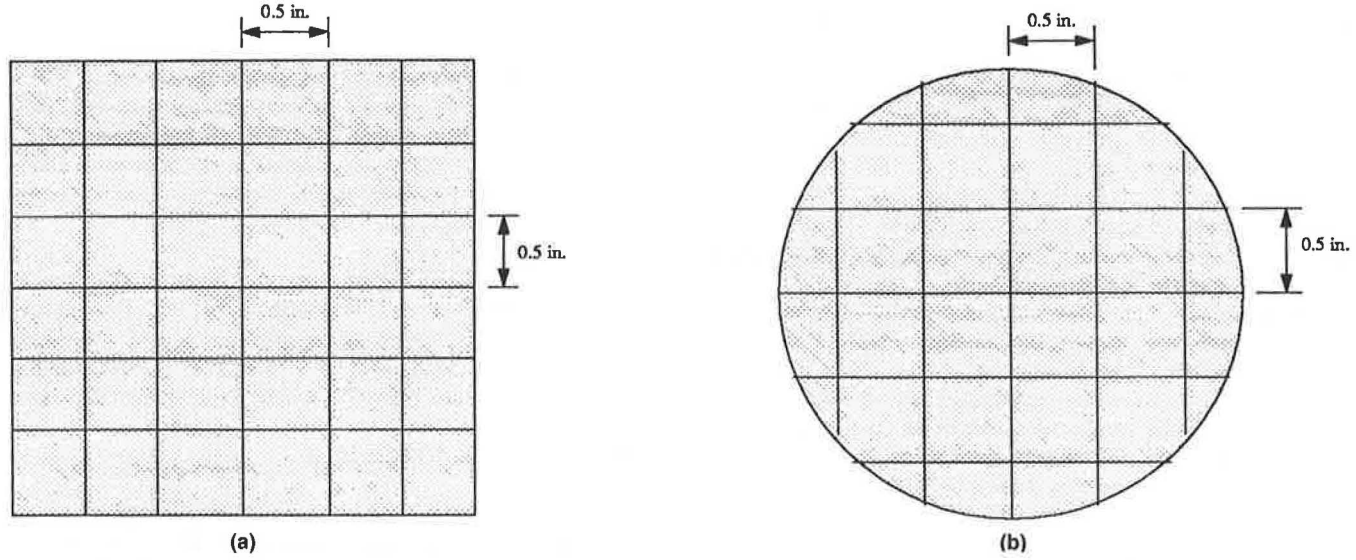

FIGURE 9 Slices ready to be viewed under the microscope, (a) longitudinal slice, and (b) transverse slice.

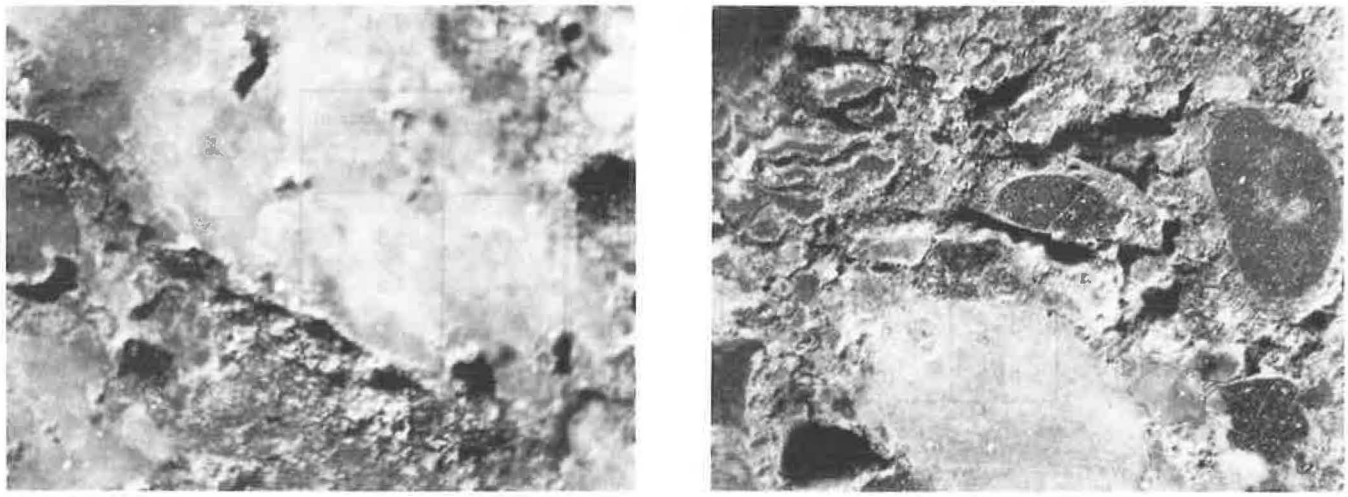

FIGURE 10 Bond cracks at (a) aggregate-cement and (b) fiber-cement interfaces.

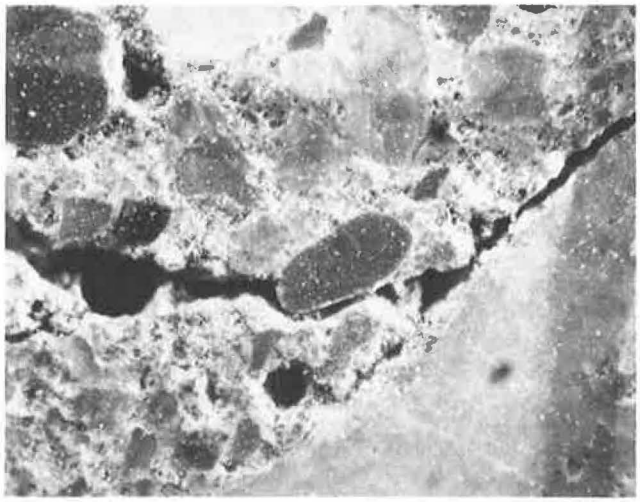

FIGURE 11 Typical matrix microcracks.

fiber-reinforced concrete (LMSFRC) materials are discussed in this section. Conclusions regarding the latex modification and fiber reinforcement effects on the failure mechanism of concrete materials are also presented.

Results of crack intensity (i.e., crack length per unit area of cross section) measurements at different compressive stress levels on plain concrete specimens for transverse and longitudinal sections are shown in Figures 12a and 12b, respectively. The crack intensity at the transverse section is more representative of the actual conditions than that obtained at the longitudinal section. This distinction results from the fact that microcracks tend to propagate in vertical planes. Hence, although a transverse section cuts many of these cracks, the longitudinal section occurs along or in between the approximately vertical crack planes and thus does not present a typical crack intensity.

Microcracks are observed in Figure 12 to be present even before loading (at 0 percent stress level). These microcracks are caused by the differential shrinkage movements, settlements, and thermal strains between aggregates and cement paste, and also by the bleeding effects. They appear dominantly at the interfaces between coarse aggregate and cement paste interfaces (see Figure 12). Similar observations using identical techniques have been made by Shah (*2*). The propagation of these microcracks under compression (which starts to take place mainly at the interfaces and then extends into the matrix as previously shown in Figure 11) is shown quantitatively in Figure 12. At the peak compressive stress, microcracks have a tendency to interconnect and localize, leading to the formation of macrocracks with increasing widths. The process of microcrack propagation takes place at an increasing rate in the postpeak region where microcracks tend to be unstable. Similar observations using identical techniques have been made previously by Shah and Sankar (*2*).

The microcrack intensity in LMC under increasing compressive stresses is shown in Figure 13. Comparison of Figures 12a and 13a, for the more representative transverse sections, indicates that the microcrack intensities tend to be reduced at lower stress levels with latex modification. In particular, microcracks occurring at aggregate-paste interfaces tend to

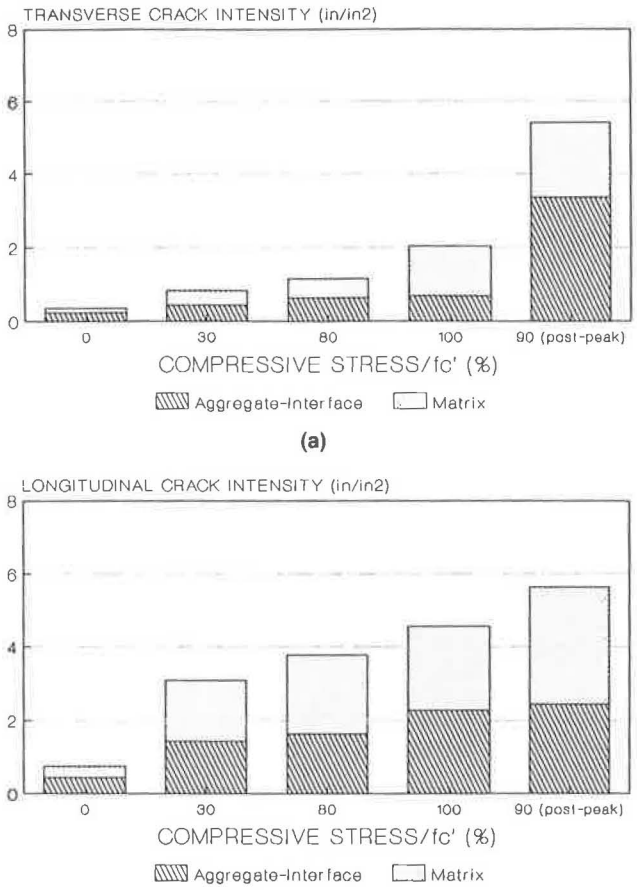

FIGURE 12 Microcrack intensities at different compressive stress levels in plain concrete for (a) transverse section, and (b) longitudinal section.

be reduced substantially in the presence of latex polymers, confirming previous findings (*3*) that latex modification provides improved bonding between the cementitious paste and aggregates. Reduced microcrack intensity in the presence of latex polymers may result from the restraint of microcrack propagation by polymer films bridging across these cracks. In the postpeak region, where the interconnection and localization of microcracks lead to the formation of macrocracks with increasing widths, the failure mechanism in LMC was comparable to that in plain concrete.

The microcrack intensities at different stress levels for SFRC are shown in Figure 14. The appearance of fiber-interface microcracks (see Figure 15), which could be initiated by the same phenomena causing aggregate-interface microcracks, is the new phenomenon that seems to have an unexpected dominant effect in deciding the failure mechanism of SFRC. The formation of fiber-interface microcracks and their relatively rapid propagation (see Figure 16) under increasing compressive stresses in the prepeak region seems to reduce the effectiveness of steel fibers in arresting the propagation of microcracks. In the postpeak region, however, the crack system seems to be more stable in SFRC (Figure 14a) than in plain concrete (Figure 12a) and in LMC (Figure 13a).

Latex modification of SFRC, as shown in Figure 17, seems to stabilize the fiber-interface microcracks under increasing

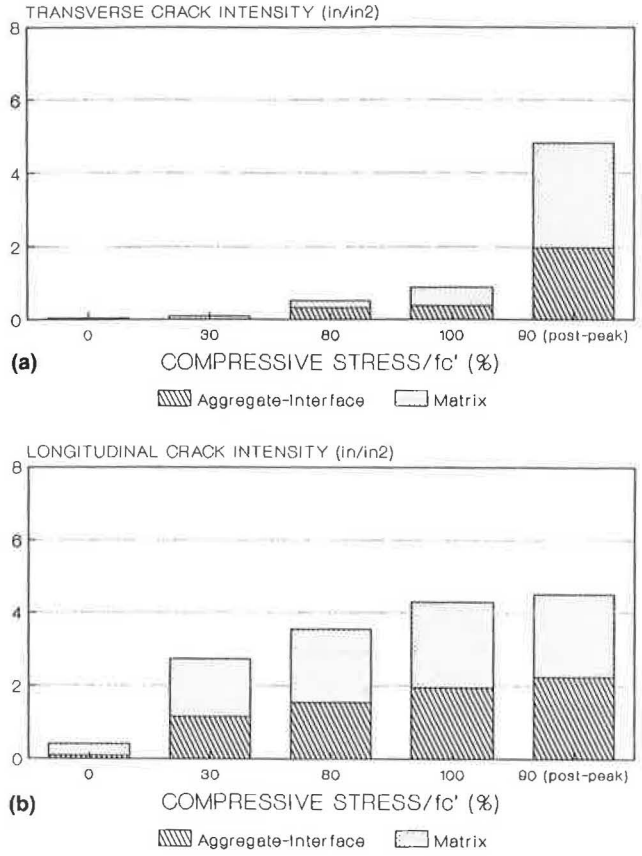

FIGURE 13 Microcrack intensities at different compressive stress levels in LMC, (a) transverse section, and (b) longitudinal section.

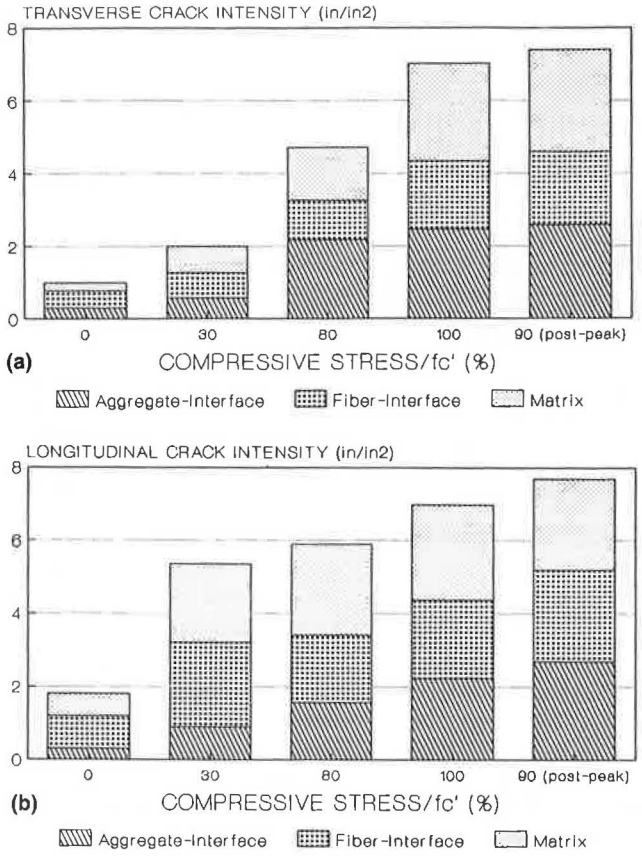

FIGURE 14 Microcrack intensities at different compressive stress levels in SFRC for (a) transverse section, and (b) longitudinal section.

compressive stresses. The aggregate-interface microcracks were also partly controlled by the presence of latex polymers in SFRC. Figure 10 shows these points by showing better fiber- and aggregate-interface bonds even at high compressive stress levels.

The matrix microcrack orientations at the longitudinal sections were generally less than 20 degrees from the longitudinal axis of the specimen (i.e., the loading direction). The microcrack orientation at the aggregate- and fiber-matrix interfaces seemed to be random.

SUMMARY AND CONCLUSIONS

The effects of latex modification and steel reinforcement on the microcracking process of failure mechanism in concrete materials subjected to compression loads were studied. For this purpose, concrete specimens were subjected to different levels of compressive stress in the prepeak and postpeak regions, and were then unloaded. Image analysis techniques were used to quantify microcrack intensities within the paste and at the aggregate- and fiber-matrix interfaces at different load levels. The results indicated that

1. Microcracks are present in concrete materials, dominantly at the coarse aggregate-matrix and fiber-matrix interfaces, even before any loading. These microcracks may be caused by differential shrinkage and thermal movements between cementitious matrices and mix inclusions (i.e., aggregates and fibers);

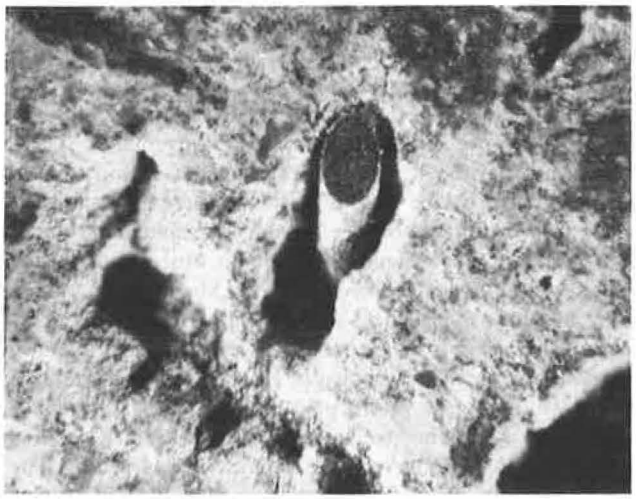

FIGURE 15 Typical fiber interface microcracks.

2. In plain concrete, microcracks tend to originate mainly at the interfaces between coarse aggregate and cement paste,

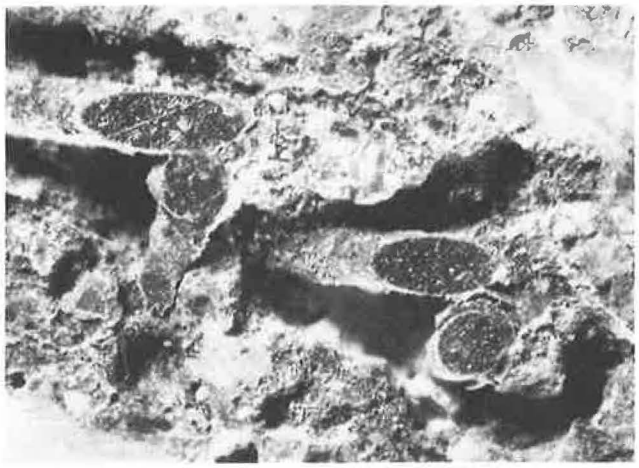

FIGURE 16 Microcracking caused by rapid fiber-interface microcrack propagation.

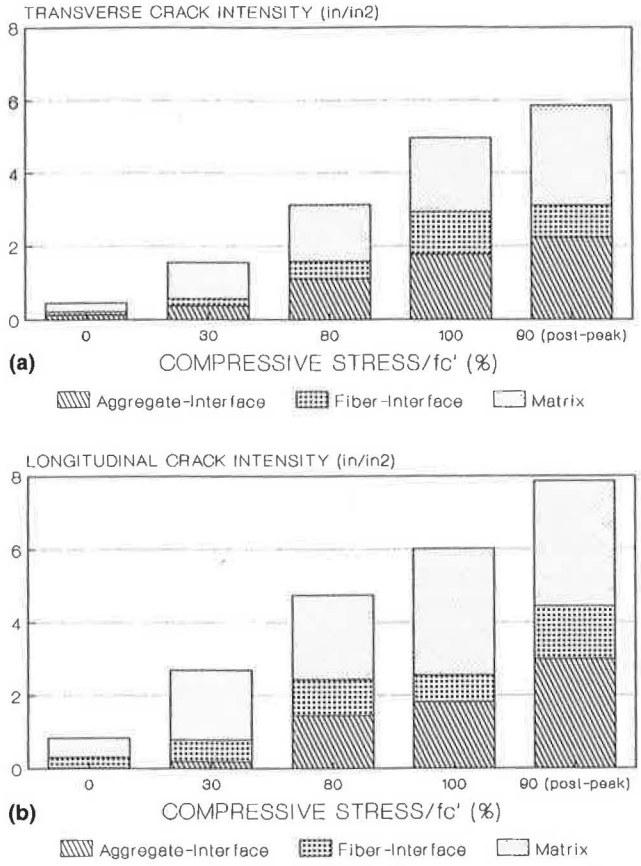

FIGURE 17 Microcrack intensities at different compressive stress levels in LMSFRC for (a) transverse section and (b) longitudinal section.

and then extend into the matrix at higher compression levels; near the peak load, microcracks tend to interconnect and localize, forming macrocracks with increasing widths; there is a rather sudden growth in microcrack intensity beyond the peak compression load;

3. In LMC, the microcrack intensities, especially at aggregate-paste interfaces, tend to be reduced, indicating improvements in bonding between the cementitious paste and aggregates as a result of latex modification; beyond the peak load, however, the sudden increase in microcrack intensity still takes place in spite of latex modification;

4. In unmodified SERC, the fiber-matrix interface microcracks seem to play a dominant role in deciding the failure mechanism of the concrete matrix because of their relatively rapid propagation under increasing compressive stress levels; steel fibers, however, control microcrack propagation in the post-peak region; and

5. Latex modification of SFRC seems to stabilize the fiber-matrix interface microcracks as well as the aggregate-matrix interface microcracks leading to a more stable microcrack system within SFRC materials.

ACKNOWLEDGMENTS

Financial support for the performance of this research was provided by BASF Canada, Inc., and the Research Excellence Fund of the State of Michigan. These contributions are gratefully acknowledged. The authors are also thankful to Kar Lok of BASF Canada, Inc., and Lawrence T. Drzal of the Composite Materials and Structures Center, Michigan State University, for their encouragement and technical support.

REFERENCES

1. S. P. Shah. *Application of Fracture Mechanics to Cementitious Composites.* Advanced Science Institute Series E, Martinus Nijhoff Publishers, Boston, Mass., 1985.
2. S. P. Shah and R. Sankar. Internal Cracking and Strain-Softening Response of Concrete Under Uniaxial Compression. *ACI Materials Journal*, American Concrete Institute, Detroit, Mich., May–June, 1987, pp. 200–212.
3. J. E. Isenberg, D. E. Rapp, E. J. Sutton, and J. W. Vanderhoff. *Microstructure and Strength of the Bond Between Concrete and Styrene-Butadiene Latex-Modified Mortar.* In *Highway Research Record 370*, TRB, National Research Council, Washington, D.C., 1971, pp. 75–89.

Publication of this paper sponsored by Committee on Mechanical Properties of Concrete.

Use of High-Volume Class F Fly Ash for Structural-Grade Concrete

TARUN R. NAIK, VASANTHY SIVASUNDARAM, AND SHIW S. SINGH

Performance of structural-grade concrete incorporating high volumes of low-calcium fly ash was investigated. Two different ASTM Class F fly ashes were used. A portland cement concrete designed to have 28-day compressive strength of 6,000 psi (41 MPa) was used as a control concrete. Concrete mixes were also designed to have fly ash substitution based on total cement weight in the range of 0 to 60 percent by weight. The water-cement ratio was maintained approximately constant and the desired workability was achieved by using a superplasticizer. Concrete was tested for compressive strength, splitting tensile strength, and modulus of elasticity in accordance with ASTM test methods. Compressive strength and splitting tensile strength of concrete were determined at ages 1, 7, and 28 days, whereas modulus of elasticity was determined at 7 and 28 days. High replacement of cement by fly ash in concrete caused reduction in compressive strength, splitting tensile strength, and modulus of elasticity within the experimental range. Compressive strength of fly ash concrete was slightly lower than the reference concrete up to fly ash addition of 60 percent. However, fly ash concretes achieved adequate strengths appropriate for structural application even at the 60 percent cement replacements.

Large amounts of fly ash have been used in mass concretes for a long time, for reducing cost and controlling temperature increase in order to reduce cracking at early ages (*1–7*). Most current uses of low-calcium fly ash are in construction of pavements. Because paving concrete contains a low water-cement ratio, workability of the concrete is considerably reduced, resulting in its possible unsuitability for structural applications. In order to improve workability for mixtures with a low water-cement ratio for structural applications, either plasticizers, water-reducing admixtures, or superplasticizers are used. Recently, researchers (*8,9*) have found that superplasticized high-volume fly ash concrete can be proportioned to have high early strength of 1,500 to 3,000 psi (10 to 20 MPa) at 3 days, and high 28-day strength of 5,000 to 8,700 psi (35 to 60 MPa), suitable for structural-grade concrete.

In the United States, most studies have been primarily concerned with use of high-volume fly ash in the construction of highway base courses and dams. However, no work has been done regarding the use of high-volume fly ash in manufacture of high-strength structural-grade concretes. This research was primarily undertaken to further developing technologies for large-scale use of Class F fly ash in production of structural-grade concrete.

Addition of low-alkali Class F fly ash in concrete generally increases durability of concrete subjected to alkali-silica reaction by reducing reactive alkali content of concrete mixes. Additionally, use of fly ash in concrete reduces its permeability, which in turn diminishes alkali aggregate reactions that can occur because of water penetration in the structures (*1*).

A number of studies have been conducted to develop Class F fly ash mortars and concretes for structural applications (*10–17*). Swamy et al. (*10*) reported that concrete mixes containing 30 percent by weight of fly ash (ASTM Class F) could be proportioned to have adequate workability and early 1-day strength and elastic modulus for structural applications. The dosage of admixtures or superplasticizers was adjusted to obtain cohesiveness and workability with slumps in excess of 4 in. (100 mm) for easy placeability in structural members with steel reinforcement. Swamy and Mahmud (*11*) developed data on mix proportions, strength, and modulus of elasticity for structural-grade concrete made with 50 percent low-calcium fly ash (ASTM Class F), and a superplasticizer. Their results indicated that for concretes with a low water-cement ratio of 0.32 to 0.42, high early strength of 1,800 to 3,000 psi (12 to 20 MPa) in 1 day, and 28-day strengths of 6,500 to 8,700 psi (45 to 60 MPa), could be produced with slump in excess of 150 mm (6 in.). Under a moist curing condition, fly ash concretes had about 50 to 100 percent higher strength at age 1 year compared with their strengths at 28-day age.

Recently, extensive research work has been conducted at CANMET concerning use of high-volume ASTM Class F fly ash in structural-grade concretes (*13–16*).

Mukerjee et al. (*13*) incorporated high volumes of fly ash in concrete with the aid of three different superplasticizers. They reported that satisfactory high-strength concrete can be achieved using large quantities of ASTM Class F fly ash. In that study, the mechanical properties of concrete containing 37 percent low-calcium fly ash were found to be superior to the properties of the reference concrete.

Malhotra and Painter (*14*) reported an optimum fly ash content in the range of 50 to 60 percent of cement replacement for structural-grade concrete with respect to compressive strength. Giaccio and Malhotra (*8*) determined properties of superplasticized concrete containing high-volume of Class F fly ash made with ASTM Type I and III cement. The properties determined were (a) compressive strength, (b) flexural strength, (c) splitting tensile strength, and (d) freezing and thawing resistance. On the basis of data obtained, the authors concluded that concrete containing high volumes of Class F fly ash possessed excellent mechanical properties for use in structural concrete elements, especially for massive sections.

Sivasundaram et al. (*9*) proportioned a number of concrete mixtures incorporating high volumes of low-calcium fly ash, superplasticizer, and air-entraining admixture. A block with dimensions of 5 × 5 × 5 ft (1.52 × 1.52 × 1.52 m) was manufactured to evaluate temperature increase caused by hy-

T. R. Naik and S. S. Singh, College of Engineering and Applied Science, University of Wisconsin—Milwaukee, P.O. Box 784, Milwaukee, Wis. 53211. V. Sivasundaram, Department of Energy, Mines, and Resources, CANMET, Ottawa, Canada.

dration of cementitious materials. The superplasticized high-volume fly ash concrete had its best performance at a water-cement ratio of about 0.32. The concrete produced had high compressive strength at both early and later ages, a high modulus of elasticity, and a reduced heat of hydration. In order to evaluate field performance of this concrete, a concrete block measuring 29 × 24 × 9 ft (8.84 × 7.32 × 2.74 m) was also cast under controlled temperature conditions. Neither the small block cast under laboratory condition nor the large block developed any observable thermal cracks, and their compressive strength and modulus of elasticity values were comparable to those obtained for laboratory specimens. In another study, Sivasundaram et al. (*15*) found that long-term performance of high-volume fly ash concrete was excellent with respect to compressive strength, modulus of elasticity, diffusion of chloride ions in concrete. etc.

Langley et al. (*16*) reported that maximum fly ash percentage might range between 55 and 60 percent of total cement content to produce structural-grade concrete. Their test results revealed that strength properties, modulus of elasticity, drying shrinkage, creep, and freeze-thaw durability of concrete with low cement and high fly ash content compared favorably to normal portland cement concrete.

Taniguchi et al. (*17*) evaluated performance of high-volume fly ash concrete for use in construction of marine structures. They reported that strength characteristics of high-volume fly ash concrete depended strongly on types and dosages of chemical activators and curing conditions. Their study of high-volume fly ash concrete with sodium chloride (NaCl) as a chemical activator indicated high initial strength and good increase in strength with age. (Of course, use of NaCl as an accelerator can cause accelerated rebar corrosion.) In addition, high-volume fly ash concrete exhibited good resistance against sea water with respect to strength characteristics and volume changes.

EXPERIMENTAL PROGRAM

A portland cement concrete was proportioned to produce the 28-day strength of 6,000 psi (41 MPa). In addition, concrete mixes were also proportioned to incorporate fly ash at various percentages of cement replacements ranging between 40 and 60 percent. Experiments were designed to evaluate performance of fly ash concretes with respect to compressive strength, splitting tensile strength, and secant modulus of elasticity.

MATERIALS

Portland cement (ASTM Type I) obtained from one source was used in this investigation.

Low-calcium fly ashes, ASTM Type F, were obtained from Oak Creek Power Plant (OCPP) in Oak Creek, Wisconsin, and Valley Power Plant (VPP) in Milwaukee, Wisconsin. These plants use Western bituminous coal obtained from Pennsylvania Mining District 2.

Chemical composition and physical properties of the fly ashes were determined using appropriate ASTM test methods. Chemical composition and physical properties data are presented in Table 1 for OCPP fly ash and in Table 2 for VPP fly ash.

TABLE 1 CHEMICAL AND PHYSICAL TEST DATA FOR THE OCPP CLASS F FLY ASH

Chemical Composition	Average, percent	ASTM-C-618
Silicon Oxide, SiO_2	49.6	-
Aluminum Oxide, Al_2O_3	24.0	-
Iron Oxide, Fe_2O_3	14.4	-
Total, SiO_2+Al_2O_3+Fe_2O_3	88.0	70.0 Min.
Sulfur Trioxide, SO_3	0.88	5.0 Max.
Calcium Oxide, CaO	3.23	-
Magnesium Oxide, MgO	0.98	5.0 Max.
Potassium Oxide, K_2O	2.46	-
Moisture Content	0.11	3.0 Max.
Loss on Ignition	3.5	6.0 Max.

Physical Tests		ASTM C-618
Fineness, % Retained on #325 Sieve	25.7	34 Max.
Pozzolanic Activity Index with Portland Cement, 28 days, % with lime, 7 days, psi	93 1110	75 Min. 800 Min.
Water Requirement, % of Control	103	105 Max.
Soundness, Autoclave Expansion, %	0.08	0.8 Max.
Specific Gravity	2.30	-

Note: 1 psi = 0.0069 MPa

TABLE 2 CHEMICAL AND PHYSICAL TEST DATA FOR THE VPP CLASS F FLY ASH

Chemical Composition	Average, percent	ASTM-C-618
Silicon Oxide, SiO_2	50.1	-
Aluminum Oxide, Al_2O_3	25.3	-
Iron Oxide, Fe_2O_3	14.7	-
Total, $SiO_2+Al_2O_3+Fe_2O_3$	90.1	70.0 Min.
Sulfur Trioxide, SO_3	0.25	5.0 Max.
Calcium Oxide, CaO	1.18	-
Magnesium Oxide, MgO	0.71	5.0 Max.
Potassium Oxide, K_2O	2.24	-
Moisture Content	0.11	3.0 Max.
Loss on Ignition	3.5	6.0 Max.

Physical Tests		ASTM C-618
Fineness, % Retained on #325 Sieve	25	34 Max.
Pozzolanic Activity Index with Portland Cement, 28 days, % with lime, 7 days, psi	88 640	75 Min. 800 Min.
Water Requirement, % of Control	106	105 Max.
Soundness, Autoclave Expansion, %	0.07	0.8 Max.
Specific Gravity	2.32	-

Note: 1 psi = 0.0069 MPa

The fine aggregate was natural sand obtained from a local ready-mix concrete producer. Natural gravel, used as a coarse aggregate, was obtained from the same local concrete producer; it had maximum size of ¾ in. (19 mm).

A Melamine-based superplasticizer was used in this investigation. The dosages of the superplasticizer were varied to achieve the desired workability of fresh concrete while maintaining the same ratio of water to cementitious material.

MIXTURE PROPORTIONING

The mix proportion for the reference portland cement concrete used in this investigation (Mix O–A) is described in Table 3. All concrete mixtures used in this investigation were non–air entrained. In addition to the reference portland cement concrete, fly ash concretes were designed to have various amounts of fly ash in the range of 40 to 60 percent by weight on the basis of total cement used.

Concrete mixtures using OCPP Class F fly ash were proportioned to contain fly ash at cement replacement of 40, 50, and 60 percent by weight. The corresponding mixtures were designated as OCPP–A, OCPP–B, and OCPP–D. The water-cement ratio, (Water)/(Cement + Fly Ash), was maintained at about 0.32. Details of the mixture proportions are presented in Table 3.

Concrete mixtures containing VPP Class F fly ash were proportioned to incorporate fly ash at cement replacement of 50 and 60 percent by weight. The corresponding mixtures were designated as VPP–E and VPP–K. The water-cement ratio was kept at approximately 0.32 for Mix O–A and VPP–E, and about 0.44 for Mix VPP–K. The details of the mix proportions are presented in Table 4. Mix O–A is the same for both sources of fly ashes.

All the concrete ingredients were kept at room temperature before mixing the materials. A rotary drum laboratory mixer was used to prepare concrete mixes. The properties of fresh concretes made with ASTM Class F fly ash obtained from OCPP are presented in Table 3. The properties of concrete containing ASTM Class F fly ash derived from VPP are presented in Table 4.

Cylindrical specimens of size 6 × 12 in. (152 × 305 mm) were cast in molds for compressive strength, tensile strength, and secant modulus of elasticity measurements for all the concrete mixtures.

The casting and curing of concrete test specimens under laboratory conditions were carried out according to the appropriate ASTM standard methods.

TESTING OF SPECIMENS

Specimens were tested for compressive strength, tensile strength, and secant modulus of elasticity in accordance with the applicable ASTM test methods. Three cylinders were tested for each experimental condition.

TABLE 3 CONCRETE MIX USING OCPP CLASS F FLY ASH—6,000-psi (41-MPa) SPECIFIED STRENGTH

Mix No.	0-A	OCPP-A	OCPP-B	OCPP-D
Specified Design Strength, psi	6000	6000	6000	6000
Cement, lbs./cu. yd.	611	355	305	244
Fly Ash, lbs./cu. yd.	0	244	305	366
Water, lbs./cu.yd.	195	195	195	195
Water to Cementitious Ratio	0.32	0.33	0.32	0.32
Sand, SSD, lbs./cu. yd.	1544	1499	1487	1476
3/4" aggregates, SSD, lbs./cu. yd.	1887	1831	1818	1804
Slump, inches	2-1/4	4	3	5-1/2
Air Temperature, degrees F	65	65	66	68
Concrete Temperature, degrees F	65	65	66	68
Concrete Density, pcf	158.4	155.2	153.6	152.8
Superplasticizer liters/cu. yd.	4.9	4.7	4.6	4.5

Note: 1 psi = 0.0069 MPa; 1 inch = 25.4 mm
1 degree C = (degree F - 32)/1.8
1 lb/cu yd = 0.593 kg/m^3; 1 pcf = 16.02 kg/m^3
1 liter = 29.57 x 10^3 oz.

TABLE 4 CONCRETE MIX USING VPP CLASS F FLY ASH—6,000-psi (41-MPa) SPECIFIED STRENGTH

Mix No.	0-A	VPP-E	VPP-K
Specified Design Strength, psi	6000	6000	6000
Cement, lbs./cu. yd.	611	305	244
Fly Ash, lbs./cu. yd.	0	305	367
Water, lbs./cu.yd.	195	195	266
Water to Cementitious Ratio	0.32	0.32	0.44
Sand, SSD, lbs./cu. yd.	1554	1501	1488
3/4" aggregates, SSD, lbs./cu. yd.	1887	1836	1870
Slump, inches	2-1/4	1-1/2	9-1/2
Air Temperature, degrees F	65	60	65
Concrete Temperature, degrees F	65	60	65
Concrete Density, pcf	158.4	151.6	155
Superplasticizer liters/cu. yd.	4.9	4.5	5.1

Note: 1 psi = 0.0069 MPa; 1 inch = 25.4 mm
1 degree C = (degree F - 32)/1.8
1 lb/cu yd = 0.593 kg/m^3; 1 pcf = 16.02 kg/m^3
1 liter = 29.57 x 10^3 oz.

RESULTS AND DISCUSSION

Compressive Strength

Compressive strength data for the concretes containing Class F fly ash obtained from OCPP fly ash are reported in Table 5. The compressive strength versus age relation is shown in Figure 1. The relation between compressive strength and percentage of OCPP fly ash is shown in Figure 2. Compressive strength was found to increase with age for all the fly ash concretes (Figure 1). In general, addition of high volumes of OCPP fly ash in concrete caused a reduction in compressive strength (Figure 2) relative to concrete containing 611 lb/yd^3 of portland cement. Compressive strength at 28 days decreased from 6,820 psi (47 MPa) to 5,016 psi (35 MPa) when fly ash inclusion was increased up to 60 percent of the cement used by weight. The fly ash concrete incorporating 60 percent fly ash demonstrated compressive strengths of 3,200 psi (22 MPa) at the 7-day age and 5,000 psi (35 MPa) at the 28-day age. These values are considered to be substantial for a concrete containing only 244 lb/yd^3 (145 kg/m^3) of portland cement. Thus, these results indicate that concrete containing up to 60 percent of low-calcium fly ash can be proportioned to meet the requirements of strength and workability for structural-grade concretes. The desired strength can be achieved by adjusting the amount of fly ash, and for the same water-cement ratio, desired workability can be obtained through the use of superplasticizer. Moisture corrections for aggregates must also be made when aggregates contain greater amounts of water than that at the saturated surface dry condition.

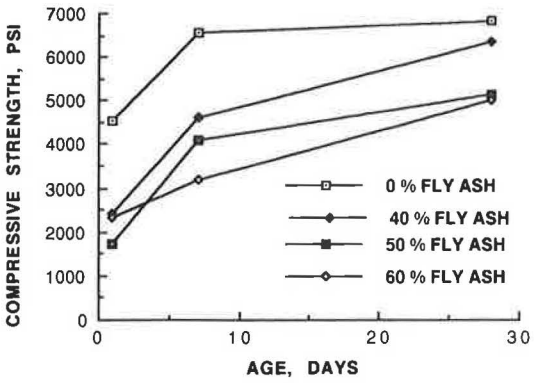

FIGURE 1 Compressive strength versus age for OCPP Class F fly ash.

Compressive strength data for concrete made with Class F fly ash obtained from VPP are presented in Table 6. Compressive strength versus age curves are shown in Figure 3. The relation between compressive strength and percentage of fly ash inclusion is shown in Figure 4. The compressive strength data obtained with VPP fly ash had the same general trend as described earlier for the structural concrete made with OCPP fly ash. However, because of variations in their physical properties between the sources of fly ash, especially in fineness and pozzolanic activity index, their reactivities varied, which caused differences in their measured performance in concrete. The concretes containing VPP fly ash produced sufficiently high compressive strength at all the ages tested up

TABLE 5 CONCRETE STRENGTH DATA USING OCPP CLASS F FLY ASH—6,000-psi (41-MPa) SPECIFIED STRENGTH

Mix No.	0-A	OCPP-A	OCPP-B	OCPP-D
Specified Strength, psi	6000	6000	6000	6000
Percent Fly Ash	0	40	50	60

Test Age, Days	Compressive Strength, psi			
1	4525	2404	1712	2346
7	6572	4604	4097	3189
28	6820	6343	5140	5016

Test Age, Days	Splitting Tensile Strength, psi			
1	365	251	158	145
7	464	362	360	236
28	541	453	439	353

Test Age, Days	Modulus of Elasticity, psi x10^{*6}			
7	4.92	3.78	-	3.27
28	5.45	4.75	-	4.77
28**	5.43	5.08	4.5	4.73

Note: 1 psi = 0.0069 MPa

*Average of three test specimens.

**Computed by ACI 318 Equation

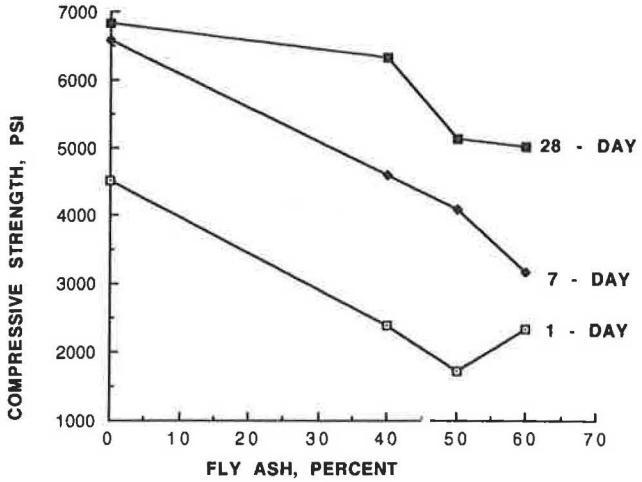

FIGURE 2 Compressive strength versus percentage of fly ash for OCPP Class F fly ash.

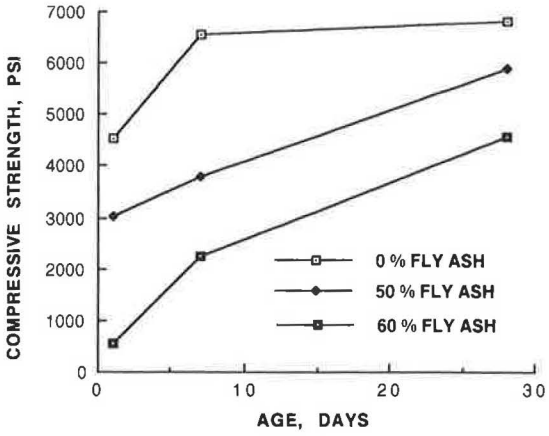

FIGURE 3 Compressive strength versus age for VPP Class F fly ash.

to 50 percent cement replacement. At 50 percent fly ash addition, concrete gained strength of about 3,000 psi (21 MPa) at 1-day age, which is high enough to meet requirements of early strength gain for most structural applications. The concrete also developed sufficient 28-day strength suitable for structural applications even at 60 percent fly ash inclusion.

Figures 2 and 4 also show that at high fly ash replacement levels, the proportion of fly ash concrete strength to reference concrete strength increased substantially from 1 to 28 days.

The high strength obtained through the use of superplasticizers is attributed to the lower water-cement ratio for a given consistency and to the densified concrete mixture. Previous microscopic studies have confirmed that addition of superplasticizers in concrete mixes produces excellent dispersion of cement particles, which in turn accelerates the rate of hydration reaction. Consequently, as observed in this project, superplasticized concretes had high compressive strength because of low water-cement ratio.

TABLE 6 CONCRETE STRENGTH DATA USING VPP CLASS F FLY ASH—6,000-psi (41-MPa) SPECIFIED STRENGTH.

Mix No.	O-A	VPP-E	VPP-K
Specified Strength, psi	6000	6000	6000
Percent Fly Ash	0	50	60
Test Age, Days	**Compressive Strength, psi**		
1	4525	3006	553
7	6572	3805	2258
28	6820	5906	4569
Test Age, Days	**Splitting Tensile Strength, psi**		
1	365	156	45
7	464	271	212
28	541	393	245
Test Age, Days	**Modulus of Elasticity, psi x10⁶**		
7	4.92	3.33	4.07
28	5.45	4.33	-
28**	5.43	4.73	4.30

Note: 1 psi = 0.0069 MPa

*Average of three test specimens.

**Computed by ACI 318 Equation.

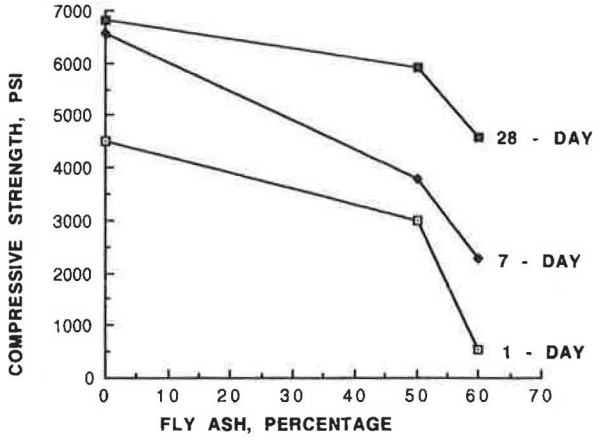

FIGURE 4 Compressive strength versus percentage fly ash for VPP Class F fly ash.

Because early-age strength for high-volume fly ash is lower compared to reference concrete, longer periods of time will be required to reach the desired strength for stripping formwork. In cases where additional curing time cannot be allowed, the mixture proportion can be adjusted to meet the job requirements in order to reach sufficient strength for stripping within a given length of time. However, except for Mix VPP–K, all concretes developed sufficient strength in 1 day to allow for the form stripping to continue without delay.

Splitting Tensile Strength

Splitting tensile strength data obtained from various concrete mixes are reported in Table 5 for concrete made with OCPP fly ash and in Table 6 for concrete made with VPP fly ash.

In general, splitting tensile strength increased with age for concretes made both with OCPP and VPP fly ashes (Tables 5 and 6). Also, in general, the tensile strength decreased with an increase in fly ash content in the concrete. However, percent decrease in tensile strength became lower at later ages.

The relation between tensile strength and age for the concrete made with the fly ash from OCPP is shown in Figure 5. The effect of fly ash addition on tensile strength of concrete is shown in Figure 6. Analysis of the results indicated that the concrete containing 50 percent Class F fly ash obtained from OCPP had 81 percent of the 28-day tensile strength of the reference concrete. A further decrease in value of the tensile strength was obtained when addition of fly ash was further increased to 60 percent.

The tensile strength versus age data for the concrete containing Class F fly ash from VPP are shown in Figure 7; the relation between tensile strength and fly ash inclusion is shown in Figure 8. This concrete achieved 73 percent of the tensile strength of the referenced concrete at fly ash addition of 50 percent and the age of 28 days (Figure 8). When fly ash addition was increased to 60 percent, the fly ash concrete attained only 45 percent of the tensile strength of reference concrete.

Modulus of Elasticity

The secant modulus of elasticity data are presented in Tables 5 and 6 for the concretes made with OCPP fly ash and VPP

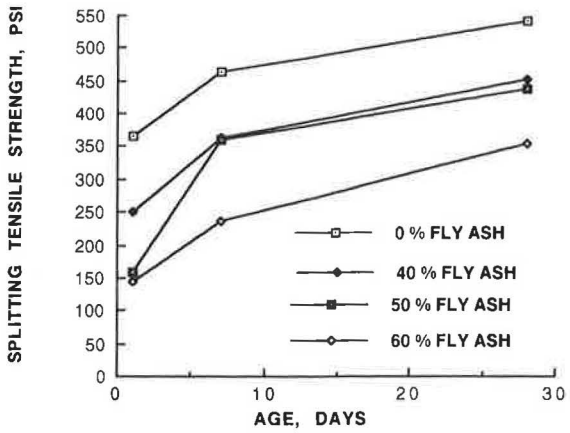

FIGURE 5 Tensile strength versus age for OCPP Class F fly ash.

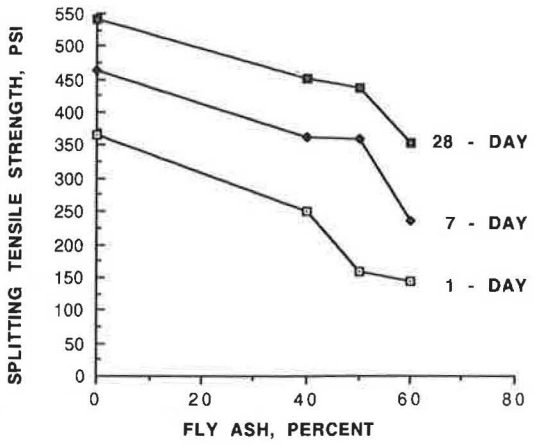

FIGURE 6 Tensile strength versus percentage fly ash for OCPP Class F fly ash.

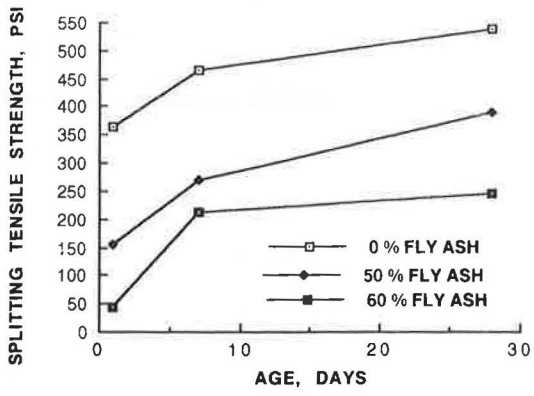

FIGURE 7 Tensile strength versus age for VPP Class F fly ash.

fly ash. In general, modulus of elasticity values increased with increase in age, and decreased with increase in fly ash content, all within a narrow range of possible testing and measuring errors.

The data presented in Tables 5 and 6 indicate that secant modulus values of the concretes made with both of these ASTM Class F fly ashes up to 60 percent fly ash inclusion are

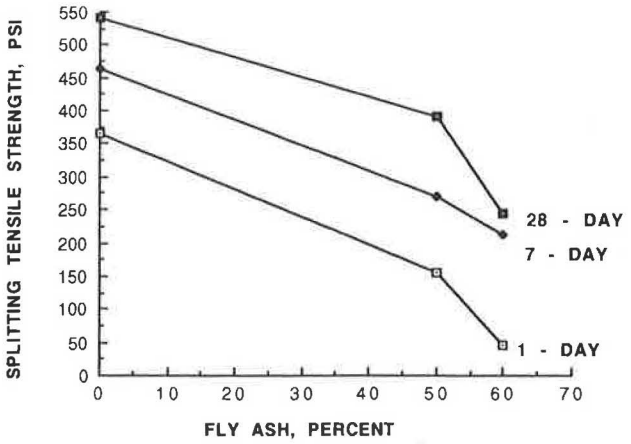

FIGURE 8 Tensile strength versus percentage fly ash for VPP Class F fly ash.

sufficient for structural applications. The modulus of elasticity was also computed using the ACI Code 318 equation:

$$E_c = (W_c^{1.5})(33 f_c^{1/2})$$

where

E_c = static modulus of elasticity, psi;
W_c = unit weight, lb/ft^3; and
f_c = 28-day compressive strength of a standard cylinder.

The values computed by the ACI Code 318 equation are presented in Tables 5 and 6 for concretes containing OCPP and VPP fly ashes, respectively. The values of modulus of elasticity computed by the ACI Code 318 equation were within a few percentage points of the actual values.

SUMMARY AND CONCLUSIONS

This study was primarily directed toward evaluation of performance of concrete incorporating a high volume of ASTM Class F fly ash. A portland cement concrete designed to have 6,000 psi (41 MPa) was used as a reference concrete. Concrete mixes containing two different types of low-calcium fly ashes were proportioned to have cement replacements between 40 and 60 percent. The water-cement ratio was maintained at approximately 0.32, and the desired workability of concrete mixes was obtained with the aid of a superplasticizer.

In general, both compressive strength and tensile splitting strength increased with age and decreased with increasing fly ash inclusions in the tested range of variables. However, the concrete containing fly ash up to 60 percent developed compressive strength in excess of 4,350 psi (30 MPa) at the 28-day age. At an early 7-day age, the concrete had high early secant modulus of elasticity, suitable for use in structural concrete.

On the basis of the recorded data, superplasticized concrete containing fly ash up to 60 percent can be proportioned to meet the strength and workability requirements for structural-grade concretes.

The chemical, physical, and mineralogical properties of fly ash can have appreciable effects on performance of fly ash in concrete. Properties of cement would also influence the performance of concrete. Therefore, it is necessary to determine the optimum mixture proportions for each cement and fly ash source before use.

REFERENCES

1. P. K. Metha. *Concrete Structure, Properties and Materials*. Prentice-Hall, Englewood Cliff, N.J., 1986.
2. P. R. Stodola. Performance of Fly Ash in Hardened Concrete. *ACI Concrete International*, Dec. 1983, pp. 64–65.
3. R. E. Davis, R. W. Carleson, and H. E. Davis. Properties of Cement and Concrete Containing Fly Ash. *ACI Journal*, Vol. 33, 1937, pp. 577–612.
4. B. Mather. Use of Concrete of Low-Portland Cement in Combination with Pozzolans and Other Admixtures in Construction of Concrete Dams. *ACI Journal*, Dec. 1974, pp. 589–599.
5. M. N. Hague, B. M. Langan, and M. A. Ward. High Fly Ash Concrete. *ACI Journal*, Vol. 81, No. 1, Jan.-Feb. 1984, pp. 54–60.
6. V. H. Dodson. High Percentage Use of Fly Ash in Concrete. In *Fly Ash Concrete*, Denver Fly Ash Concrete, Inc., and Los Angeles Fly Ash Symposium, Inc., 1983, pp. 801-01–802-21.
7. E. E. Berry and V. M. Malhotra. Fly Ash in Concrete. In *Supplementary Cementing Materials for Concrete*, V. M. Malhotra, ed., Minister of Supplies and Services, Canada, 1987, pp. 36–163.
8. G. M. Giaccio and V. M. Malhotra. Concrete Incorporating High-Volumes of ASTM Class F Fly Ash. *ASTM Cement, Concrete and Aggregates*, Winter 1988, pp. 88–95.
9. V. Sivasundaram, G. G. Carette, and V. M. Malhotra. Superplasticized High-Volume Fly Ash System to Reduce Temperature Rise in Mass Concrete. *Proc., 8th International Coal Ash Utilization Symposium*, Vol. 2, Electric Power Research Institute, Washington, D.C., Oct. 1987.
10. R. N. Swamy, A. R. A. Sami, and D. D. Theodorakopoulos. Early Strength of Fly Ash Concrete for Structural Applications. *ACI Journal*, Sept.-Oct. 1983, pp. 414–423.
11. R. N. Swamy and H. B. Mahmud. Shrinkage and Creep Behavior of High Fly Ash Content Concrete. *Proc., 3rd CANMET/ACI International Conference on Fly Ash, Silica Fume, Slag, and Natural Pozzolans in Concrete*, V. M. Malhotra, ed., Trondheim, Norway, Vol. 1, ACI SP–114, American Concrete Institute, Detroit, Mich., 1989, pp. 453–475.
12. R. N. Swamy and H. B. Mahmud. Mix Proportions and Strength Characteristics of Concrete Containing 50% Low-Calcium Fly Ash. In *Proc., 2nd International Conference on Fly Ash, Silica Fume, Slag and Natural Pozzolans in Concretes*, Vol. 1, ACI Publication SP–91, American Concrete Institute, Detroit, Mich., April 1986, pp. 413–432.
13. P. K. Mukherjee, M. T. Loughborough, and V. M. Malhotra. Development of High-Strength Concrete Incorporating Large Percentages of Fly Ash and Superplasticizers. *ASTM Cement, Concrete and Aggregates*, Vol. 4, No. 2, Winter 1983, pp. 81–86.
14. V. M. Malhotra and K. E. Painter. Early-Age Strength Properties, and Freezing and Thawing Resistance of Concrete Incorporating High-Volumes of ASTM Class F Fly Ash. *International Journal of Cement Composites and Lightweight Concrete*, Vol. 11, No. 2, Feb. 1988.
15. V. Sivasundaram, G. G. Carette and V. M. Malhotra. Long-Term Strength Development of High-Volume Fly Ash Concrete. Presented at the 3rd International Conference on the Use of Fly Ash, Silica Fume, Slag, and Natural Pozzolans in Concrete, Trondheim, Norway, June 1989.
16. W. S. Langley, G. G. Carette, and V. M. Malhotra. Structural Concrete Incorporating High Volumes of ASTM Class F Fly Ash. *ACI Materials Journal*, Vol. 86, No. 5, Sept.-Oct. 1989, pp. 507–514.
17. K. Taniguchi, T. Suzuki, Y. Shimomura, H. Ohga, and S. Nagataki. Applicability of High-Volume Fly Ash Concrete to Marine Structures. *Proc., 3rd CANMET/ACI International Conference on Fly Ash, Silica Fume, Slag, and Natural Pozzolans in Concrete, Supplementary Papers*, M. Alasali, ed., Trondheim, Norway, 1989, pp. 66–81.

Publication of this paper sponsored by Committee on Mechanical Properties of Concrete.

Evaluation of Particle Shape and Texture: Manufactured Versus Natural Sands

PRITHVI S. KANDHAL, JOHN B. MOTTER, AND MAQBOOL A. KHATRI

Many highway agencies now limit the amount of natural sand in hot mix asphalt (HMA) when used on heavy-duty pavements to minimize rutting. This procedure is usually accomplished by generically specifying the maximum allowable percentage of natural sand. Generally, natural sands tend to be rounded, whereas manufactured sands tend to be angular. However, there are some natural sands that are subangular rather than rounded. Also, some manufactured or crushed sands can be subrounded rather than completely angular. There is a definite need to quantify the shape and texture of the fine aggregate so that it can be specified on a rational basis rather than generically. Fine aggregates (8 natural and 10 manufactured sands) of different mineralogical compositions were sampled from various sources in Pennsylvania. Particle shape and texture data were obtained using ASTM D3398, and two proposed methods of the National Aggregate Association (NAA). On the basis of ASTM D3398, a particle index value of 14 appears to divide the natural and manufactured sands, and therefore, can be used for specification purposes. However, because each sieve size fraction needs to be tested individually and results combined, the current ASTM D3398 test procedures are too time consuming. However, test data indicate that only the major fraction needs to be tested because its particle index has a fairly good correlation with the average particle index. Moreover, both NAA proposed Methods A and B show good correlations (R^2 = 0.97) with the ASTM D3398 method. These methods are straightforward and less time consuming. Equations needed to compute ASTM D3398 weighted-average particle index values from two NAA methods are described.

Natural sand generally has rounded particles and, when used in hot mix asphalt (HMA), tends to lower its resistance to permanent deformation (rutting). As such, many highway agencies now limit the amount of natural sand in HMA for heavy-duty pavements to minimize permanent deformation. However, the use of generic terms such as natural or manufactured sand in specifications is not rational. The shape and texture of the sands actually determine the resistance to permanent deformation of HMA mixes in which they are used. Some natural sands are subangular rather than rounded, and on the other hand some crushed or manufactured sands are subrounded rather than completely angular. There is a definite need to quantify the shape and texture of the fine aggregate to specify sands in a more rational manner rather than specifying them generically.

OBJECTIVES

This study was undertaken to achieve the following objectives:

1. Quantify the particle shape and texture of various natural and manufactured (crushed) sands of different mineralogical compositions from Pennsylvania using ASTM D3398 (Index of Particle Shape and Texture), and proposed Methods A and B of the National Aggregate Association (NAA) using uncompacted void content.
2. Compare and evaluate the differences between the particle shape and texture of natural and manufactured sands obtained by the three methods.
3. Examine the ASTM D3398 method, which is time consuming because several sieve size fractions have to be tested individually, to see if it can be shortened without significantly affecting the particle shape and texture index values.
4. Compare the results from the ASTM D3398 method with the NAA Methods A and B, and examine if either of the NAA methods can be used in lieu of ASTM D3398.

P. S. Kandhal and M. A. Khatri, National Center for Asphalt Technology, 211 Ramsay Hall, Auburn University, Auburn, Ala. 36849–5354. J. B. Motter, Pennsylvania Department of Transportation, P.O. Box 2926, Harrisburg, Pa. 17105.

REVIEW OF LITERATURE

Aggregate shape is discussed in the literature in terms of differences between natural aggregates (gravels) and crushed aggregates. The particle shape of fine aggregate is apparently more important than that of coarse aggregate in improving the stability of HMA mixtures and increasing their resistance to permanent deformation.

Herrin and Goetz (*1*) studied the effect of aggregate shape on the stability of HMA mixtures and concluded that the addition of crushed gravel in the coarse aggregate fraction increased the strength for one-size mixtures but was of little importance in the dense-graded mixtures.

Lottman and Goetz (*2*) have reported the effect of crushed gravel fine aggregate in improving the strength of dense-graded asphaltic surfacing mixtures. Shklarsky and Livneh (*3*) made a very extensive study of the difference between natural gravel and crushed-stone aggregates in combination with natural sand and crushed-stone fine aggregates. Several variables were studied including the Marshall stability and flow, angle of internal friction and cohesion as measured in triaxial shear, resistance to moving wheel loading, resistance to splitting, immersion-compression strengths, and permeability. They reported as follows:

> Replacement of the natural sand with crushed fines improves incomparably the properties of the product, increases its stability, reduces rutting, improves water resistance, reduces bitumen sensitivity, increases the void ratio, and brings the mixture (with gravel coarse aggregate) to the quality level of one with crushed coarse and fine aggregate. On the other hand, replacement of the coarse material with crushed coarse aggregate entails no such decisive effect.

Griffith and Kallas (*4*) studied the effect of different aggregate types on the aggregate void characteristics of bituminous pav-

ing mixtures. They reported that natural gravel aggregates would generally require less asphalt than the crushed stone mixtures would, because natural gravels developed lower aggregate voids compared with the crushed stone mixtures having the same gradation.

Significant increases in stability have been reported by Wedding and Gaynor (*5*) when using crushed gravel in place of natural gravel. They concluded that the use of crushed gravel sand in place of natural sand is nearly equal in effectively raising stability as the use of 25 percent crushed gravel in the coarse aggregate.

Maupin (*6*) has reported a laboratory investigation of the effects of particle shape on the fatigue behavior of an asphalt surface mixture. He used three aggregates: round gravel, crushed limestone, and slabby slate. From constant-strain mode fatigue tests, it was demonstrated that the mixture containing round gravel had longer fatigue life than the other mixtures.

Marshall mix designs were run by Moore and Welke (*7*) on 110 sands from throughout the state of Michigan in which the coarse aggregate, asphalt content, and mineral filler were held constant. Both the angularity of the fine aggregate and the gradation of the mixture are critical for acquiring higher stabilities. The more angular the fine aggregate, the higher the stability. As for gradation, the closer the gradation is to the Fuller curve for maximum density, the higher is the stability. Rounded sands of relatively uniform size result in lower stabilities. Moreover, manufactured sands (slag or crusher sands) have highly angular particle shapes and are made for extremely high stabilities.

Foster (*8*) tested two sections of sand-asphalt mix and of mixes made with two different coarse aggregates and the same fine aggregate used in the sand-asphalt. After observation of the performance of the pavements, he concluded that the true capacity of dense-graded mixes to resist traffic-induced stresses is controlled by the characteristics of the fine aggregate.

Various methods have been reported in the literature for evaluating particle shape and texture of fine aggregates. These test methods can be divided generally into two categories—direct and indirect. Direct methods may be defined as those wherein particle shape and texture are measured, described qualitatively, and possibly quantified through direct measurement of individual particles. In indirect methods, measurement of the bulk properties of the fine aggregate are made separately or as mixed in the end product. A brief summary of the test methods found in the literature follows. (ASTM D3398 is the only test method for determination of particle shape and texture that has been standardized. Efforts are currently underway to propose the NAA methods A and B as ASTM standards.)

Direct Tests

Corps of Engineers' Method CRD-C120-55, Method of Test for Flat and Elongated Particles in Fine Aggregate

In this method, particle shape is evaluated by observation with a microscope. The sample is separated into five sizes and the number of particles having a length-to-width ratio of more than 3 in each group is counted and reported as a percentage. This method evaluates only the particle shape and not the surface texture of the particles.

Laughlin Method

In this method (*9*), which was developed for fine aggregate used in portland cement concrete, measurements are made using enlarged photographs of particles retained on various sieves. The radii of curvature of the particles and the radius of an inscribing circle are measured. Using these measurements, a parameter referred to as the roundness of the particles is then computed. Again, this method only tests the angularity (or roundness) of the particles and not the surface texture.

Indirect Tests

ASTM D3398, Standard Test Method for Index of Aggregate Particle Shape and Texture

In this method, the sample is first broken down into individual sieve fractions. Thus, the gradation of the sample is determined. Each size of material is then separately compacted in a cylindrical mold using a tamping rod at 10 and 50 drops from a height of 2 in. The mold is filled completely by adding extra material so that it just levels off with the top of the mold. Weight of the material in the mold at each compactive effort is determined and the percent voids computed. A particle index for each size fraction is then computed and, using the gradation of the sample, a weighted average particle index for the entire sample is also calculated.

National Aggregate Association's Proposed Method of Test for Particle Shape and Texture of Fine Aggregate using Uncompacted Void Content

In this method, a 100-cm^3 cylinder is filled with fine aggregate of prescribed gradation by allowing the sample to flow through the orifice of a funnel into the calibrated cylinder. Excess material is struck off and the cylinder with aggregate is weighed. Uncompacted void content of the sample is then computed using this weight and the bulk dry specific gravity of the aggregate. Two variations of the method are proposed. Method A uses a graded sample of specified gradation; in method B the void content is calculated using the void content results of three individual size fractions: Nos. 8 to 16, Nos. 16 to 30, and Nos. 30 to 50.

New Zealand Method

This method (*10*) is a flow test similar to NAA's proposed method. Here the orifice is ½ in. in diameter, and any material larger than the 5/16-in. sieve is removed. The void content and time required by 1,000 g of the material to flow through the orifice is measured and reported as a basic measure of particle shape and texture.

National Crushed Stone Association (NCSA) Method

In this flow test (*11*), the material is broken down into three sizes. Void content of each size fraction is determined separately by allowing to flow through an orifice of 1-in. diameter. The arithmetic mean of the void contents of the three sizes is computed as the basic measure of particle shape and texture.

Virginia Method

This method (*12*) is basically the same as the NCSA method.

National Sand and Gravel Association (NSGA) Method

This method (*13*) is basically the same test developed by Rex and Peck (*14*) and later used by Bloem and Gaynor (*15*) and Wills (*16*), but with different details. This is also a flow test with the size of an orifice of 0.4-in. diameter. Sample is broken down into four size fractions and then recombined in specified proportions. Void content of the sample thus prepared is determined and reported as the basic measure of particle shape and texture.

Ishai and Tons Method

In this test (*17*), results from a flow test are related to more basic measures of geometric irregularity of particles, i.e., macroscopic and microscopic voids in particles. The size of the orifice depends on the size of the particles being tested. The sample may be broken down into as many as six size fractions. One-sized glass beads are needed for each fraction. Flow test performance is reported on one-sized aggregate and corresponding one-sized glass beads.

Specific Rugosity by Packing Volume

This flow test method (*18*) was used for direct measurement of the packing specific gravity of one-sized aggregate particles. Aggregate sample was broken into four sizes and each placed in a cone-shaped bin and then poured into a calibrated constant-volume container. Packing specific gravity was computed using the weight of this calibrated volume of aggregate. The macro- and microsurface voids were computed using the apparent, bulk, and packing specific gravities. The addition of the macro- and microsurface voids thus obtained was done to arrive at the specific rugosity.

Direct Shear Test

This test method is used to measure the internal friction angle of a fine aggregate under different normal stress conditions. A prepared sample of the aggregate under consideration is consolidated in a shear mold. The sample is then placed in a direct shear device and sheared by a horizontal force while a known normal stress is applied.

MATERIALS

Fine aggregates used in this study comprised 8 natural and 10 manufactured sands of different mineralogical composition and came from various sources in Pennsylvania. Table 1 presents the source, type of aggregate, and its bulk specific gravity and water absorption data obtained using ASTM C128. Table 2 presents the as-received gradations of all the aggregates used in the study. All natural sands were uncrushed and came from pit run or bank run gravel sources while all manufactured sands except one were crushed from different stone types including limestone, sandstone, calcareous sandstone, siltstone, dolomite, argillite, and hornfels. One of the manufactured sands was blast furnace slag (fine aggregate No. 10).

TEST METHODS

ASTM D3398

This standard is the ASTM Standard Test Method for Index of Aggregate Particle Shape and Texture. Only one size of standard mold was used for this study, a 3-in.-diameter mold (Mold D). The sample was washed on a No. 200 sieve and dried in the oven at 230°F ± 9°F. It was then sieved to separate the total material into individual size fractions using ASTM C136. Bulk specific gravity of the material was determined in accordance with ASTM C128. The individual size fractions were then compacted using 10 and 50 drops of the tamping rod to determine the voids and hence the particle index for each size fraction. The weighted average particle index was then computed by averaging the particle index data for each size fraction, weighted on the basis of the percentage of the fractions in the original grading of the sample as received.

NAA Methods

Both Methods A and B were used during this study. In Method A, the specified standard grading was used to make the sample by using the following quantities of dry sand from each size:

Individual Size Fraction	*Weight, g*
#8 to #16	44
#16 to #30	57
#30 to #50	72
#50 to #100	17
Total	190

In Method B, 190 g of dry fine aggregate was used for each of the sizes Nos. 8 to 16, Nos. 16 to 30, and Nos. 30 to 50.

The samples were dried in the oven at 230°F ± 9°F before determination of voids content. The cylinder used was a standard 100-cm^3 cylinder. Void contents were determined by allowing the sample to flow through a funnel (of 0.375-in.-diameter orifice) from a height of 4.50 in. above the top of the cylinder. For the graded sample (Method A), the void content so determined was used directly. For the individual fractions (Method B), the mean void content percent was calculated on the basis of the void contents for individual size fractions.

TABLE 1 GENERAL DATA FOR AGGREGATES USED

S.No.	County	* Type	** Type Agg.	Bulk Sp. Gr.	Water Asborption (percent)
1	Crawford	N	GL	2.582	1.38
2	Ohio	N	GL	2.560	1.24
3	Erie	N	GL	2.587	1.26
4	Bucks	N	GL	2.556	1.59
5	Bedford	M	LS	2.610	1.14
6	Warren	N	GL	2.580	0.98
7	Monroe	N	GL	2.570	2.32
8	Wyoming	N	GL	2.593	0.95
9	Westmonland	N	GL	2.564	1.26
10	Westmonland	M	SB	2.430	4.33
11	Cumberland	M	SS	2.627	0.40
12	Fayette	M	CS	2.670	0.27
13	Westmonland	M	CS-CG	2.673	0.60
14	Perry	M	SL	2.648	0.96
15	Berks	M	DO-LS	2.728	0.47
16	Northumberland	M	SS-CG	2.664	0.36
17	Bucks	M	AR	2.660	0.52
18	Adams	M	HF	2.668	0.58

*
N = Natural fine aggregate
M = Manufactured fine aggregate

**
GL = Gravel Sand
LS = Limestone
SB = Blast Furnace Slag
CS = Calcareous Sandstone
SS = Sandstone
CS-CG = Calcareous Sandstone Conglomerate
SL = Siltstone
DO-LS = Dolomitic Limestone
SS-CG = Sandstone Conglomerate
AR = Argillite
HF = Hornfels

TABLE 2 AS-RECEIVED GRADATIONS FOR AGGREGATES USED

S.No.	* Type	Type Aggregate	Percent Passing							
			3/8 in	#4	#8	#16	#30	#50	#100	#200
1	N	GL	100.0	96.0	80.1	63.3	43.1	15.4	3.5	1.4
2	N	GL	100.0	97.5	77.9	55.2	29.5	6.1	0.9	0.5
3	N	GL	100.0	95.1	78.2	61.9	45.8	25.7	9.4	3.2
4	N	GL	100.0	94.8	79.3	68.7	53.9	16.6	2.8	1.4
5	M	LS	100.0	99.8	77.9	39.3	18.1	8.2	4.8	3.5
6	N	GL	100.0	95.8	77.2	55.8	38.4	21.2	12.4	3.7
7	N	GL	100.0	96.2	77.4	58.2	36.3	19.4	7.9	2.0
8	N	GL	100.0	98.0	72.6	55.5	42.0	15.3	4.2	1.8
9	N	GL	100.0	98.1	70.2	49.9	36.9	19.6	4.3	0.9
10	M	SB	100.0	99.6	82.0	58.1	37.8	20.0	9.5	4.1
11	M	SS	100.0	99.3	85.9	69.6	49.7	26.4	7.3	1.3
12	M	CS	100.0	100.0	75.3	46.9	31.2	18.0	8.6	4.2
13	M	CS-CG	100.0	98.1	77.0	45.7	27.4	13.5	4.4	2.0
14	M	SL	100.0	99.8	73.3	42.3	24.1	13.7	8.7	5.1
15	M	DO-LS	100.0	99.8	84.0	44.8	25.9	14.5	7.8	3.2
16	M	SS-CG	100.0	100.0	84.5	50.1	32.4	16.4	7.7	3.3
17	M	AR	100.0	99.1	79.4	53.2	33.0	16.8	11.2	6.5
18	M	HF	100.0	99.8	88.1	57.4	31.4	15.7	8.0	4.7

*
N = Natural fine aggregate
M = Manufactured fine sand

TEST DATA AND DISCUSSION

The test data obtained for particle (shape and texture) index (I_a) using ASTM D3398 are presented in Table 3. The results are arranged in order of increasing I_a values. A plot of the weighted average particle index values for various fine aggregates used in this study is shown in Figure 1. The results obtained using the NAA proposed Methods A and B are presented in Table 4. These results are also shown in Figure 2. A general trend of values obtained by the two methods is shown in Figure 3. A discussion of the results obtained follows.

Differences Between Natural and Manufactured Sands

On the basis of the ASTM D3398 data shown in Figure 1, natural sands appear to exhibit lower I_a values compared with manufactured sands. There is one exception, however, in that one of the manufactured sands (Fine Aggregate No. 5—limestone) falls with the natural sands. Generally, a particle index value of 14 delineates the natural and manufactured sands. As indicated in Table 3, the average particle index for natural sands is 12.3 with a standard deviation of 1.26; thus the 95 percent confidence limits for I_a values of natural sands are 9.8 and 14.8. Similarly, the average particle index for manufactured sands is found to be 18.2 with a standard deviation of 2.72; thus the 95 percent confidence limits of the particle index for manufactured sands are 12.9 and 23.5. On the basis of the 95 percent confidence limits, natural and manufactured sands overlap in the particle index range of 12.9 to 14.8. From trial-and-error procedures, this overlap would cease to exist at a confidence level of 86 percent, yielding a dividing value of the particle index of 14.1. A minimum value of I_a of 14 thus can probably be used in the specifications in lieu of specifying manufactured sand generically.

Similar trends are observed for data obtained using NAA Methods A and B as indicated in Figure 2. The average values, standard deviations, and 95 percent confidence limits for uncompacted void contents obtained using NAA methods are as follows:

Method	*Type of Aggregate*	*Average*	*Standard Deviation*	*95 percent Confidence Limits*
A	Natural	42.5	1.51	39.5–45.5
A	Manufactured	48.1	2.68	42.8–53.4
B	Natural	46.1	1.58	43.0–49.2
B	Manufactured	51.9	2.59	46.8–57.0

Again, on the basis of the 95 percent confidence limits, the uncompacted void contents for natural and manufactured sands overlap in the range of 42.8 to 45.5 using Method A and in the range of 46.8 to 49.2 using Method B. These overlap regions can be avoided at a confidence level of 82 percent for Method A and 84 percent for Method B, yielding delineating values of uncompacted void content separating the natural and manufactured sands as 44.5 (Method A) and 48.4 (Method B), respectively. On the average, the uncompacted void content obtained by Method A is lower than that obtained using Method B. The difference appears to be reasonably uniform as indicated in Figure 2, and, therefore, either Method A or B can be used.

Evaluation of ASTM D3398

Because of the time-consuming nature of ASTM D3398 procedure, alternative approaches were sought during the present study. Correlations were run between the average particle index obtained using ASTM D3398 and the particle indexes for the individual major fraction, and major fraction plus second-major fractions to see whether these could be used instead. These correlations are shown in Figures 4–6. These

TABLE 3 PARTICLE SHAPE INDEX DATA USING ASTM D3398

S. No.	* Type	Type of Aggregate	Sieve Fraction -3/8"+#4	-#4+#8	-#8+#16	-#16+#30	-#30+#50	-#50+#100	-#100+#200	-#200	Weighted Particle Index
1	N	GL	8.9	8.9	9.3	10.5	10.6	11.0	11.0	11.0	10.1
2	N	GL	10.6	10.6	11.2	10.1	9.8	11.2	11.2	11.2	10.5
3	N	GL	11.1	12.0	13.1	13.4	12.7	12.3	12.3	12.3	12.6
4	N	GL	11.7	13.8	13.5	12.2	11.9	13.4	13.4	13.4	12.6
5	M	LS	12.5	12.5	12.7	12.7	13.3	13.3	13.3	13.3	12.8
6	N	GL	9.3	10.0	13.4	13.5	13.2	14.9	15.5	15.5	13.0
7	N	GL	11.7	12.4	12.2	13.0	13.9	13.8	13.8	13.8	13.0
8	N	GL	11.3	11.3	14.8	14.9	12.5	13.8	13.8	13.8	13.1
9	N	GL	11.3	11.3	15.4	15.2	12.8	14.1	14.1	14.1	13.4
10	M	SB	16.1	16.1	15.2	13.1	14.5	16.0	16.0	16.0	15.0
11	M	SS	16.9	16.9	17.1	16.2	15.5	16.5	16.5	16.5	16.4
12	M	CS	0.0	17.8	19.5	20.1	17.2	16.2	16.2	16.2	18.3
13	M	CS-CG	19.7	19.7	19.9	19.0	17.4	16.3	16.3	16.3	18.9
14	M	SL	19.0	19.0	18.8	19.1	19.8	20.8	20.8	20.8	19.3
15	M	DO-LS	20.3	20.3	19.8	18.9	18.6	18.7	18.7	18.7	19.4
16	M	SS-CG	0.0	18.8	19.7	20.2	20.1	21.3	21.3	21.3	20.0
17	M	AR	20.5	20.5	21.6	21.0	20.0	21.6	21.6	21.6	21.0
18	M	HF	19.8	19.8	20.6	22.0	22.1	22.1	22.1	22.1	21.3

Average for Natural Sands	12.3
Standard Deviation	1.26
Average for Manufactured Sands	18.2
Standard Deviation	2.72

* N = Natural fine aggregate
M = Manufatured fine aggregate

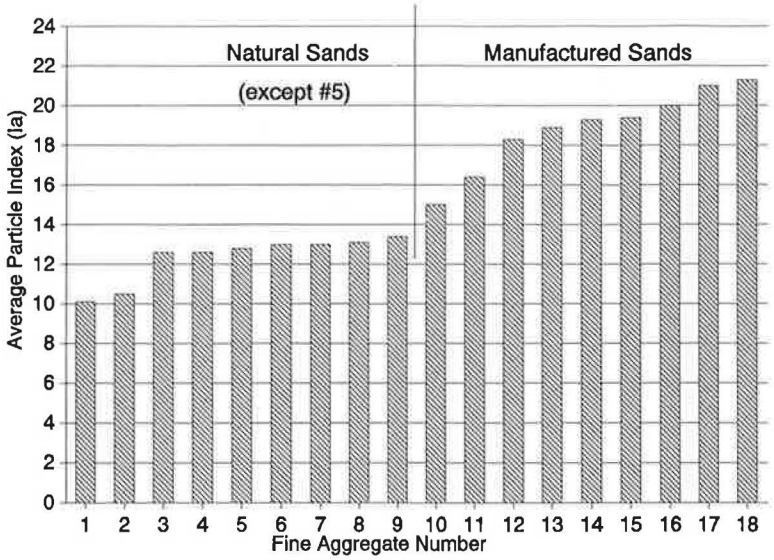

FIGURE 1 Average particle index using ASTM D3398.

TABLE 4 PARTICLE SHAPE AND TEXTURE DATA USING NAA METHODS A AND B

S.No.	Type*	Type Aggregate	Method A	Method B
1	N	GL	40.6	43.9
2	N	GL	40.2	43.5
3	N	GL	42.2	47.5
4	N	GL	42.7	46.0
5	M	LS	43.1	47.5
6	N	GL	43.9	46.6
7	N	GL	43.8	46.9
8	N	GL	42.4	46.3
9	N	GL	44.3	47.8
10	M	SB	45.4	49.0
11	M	SS	45.7	48.8
12	M	CS	48.5	52.7
13	M	CS-CG	47.7	52.3
14	M	SL	48.7	52.6
15	M	DO-LS	49.2	53.2
16	M	SS-CG	49.3	53.5
17	M	AR	50.9	54.7
18	M	HF	52.0	55.0

* N = Natural fine aggregate
M = Manufactured fine aggregate

figures indicate correlations for (a) the whole data including both natural and manufactured sands, (b) natural sands only, and (c) manufactured sands only, respectively. Good correlations exist between the average particle index and particle indexes for major fraction, and major plus second major fractions for the whole data as well as for data on manufactured sands. Coefficient of determination (R^2) values are found to range between 0.94 and 0.98. Natural sands, however, have some scatter and the R^2 values are 0.59 and 0.80 for major-fraction, and major-fraction plus second-major-fraction particle index values, respectively. The equations relating the weighted average particle index (I_a) with major-fraction particle index (I_m) are as follows:

$$I_a = 0.92I_m + 1.3 \quad \text{for combined data}$$

$$I_a = 0.82I_m + 2.5 \quad \text{for natural sands}$$

$$I_a = 0.92I_m + 1.4 \quad \text{for manufactured sands}$$

Similarly, the equations relating weighted average particle index (I_a) with major plus second-major-fraction particle index (I_{mpsm}) are as follows:

$$I_a = 0.93I_{mpsm} + 1.3 \quad \text{for combined data}$$

$$I_a = 1.08I_{mpsm} - 0.6 \quad \text{for natural sands}$$

$$I_a = 0.90I_{mpsm} + 1.8 \quad \text{for manufactured sands}$$

In general, the particle index values within the sieve fraction increase as the sieve size decreases. No general trends can be found as to whether the distribution within the sand is normal or skewed.

The particle index may be used for the major fraction of a sand in place of its weighted average particle index. On average, the major-fraction particle index differs from the weighted-average particle index by 0.1, which is practically insignificant. If increased accuracy is desired, then both the major fraction and second-major fraction can be tested and the results combined to yield a weighted average value.

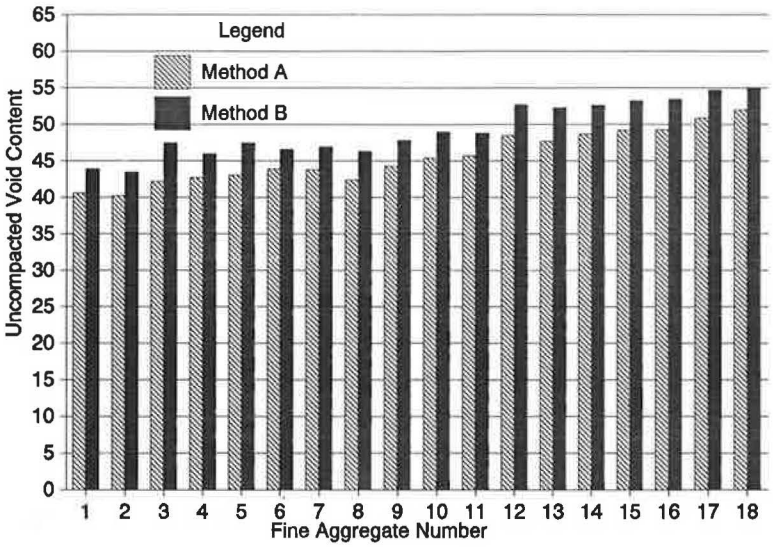

FIGURE 2 Uncompacted void content using NAA proposed Methods A and B.

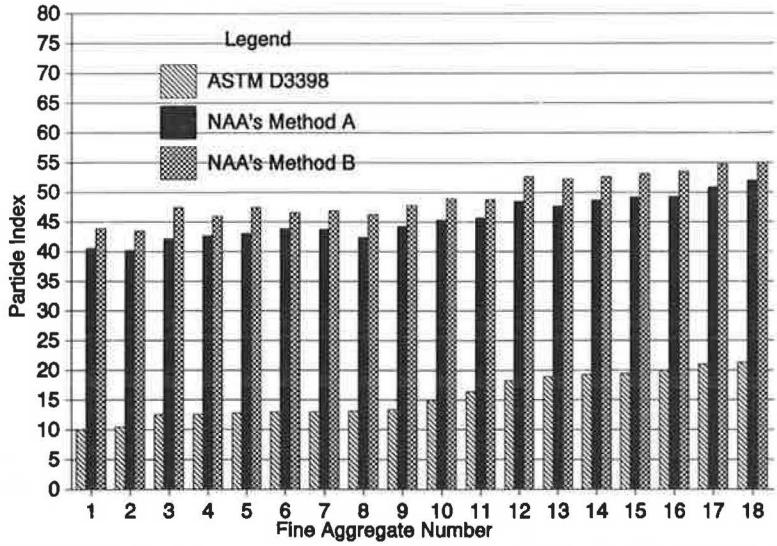

FIGURE 3 Particle index using ASTM D3398 and NAA proposed Methods A and B.

Comparison of ASTM D3398 and NAA Methods

Data obtained using NAA Methods A and B were correlated with the weighted average particle index data obtained using ASTM D3398. These correlations are shown in Figure 7. The coefficient of determination (R^2) for both methods was 0.97. On the basis of the data obtained for the 18 fine aggregates, the NAA methods can successfully be used in place of ASTM D3398. With the slope value of almost one, the data are observed to have only a shift factor for translating NAA method results to ASTM D3398 results. This shift for Method A is −31.2; for Method B, −33.5. The following equations may be used for transforming NAA method results to ASTM D3398 results.

$$I_a = 1.03V_{NAA} - 31.2 \quad \text{for Method A}$$

$$I_a = 1.00V_{NAA} - 33.5 \quad \text{for Method B}$$

where V_{NAA} is the uncompacted voids content measure of particle shape and texture obtained by NAA methods.

CONCLUSIONS

On the basis of the particle shape and texture index values obtained for the various natural and manufactured sands tested using ASTM D3398 and NAA proposed Methods A and B, the following conclusions can be drawn:

1. A particle index value of about 14 divides the natural and manufactured sands when using ASTM D3398. This value can probably be used for specification purposes when ASTM D3398 is used. All manufactured sands except one exhibit higher particle index values and all natural sands have lower particle index values. A similar trend is observed for NAA Methods A and B as well in which uncompacted void content values of 44.5 and 48.3, divide the natural and manufactured sands, respectively.
2. Correlations between the major-fraction, and major-fraction plus second-major-fraction particle indexes with the weighted-average particle index using ASTM D3398 are fairly good for the overall data. This agreement suggests that a particle index value for the major fraction or major fraction

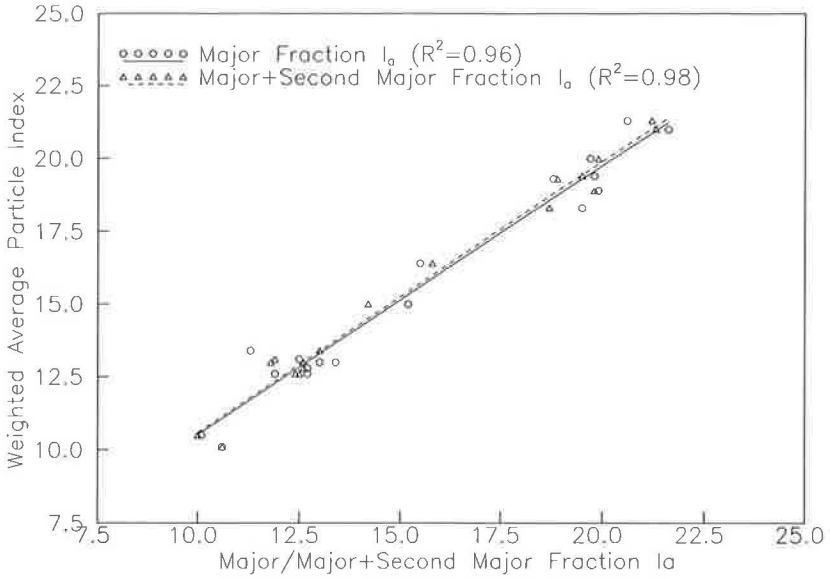

FIGURE 4 Weighted-average particle index versus major-fraction and major-fraction plus second-major-fraction particle indexes (combined data).

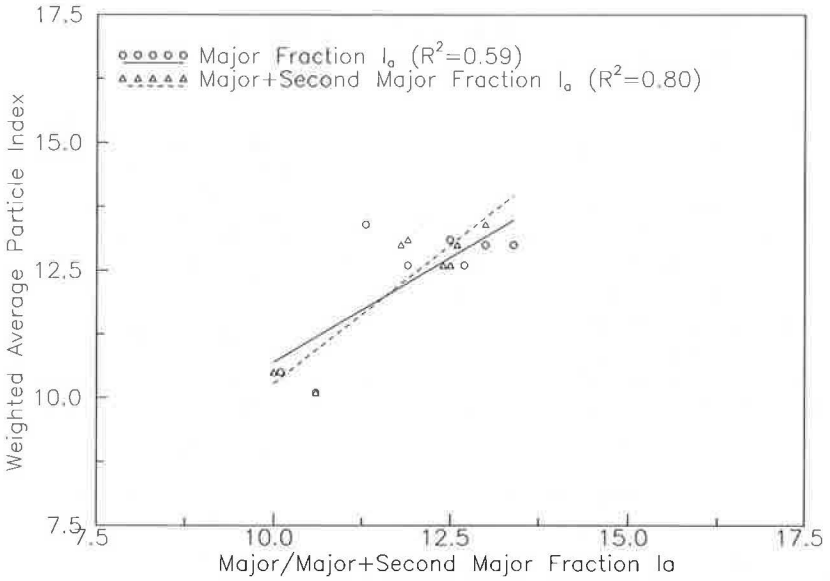

FIGURE 5 Weighted-average particle index versus major-fraction and major-fraction plus second-major-fraction particle indexes (natural sands only).

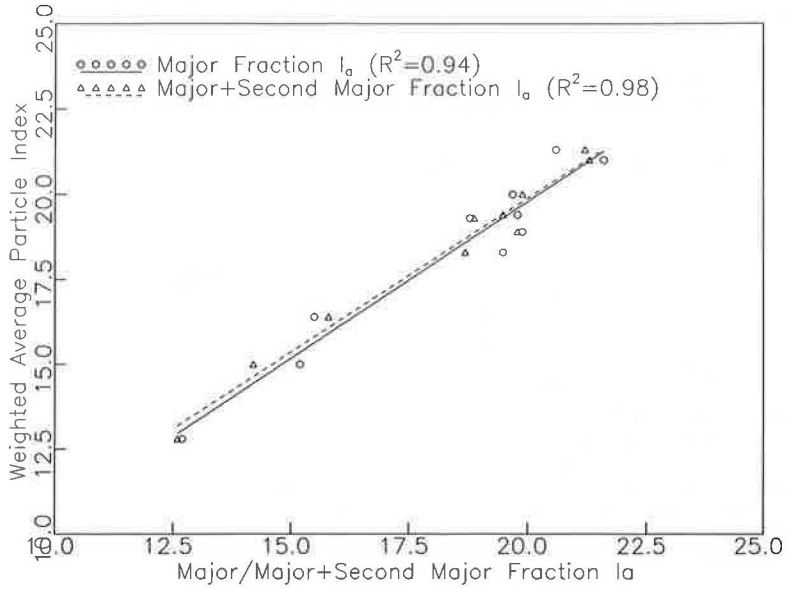

FIGURE 6 Weighted-average particle index versus major-fraction and major-fraction plus second-major-fraction particle indexes (manufactured sands only).

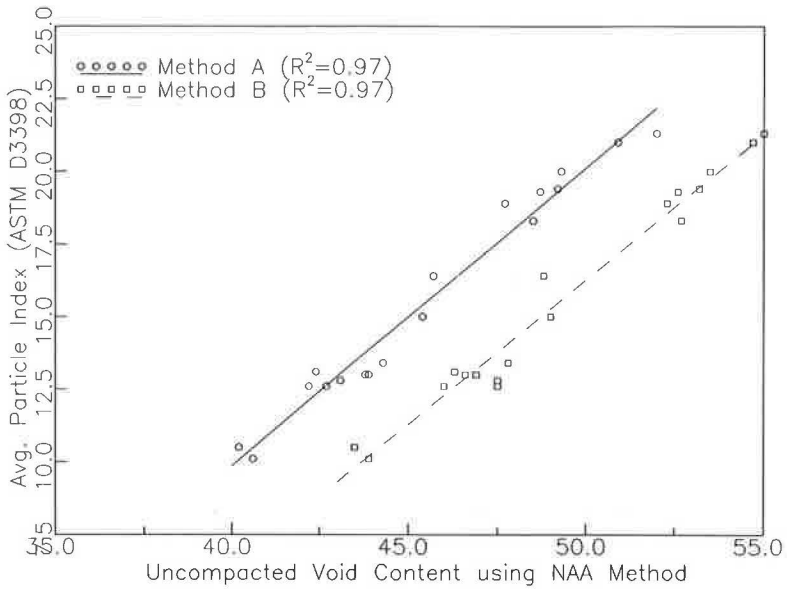

FIGURE 7 Average particle index using ASTM D3398 versus uncompacted void content using NAA Methods A and B.

plus second-major fraction of the fine aggregate may be used as the average particle index for the combined gradation. This result would save time and effort in testing.

3. Both NAA Methods A and B show high correlations (R^2 = 0.97) with the ASTM D3398 method. This correlation indicates the viability of substituting the NAA methods for ASTM D3398 as the standard methods for determining particle shape and texture of fine aggregates. NAA methods are both straightforward and time saving as compared with ASTM D3398. Equations for computing the ASTM D3398 weighted-average particle index from the NAA method results are described for the aggregates tested in this study.

Currently, research is under way at the National Center for Asphalt Technology, Auburn, Alabama, to correlate the fine aggregate particle index with the permanent deformation (rutting) behavior of the HMA mixes so that minimum values of particle index can be specified for heavy-duty pavements.

ACKNOWLEDGMENTS

All tests on aggregates were conducted by the personnel of Bituminous Testing Laboratory of the Pennsylvania Department of Transportation, Harrisburg, Pennsylvania. Statistical analysis of the test data was performed by the National Center for Asphalt Technology.

REFERENCES

1. M. Herrin and W. H. Goetz. Effect of Aggregate Shape on Stability of Bituminous Mixes. *HRB Proc.*, Vol. 33, 1954.
2. R. R. Lottman and W. H. Goetz. *Effect of Crushed Gravel Fine Aggregate on the Strength of Asphaltic Surfacing Mixtures.* Circular 63, National Sand Gravel Association, 1956.
3. E. Shklarsky and M. Livneh. The Use of Gravels for Bituminous Paving Mixtures. *Proc., AAPT*, Vol. 33, 1964.
4. J. M. Griffith and B. F. Kallas. Aggregate Voids Characteristics in Asphalt Paving Mixes. *HRB Proc.*, Vol. 36, 1957.
5. P. A. Wedding and R. D. Gaynor. The Effects of Using Crushed Gravel as the Coarse and Fine Aggregate in Dense Graded Bituminous Mixtures. *Proc., AAPT*, Vol. 30, 1961.
6. G. W. Maupin. Effect of Particle Shape and Surface Texture on the Fatigue Behavior of Asphaltic Concrete. In *Highway Research Record 313*, HRB, National Research Council, Washington, D.C., 1970, pp. 55–62.
7. R. B. Moore and R. A. Welke. *Effects of Fine Aggregate on Stability of Bituminous Mixes.* Research Report 78 TB-34-79F, Testing and Research Division, Testing Laboratory Section, Michigan Department of Transportation, 1979.
8. C. R. Foster. Dominant Effect of Fine Aggregate on Strength of Dense-Graded Asphalt Mixes. Special Report 109. HRB, National Research Council, Washington, D.C., 1970, pp. 1–3.
9. G. R. Laughlin. *Limestone Fine Aggregate in Portland Cement Concrete.* Highway Research Laboratory, Lexington, Ky., 1960.
10. *Method of Determining Voids Content, Flow Time, and Percentage Oversize Material in Sand.* Des. C121-69. Central Laboratories, New Zealand Ministry of Works, Wellington, 1969.
11. J. E. Gray and J. E. Bell. *Stone Sand.* National Crushed Stone Association Engineering Bulletin 13, 1964.
12. *Road and Bridge Specifications.* Virginia Department of Highways, Richmond, 1970.
13. *Tentative Method of Test for Uncompacted Void Content of Fine Aggregate.* National Sand and Gravel Association and National Ready-Mix Concrete Association, Washington, D.C., Undated.
14. H. M. Rex and R. A. Peck. A Laboratory Test to Evaluate the Shape and Surface Texture of Fine Aggregate Particles. *Public Roads*, Vol. 29, No. 5, 1956.
15. D. L. Bloem and R. D. Gaynor. Effect of Aggregate Properties on Strength of Concrete. *Journal of American Concrete Institute*, Vol. 60, No. 10, 1963.
16. M. H. Wills, Jr. How Aggregate Particle Shape Influences Concrete Mixing Water Requirement and Strength. *ASTM Journal of Materials*, Vol. 2, No. 4, 1967.
17. I. Ishai and E. Tons. A Concept and a Test Method for a Unified Characterization of the Geometric Irregularity of Aggregate Particles. *ASTM Journal of Testing and Evaluation*, Vol. 5, No. 1, 1977.
18. E. Tons and W. H. Goetz. Packing Volume Concept for Aggregates. In *Highway Research Record 236*, HRB, National Research Council, Washington, D.C., 1968, pp. 76–96.

The opinions, findings, and conclusions expressed here are those of the authors and not necessarily those of the National Center for Asphalt Technology, Pennsylvania Department of Transportation, or Auburn University.
Publication of this paper sponsored by Committee on Mineral Aggregates.

Comparison of Four Aggregates Using the Washington Hydraulic Fracture Test

DONALD J. JANSSEN AND DAVID K. ALMOND

The importance of identifying D-cracking susceptible aggregates has led to a considerable number of aggregate identification test procedures. Unfortunately, the more reliable of the procedures may require 8 weeks or longer, expensive equipment, and highly skilled operators. In response to this problem, the Strategic Highway Research Program (SHRP) has issued a research contract to develop a rapid, reliable test method for identifying aggregates susceptible to D-cracking. The new test method being developed is used to examine four aggregates: two that have produced D-cracking in the field, and two with a performance history of no D-cracking. The test method involves covering an oven-dried aggregate sample with water, and then pressurizing the water to 1,150 psi (7,930 kPa). The pressure is quickly released, and then the pressurization and release cycle is repeated. Ten cycles per day are run for a total of 50 cycles. The amount of aggregate fracturing is determined and indicates D- cracking potential. The D-cracking susceptibility of the four aggregates tested was clearly identified even though the samples were different materials from diverse origins and locations

D-cracking refers to the distress in concrete that results from the disintegration of coarse aggregates after they have become saturated and have been subjected to repeated cycles of freezing and thawing (*1*). Although D-cracking has been known to exist since the 1930s (*2*), a fast, reliable, reproducible, easily performed, and inexpensive test for identifying aggregates susceptible to D-cracking has not been developed. The effectiveness of a modification to a newly developed procedure for identifying D-cracking susceptible aggregates is examined, and four aggregates—a D-cracking susceptible gravel, a non-D-cracking susceptible gravel, a D-cracking susceptible limestone, and a non-D-cracking susceptible limestone—are compared with the new test procedure.

BACKGROUND

The mechanisms of D-cracking have not yet been completely clarified and continue to be intensively studied (*3*). Some general characteristics about aggregates that are susceptible to D-cracking have been identified.

Kaneuji et al. (*4*) observed qualitative correlations between concrete durability and pore size distributions of aggregates. At a constant total pore volume, aggregates with smaller pore sizes have a lower durability. For aggregates with similar predominating pore sizes, a greater pore volume means a less durable aggregate. By correlating aggregate service records with mercury porosimeter studies, Marks and Dubberke (*5*) found that, with one exception, the nondurable aggregates they analyzed exhibited a predominance of pore sizes in the 0.04- to 0.2-μm-diameter range, whereas aggregates with good-to-excellent service records did not exhibit a predominance of 0.04- to 0.2-μm-diameter pore sizes.

Using Washburn's (*6*) equation:

$$P = 4T \cos \theta / d \quad (1)$$

where

T = surface tension (72 dynes/cm for water),
θ = contact angle (assumed 0° for water-aggregate contact), and
d = pore diameter.

absolute pressures between 210 psi (1,450 kPa) and 1,050 psi (7,240 kPa) could be used to force water into aggregate pore diameters within the range 0.04 to 0.2 μm.

EXISTING TEST METHODS

Because of the complex interrelationship of variables that affect the performance of aggregates in concrete, many tests have been devised to provide a reliable means of separating durable and nondurable aggregate (*7*). The test methods developed identify the resistance of aggregate to frost action and can be placed into two primary groups (*8,9*). One group consists of tests that try to simulate the environmental conditions to which the concrete aggregate is exposed. The other group consists of tests that correlate aggregate properties with known field performances and results from environmental tests.

Environmental Simulation

The environmental simulation tests include the following:

1. Sulfate soundness test,
2. Unconfined aggregate freeze-thaw test,
3. Rapid freeze-thaw test,
4. Powers slow-cool test, and
5. VPI single-cycle slow-freeze test.

Sulfate Soundness (AASHTO T104)

This test is favored by many over other test methods because of the small amount of equipment involved and the short

Washington State Transportation Center (TRAC), University of Washington, JE-10, Corbet Building, Suite 204, 4507 University Way, N.E., Seattle, Wash. 98105.

amount of time required to run the test (*7*). In the sulfate soundness test, aggregate is soaked in a sodium or magnesium sulfate solution and then dried. Repeated cycles result in salt crystal growth in the aggregate pores. The expansive forces generated by the crystal growth supposedly simulate the expansive forces caused by the formation of ice in aggregate pores. However, the major natural cause of disintegration in aggregates, according to some theories, is the hydraulic pressure produced when water attempts to leave the zone of freezing (*7*). The growth of the sulfate crystals may not generate hydraulic pressures, and may not be related to the pore sizes believed to contribute to damage from freezing. Additionally, the sulfate test does not account for the effects of confining the aggregate by mortar, which determines the rate and amount of moisture movement into and out of the aggregate.

Unconfined-Aggregate Freeze-Thaw (AASHTO T103)

The unconfined-aggregate freeze-thaw test is an outgrowth of the sulfate test (*7*). The test has three variations; however, the basic procedure consists of subjecting the aggregate to repeated freezing in water and thawing. As with the sulfate test, the unconfined freezing and thawing test does not duplicate confinement of the aggregate by mortar. This test can be less reproducible because of the number of variables involved. These variables include rate of cooling and final temperature, rate of thawing, the moisture conditions of the samples before each cycle, and the length of time the samples remain frozen and thawed.

Rapid Freezing and Thawing (ASTM C666)

The Standard Test Method for Resistance of Concrete to Rapid Freezing and Thawing has two methods, A and B. Method A consists of freezing and thawing specimens in water, and Method B consists of freezing specimens in air and thawing them in water (*10*). The test can be conducted with concrete cylinder or prism specimens, although prism specimens are most commonly used (*1*). A freeze-thaw cycle is completed by lowering the specimen temperature from 40°F (4°C) to 0°F (−18°C) and raising it back to 40°F (4°C) within a 2- to 5-hr period. Specimen length change and a durability factor, calculated from the relative dynamic modulus of elasticity (ASTM C215), are determined from the test. Measurements are initially taken and repeated after every 36 cycles until completion. The test is completed after 300 cycles or until the modulus is reduced to 60 percent of the initial modulus, whichever occurs first.

Presently, standard specifications provide limited guidance on what constitutes good or bad performance. Except for ranking in relative order of frost resistance, no criteria have been established nationally for the acceptance or rejection of aggregates on the basis of ASTM C666 (*11*), although some states have established their own criteria. Furthermore, although this test better simulates the confining nature of mortar in concrete, aggregate evaluations may take nearly 5 months to complete (*5*).

Powers Slow Cool (ASTM C671)

In this test, concrete specimens are maintained in a constant temperature bath at 35°F (2°C) (*10*). Once every 2 weeks, the specimens are immersed in a water-saturated kerosene bath and the temperature is lowered from 35°F (2°C) to 15°F (−9°C) at the rate of 5 F° (2.8 C°) per hour. Length changes are measured continuously during cooling. After having cooled, the specimens are returned to the original water bath. Typical behavior consists of an initial decrease in specimen length with cooling, followed by some amount of expansion and then an additional decrease in length. The dilation is determined by measuring the difference between the length at maximum expansion and the projected length had the specimen continued to decrease in length rather than expanding. Dilation typically remains relatively constant for a number of cycles and then increases sharply (by a factor of two or more). Critical dilation is the dilation during the last cycle before the dilation begins to increase by a factor of two or more. The test is terminated once the specimens have exceeded critical dilation or until the specimens have completed a desired number of cycles. The number of cycles before critical dilation is termed the period of frost immunity. Some highly frost-resistant aggregates may never produce critical dilations.

As with the rapid freeze-thaw test, this test is time intensive and requires costly equipment.

VPI Single-Cycle Slow Freeze (12)

This test uses concrete specimens made and cured in accordance with ASTM C192. Stainless steel strain plugs are placed, 10 in. (25 cm) apart, into prisms. Initial measurements of transverse frequency, weight, and length are recorded. The specimens are then placed in a freezing apparatus with an air temperature of 0°F (−18°C). Length change measurements are made at 5- to 15-min intervals over a 4-hr cooling period.

From the results, two primary correlations are developed. The first is temperature versus length change. The minimum 5°F (2.8°C) temperature slope, b_1, is the minimum slope that can be found, within a 5°F (2.8°C) or more range, on the length change-temperature curve obtained during the first freeze of a specimen. The second correlation is time versus length change. The cumulative length change is plotted versus time, and the time slope, b_1, is determined as the minimum slope that can be found within a ⅓-hr or greater time range.

This test requires approximately 3 days to perform once curing has been completed. It produces fairly accurate distinctions between durable and nondurable aggregates. However, for aggregates of questionable durability, the rapid freeze-thaw test should be performed.

Aggregate Properties and Field Performance

The tests developed to correlate aggregate properties and field performance are easy to run, relatively quick, and with one

exception, require relatively inexpensive equipment. These tests include the following:

1. Mercury intrusion porosimeter,
2. Iowa pore index,
3. Absorption-adsorption, and
4. Petrographic analysis.

Mercury Intrusion Porosimeter

One of the primary methods of determining the pore size distribution of a porous solid is mercury porosimetry, which is based on a relation presented by Washburn (*13*). The mercury intrusion porosimeter apparatus has been used in many studies of the pore characteristics of aggregates (*4,5,14–17*). The nonwetting liquid is almost always mercury because of its low vapor pressure and relative inertness to chemical reaction with the aggregate, and because it is nonwetting for most surfaces (*14*). However, the problems with this test include the following:

1. Washburn's (*6*) equation is for pores that are cylindrical and interconnected. This is not normally the case with aggregate. The pore size distribution is weighted toward smaller pore sizes because the void volumes of pores with entrances narrower than the body, termed "ink-bottle pores," will be recorded according to the entrance size.
2. Values must be assumed for the contact angle and surface tension of the nonwetting liquid.
3. The sample size is small, usually 2 to 5 g. Therefore, the test may not yield a representative result, especially when the sample is from a heterogeneous source.
4. The equipment is expensive and requires special handling.
5. After testing, specimens may be considered hazardous waste because of mercury contamination.

Iowa Pore Index Test

The Iowa pore index test (IPIT) was developed on the basis of earlier evidence that D-cracking is related to freeze-thaw actions and, more specifically, to the pore sizes of coarse aggregate (*5*). The objective in developing the test was to readily identify a correlation between an aggregate's susceptibility to critical saturation and its potential to cause D-cracking (*1*).

The test procedure consists of placing a 9,000-g, oven-dried aggregate sample in a modified air pressure meter container, filling the container with water, and then applying 35 psi (242 kPa) of air pressure (*5*). The primary load is defined as the amount of water injected during the first minute. This reading corresponds to the filling of the aggregate's macropores. A large primary load is considered to indicate a beneficial limestone property.

The amount of water injected between 1 and 15 min is the secondary load and represents the quantity of water injected into the aggregate's micropore system. The secondary load is the pore index test result.

Aggregates with histories of producing D-cracking concrete have had pore index readings of 27 ml or more (*1,5*). After comparing the IPIT and the mercury intrusion porosimeter to aggregate field performance, Shakoor and Scholer (*16*) concluded that the pore index test is a reliable, less expensive, and quicker replacement for mercury intrusion porosimetry. They also stated that IPIT results are more representative of the parent rock because of the large sample volume used.

Other studies have found problems with the IPIT (*18,19*). These problems include variable and erroneous results for aggregates with reasonably rapid rates of early absorption and no discernible trends in the results from gravels. Furthermore, the IPIT cannot indicate to what extent a reduction in maximum aggregate size will improve performance, and the test does not discriminate between absorption by a few highly porous particles or absorption by many moderately porous particles.

Absorption-Adsorption

An extensive study of D-cracking by Klieger et al. (*20*) in Ohio included an attempt to develop a test that would distinguish between durable and nondurable aggregate and that would require a minimum amount of sample preparation, time, and test equipment. They developed an absorption-adsorption test and compared the test results to pavement service records.

After conducting this test with a large variety of aggregate sources, they concluded that the absorption-adsorption test tended to be overly conservative in its identification of durable and potentially nondurable aggregates. The test predicted poor freeze-thaw resistance for a large percentage of material from several sources with good service records.

Petrographic Analysis (ASTM C295)

Many studies of aggregate freeze-thaw resistance have incorporated petrographic analysis either to identify aggregate properties that affect concrete durability or to predict aggregate performance in freeze-thaw tests (*9,12,21–24*). Petrographic examination is a visual examination and analysis of aggregate in terms of both lithology and individual particle properties (*25,26*). It requires the skills of a well-trained and experienced petrographer. The examination uses small sample sizes, which require a large amount of work to provide accurate results (*26*). Also, the analysis is not able to provide definite specification limits because information so obtained is the result of subjective appraisal by the petrographer and can be reduced to a numerical quantity only through personal interpretation (*25*).

WASHINGTON HYDRAULIC FRACTURE TEST

This test method is based on the assumption that the hydraulic pressures expected in concrete aggregates during freeze-thaw cycling can be simulated by subjecting sample aggregates, submerged in water, to high pressures. As the external chamber pressure increases, the water penetrates into smaller and smaller pores. With adequate pressure, the water can penetrate pores in the size range associated with D-cracking. If

this external pressure is rapidly released, air compressed within any pores will tend to push the water back out, thereby simulating the internal pressures generated during freezing. Aggregate fracturing should result if the pressure in the pores cannot be dissipated quickly and the aggregate is unable to elastically accommodate the high internal pressure. As discussed, a pressure in the range of 1,050 psi (7240 kPa) is necessary to force water into the pore size range generally associated with D-cracking aggregates; this test procedure uses a pressure of 1,150 psi (7930 kPa).

The advantages of this test are as follows:

1. Theoretically, the test should be able to simulate the internal pressures that are believed to cause D-cracking in nondurable aggregates;
2. The escape path necessary for pressure dissipation could make this procedure sensitive to aggregate size, which is in agreement with field experience (*2*);
3. The cost for special equipment is relatively low (under $10,000);
4. Compared to most tests, this test is relatively fast (approximately 6 days are required for testing, with daily operator time under 1 hr per specimen) and, therefore, economical; and
5. The uniform pressure applied to individual aggregate particles within the chamber, along with standardization of the pressure and holding time, should make this test highly reproducible.

TESTING APPARATUS

The main part of the testing apparatus is the pressure chamber (Figure 1), which was developed from a commercially available membrane extractor at 100-bar (1,500-psi) pressure. A schematic of the apparatus is shown in Figure 2, and a pho-

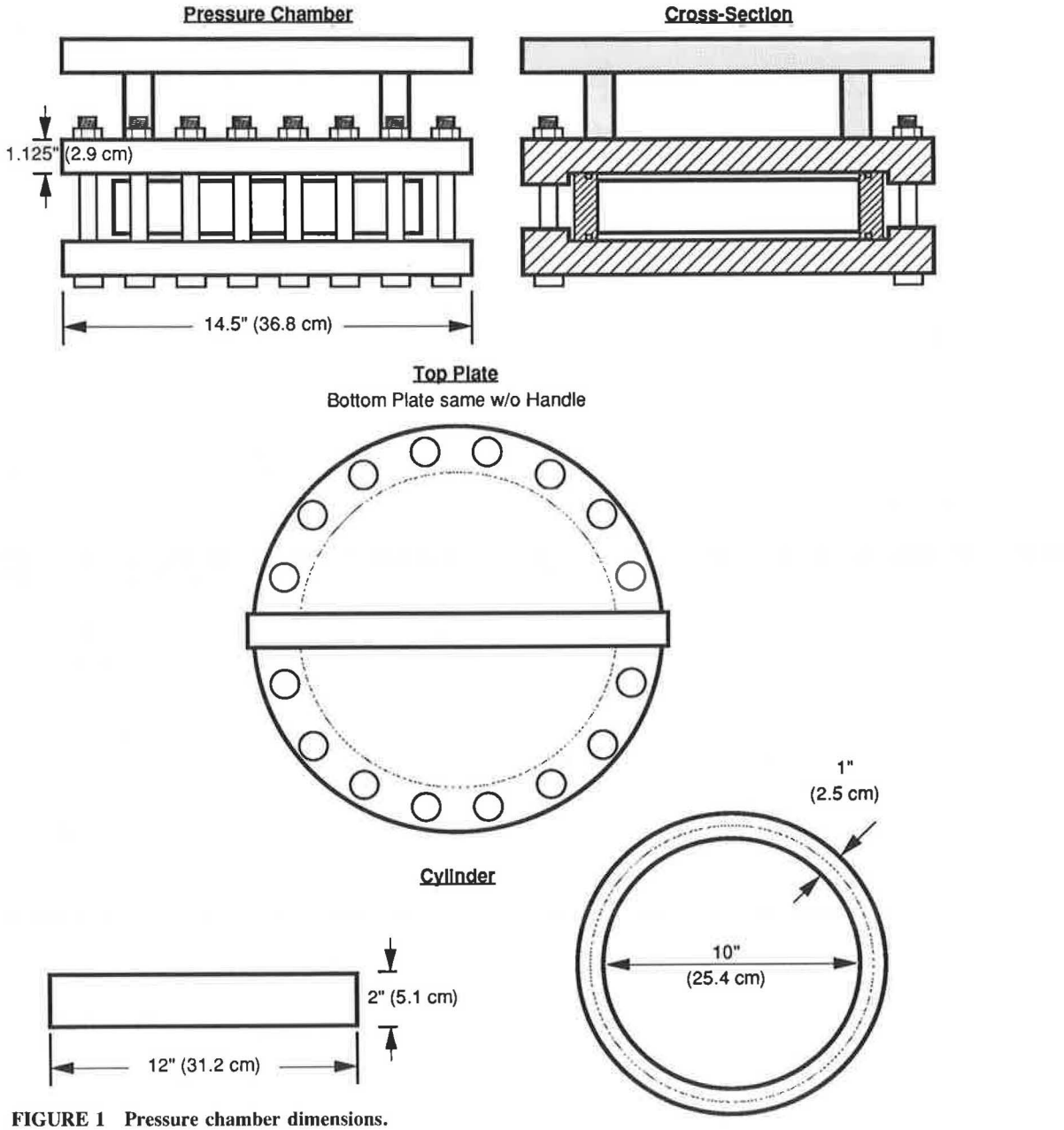

FIGURE 1 Pressure chamber dimensions.

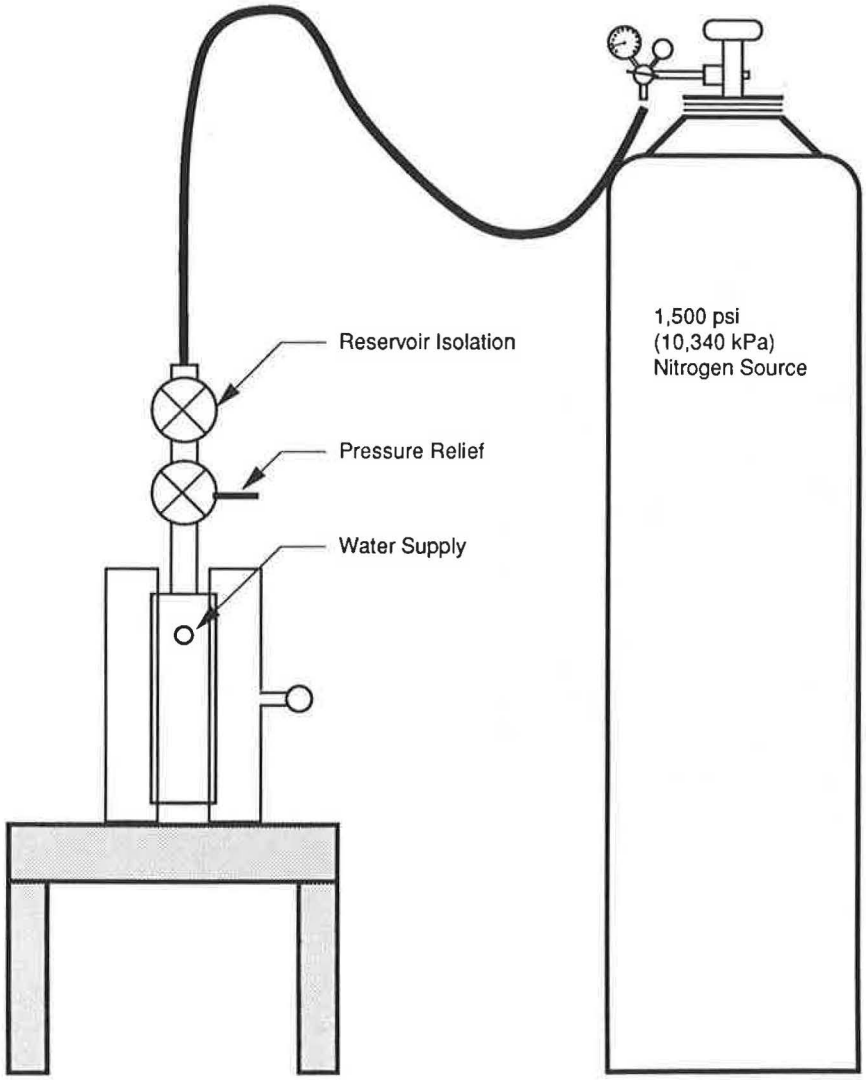

FIGURE 2 Equipment schematic.

tograph is shown in Figure 3. Full details of the testing apparatus have been presented elsewhere (*27,28*). Because the pressures used are quite high, 1,150 psi (7930 kPa), the authors do not recommend constructing the equipment from other than the commercially available pressure membrane extractor, unless appropriate pressure certification is obtained before the equipment is used.

TESTING PROCEDURE

The testing procedure consists of the following:

1. Placing a washed, oven-dried specimen of known mass, number of particles, and size range into the pressure chamber,
2. Bolting the chamber shut and filling it with water,
3. Applying an internal pressure of 1,150 psi (7930 kPa) to the chamber, and
4. Rapidly releasing the chamber pressure.

After 10 repetitions of Steps 3 and 4, the specimen is removed from the chamber, oven-dried, and counted. One day is required for specimen preparation, including washing, oven-drying, and grading. An additional day is needed for each 10 pressurization cycles (actual operator time is less than 1 hr per specimen per day), for a total of six required days. The result is an increase in the number of pieces larger than the No. 4 sieve, which is recorded as a percentage of the total number of initial pieces. This is termed the "percentage of fracture." Additional details on the testing procedure are presented elsewhere (*27,28*).

SPECIMEN SIZE

The pressure chamber is able to handle a sample size of approximately 3,200 g (7.0 lb), depending on the specimen particle shape and size range analyzed. This size is equivalent to approximately 450 pieces in the ½-in. (12.5-mm) to ¾-in. (19-mm) range and 125 to 225 pieces in the ¾-in. (19-mm) to 1¼-in. (32-mm) range. (The number of particles that can fit in the apparatus at one time is sensitive to particle angularity, especially at larger particle sizes.) Preliminary work suggests that a single filling of the chamber is sufficient for sizes

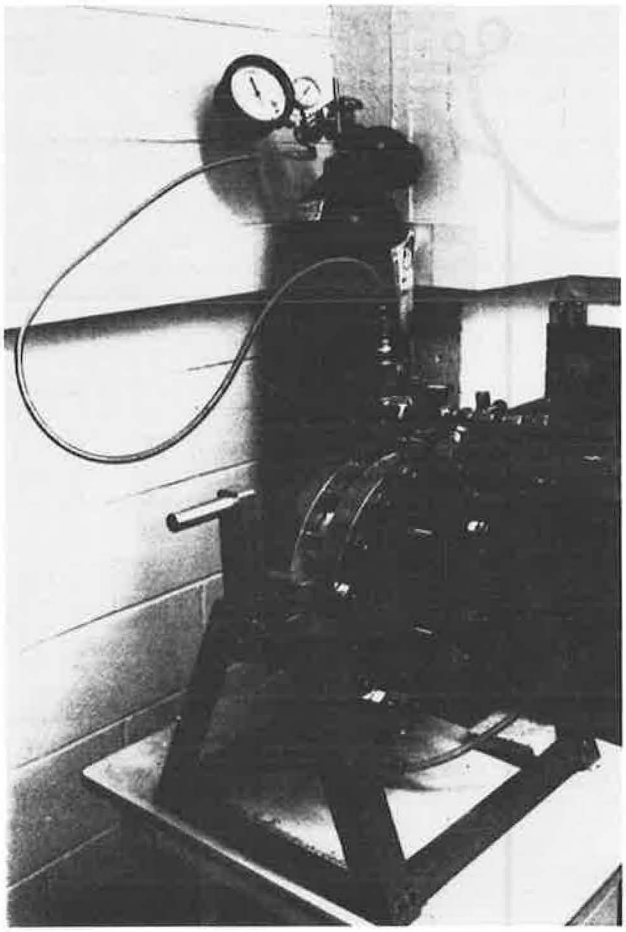

FIGURE 3 Photograph of equipment.

smaller than ¾ in. (19 mm), but combining results of multiple specimens is recommended for sizes larger than ¾ in. (19 mm) (*27*).

PROBLEMS WITH THE CURRENT PROCEDURE

The testing procedure depends on pressure forcing water into the aggregate pores, and then a release of the pressure from inside to outside the aggregate to create a sufficient critical gradient of pressure to cause fracturing. Winslow (*19*) pointed out that some aggregates absorb water extremely quickly. If an aggregate is at a relatively high degree of saturation before pressurization in the Washington hydraulic fracture procedure, the pressure gradient necessary for fracture after the pressure has been released may not develop. Modifications to the procedure are necessary to accommodate rapid-absorbing aggregates. Such a modification is described in the following sections.

MATERIALS

The aggregates tested in this comparison consisted of two gravels and two crushed limestones. One of the gravels and one of the limestones had histories of producing D-cracking in the field, and the other limestone and gravel produced durable concrete. The samples tested passed the 1¼-in (32-mm) and were retained on the ¾-in. (19-mm) sieve. The specific gravities and absorptions, along with the D-cracking susceptibilities of the four aggregates, are presented in Table 1.

Winslow absorption rates (*19*) are shown in Figure 4. Both gravels and one of the limestones (the non-D-cracking limestone) had similar absorption rates, whereas the other limestone (which is D-cracking susceptible) had a much higher absorption rate. Although absorption rate itself is not an indicator of D-cracking susceptibility (*19*), the higher absorption rate indicated possible problems with the results from the Washington hydraulic fracture test.

TESTING PROCEDURE

Two specimens of each of the four aggregates were tested according to the Washington hydraulic fracture test procedure. In addition, two specimens of each of the limestones were treated with a water-soluble silane-based sealer. The purpose of this treatment was to reduce the absorption rate of the rapidly absorbing limestone (ILA). The literature (*29*,*30*) suggests that the primary effect of the silane is to change the water-solid contact angle in the aggregate pores. This change does not affect the pore size, but it does affect the way surface tension absorbs water into the pore. Figure 5 is a plot of the absorption rates for the untreated and treated ILA limestone. As the figure shows, the absorption rate indeed decreased.

For comparison purposes, the slower absorbing limestone (ILB) was also treated. Almond (*27*) has shown that the treatment does not affect the fracture results of slow-absorbing

TABLE 1 SPECIFIC GRAVITIES AND ABSORPTIONS OF AGGREGATES TESTED

ID Number	Source	D-Cracking Suscept.	Apparent Specific Gravity	Absorption (percent)
ILA	Illinois Limestone	YES	2.70	1.46
ILB	Illinois Limestone	NO	2.69	0.92
MIA	Michigan Gravel	YES	2.76	1.15
MIB	Michigan Gravel	NO	2.72	1.06

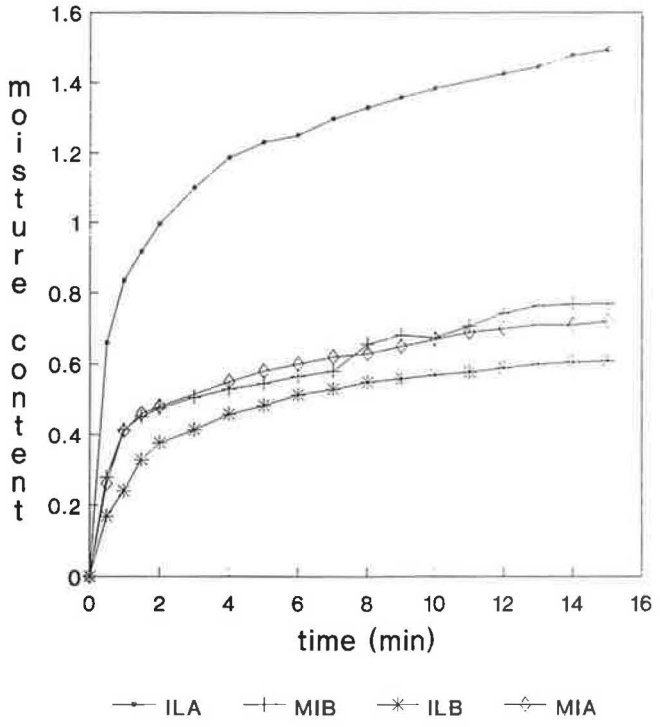

FIGURE 4 Winslow rapid absorptions (*19*).

aggregates. The treatment consisted of covering the washed and oven-dried specimens with the sealer solution, allowing the water in the sealer to evaporate at room temperature for 24 hr, and then oven-drying the specimens overnight. Testing was then continued in the normal Washington hydraulic fracture test procedure.

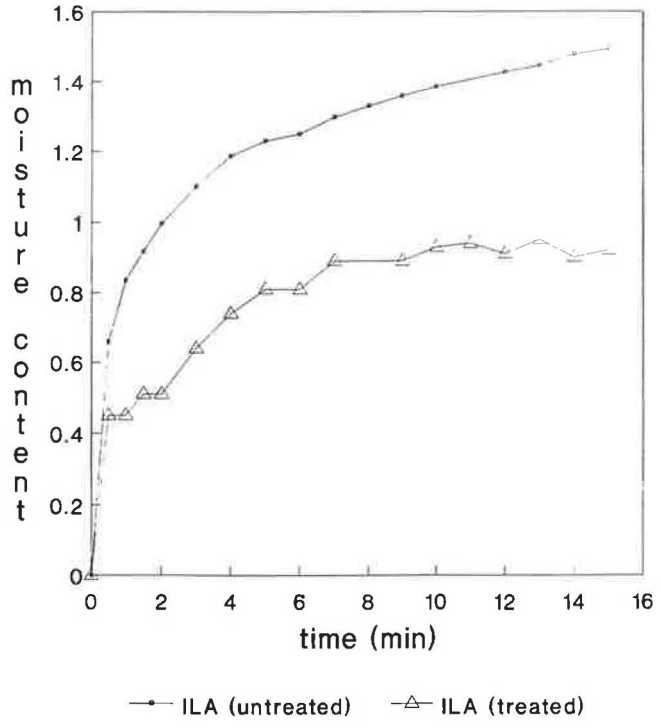

FIGURE 5 Winslow absorptions for untreated and treated ILA limestone (*19*).

RESULTS

Data

The total number of pieces counted after each series of 10 pressurization cycles for each duplication of the four aggregates is presented in Table 2. The numbers of pieces are given both for the plus ⅜-in. (9.5-mm) sieve and for the minus ⅜-in. (9.5-mm) sieve, and for the No. 4 sieve sizes. Material that passed the No. 4 sieve was not counted. The initial samples were all retained on the ¾-in. (19-mm) sieve. The results for the silane-treated limestones are also presented in Table 2. Table 3 gives the percentage of fractures for each series of 10 pressurization cycles for each of the aggregates. The results from the duplicate specimens were combined to determine these percentages. The percentage of fractures was calculated by dividing the number of additional pieces by the original number of aggregate pieces before any pressurization. This calculation is as follows:

$$FP_i = 100\ (n4_i + n_i - n_0)/n_0 \qquad (2)$$

where

FP_i = the percentage of fractures after i pressurization cycles,
$n4_i$ = The number of pieces that pass the ⅜-in. (9.5-mm) sieve but are retained on the No. 4 sieve after i pressurization cycles,
n_i = The number of pieces that are retained on the ⅜-in. (9.5-mm) sieve after i pressurization cycles, and
n_0 = The initial number of pieces tested.

Analysis

The effect of the silane treatment can be seen in Figure 6. Without treatment, the ILA aggregate (D-cracking susceptible) showed fracturing of less than about 6 percent after 50 pressurization cycles. With treatment, the fracturing increased to about 15 percent after 50 cycles. For this rapid-absorbing aggregate, the silane treatment appeared to increase the amount of fracturing, indicating that this aggregate was probably D-cracking susceptible. Without the treatment, the results indicated that the aggregate might not have D-cracking potential, which was contrary to field experience with this aggregate. Figure 7 shows the influence of the silane treatment on the non-D-cracking susceptible limestone. The treatment had almost no effect on this aggregate. This result agreed with previous work (*27*), which indicated that silane treatment of a non-D-cracking susceptible aggregate did not affect the amount of fracturing in the Washington hydraulic fracture test.

Figure 8 shows the combined results for all four aggregates tested. The two D-cracking susceptible aggregates showed similar fracture percentages, even though one was a limestone and one was a gravel. Both easily produced fracturing of greater than 10 percent in the 50 pressurization cycles. The two nonsusceptible aggregates showed similar results—fracturing of less than 5 percent in 50 pressurization cycles—

TABLE 2 PARTICLE COUNT RESULTS

Sample ID	Number of Cycles	+ 3/8 Pieces	- 3/8, + #4 Pieces
IL02A	0	135	0
	10	135	0
	20	135	0
	30	136	2
	40	136	3
	50	137	4
IL05A	0	150	0
	10	152	0
	20	152	2
	30	155	4
	40	156	5
	50	156	6
IL03A (Treated)	0	150	0
	10	155	6
	20	156	7
	30	156	9
	40	157	10
	50	158	15
IL04A (Treated)	0	150	0
	10	151	4
	20	156	12
	30	156	12
	40	156	12
	50	156	15
IL05B	0	200	0
	10	200	4
	20	201	6
	30	200	8
	40	200	8
	50	200	10
IL06B	0	200	0
	10	201	1
	20	201	2
	30	201	2
	40	201	4
	50	204	8
IL03B (treated)	0	200	0
	10	201	2
	20	201	2
	30	201	3
	40	201	3
	50	201	5
IL04B (Treated)	0	200	0
	10	200	0
	20	200	2
	30	201	2
	40	201	2
	50	201	5
MI06A	0	200	0
	10	209	14
	20	211	18
	30	211	23
	40	213	25
	50	214	30
MI08A	0	200	0
	10	200	4
	20	201	5
	30	201	9
	40	203	13
	50	205	22
MI01B	0	210	0
	10	210	0
	20	210	1
	30	211	2
	40	211	3
	50	211	6
MI03B	0	200	0
	10	202	1
	20	202	3
	30	203	3
	40	203	3
	50	203	3

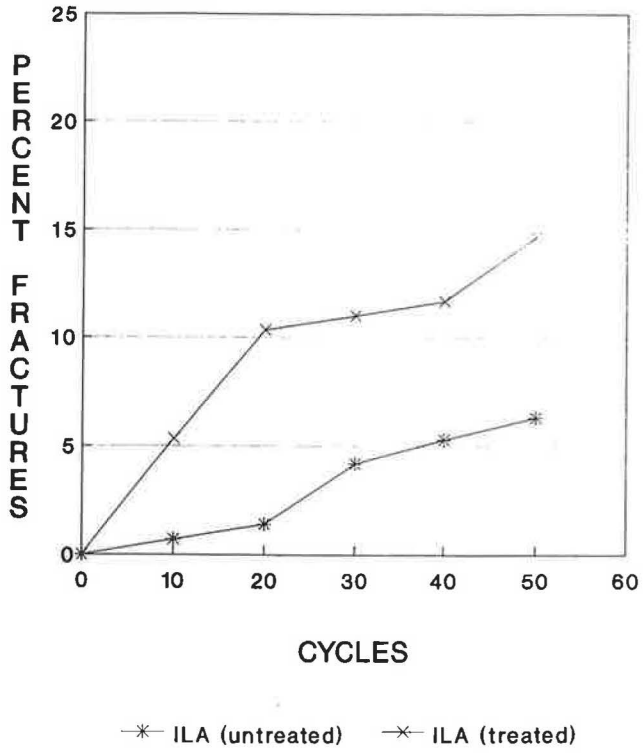

FIGURE 6 Comparison of treated and untreated ILA aggregate (D-cracking-susceptible limestone).

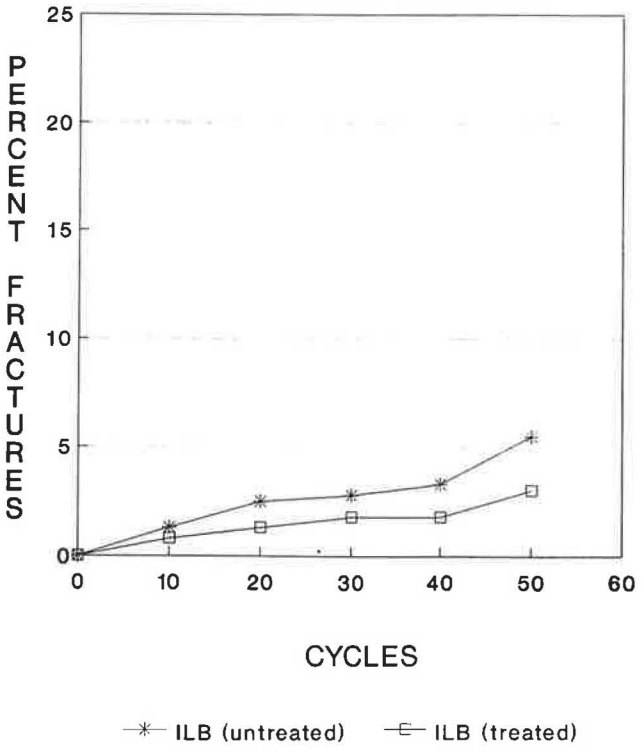

FIGURE 7 Comparison of treated and untreated ILB aggregate (non-D-cracking-susceptible limestone).

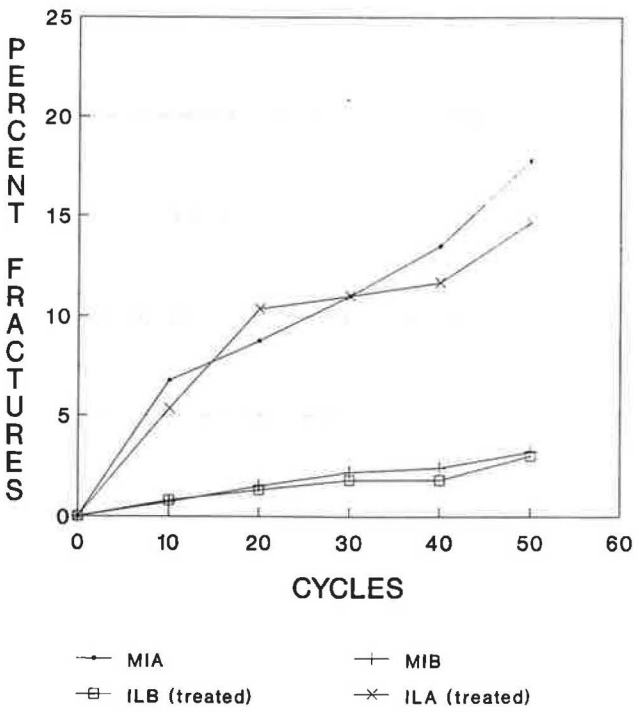

FIGURE 8 Comparison of four aggregates.

despite their different origins (one a gravel and one a limestone). The D-cracking susceptibility of the four aggregates tested was clearly indicated by the Washington hydraulic fracture test.

CONCLUSIONS AND RECOMMENDATIONS

The Washington hydraulic fracture test produces fracturing in concrete aggregates and produces substantially more fracturing in aggregates susceptible to D-cracking than in aggregates not susceptible to D-cracking. The procedure is not limited to relatively uniform aggregates, such as crushed limestones, but is also applicable to materials such as gravels from glaciated regions. The promising results from the tests of diverse aggregates support the validity of the mechanism used in the test procedure.

The major shortcoming of the test procedure, its inability to deal with rapidly absorbing aggregates, appears to be solved by use of a water-soluble, saline-based sealer. The assumed effect of the sealer treatment in reducing the surface tension absorption of water into the aggregate pores appears to allow the pressurization mechanism to function properly.

Ongoing research work is continuing to validate the procedure for a larger number of aggregates to determine pass or fail criteria (such as the number of cycles required to produce fracturing of 10 percent, or the total amount of fracturing produced at the end of 50 cycles), and to develop precision statements. Because of the pressures involved, building the equipment in-house is not recommended unless pressure certification is obtained for the finished equipment.

TABLE 3 PERCENT FRACTURE

Sample ID	Number of Cycles	Percent Fractures
ILA	10	0.7
	20	1.4
	30	4.2
	40	5.3
	50	6.3
ILA (Treated)	10	5.3
	20	10.3
	30	11.0
	40	11.7
	50	14.7
ILB	10	1.3
	20	2.5
	30	2.8
	40	3.3
	50	5.5
ILB (Treated)	10	0.8
	20	1.3
	30	1.8
	40	1.8
	50	3.0
MIA	10	6.8
	20	8.8
	30	11.0
	40	13.5
	50	17.8
MIB	10	0.7
	20	1.5
	30	2.2
	40	2.4
	50	3.2

REFERENCES

1. D. Schwartz. *NCHRP Synthesis of Highway Practice 134: D-Cracking of Concrete Pavements*. TRB, National Research Council, Washington, D.C., 1987.
2. D. Stark and P. Kleiger. Effects of Maximum Size of Coarse Aggregate on D-Cracking in Concrete Pavements. In *Highway Research Record 441*, HRB, National Research Council, Washington, D.C., 1973, pp. 33–43.
3. Bjegovic, D. Mikulic, and V. Ukraincik. Theoretical Aspect and Methods of Testing Concrete Resistance to Freezing and Deicing Chemicals. *Concrete Durability SP 100*, Vol. 1, 1987, pp. 947–971.
4. M. Kaneuji, D. N. Winslow, and W. L. Dolch. The Relationship Between An Aggregate's Pore Size Distribution and Its Freeze Thaw Durability in Concrete. *Cement and Concrete Research*, Vol. 10, 1980, pp. 433–441.
5. V. J. Marks and W. Dubberke. Durability of Concrete and the Iowa Pore Index Test. In *Transportation Research Record 853*, TRB, National Research Council, Washington, D.C., 1982, pp. 25–30.
6. E.W. Washburn. Note on a Method of Determining the Distribution of Pore Sizes in a Porous Material. *Proc., National Academy of Sciences*, Vol. 7, 1921, pp. 115–116.
7. T. Larson, P. D. Cady, M. Franzen, and J. Reed. *Special Report 80: A Critical Review of Literature Treating Methods of Identifying Aggregates Subject to Destructive Volume Change When Frozen in Concrete and a Proposed Program of Research*. HRB, National Research Council, Washington, D.C., 1964.
8. S. R. Thompson, M. P. Olsen, and B. J. Dempsey. *D-Cracking in Portland Cement Concrete Pavements*. Synthesis Report, Transportation Engineering Series No. 29. Department of Civil Engineering Experiment Station, University of Illinois, Urbana, June 1980.
9. T. D. Larson and P. D. Cady. *NCHRP Report 66: Identification of Frost-Susceptible Particles in Concrete Aggregates*. HRB, National Research Council, Washington, D.C., 1969.
10. *Annual Book of ASTM Standards, Volume 04.02, Concrete and Aggregates*. ASTM, Philadelphia, Pa., 1990.
11. V. Sturrup, R. Hooton, P. Mukherjee, and T. Carmichael. Evaluation and Prediction of Concrete Durability—Ontario Hydro's Experience. *Katharine and Bryant Mather International Symposium on Concrete Durability, SP-100*, American Concrete Institute, Detroit, Mich., Vol. 2, 1987, pp. 1121–1154.
12. R. D. Walker. *NCHRP Report 12: Identification of Aggregates Causing Poor Concrete Performance When Frozen*. HRB, National Research Council, Washington, D.C., 1965.
13. W. L. Dolch. *Porosity*. Special Technical Publication 169B. ASTM, Philadelphia, Pa., 1978, pp. 646–656.
14. D. N. Winslow and S. Diamond. A Mercury Porosimetry Study of the Evolution of Porosity in Portland Cement. *Journal of Materials*, Vol. 5, No. 3, Sept. 1970, pp. 564–585.
15. C. L. Hiltrop and J. Lemish. Relationship of Pore-Size Distribution and Other Rock Properties to Serviceability of Some Carbonate Aggregates. *Bulletin 239*, HRB, National Research Council, 1960, pp. 1–23.
16. A. Shakoor and C. F. Scholer. Comparison of Aggregate Pore Characteristics as measured by Mercury Intrusion Porosimeter and Iowa Pore Index Tests. *Journal of the American Concrete Institute*, Vol. 82, July/Aug. 1985, pp. 453–458.
17. R. D. Walker and T. Hsieh. Relationship Between Aggregate Pore Characteristics and Durability of Concrete Exposed to Freezing and Thawing. In *Highway Research Record 226*, HRB, National Research Council, Washington, D.C., 1968, pp. 41–49.

18. M. L. Traylor. Efforts to Eliminate D-Cracking in Illinois. In *Transportation Research Record 853*, TRB, National Research Council, Washington, D.C., 1982, pp. 9–14.
19. D. N. Winslow. The Rate of Absorption of Aggregates. *Cement, Concrete, and Aggregates*, Vol. 9, No. 2, 1987, pp. 154–158.
20. P. Klieger, G. Monfore, D. Stark, and W. Teske. *D-Cracking of Concrete Pavements in Ohio*. Ohio-DOT-11-74. 1974.
21. J. W. Harman, P. D. Cady, and N. B. Bolling. Slow-Cooling Tests for Frost Susceptibility of Pennsylvania Aggregates. In *Highway Research Record 328*, HRB, National Research Council, Washington, D.C., 1970, pp. 26–37.
22. T. D. Larson, A. Boettcher, P. Cady, M. Franzen, and J. Reed. *NCHRP Report 15: Identification of Concrete Aggregates Exhibiting Frost Susceptibility*. HRB, National Research Council, Washington, D.C., 1965.
23. W. K. Mysyk. Petrological Studies on Carbonate Aggregate Responsible for Pavement D-Cracking in Southern Manitoba, Canada. In *Transportation Research Record 1110*, TRB, National Research Council, Washington, D.C., 1987, pp. 10–15.
24. R. D. Walker, H. J. Pence, W. H. Hazlett, and W. J. Ong. *NCHRP Report 65: One-Cycle Slow-Freeze Test For Evaluating Aggregate Performance In Frozen Concrete*. HRB, National Research Council, Washington, D.C., 1969.
25. R. Rhoades and R. C. Mielenz. Petrography of Concrete Aggregate. *Journal of the American Concrete Institute*, Vol. 17, No. 6, June 1946, pp. 581–600.
26. ACI Committee 621. Selection and Use of Aggregates for Concrete. *Journal of American Concrete Institute*, No. 58–24, Nov. 1961, pp. 513–541.
27. D. K. Almond. *A Test for Identifying Aggregates Susceptible to Freeze-Thaw Damage*. Masters' thesis. University of Washington, Seattle, June 1990.
28. D. K. Almond and D. J. Janssen. The Washington Hydraulic Fracture Test for Concrete Aggregates Exposed to Freezing and Thawing. Supplementary Paper, 2nd CANMET/ACI International Conference on Durability of Concrete, Montreal, Canada, 1991.
29. W. F. Perenchio. Durability of Concrete Tested with Silanes. *Concrete International*, Nov. 1988, pp. 34–40.
30. CHEM-TRETE Product Literature. HULS-06-SIW 50M I89, Hüls America, Inc., Piscataway, N.J., 1988.

Publication of this paper sponsored by Committee on Mineral Aggregates.

Micro-Deval Test for Evaluating the Quality of Fine Aggregate for Concrete and Asphalt

C. A. ROGERS, M. L. BAILEY, AND B. PRICE

The sulfate soundness test has been used for many years for evaluating the physical suitability of fine aggregate. This test suffers from poor within-laboratory and multilaboratory precision; it is a time-consuming and expensive test. The work described here was an evaluation of alternative tests for measuring soundness of fine aggregate. The tests studied were the attrition test and a modified version of the French micro-Deval test usually used for coarse aggregate. The micro-Deval test was found to have a significant correlation with magnesium sulfate soundness loss and water absorption of fine aggregate. Unlike the attrition test, the micro-Deval test is relatively insensitive to the gradation of the sand being tested and has excellent precision. The test is conducted by placing 500 g of water-saturated sand in a ball mill with 1250 g of 9.5-mm steel balls and 750 ml of water. The mill is rotated at 100 rpm for 15 min. The aggregate is washed over a 75-μm sieve and the loss is calculated as a mass percent of the original oven-dry weight. The test may be completed in less than 48 hr. Aggregates that give more than 25 percent loss are judged to be marginal for use in portland cement concrete and asphaltic concrete. The Ontario Ministry of Transportation has adopted the micro-Deval test for measuring the quality of fine aggregate for concrete and asphalt.

In many areas of North America, especially near urban areas, it is recognized that construction aggregates are a depleting resource. The sterilization of resources by restrictive zoning regulations, building development, and "not in my back yard" (NIMBY) groups further contribute to shortages of moderate-cost aggregates. As a result, there is often pressure to use lower-quality or marginal-aggregate sources. At the same time, there is a demand from engineers to use higher-quality aggregates than were used in the past. For instance, where higher truck tire pressures and axle loads are causing rutting of asphalt pavements made with natural sand and gravel aggregates, the solution is to use quarried aggregates, excluding some traditional sources. Higher traffic volumes call for the use of pavement surfacing aggregates of better frictional properties, again excluding some traditional sources. There is, thus, a conflict between development, which tends to reduce aggregate resources, and an increasing demand for high-quality aggregates as a result of this development.

Aggregate testing and evaluation procedures and specifications have not kept pace with the modern technology. Some of the testing procedures used today are not necessarily the best available for the evaluation of the suitability of aggregates. Aggregates are often rejected for certain uses when they fail to meet one or more specifications, yet the actual field performance in concrete or asphalt may be satisfactory. The automatic rejection of aggregates that fail to meet existing specification requirements can lead to a reduction in available aggregate resources. The use of tests with an improved correlation with field performance and better precision than some of the current tests would allow the selection of some of the so-called marginal aggregates with greater assurance that they will be suitable.

One of the most commonly used aggregate tests in North America is the magnesium sulfate soundness test. The forerunner of the present magnesium sulfate soundness test was developed in 1828. The purpose was to simulate the forces generated by freezing water in building stone. In the early 19th century, there was no means of freezing water in the laboratory so this test served well. The magnesium sulfate soundness test has been used for many years for testing fine aggregate. On fine aggregate, the sulfate soundness test unfortunately has poor multilaboratory precision. In repeated studies of the multilaboratory variation in five Ministry of Transportation laboratories, it was found (*1*) that the average coefficient of variation was 10.5 percent, and the 95 percent difference limits were 30 percent (over a range in values from 7 to 22 percent loss). In other words, in repeated testing of a sand with an average loss of 16 percent, the range in values reported by various laboratories will be from 13.6 to 18.4 percent, 19 times in 20. ASTM (C 88) does not give precision data for the fine aggregate test, but notes that: "Since the precision of this test method is poor . . . it may not be suitable for outright rejection of aggregates without confirmation from other tests more closely related to the specific service intended."

In the late 1970s, work by the Ontario Ministry of Transportation found a significant correlation ($r = 0.68$) between the wet attrition test of Davis et al. (*2*) and sulfate soundness loss of fine aggregates (*3*). In the late 1980s, it was decided to study this relationship further in the testing program reported in the following sections. It was thought that wet abrasion or attrition tests would be more precise than the sulfate soundness test, be quicker, and measure more or less the same properties as the sulfate soundness test. A number of wet abrasion tests were selected for study.

TESTING PROGRAM

ASTM Attrition Test

This test has been adopted by ASTM (C 1137–90). It consists of placing a washed, graded, 500-g sample of sand in an eight-

Ministry of Transportation, 1201 Wilson Ave., Downsview, Ontario, M3M 1J8, Canada.

sided container where it is subjected to vigorous abrasive action with a high-speed impeller at 850 rpm in the presence of 175 ml of water. Loss is measured by the decrease in fineness modulus or the increase in the amount of material passing the 75-μm sieve. In this study, the ASTM procedure was used with a WEMCO impeller and tank with the following modifications: test duration was extended from 6 to 10 min because 6 min seemed somewhat arbitrary and causing significant loss in the test was desired. The sands were washed over a 75-μm sieve and dried before testing but were not graded to a standard grading. Change in fineness modulus (FM) was not reported.

MTO Attrition Test

This test is similar to the ASTM attrition test. It has been used by the Ministry of Transportation Ontario (MTO) for 10 years for evaluating the objectionable mud-producing properties of sand spread on icy road surfaces (*3*). The impeller device, more robust than that used in the ASTM procedure, was that specified by Davis et al. (*2*). A 500-g sample was tested in 175 ml of water for 10 min at an impeller speed of 390 rpm. This speed was adopted several years ago because the 850 rpm originally used by Davis et al. (*2*) was found to cause excessive splashing.

Micro-Deval Abrasion Test

This test has been developed in France (*4–6*) for the evaluation of coarse aggregate. It has since been adopted in the province of Québec (*7*). It consists of abrading a sample of 500 g of stone with 5000 g of 9.5-mm-diameter steel balls and 2.5 L of water in a 5-L steel jar, 200 mm in diameter. The jar is rotated at 100 rpm for 2 hr. Loss is measured by measuring the amount of material passing a 1.25-mm sieve. For testing fine aggregate, the test was modified as follows: A 700-g sample of sand was washed on a 75-μm sieve and oven-dried. A representative oven-dry subsample of 500 ± 5 g was prepared and immersed in tap water at room temperature for 24 hr. Excess water was poured off and the sample placed in a steel jar with 1250 g of steel balls and 750 ml of water. The jar was rotated at 100 rpm for 15 min. The sample was washed over a 75-μm sieve and oven-dried to constant mass. Loss was expressed as percent by mass of the original sample mass.

Samples were also tested to determine their gradation, absorption, relative density, and loss in the magnesium sulfate soundness test.

SAMPLE COLLECTION

Ideally, it would have been desirable to test a group of samples that had a field performance history ranging from good to bad. After over 40 years of experience, the Ministry of Transportation has never used a fine aggregate that caused or resulted in premature failure of concrete or asphalt that could be attributed to inadequate physical properties measured by the sulfate soundness test. Asphalt pavements have failed because of unsatisfactory fine aggregate particle shape or unsatisfactory grading. Concrete has failed because of some alkali-silica reactive component in the sand, poor grading, or the presence of objectionable quantities of organic acids. It has not been possible to attribute failure to an unsatisfactory property measured in the sulfate soundness test. Fine aggregates that had a sulfate soundness loss of up to 45 percent have occasionally been used in asphaltic concrete without apparent failure. This experience created a problem in devising a satisfactory sampling system.

A number of natural sands and crusher screenings that are used in Ontario exceed the sulfate soundness requirements for various applications. The Ministry of Transportation has specifications for maximum magnesium sulfate soundness loss for concrete and asphalt fine aggregate. The limit for portland cement concrete and high-quality asphaltic concrete use is a maximum of 16 percent loss, and 20 percent for lower-quality asphaltic concrete use. The specifications allow these limits to be exceeded if satisfactory field performance of concrete or asphalt and results of accelerated freeze-thaw testing of concrete can be shown to be satisfactory. For instance, natural sands found in the vicinity of the Niagara Escarpment typically contain large amounts of cemented particles and porous sandy carbonates that result in sulfate soundness losses of up to 25 percent. These sands perform well in asphalt and concrete and are approved and used for these applications (*8*). In 1989, a portland cement concrete supplier in Eastern Ontario was able to demonstrate that a natural sand performed well in field concrete and in accelerated laboratory tests. Despite sulfate soundness losses of up to 25 percent this material was approved for use in Ontario highway work. There are other examples, particularly with the crusher screenings from carbonate quarries that typically yield high sulfate soundness losses, yet perform well in asphaltic concrete. The reason for their high losses is not exclusively caused by any large amount of weak or otherwise unsound particles but is partly caused by the coarseness of gradation of these screenings, which in the test calculations, can unfairly penalize them. New York State has also recognized this problem with coarse sands giving high sulfate losses, and now calculates loss in this test using a standard grading, irrespective of the grading of the sand tested.

In order to aid in setting specification limits for any new test that was adopted as a substitute for the sulfate soundness test, testing those sands that had a record of satisfactory field performance but exceeded the current specification limits was desired. A suite was selected of about 110 samples of fine aggregate that had a history of satisfactory performance in portland cement concrete or asphaltic concrete, or both. These samples were selected and sampled by highway engineers in the five administrative regions in Ontario. The location and nature of the samples tested are described elsewhere (*9*). The samples consisted of 86 natural sands and 21 quarry screenings. The quarry screenings were nearly all from Paleozoic carbonate quarries in southern Ontario. The natural sands consisted either of 100 percent of siliceous particles of Precambrian age from northern Ontario, or mixtures of Precambrian siliceous particles and Paleozoic sediments (carbonate, siltstone, sandstone, sandy carbonate, and shale) found in southern Ontario.

RESULTS AND DISCUSSION

The first task was an investigation of the influence of sample grading on degradation in the wet attrition and abrasion tests. A good-quality natural sand and crusher screenings from a

shaley limestone quarry were prepared to four different gradings. The FM varied from 2.15 to 3.77. Samples of these materials were then tested in the ASTM and MTO attrition tests and the micro-Deval test. Results are shown in Figures 1 and 2. For the case of the attrition tests, the finer graded samples gave significantly lower losses than the coarse samples. In these tests, it is postulated that the larger particles have greater kinetic energy than the smaller particles, which led to greater disintegration on impact with the walls of the container. Alternatively, larger particles may simply be less resistant to damage than smaller particles. This observation indicated that, in future development, samples should be tested at a standard grading to remove the bias introduced by either coarser or finer gradings.

In contrast, the micro-Deval test demonstrated a negligible or reverse response. The finer the grading of the sample, the greater the loss. This influence of grading was relatively small at low losses (<20 percent), but became more obvious with higher-loss materials. This test is conducted at low speed in contrast to the attrition test. The particles have little kinetic energy and the main means of disintegration is a grinding action between the particles and between the particles and the steel balls. In this case, it would be expected that the amount of breakdown would be a direct function of energy

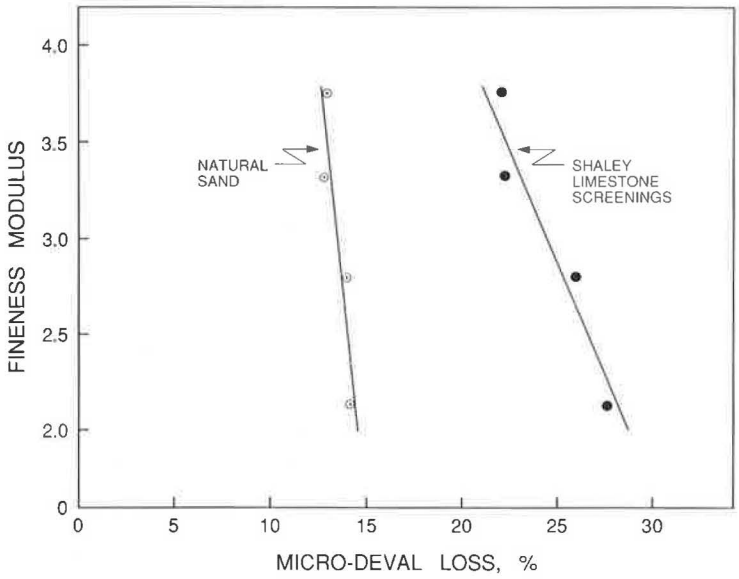

FIGURE 1 Attrition loss versus fineness modulus of sand and screenings.

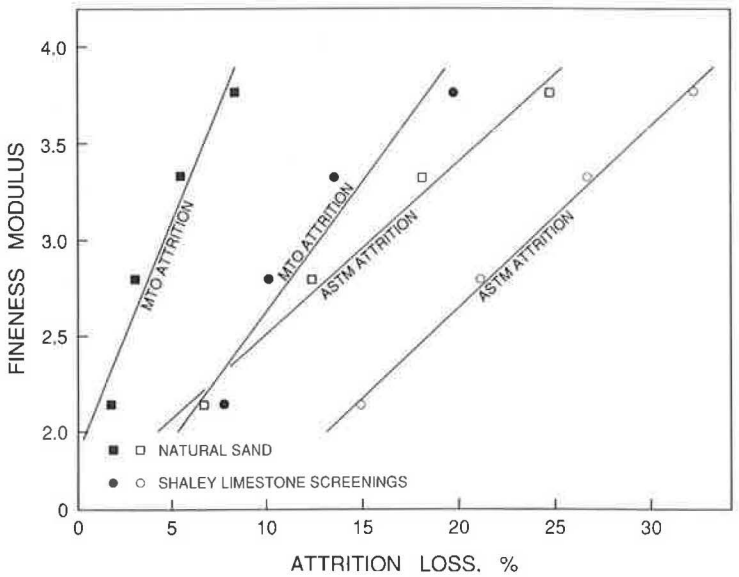

FIGURE 2 Micro-Deval loss versus fineness modulus of sand and screenings.

expended and also the original size of the particles. Less work has to be done on a fine than on a coarse graded sample to cause material to break down to pass the 75-μm sieve. This observation was confirmed by testing a further eight different materials at the four different gradings.

The within-laboratory variability of the three tests was determined by testing 10 replicate samples of natural sand and shaley limestone screenings. The results are presented in Table 1. The ASTM attrition tests gave the highest loss with the shaley limestone, but also had a wide variation. With the low-loss natural sand, the MTO attrition test has the widest variation, but this is mainly because of the low mean loss of 4.1 percent obtained in this test with this material, which distorts variability when using coefficient of variation. The micro-Deval test had the lowest within-laboratory variation of about 1 to 2 percent.

The micro-Deval test was thus found to be relatively insensitive to sample grading and also to have the lowest within-laboratory variation. These two attributes are much desired. The requirement to prepare samples to a standard grading before testing is time consuming and expensive. In the case of very fine or very coarse materials, large amounts of material must be sieved to obtain the desired standard grading. In some cases, such as with fine sands, it is difficult to obtain enough coarse material to make up a sample to a standard grading. In any event, such a sample can hardly be representative.

In order to investigate likely multilaboratory variation in the micro-Deval test, an experiment was devised. Replicate samples of 58 different materials were tested in different equipment at different times by different technicians. The micro-Deval loss of the materials ranged from 5 to 31 percent; the average coefficient of variation was 3.2 percent. In practical terms, this means that testing of replicate samples of a material with a mean loss of 20 percent in different laboratories should give results between 18.2 and 21.8 percent, 95 percent of the time. This variation is wider than that found in the within-laboratory investigations (Table 1) but it is still excellent compared to many other materials tests.

In spite of the marked effect of grading on loss in the attrition tests, they were conducted without using a standard grading. The samples were washed, dried, and prepared to 500 g, but no attempt was made to grade the material to a constant grading. It was desired to see if, despite the effect of grading on loss, any useful relationship existed between these tests. Figure 3 shows the relationship between the ASTM and MTO attrition tests. As should be expected, there is an excellent correlation, but there is a marked difference in performance in the two tests. On average, there is about 3 times more loss in the ASTM attrition test. This is because of the higher speed of the impeller (850 rpm) in this test compared to the MTO test (390 rpm). Over the course of testing the 110 samples, there was considerable wear on the ASTM impeller and this had a marked effect on loss in the test. After every 10 samples were tested, a replicate sample of laboratory sand was tested. There was a consistent and gradual reduction in loss in this test from the start of the program to completion, from 42 to 36 percent loss for shaley limestone screenings and from 16 to 12 percent with natural sand. After 110 samples had been tested, a new impeller was fitted to the ASTM attrition device, and loss of these materials increased to the original values of 42 and 16 percent. In any future development of the ASTM attrition test, this problem will have to be compensated for. Because more robust blades are mounted on the impeller, the MTO attrition test did not show this problem, and results of testing replicate samples remained consistent throughout the program.

Figure 4 shows the relationship between the ASTM attrition test and magnesium sulfate soundness loss. There is a significant correlation both for natural sands and screenings. The attrition loss of the screenings was considerably greater than that for natural sands, probably because of the coarser gradation of screenings compared with natural sands. Had testing been conducted at constant grading, such a marked difference would probably not have been observed. However, there is a relationship that could be used to predict sulfate soundness loss.

The relationship between micro-Deval and magnesium sulfate soundness loss of all samples is shown in Figure 5, that for concrete sands in Figure 6, and that for asphalt sands and screenings in Figure 7. There is excellent correlation for both natural sands and for crusher screenings. In Figures 6 and 7, proposed new requirements are shown for various applications. They will replace the existing magnesium sulfate soundness specifications. In Figure 7, the proposed requirement for hot-laid (HL) 1 and 3 fine aggregates refers to the highest-quality asphaltic concrete used exclusively for surface courses. The requirements for HL 2, 4, and 8 refer to lower-quality asphaltic concrete used in surface courses on secondary highways and in binder courses. In May 1990, on an experimental basis, these requirements were adopted for some Ontario highway contracts. Adoption of these new criteria will result in the acceptance of some materials that had previously not met the soundness requirements. This is intentional. At the time materials were selected for sampling, it was specified

TABLE 1 WITHIN-LABORATORY VARIABILITY OF ATTRITION AND MICRO-DEVAL TESTS

	NATURAL SAND		SHALEY LIMESTONE SCREENINGS	
	Mean loss	C of V.	Mean loss	C of V.
micro-Deval	13.8%	1.9%	23.4%	1.1%
ASTM Attrition	13.3%	11.0%	38.8%	6.8%
MTO Attrition	4.1%	14.1%	20.1%	5.4%

Number of replicates = 10, C of V = coefficient of variation

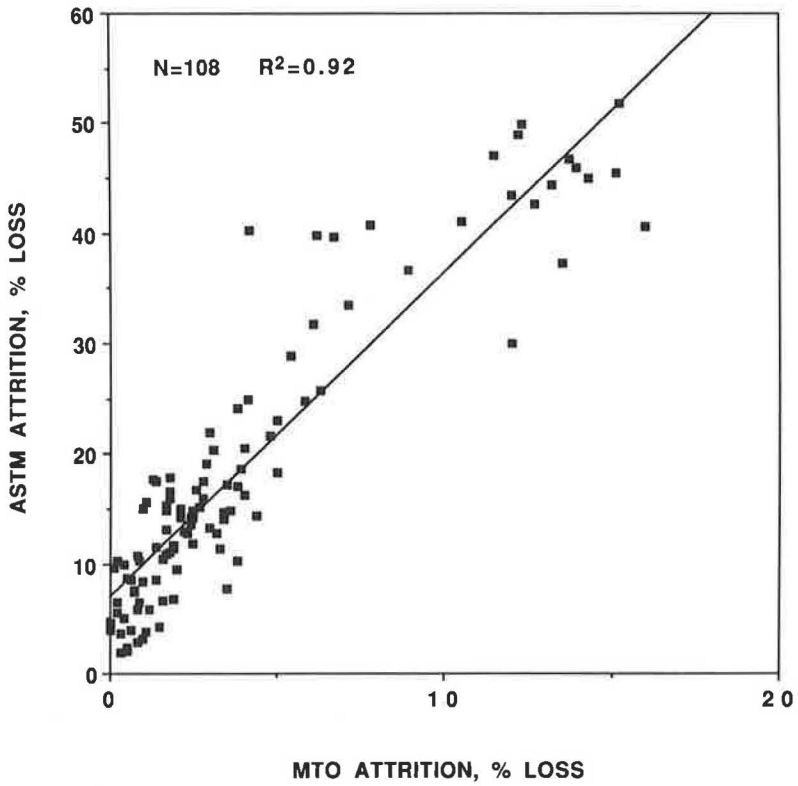

FIGURE 3 ASTM attrition loss versus MTO attrition loss for sands and screenings.

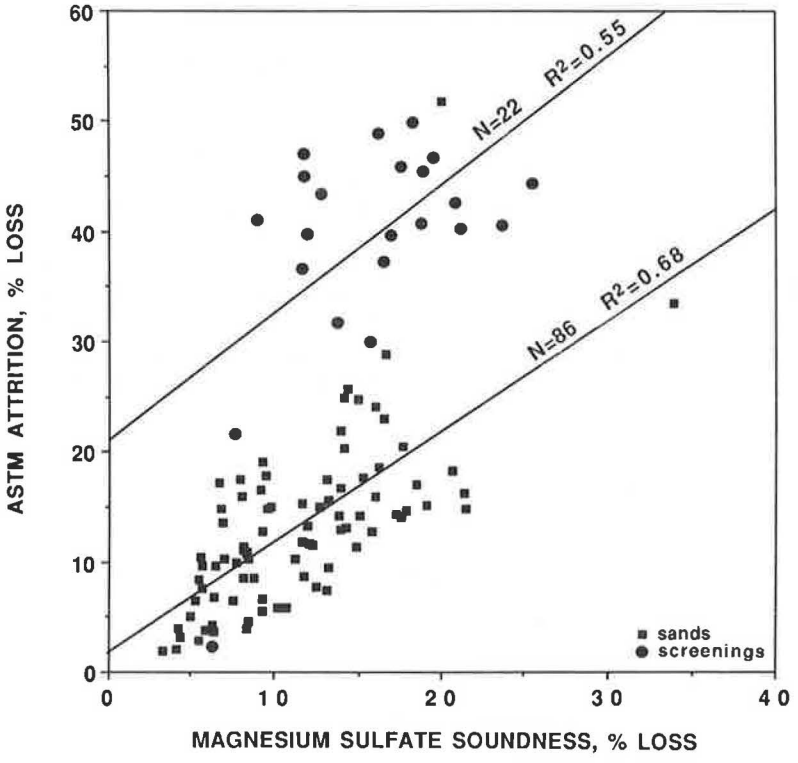

FIGURE 4 ASTM attrition loss versus magnesium sulfate soundness loss.

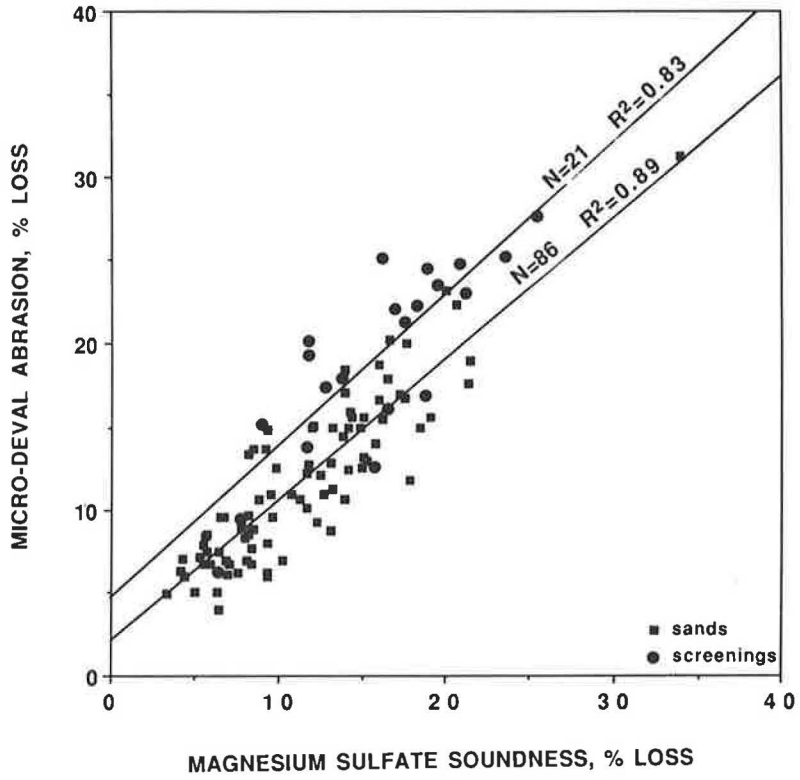

FIGURE 5 Micro-Deval abrasion loss versus magnesium sulfate soundness loss for sands and screenings.

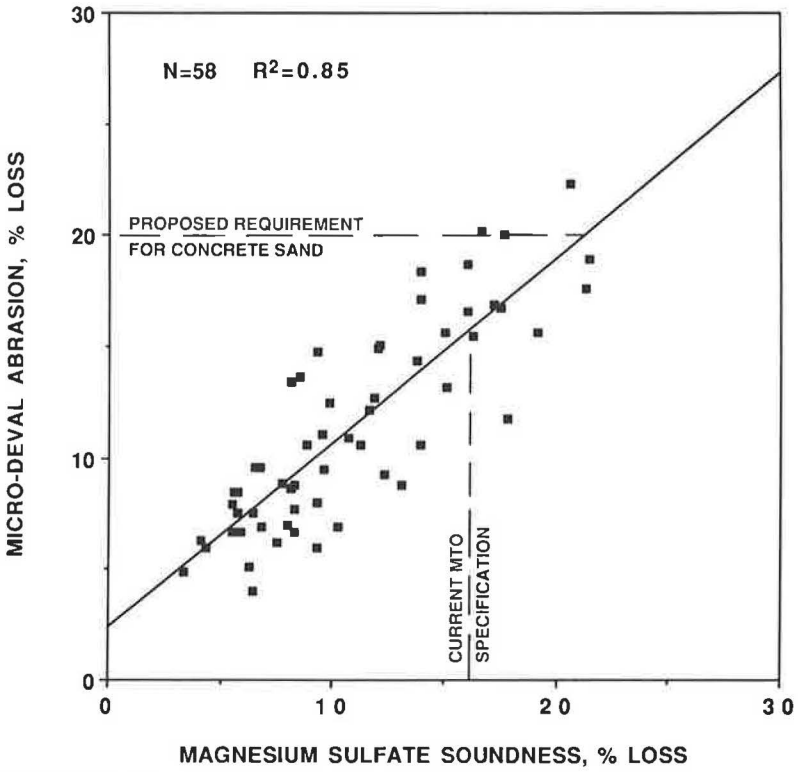

FIGURE 6 Micro-Deval abrasion loss versus magnesium sulfate soundness loss for concrete sands.

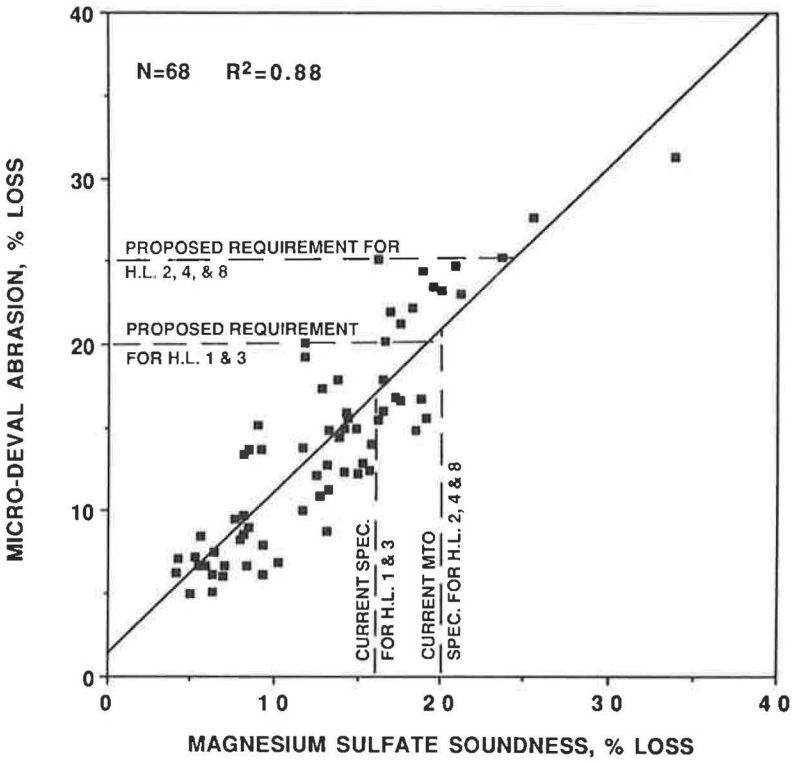

FIGURE 7 Micro-Deval abrasion loss versus magnesium sulfate soundness loss for asphalt sands and screenings.

that the materials should be those currently used on MTO work, even if they exceeded the current soundness specifications. These materials had a record of having been used without any known or obvious deleterious effect, so an adjustment to selection criteria is justified.

In order to see how reliable the micro-Deval test was at measuring the quantity of low-quality material in an otherwise satisfactory sand, a low-strength, slaking shale (Queenston) was oven-dried, crushed, and sieved. This shale was then blended with a high-strength quartz sand (from Ottawa, Illinois) at various levels of substitution. The results, shown in Figure 8, indicated an excellent relationship between amount of shale and loss in the test.

Significant correlation was found between water absorption and performance in the various tests. In the wet attrition/abrasion tests, this is probably partly caused by a slaking effect. Material that is susceptible to slaking has a high microporosity (shales, clays, and shaley limestones). The more po-

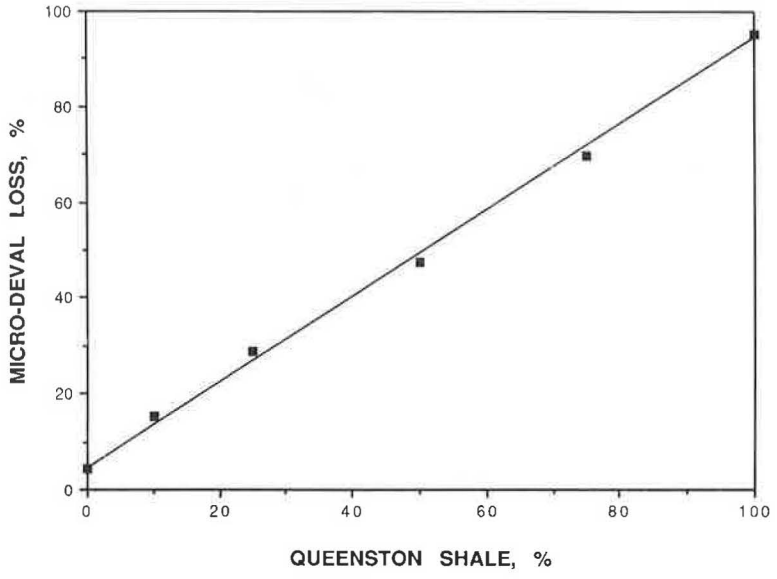

FIGURE 8 Micro-Deval loss versus amount of low-strength Queenston shale in quartz sand.

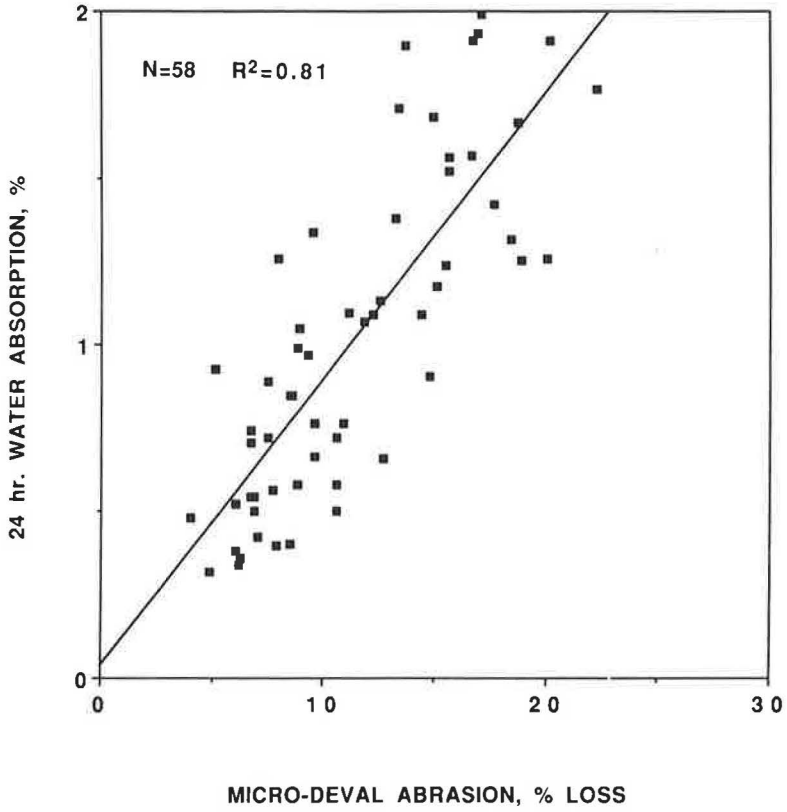

FIGURE 9 Twenty-four-hour water absorption versus micro-Deval abrasion loss for concrete sands.

rous materials will generally be weaker and break down more readily when subjected to abrasion or attrition. The correlation between natural concrete sand and micro-Deval loss shown in Figure 9 is particularly striking. A significant correlation was also found between water absorption and magnesium sulfate soundness loss ($r = 0.64$) and between water absorption and ASTM attrition loss ($r = 0.71$). Adams and Pratt (*10*), Mather (*11*), and Chamberlin (*12*) all found high positive correlations between water absorption of natural sands and loss in magnesium sulfate soundness tests ($r = 0.81, 0.81$, and 0.82, respectively). This relationship is logical, because the higher the porosity, the more sulfate solution that can enter the particles and exert destructive pressure when crystallized in the drying cycle of the test.

IMPLEMENTATION

A detailed procedure for the micro-Deval test has been written (*9*). A feature of the test is a requirement to periodically test a reference material to observe and control within and between laboratory variation. It is intended that after every 9 samples are tested, a 10th sample, which is the reference aggregate, should be tested and results plotted on a control chart. If a laboratory only rarely conducts the test, then testing of the reference aggregate should be conducted whenever the test is performed. MTO has purchased a 15-tonne stockpile of shaley limestone screenings that is being used as reference material.

CONCLUSIONS

The magnesium sulfate soundness test for fine aggregate has a poor multilaboratory precision and is not always suitable if rigid specification criteria are applied. The test is time consuming, taking 10 days.

The micro-Deval test is a rapid, simple test. Results can be obtained within 2 days. It has good correlation with the sulfate soundness test. The predicted within-laboratory and multilaboratory variability of the micro-Deval test is good, and can be easily controlled using a reference material. The test is suitable for identifying fine aggregates that contain significant amounts of poor or weak rock types.

ACKNOWLEDGMENTS

The observations described in this paper are the result of dedicated, painstaking work by many people who assisted with various tasks from the initial sample collection through to the final typing. We wish to thank the following for their assistance: C. Barber, E. Betts, D. Boothe, R. DuBois, L. Denomme, J. Dumond, D. Fox, G. Gage, M. Gibbens, K. Junor, B. Smith, H. Stankatis, and G. VanKan.

REFERENCES

1. C. A. Rogers and I. Bullen. Interlaboratory Study of the Precision of Soils and Aggregate Test Methods. Report MI-31. Engineering Materials Office, Ontario Ministry of Transportation, Downsview, 1981.
2. R. E. Davis, R. C. Mielenz, and M. Polivka. Importance of Petrographic Analysis and Special Tests not Usually Required in Judging Quality of Concrete Sand. *Journal of Materials, ASTM*, Vol. 2, No. 3, 1967, pp. 461–486.
3. C. A. Rogers and I. Bullen. The Development of an Attrition Test for Evaluating Ice Control Sand. Report EM-26. Ontario Ministry of Transportation, Engineering Materials Office, Downsview, 1979, 40 pp.
4. R. L'Haridon. Essai Micro-Deval Destiné a Prévoir à Partir de Petits Échantillons, les Qualités Routières des Roches Carottées. Bulletin Liaison Laboratoire Routières Ponts et Chausées, No. 14, Paris, France, 1965, pp. 1–17 to 1–21.
5. G. Chevassu. Variation des Résultats de l'Essai Deval Humide en Fonction du Nombre de Pierres Tendres. Bulletin Liaison Laboratoire Routières Ponts et Chausées, No. 41, Paris, France, 1969, pp. 43–45.
6. C. Tourenq. L'Essai Micro-Deval. Bulletin Liaison Laboratoire Routières Ponts et Chausées, No. 50, Paris, France, 1971, pp. 69–76.
7. Détermination du Coefficient d'Usure par Attrition à l'Aide de l'Appareil Micro-Deval. BNQ-2560-070. Bureau de Normalisation du Québec, Ministère de L'Industrie, du Commerce et du Tourisme, Québec.
8. C. A. Rogers and P. K. Mukherjee. Influence of Cementations in Sand from Fonthill on Durability and Strength of Concrete. Report MI-19. Ontario Ministry of Transportation, Engineering Materials Office, Downsview, 1979, 11 pp.
9. C. A. Rogers, M. Bailey, and B. Price. The Micro-Deval Test for Evaluating the Quality of Fine Aggregate for Concrete and Asphalt. Report EM-96. Ontario Ministry of Transportation, Engineering Materials Office, Downsview, 1990.
10. A. Adams and M. A. Pratt. A Comparison of Absorption and Soundness Test on Maine Sands. *ASTM Proc.*, Vol. 45, ASTM, Philadelphia, Pa., 1945, p. 771.
11. K. Mather. Relation of Absorption and Sulfate Test Results on Concrete Sands. Bulletin No. 144, ASTM, Philadelphia, Pa., Jan. 1947, pp. 26–31.
12. W. P. Chamberlin. Influence of Natural Sand Fine Aggregate on Some Properties of Hardened Concrete Mortar. In *Highway Research Record 124*, HRB, National Research Council, Washington, D.C., 1966, pp. 18–40.

Publication of this paper sponsored by Committee on Mineral Aggregates.

Effects of Los Angeles Abrasion Test Values on the Strengths of Laboratory-Prepared Marshall Specimens

SERJI N. AMIRKHANIAN, DOUGLAS KACZMAREK, AND JAMES L. BURATI, JR.

In the United States, approximately 93 percent of hard-surfaced roads are surfaced with asphaltic concrete mixtures. These mixtures are a combination of high-quality aggregates and an asphalt cement. The aggregates must be able to resist abrasion and degradation during manufacturing, placing, and compacting. For decades, researchers studied the resistance of aggregates to abrasion and impact. The most common test used to measure this resistance is the Los Angeles (LA) abrasion test. The LA test has been used for many years throughout the United States and has a local history. From this history, acceptance specifications have been written. The objectives were to determine (a) the extent of the use of LA values in the United States; (b) any discernible difference in the level of performance (i.e. strengths) between laboratory-prepared Marshall specimens using different aggregate sources; and (c) the level of degradation of extracted aggregates. In general, the majority of states use the LA abrasion test for writing specifications. In some cases, there were not significant differences between the dry and wet indirect tensile strength and resilient modulus values of specimens prepared with aggregates with low LA values versus specimens prepared with aggregates with high LA values. The gradation analysis of the recovered aggregates indicated that no major degradation of aggregates occurred with various compactive efforts.

In the United States, approximately 93 percent of hard-surfaced roads are surfaced with asphaltic concrete mixtures. This percentage accounts for nearly 2 million miles of flexible pavements (*1*). Flexible pavements are a combination of an asphalt cement and high-quality aggregates. The aggregates must be able to resist abrasion and degradation during manufacturing, placing, and compaction of the asphaltic concrete mixtures. In addition, the aggregates must be able to resist the forces applied by the traffic during the service life of the pavement (*2*). As a result, there is a constant demand for high-quality aggregates. For decades, research has been directed toward determining quantitatively the effects of aggregate properties on asphaltic concrete mixtures. One property studied is the resistance of aggregates to abrasion and impact.

Toughness can be defined as the ability of an aggregate to resist the impacting and grinding forces applied during manufacturing, placing, and compacting. The tests to measure the toughness of aggregate particles are described in ASTM C131, *Resistance to Degradation of Small-Size Coarse Aggregate by Abrasion and Impact in the Los Angeles Machine;* ASTM C535, *Resistance to Degradation of Large-Size Coarse Aggregate by Abrasion and Impact in the Los Angeles Machine;* and AASHTO T96, *Resistance to Abrasion of Small Size Coarse Aggregate by Use of Los Angeles Machine.*

The Los Angeles (LA) degradation test measures an aggregate's resistance to wear or abrasion. In this test (i.e., ASTM C535), approximately 10,000 g of sample is placed in the Los Angeles abrasion testing machine and rotated 1,000 revolutions at 30 to 33 rpm. The abrasive and impacting forces are applied by 12 steel spheres averaging 1.84 in. in diameter and weighing between 390 and 445 g, and having a total weight of approximately 5000 g. The percentage wear (LA value) is calculated using the following relationship:

$$\text{Percentage LA Loss} = [(\text{Original weight} - \text{Final weight})/(\text{Original weight})] \times 100$$

BACKGROUND

Before the LA abrasion test was tentatively adopted in 1937, the Deval method of testing was the only accepted method to determine the toughness of aggregates. The Deval test was developed in France in the 1870s and was adopted as a standard test for use on road materials by ASTM in 1908 and revised in 1926 (*3*). Because the LA abrasion test related closer with the performance of aggregates in pavements than the Deval test, in 1940 this test was adopted as a standard test for measuring the wear of aggregates (*3*).

Woolf (*4*) and Woolf and Runner (*5*) reported that a relation exists between the abrasion loss from the LA abrasion test and the service records of materials used in bituminous construction, surface treatment, and portland cement concrete. They also concluded that this test gives an accurate indication of the quality of materials tested and that the results can be used in specifications controlling the acceptance of coarse aggregates.

Hatt (*6*) also reported that a relation exists between the results of the LA abrasion test and the action of the road roller on the aggregates in place. Hatt found a large amount of degradation of aggregates in bituminous surface treatments caused by the compaction efforts of rollers. Hatt also noted the gradual degradation of aggregates in the surface treatment tested because of traffic conditions.

Civil Engineering Department, Clemson University, Clemson, S.C. 29634-0911.

However, the results of a laboratory-field study by Goode and Owings (*7*) indicated that the degradation of aggregates caused both by compaction and traffic was insignificant in most instances and in no instance was sufficient to affect the service behavior of the respective pavements.

In 1971, to obtain information regarding aggregate degradation, Committee A2G201, Mineral Aggregates, of the Highway Research Board, prepared and distributed a questionnaire on aggregate degradation (*8*). The responses among agencies that were using solely an abrasion test (e.g., the LA abrasion test) indicated that only 36 percent felt protected against accepting problem aggregates. The level of confidence increased to 87 percent when the abrasion test was used in combination with soundness and wet abrasion tests (*8*).

Lappalainen (*9*) studied the factors influencing wear resistance of pavements. He concluded that in many cases the strength values (i.e., from the LA abrasion test) determined in the laboratories have proved to be misleading. He also noted that the strength and wear resistance of aggregates cannot be determined only on the basis of rock type.

Woodside and Peden (*10*) studied the integrity of standard tests used in Ireland. Ten quarries were used to obtain the aggregate samples to calculate the LA abrasion loss. The authors found that the LA abrasion test was a consistent method of detecting weak materials and was a means of predicting aggregate impact value and aggregate crushing value.

Wylde (*11*) reviewed and investigated the road failures, aggregates, and test methods used in Australia. He concluded that the absolute significance of test results was not apparent. He also found that the consensus was that the results of a range of test methods should be interpreted in the light of experience with the aggregate in service.

West et al. (*12*) investigated tests for evaluating degradation of base course aggregates. They concluded that the LA abrasion test appears to be a good indicator of the degradation properties of carbonate rocks, but not of basalt rocks. They also noted that the textural parameters (e.g., grain size and roundness) were related to the LA abrasion wear value.

OBJECTIVES

The objectives of this research study were to

1. Conduct a survey, through a questionnaire, to determine the use of LA test results in various state highway agencies throughout the United States;
2. Evaluate the effects of low and high LA values on the strengths of asphaltic concrete mixtures; and
3. Evaluate the effects of low and high LA values on the degradation of aggregates by using different compactive efforts (blows per side) on the laboratory-prepared Marshall specimens.

SCOPE

A questionnaire was sent to all state and federal highway agencies throughout the United States. This survey was conducted to obtain specific information regarding the use of the LA test for highway specifications.

In addition, 288 laboratory-prepared Marshall specimens were made and tested. Four aggregate sources with a range of LA values from 28 to 55 were selected for this study. Four different compactive efforts (i.e., 25, 50, 75, and 100 blows per side) were used to prepare the specimens. The specimens were divided into two moisture conditioning groups: dry and wet. The Tunnicliff and Root (*13*) method of moisture conditioning was used for testing the wet specimens.

In order to study the effects of high and low LA values on the degradation of aggregates, the aggregates were extracted from randomly selected laboratory-prepared Marshall specimens made with various compactive efforts. Gradation analyses were performed to determine the amount of degradation.

For each specimen, the dry and wet resilient modulus (MR), and dry and wet indirect tensile strength (ITS) values were obtained. The tensile strength retained (TSR) and resilient modulus ratio (MRR) were calculated for each pair of dry- and wet-conditioned specimens prepared with the same aggregate source and number of blows per side.

MATERIALS

The materials used in the preparation of laboratory-prepared Marshall specimens included four aggregate sources (denoted as A, B, C, and D) and one asphalt cement source (AC–20). Aggregates A, B, C, and D (all granite) had LA values of 55, 48, 30, and 28, respectively. The LA value was determined using aggregates of Grading B from each source. All of the mixtures are used for surface courses in South Carolina.

TESTING PROCEDURES

For each aggregate source, the Marshall method of mix design was performed to obtain the optimum asphalt content according to the Asphalt Institute's Manual Series 2 (MS–2) (*14*). A total of 288 specimens were prepared and tested. The specimens were randomly selected and separated into two testing groups; wet and dry. Dry specimens were placed in a temperature control cabinet (77°F ± 2°F) for 24 hr. Wet specimens were subjected to Tunnicliff and Root's (*13*) moisture susceptibility test. This test requires each specimen to be submerged in water with a vacuum of 20 psi for 5 min. Then, the specimen must be placed in a water bath (140°F ± 2°F) for 24 hr and then placed in another water bath (77°F ± 2°F) for 1 hr before testing.

Both wet and dry specimens were tested, at 77°F ± 2°F, for MR (ASTM D–4123) using a Retsina Mark VI resilient modulus testing machine. Each specimen was placed on its circular side in the measuring yoke. Horizontal deformations were measured when the specimen was subjected to repeated vertical loads (10 repetitions in 30 sec) of approximately 70 lb. Each specimen was then turned 90 degrees on its circular side and tested again. The mean of the two test values was used as the MR value for that specimen.

All specimens were then tested for ITS (at 77°F ± 2°F) after 2 hr of dry or wet storage. The ITS was obtained using a Marshall testing machine (deformation rate of 2 in./min) with a testing head that was modified by the addition of half-inch metal strips.

The TSR and MRR were calculated by dividing the wet strength value by the respective dry value. These values indicated the percentage of strength that is retained when the specimen is saturated. Four of the samples within each group (i.e., aggregate source and number of blows per side) were randomly chosen and sieve analyses (ASTM C–136) were performed on the extracted aggregates.

STATISTICAL DESIGN

A complete random design (CRD) was used for the statistical design because the laboratory-prepared specimens were essentially homogeneous. The laboratory treatments (i.e., aggregate sources and number of blows per side) on some of the physical characteristics (ITS, MR, TSR, and MRR) of the asphaltic concrete mixtures were measured using analysis of variance (ANOVA).

Figure 1 shows the experimental design used to prepare and test the specimens. In this project, there were 32 combinations of variables (i.e., 4 aggregate sources × 2 moisture conditions × 4 blows per side). There were 288 Marshall specimens (32 combinations × 9 replicates) made and tested. Thirty-two specimens were prepared and tested each day. The preparation order within each replicate was randomly selected to ensure that the preparation was not biased. During Tunnicliff and Root's testing procedures, one of the specimens (i.e., A–55, 25 blows per side) fell apart in 140°F water bath.

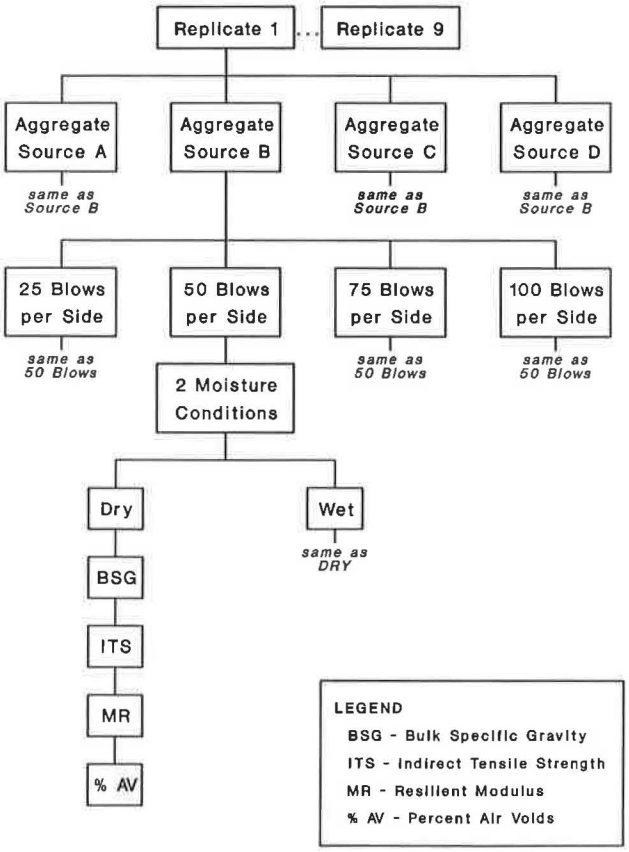

FIGURE 1 Flow chart of the experimental design for the laboratory-prepared Marshall specimens.

ANALYSIS OF QUESTIONNAIRE

Seventy-three questionnaires were sent to various authorities including all of the state highway agencies in the United States. The response rate was approximately 68 percent. The questions on the questionnaire and a summary of responses were as follows:

1. Does your department use LA abrasion loss as a specification requirement? If so, what maximum value is allowed?

Number of Responses	*Response Rate (%)*	*Maximum Allowable Loss (%)*
4	8	30
20	40	35
21	42	45
3	6	>45 but <55
2	4	Do not use LA abrasion as a specification requirement

2. How was this value established?

Number of Responses	*Response Rate (%)*	*Source*
20	43	past experience or historical data
12	25	Unaware of the origin
13	28	Adopted from ASTM, AASHTO, or FHWA
2	4	Conducted research to establish the value

3. What do you think is the major cause of deterioration of aggregates used in the surface course (impact, abrasion, grinding, etc.)?

Number of Responses	*Cause of Deterioration*
23	Abrasion caused by rolling wheel
8	Freeze thaw
7	Wear due to studded tires
6	Impact
5	Aggregate crushing (heavy load)
4	Grinding
4	Weathering of aggregates
4	Chemical action of deicing agents
6	No deterioration of aggregates

Most of the responses quoted one or more of the above forms of deterioration.

4. Do you think that surface moisture and skid resistance are given sufficient weighage in pavement and mix design procedures?

Only 4 responses indicated that they were not satisfied with the present mix design procedures.

5. Can you comment on the performance of two major roads in your area, where aggregates of high LA value and low LA value have been used?

Few responded to this question. However, none of the responses indicated that there was a correlation between the performance of flexible pavements and LA value. In addition, the answers indicated that in some cases aggregates with high LA value performed well in the field, and in some other cases those with low LA values failed in the field.

6. Do you feel that LA abrasion loss should be a specification requirement, and, if so, what value should be used for the specification limits?

> Almost all of the respondents indicated that the LA abrasion loss should be a specification requirement and that they were satisfied with the value that their agency had adopted.

STATISTICAL RESULTS

A summary of statistical results (mean, standard deviation, and coefficient of variance) of dry and wet ITS, dry and wet MR, TSR, and MRR values are presented in Tables 1–3. In addition, Table 4 indicates the sieve analyses results conducted on the original (i.e., from the quarry) aggregates and the extracted aggregates. The effects of low and high LA values on strength of laboratory-prepared Marshall specimens and degradation of aggregates due to different compactive efforts are described in the following sections.

Effects of LA values on Strength of Marshall Specimens

The statistical results of analyses of least squares difference (LSD) comparisons, at the 5 percent level, for each aggregate-blows per side combination are shown in Tables 5–7. The letters "*N*" and "*S*" in these tables indicate "not significantly different" and "significantly different" at the 5 percent level, respectively. In addition, the numbers in parentheses indicate the probability of obtaining a *t*-value as large as the one computed if the means are actually equal. Each cell in these tables is based on the average of nine specimens with the exception of aggregate Source A (25 blows per side) in wet condition which contained eight specimens.

For instance, Table 5 indicates that the difference between average dry ITS of specimens made with aggregate Source A versus Source D (both 25 blows per side) is significant at the 5 percent level [i.e., Row 1, column 4; *S* (0.0003)]. However, the difference between average dry ITS of specimens made with aggregate Source A versus Source C (both 25 blows per side) is not significant at the 5 percent level [i.e., Row 1, Column 2: *N* (0.2522)].

Figures 2–4 show the effects of various LA values on dry and wet ITS, dry and wet MR, TSR, and MRR values. Figure 2a indicates that in all cases of compactive efforts (i.e., 25, 50, etc.), specimens prepared with aggregate Sources A (LA = 55) and B (LA = 48) had higher dry ITs values than specimens prepared with aggregate Source C (LA = 30). However, Table 5 indicates that only 3 out of 8 comparisons were significantly different at the 5% level.

Figures 2b and 3 indicate that in all cases the specimens prepared with aggregate source B (LA = 48) produced higher wet ITS, dry and wet MR values than specimens containing aggregate Source C (LA = 30). Tables 5 and 6 indicate that only 2 out of 12 comparisons were significantly different at the 5 percent level.

In all cases, except one, the specimens prepared with aggregate Source D (LA = 28) produced higher dry and wet ITS and MR values than those of specimens prepared with other aggregate sources (Figures 2 and 3). However, Tables 5 and 6 indicate that 39 out of 48 comparisons were significantly different at the 5 percent level. Figure 4 indicates that in most cases the specimens prepared with aggregate Sources C (LA = 30) and D (LA = 28) produced higher TSR and MRR values than specimens made with aggregate Sources A (LA = 55) and B (LA = 48). Table 7 indicates that 11 out of 24 comparisons were significantly different at the 5 percent level.

Degradation of Aggregates Because of Compactive Efforts

Figures 5–7 show the effects of compactive efforts for each aggregate source. In most cases, specimens prepared with

TABLE 1 MEAN, STANDARD DEVIATION, AND COEFFICIENT OF VARIANCE OF DRY AND WET ITS VALUES FOR LABORATORY-PREPARED MARSHALL SPECIMENS (N = 9)

Aggregate Source - LA Value	Blows/Side	$\bar{X}$ ITS Dry (psi)	STD DEV (psi)	COEF VAR (%)	$\bar{X}$ ITS Wet (psi)	STD DEV (psi)	COEF VAR (%)
A-55	25	70.1	12.2	17.4	34.3*	13.3	38.8
	50	89.4	22.6	25.3	46.5	21.8	47.0
	75	112.1	16.2	14.4	50.6	29.5	58.4
	100	108.7	18.5	17.0	66.3	27.1	41.0
B-48	25	90.7	16.1	17.8	45.8	11.2	24.4
	50	96.3	25.1	26.1	65.3	21.6	33.1
	75	120.3	15.8	13.1	78.8	12.2	15.5
	100	118.8	12.1	10.2	104.8	24.2	23.1
C-30	25	60.5	10.4	17.3	45.3	10.7	23.7
	50	81.8	16.2	19.8	53.5	12.3	23.1
	75	96.2	21.4	22.2	74.5	13.3	17.8
	100	99.5	22.3	22.4	88.8	15.1	17.0
D-28	25	101.4	12.9	12.8	77.2	14.2	18.4
	50	122.5	14.5	11.8	108.6	17.2	15.8
	75	141.8	22.7	16.0	116.1	37.1	32.0
	100	135.7	15.2	11.2	135.2	25.1	18.6

TABLE 2 MEAN, STANDARD DEVIATION, AND COEFFICIENT OF VARIANCE OF DRY AND WET MR STRENGTHS FOR LABORATORY-PREPARED MARSHALL SPECIMENS (N = 9)

Aggregate Source - LA Value	Blows/Side	$\bar{X}$ MR Dry (ksi)	STD DEV (ksi)	COEF VAR (%)	$\bar{X}$ MR Wet (ksi)	STD DEV (ksi)	COEF VAR (%)
A-55	25	138.2	42.2	30.5	55.4*	24.3	43.9
	50	157.6	29.1	18.4	85.1	45.1	53.0
	75	200.4	50.6	25.2	73.0	40.7	55.8
	100	213.5	81.3	38.1	118.0	42.0	35.6
B-48	25	256.2	144.4	56.4	100.2	36.4	36.3
	50	238.2	60.5	25.4	136.4	61.8	45.3
	75	267.8	77.6	29.0	157.7	49.2	31.2
	100	287.8	95.4	33.2	275.7	114.3	41.8
C-30	25	142.4	47.5	33.4	87.6	34.9	39.8
	50	182.1	54.1	29.7	110.6	34.0	30.7
	75	218.8	74.2	33.9	146.3	37.2	25.5
	100	241.6	92.6	38.3	204.0	59.4	29.1
D-28	25	236.7	51.6	21.8	150.0	42.1	28.1
	50	250.3	46.9	18.7	202.2	46.9	23.2
	75	305.7	103.9	34.0	232.5	51.6	22.2
	100	289.4	58.7	20.3	323.7	154.1	47.6

* n=8

TABLE 3 MEAN, STANDARD DEVIATION, AND COEFFICIENT OF VARIANCE FOR THE INDIRECT TSR AND THE MRR VALUES FOR LABORATORY-PREPARED MARSHALL SPECIMENS (N = 9)

Aggregate Source - LA Value	Blows/Side	$\bar{X}$ TSR (%)	STD DEV (%)	COEF VAR (%)	$\bar{X}$ MRR (%)	STD DEV (%)	COEF VAR (%)
A-55	25	49.1*	16.3	33.1	44.7*	30.2	67.7
	50	54.1	30.8	57.0	58.3	41.5	71.1
	75	46.6	30.5	65.4	42.4	33.8	79.6
	100	62.1	25.3	40.7	65.4	37.7	57.6
B-48	25	51.2	13.2	25.8	45.6	26.1	57.2
	50	68.9	17.9	26.0	60.5	29.6	48.8
	75	65.8	9.3	14.1	62.6	26.0	40.8
	100	89.1	22.1	24.8	111.2	80.0	71.9
C-30	25	77.1	25.2	32.7	65.6	28.3	43.1
	50	66.0	11.8	17.9	64.7	30.9	47.8
	75	82.5	31.9	38.7	74.0	33.9	45.9
	100	93.4	29.0	31.1	91.5	33.5	36.7
D-28	25	77.6	20.3	26.1	66.8	27.8	35.5
	50	88.8	10.4	11.7	83.7	26.7	32.0
	75	81.5	21.4	26.2	80.8	25.2	31.2
	100	100.9	23.1	22.9	112.5	44.9	39.9

* n=8

Note: 1. TSR = (ITS wet / ITS dry)*100%
2. MRR = (MR wet / MR dry)*100%

TABLE 4 MEAN AND STANDARD DEVIATION OF SIEVE ANALYSES (PERCENT PASSING) FOR THE ORIGINAL AGGREGATES AND FOR EXTRACTED AGGREGATES OF LABORATORY-PREPARED MARSHALL SPECIMENS (N = 4)

	Percent Passing (Standard Deviation) Aggregate Source - Blows/Side									
Sieve Size		LA = 55					LA = 48			
	ORG*	A-25	A-50	A-75	A-100	ORG	B-25	B-50	B-75	B-100
3/8in	78.8	89.2 (2.9)	86.8 (3.0)	87.3 (2.4)	90.3 (1.5)	93.3	94.2 (2.0)	96.8 (1.9)	95.4 (1.0)	94.8 (1.2)
#4	65.0	69.1 (6.8)	67.1 (3.8)	65.5 (3.7)	65.0 (5.0)	61.5	63.7 (2.0)	67.4 (4.2)	65.5 (2.0)	66.9 (3.1)
#8	53.0	56.7 (7.6)	54.3 (3.4)	53.0 (3.7)	51.5 (5.3)	48.3	49.8 (1.9)	53.6 (4.8)	51.9 (1.6)	53.2 (3.0)
#30	-	33.4 (5.4)	31.8 (2.3)	30.9 (2.3)	31.7 (4.1)	-	33.2 (1.4)	32.3 (3.7)	35.6 (1.2)	36.4 (2.2)
#100	-	12.8 (2.2)	11.9 (0.9)	11.3 (0.9)	11.9 (1.7)	-	14.1 (0.5)	13.2 (1.7)	16.3 (0.5)	16.8 (1.0)
#200	-	6.3 (1.1)	5.7 (0.3)	5.2 (0.4)	5.5 (0.8)	-	7.3 (0.2)	6.7 (0.8)	8.8 (0.3)	9.2 (0.5)
	Aggregate Source - Blows/Side									
Sieve Size		LA = 30					LA = 28			
	ORG	C-25	C-50	C-75	C-100	ORG	D-25	D-50	D-75	D-100
3/8in	94.8	95.4 (1.9)	95.4 (0.5)	95.7 (1.8)	96.1 (1.7)	99.0	99.2 (0.3)	99.0 (0.3)	99.1 (0.2)	99.1 (0.9)
#4	65.8	68.8 (5.5)	67.6 (3.8)	69.4 (5.6)	70.5 (4.4)	73.3	77.8 (1.3)	77.7 (3.5)	76.9 (2.5)	77.9 (3.6)
#8	49.8	53.1 (5.8)	52.0 (5.1)	51.7 (5.5)	54.1 (5.6)	53.2	56.7 (1.6)	55.6 (3.8)	56.7 (3.4)	54.9 (4.0)
#30	-	25.1 (3.3)	25.4 (1.7)	23.8 (4.8)	26.6 (5.0)	-	35.2 (1.1)	32.9 (2.7)	34.9 (2.5)	33.6 (2.9)
#100	-	9.2 (1.2)	8.7 (0.6)	8.5 (1.7)	10.6 (2.0)	-	18.5 (0.6)	16.3 (1.4)	19.0 (1.4)	17.9 (1.6)
#200	-	4.9 (0.5)	4.6 (0.3)	4.6 (0.9)	5.8 (1.1)	-	10.1 (0.3)	8.9 (0.8)	10.8 (0.8)	10.3 (0.9)

* ORG: Original (i.e., from the quarry) gradation

TABLE 5 LEAST SIGNIFICANT DIFFERENCE COMPARISONS (α = 0.05) OF DRY AND WET ITS VALUES FOR LABORATORY-PREPARED SPECIMENS (N = 9)

Aggregate Source - Blows/Side	Dry ITS			Wet ITS		
	B-25	C-25	D-25	B-25	C-25	D-25
A-25	S(.0149)	N(.2522)	S(.0003)	N(.2545)	N(.2755)	S(.0001)
B-25	-	S(.0004)	N(.2000)	-	N(.9596)	S(.0015)
C-25	-	-	S(.0001)	-	-	S(.0013)
	B-50	C-50	D-50	B-50	C-50	D-50
A-50	N(.4064)	N(.3639)	S(.0001)	N(.0557)	N(.4735)	S(.0001)
B-50	-	N(.0835)	S(.0021)	-	N(.2276)	S(.0001)
C-50	-	-	S(.0001)	-	-	S(.0001)
	B-75	C-75	D-75	B-75	C-75	D-75
A-75	N(.3261)	N(.0587)	S(.0005)	S(.0044)	S(.0149)	S(.0001)
B-75	-	S(.0045)	S(.0112)	-	N(.6643)	S(.0002)
C-75	-	-	S(.0001)	-	-	S(.0001)
	B-100	C-100	D-100	B-100	C-100	D-100
A-100	N(.2293)	N(.2725)	S(.0015)	S(.0001)	S(.0221)	S(.0001)
B-100	-	S(.0225)	S(.0443)	-	N(.1011)	S(.0022)
C-100	-	-	S(.0001)	-	-	S(.0001)

Notes: 1. N and S denote not significantly and significantly different at the 5 percent level, respectively.
2. The numbers in parentheses indicate the probability of obtaining a t-value as large as the one computed if the means are actually equal.
3. Wet ITS of aggregate source A (LA=55) and 25 blows per side: n=8

TABLE 6 LEAST SIGNIFICANT DIFFERENCE COMPARISONS (α = 0.05) OF DRY AND WET MRR VALUES FOR LABORATORY-PREPARED SPECIMENS (N = 9)

Aggregate Source - Blows/Side	Dry MR			Wet MR		
	B-25	C-25	D-25	B-25	C-25	D-25
A-25	S(.0011)	N(.9068)	S(.0061)	N(.1498)	N(.3001)	S(.0028)
B-25	-	S(.0016)	N(.5808)	-	N(.6743)	N(.1024)
C-25	-	-	S(.0086)	-	-	S(.0408)
	B-50	C-50	D-50	B-50	C-50	D-50
A-50	S(.0242)	N(.4898)	S(.0097)	N(.0900)	N(.3964)	S(.0002)
B-50	-	N(.1146)	N(.7312)	-	N(.3928)	S(.0299)
C-50	-	-	N(.0555)	-	-	S(.0028)
	B-75	C-75	D-75	B-75	C-75	D-75
A-75	N(.0584)	N(.6024)	S(.0034)	S(.0055)	S(.0159)	S(.0001)
B-75	-	N(.1678)	N(.2850)	-	N(.7034)	S(.0140)
C-75	-	-	S(.0152)	-	-	S(.0048)
	B-100	C-100	D-100	B-100	C-100	D-100
A-100	S(.0374)	N(.4275)	S(.0334)	S(.0001)	S(.0049)	S(.0001)
B-100	-	N(.1936)	N(.9625)	-	S(.0216)	N(.0986)
C-100	-	-	N(.1782)	-	-	S(.0001)

Notes: 1. N and S denote not significantly and significantly different at the 5 percent level, respectively.
2. The numbers in parentheses indicate the probability of obtaining a t-value as large as the one computed if the means are actually equal.
3. Wet MR of aggregate source A (LA-55) and 25 blows per side: n=8

TABLE 7 LEAST SIGNIFICANT DIFFERENCE COMPARISONS (α = 0.05) OF TSR AND MRR VALUES FOR LABORATORY-PREPARED SPECIMENS (N = 9)

Aggregate Source - Blows/Side	TSR			MRR		
	B-25	C-25	D-25	B-25	C-25	D-25
A-25	N(.8495)	S(.0112)	S(.0099)	N(.9610)	N(.2494)	N(.2230)
B-25	-	S(.0154)	S(.0135)	-	N(.2555)	N(.2278)
C-25	-	-	N(.9624)	-	-	N(.9446)
	B-50	C-50	D-50	B-50	C-50	D-50
A-50	N(.1616)	N(.2594)	S(.0013)	N(.8993)	N(.7150)	N(.1495)
B-50	-	N(.7836)	N(.0622)	-	N(.8114)	N(.1881)
C-50	-	-	S(.0329)	-	-	N(.2803)
	B-75	C-75	D-75	B-75	C-75	D-75
A-75	N(.0706)	S(.0009)	S(.0012)	N(.2284)	N(.0736)	S(.0300)
B-75	-	N(.1159)	N(.1411)	-	N(.5536)	N(.3270)
C-75	-	-	N(.9189)	-	-	N(.6970)
Blows/Side	B-100	C-100	D-100	B-100	C-100	D-100
A-100	S(.0118)	S(.0037)	S(.0004)	S(.0099)	N(.1386)	S(.0080)
B-100	-	N(.6858)	N(.2666)	-	N(.2609)	N(.9417)
C-100	-	-	N(.4788)	-	-	N(.2314)

Notes: 1. N and S denote not significantly and significantly different at the 5 percent level, respectively.
2. The numbers in parentheses indicate the probability of obtaining a t-value as large as the one computed if the means are actually equal.
3. MRR and TSR of aggregate source A (LA-55) and 25 blows per side: n=8

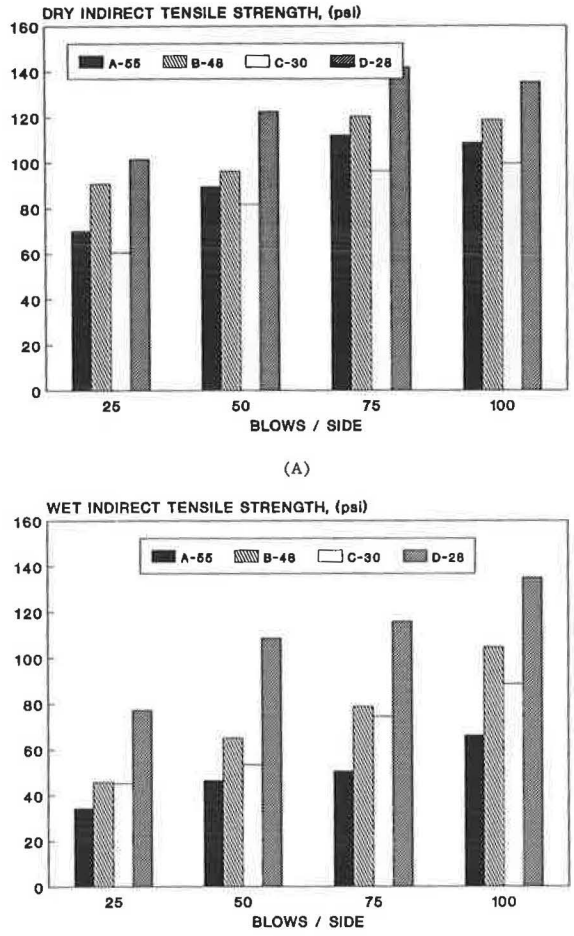

FIGURE 2 Mean of (a) dry ITS, and (b) wet ITS, of laboratory-prepared Marshall specimens compared by levels of compactive effort.

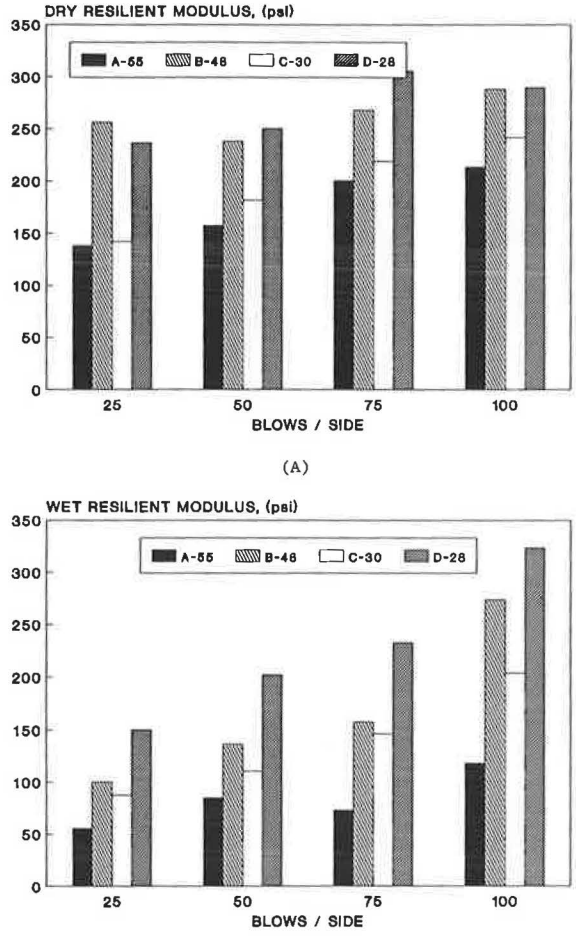

FIGURE 3 Mean of (a) dry MR, and (b) wet MR, of laboratory-prepared Marshall specimens compared by levels of compactive effort.

compactive efforts of 25 blows per side, for each aggregate source, produced lower dry and wet ITS, dry and wet MR, TSR, and MRR values than other compactive efforts. The statistical analysis indicated that 32 out of 72 comparisons were significantly different at the 5 percent level.

Four randomly selected specimens were used from each combination of aggregate source and compactive effort to obtain a representative sample for extracted aggregate gradation analyses. The statistical results indicated that for all aggregates and all compactive level efforts, for certain sieves (i.e., ⅜-in. Nos. 4, 8, and 30) there were not significant differences for percent passing of extracted aggregates. This result indicated that no major degradation occurred because of compactive efforts for these aggregates. However, the results indicated that various compactive efforts for aggregate Sources A and B, for sieves Nos. 100 and 200, produced significantly different percent passing. Aggregates (Sources C and D) with lower LA values produced similar results.

SUMMARY AND CONCLUSIONS

Seventy-three questionnaires were sent to all state and federal highway agencies in the United States to determine the use of LA abrasion test values in their specifications. The response rate was approximately 68 percent (i.e., 50 surveys were returned).

The effects of low and high LA values on the strengths of laboratory-prepared Marshall specimens were investigated. In addition, different compactive efforts were used to prepare the laboratory specimens to study the effects of low and high LA values on the degradation of extracted aggregates. Four aggregate sources with LA values of 55, 48, 30, and 28 and four compactive efforts (i.e., 25, 50, 75, and 100) were used in this research study. The following conclusions could be drawn:

1. The results of the survey indicated that the majority of state highway agencies in the United States use the LA abrasion loss value as a specification requirement.
2. Approximately 26 percent of the surveyed agencies indicated that they were unaware of the origin of the LA values used for their specifications. Approximately 43 and 27 percent of the responses indicated that the LA values were based on past experiences and adopted from ASTM or similar organizations, respectively.
3. Most of the responses indicated that the major cause of deterioration of aggregates used in the surface course was

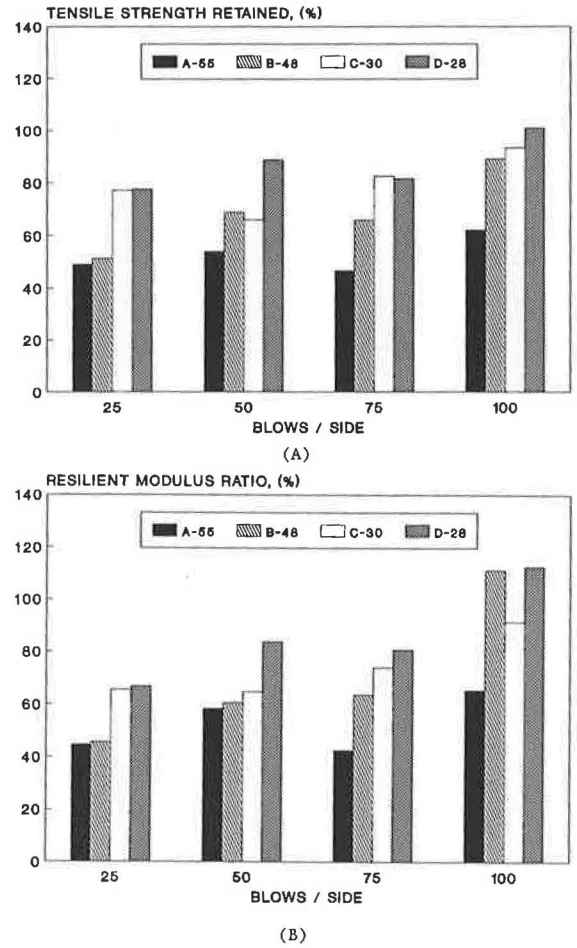

FIGURE 4 Mean of (a) TSR, and (b) MRR, of laboratory-prepared Marshall specimens compared by levels of compactive effort.

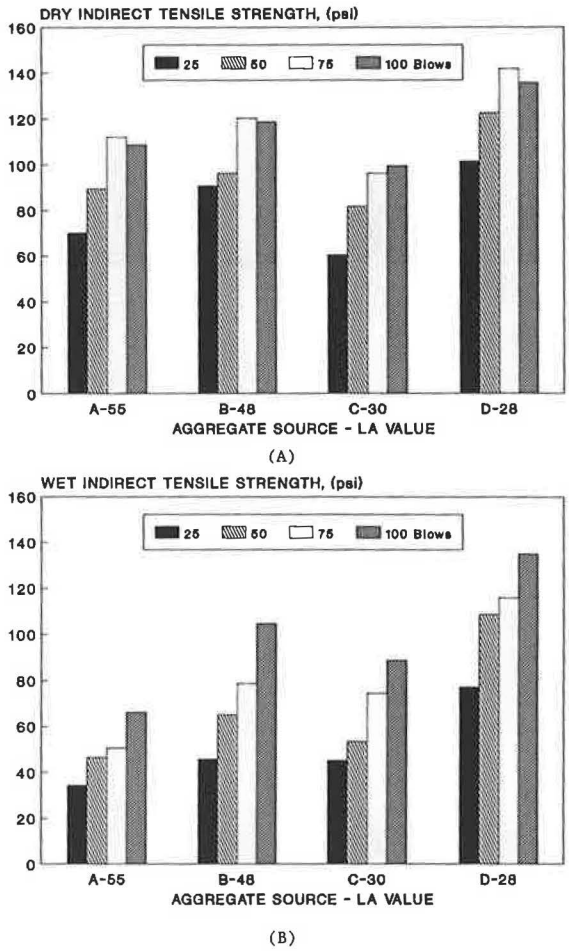

FIGURE 5 Mean of (a) dry ITS, and (b) wet ITS, of laboratory-prepared Marshall specimens compared by aggregate source.

abrasion caused by compaction. In addition, almost all states indicated that the LA abrasion loss should be a specification requirement and they were satisfied with the value that their agency had adopted.

4. The laboratory results indicated that in all compactive efforts, the specimens prepared with aggregates Sources A, B, and C (LA values of 55, 48, and 30, respectively) produced significantly lower, at a 5 percent level, dry and wet ITS values (Figure 2), than the specimens made with aggregate Source D (LA = 28).

5. In most cases, the specimens prepared with aggregate Source A (LA = 55), at all compactive efforts, produced significantly lower TSR and MRR values than the specimens made with aggregate Source D (LA = 28), as shown in Figure 4.

6. In general, the results indicated that specimens made with aggregate Source D (lowest LA value) produced significantly higher dry and wet ITS values (Table 5 and Figure 2). However, only in 50 percent of cases, the TSR values of the specimens prepared with this aggregate were significantly different (Table 7 and Figure 4a).

7. In most cases, specimens prepared with compactive efforts of 25 blows per side for each aggregate source produced significantly lower dry and wet ITS values compared with other compactive efforts (Figure 5). In most cases, there were no significant differences between TSR and MRR of specimens made with 25 blows per side compared with specimens prepared with 50, 75, and 100 blows per side (Figure 7).

8. In general, the results indicated that dry and wet ITS values of specimens prepared with aggregates of high LA value were not, in every case, lower than dry and wet ITS values of specimens made with aggregates of low LA value.

9. In general, the dry and wet MR results indicated that the strengths of specimens did not increase with a decrease in LA value of aggregates used to prepare the specimens.

10. Overall, TSR and MRR results indicated that, in most cases, specimens prepared with aggregates of low LA did not necessarily produce higher TSR and MRR values than those specimens made with aggregates of high LA.

11. The results of the sieve analyses on the extracted aggregates indicated that with the exception of percent passing sieves Nos. 100 and 200, there were no significant differences between various compactive efforts.

12. When considering the degradation of the aggregates, the results indicated that there were not significant differences between aggregates with high LA and those with low LA values.

13. Overall, these results indicated that, in most cases, for all aggregates tested, the TSR and MRR values were not influenced by compactive efforts.

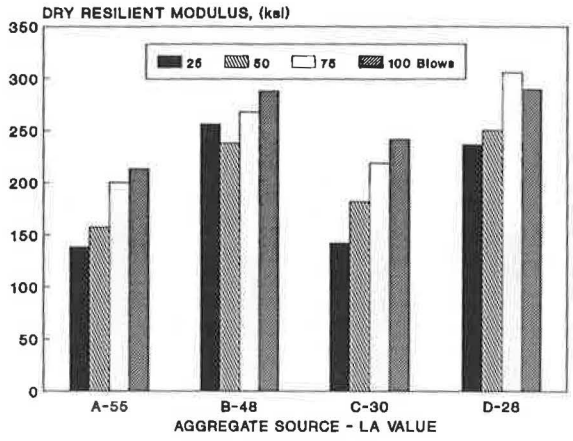

(A)

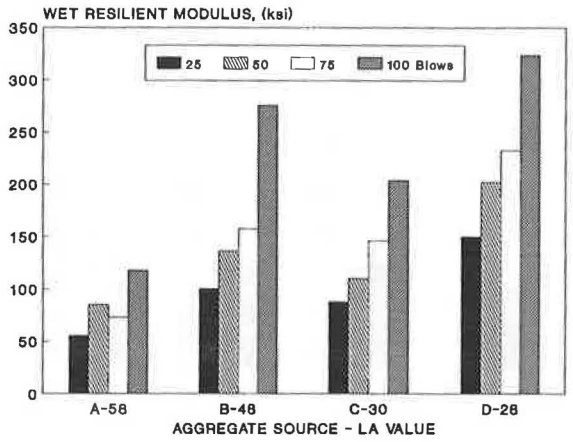

(B)

FIGURE 6 Mean of (a) dry MR, and (b) wet MR, of laboratory-prepared Marshall specimens compared by aggregate source.

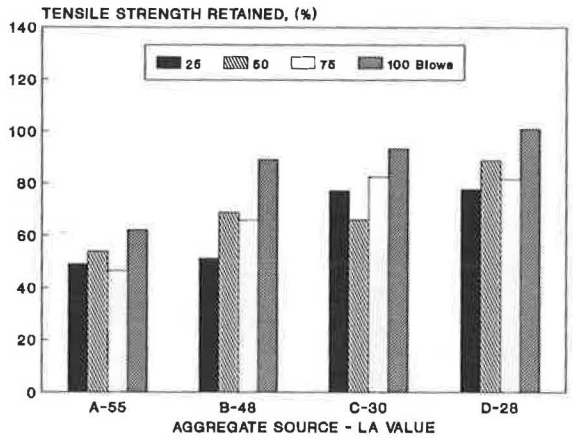

(A)

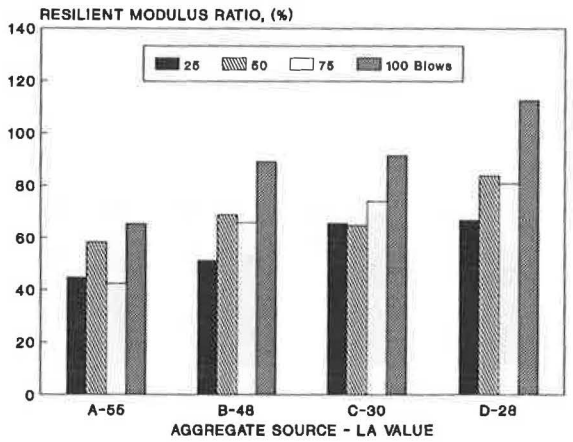

(B)

FIGURE 7 Mean of (a) TSR, and (b) MRR, of Laboratory-Prepared Marshall specimens compared by aggregate source.

REFERENCES

1. *Special Report 202: America's Highways, Accelerating the Search for Innovation.* TRB, National Research Council, Washington, D.C., 1984.
2. *The Asphalt Handbook.* Manual Series No. 4 (MS–4), The Asphalt Institute, College Park, Md., 1989.
3. H. S. Sweet. Physical and Chemical Tests of Mineral Aggregate and Their Significance. Special Technical Publication 83, *Symposium on Mineral Aggregates*, ASTM, Philadelphia, Pa., 1948, pp. 49–73.
4. D. O. Woolf. Report of Committee on Correlation of Research in Mineral Aggregate—The Relation between the Los Angeles Abrasion Test Results and the Service Records of Coarse Aggregates. *HRB Proc.*, Vol. 17, 1937, pp. 350–359.
5. D. O. Woolf and D. G. Runner. The Los Angeles Abrasion Machine for Determining the Quality of Coarse Aggregate. ASTM, Vol. 35, Part II, 1935, pp. 511–532.
6. W. K. Hatt. The Cooperative Research Project—Purdue University and Indiana Highway Commission—Progress Report. *HRB Proc.*, Vol. 18, Part I, 1938, pp. 255–263.
7. J. H. Goode and E. P. Owings. A Laboratory-Field Study of Hot Asphaltic Concrete Wearing Course Mixtures. *Public Roads*, Vol. 31, No. 11, Dec. 1961.
8. L. G. Hendrickson and R. D. Shumway. *Highway Research Circular 144: Analysis of Questionnaire on Aggregate Degradation.* HRB, National Research Council, Washington, D.C., July 1973.
9. K. Lappalainen. On Aggregate Factors Influencing Wear Resistance of Pavements. *Tie ja Liikenne*, Vol. 57, No. 1–2, 1987, pp. 26–29.
10. A. R. Woodside and R. A. Peden. Durability Characteristics of Roadstone. *Quarry Management and Products*, Vol. 10, No. 8, Aug. 1983, pp. 493–497.
11. L. J. Wylde. *Literature Review: Crushed Rock and Aggregate for Road Construction—Some Aspects of Performance, Test Methods and Research Needs.* Report 43, Australian Road Research Board, Nunawading, Jan. 1976.
12. T. R. West, R. B. Johnson, and N. M. Smith. *NCHRP Report 98: Tests for Evaluating Degradation of Base Course Aggregates.* HRB, National Research Council, Washington, D.C., 1970.
13. D. G. Tunnicliff and R. E. Root. *NCHRP Report 274: Use of Antistrip Additives in Asphalt Concrete Mixtures.* TRB, National Research Council, Washington, D.C., 1984.
14. *Mix Design Methods for Asphalt Concrete.* Manual Series No. 2 (MS–2), The Asphalt Institute, College Park, Md., May 1984.

Publication of this paper sponsored by Committee on Mineral Aggregates.

Laboratory Evaluation of the Alkali Carbonate Reaction

JACK CROTEAU, JOHN QUINN, AND KIRAN SHELAT

New Jersey's carbonate rock study was undertaken to develop a procedure to evaluate local sources for potential alkali carbonate reaction. Laboratory tests were performed on rock samples obtained from eight local sources with unknown reactive characteristics and three control samples with well-known reactive characteristics. The screening criteria described in the paper identified the known reactive sources, and also indicated that some local sources are potentially reactive at higher alkali levels. It is recommended that use of carbonate aggregate be conditioned on demonstrated nonreactivity under the described battery of tests. As a precautionary measure, low-alkali cement (alkali levels less than 0.7 percent) should be used with carbonate rock aggregate to mitigate the effect of any failure to detect aggregate reactivity.

A laboratory investigation of the alkali-carbonate reaction undertaken to develop a screening and acceptance procedure for carbonate rock proposed for use in New Jersey Department of Transportation (NJDOT) concrete mixes is described.

New Jersey's current specifications prohibit the use of carbonate rock as an aggregate for concrete surface courses, culverts, and bridges. This restriction is based on two factors. The first of these is the potential for skid resistance problems. That is, because of the well-known tendency for carbonate rock to polish under the action of traffic, it is deemed generally unsuitable for riding surfaces. The second concern regarding carbonate aggregates is the potential development of destructive expansive stresses resulting from the so-called "alkali-aggregate reaction" (AAR).

The potential of carbonate rock for creating skid resistance problems is well documented. On the other hand, the potential for distress resulting from the alkali-aggregate reaction, although recognized as a widespread problem nationally, has until recently been based primarily on anecdotal observations in New Jersey. Perhaps the most frequently cited New Jersey example of alkali-carbonate rock distress—the Magnolia Street Bridge on Routes 1 and 9—concerns a structure constructed in the mid-1930s.

The blanket prohibition of carbonate rock as a concrete aggregate is a significant factor in an existing problem of aggregate supply in New Jersey's southern (coastal plain) areas. Absent this restriction, the potential sources of supply could increase significantly. About one-quarter of the aggregate sources presently supplying NJDOT projects are carbonate rock quarries.

This study was undertaken to evaluate the alkali-aggregate reactivity of carbonate rocks from quarries in the New Jersey-Pennsylvania region to determine whether some carbonate aggregates could safely be used in Department of Transportation concrete mixes other than for riding surfaces.

The work basically consisted of a program of laboratory testing designed to determine the expansion characteristics of a representative sample of carbonate rock from eight nearby quarries. In order to provide a basis of comparison for these results, three carbonate rock samples known to be unacceptably reactive were subjected to similar tests.

New Jersey Department of Transportation, 1035 Parkway Avenue, CN 600, Trenton, N.J. 08625

NATURE OF THE ALKALI-AGGREGATE REACTION

Two reactions involving concrete aggregates and free alkali from cement have been identified, namely the alkali-silica reaction (ASR) and the alkali-carbonate reaction (ACR). These reactions involve susceptible siliceous and carbonate rocks, respectively. Collectively, these reactions are referred to as the alkali-aggregate reaction (AAR). As a result of either of these two reactions, the aggregate undergoes expansion that results in map cracking of the concrete. Water that accumulates in these cracks undergoes freezing and thawing cycles that in turn create spalling. The associated "growth" of the concrete can damage pavement joints and adjoining structures.

This reaction was first identified in the 1940s in California and in the 1950s in Virginia. A 1956 paper entitled *A Canadian Reactive Aggregate Undetected by ASTM Tests* generated significant interest among concrete mix designers, because it had been assumed that aggregates remained chemically inert during and after the hydration process. Today, AAR is of worldwide concern, with over 100 research papers having been presented in the United States and Canada.

Until recently, New Jersey pavements and structures had not displayed alkali-reactivity related damage. However, in 1988 approximately 12 lane-miles of distressed pavement on Route I-295 in Burlington County were identified (*1*) as undergoing the alkali-silica reaction. Figure 1 shows the typical pattern of map cracking associated with the alkali-aggregate reaction on the I-295 pavement. Figure 2 shows full-width cracks at the pavement joints resulting from the progressive "growth" of the pavement.

The principal concern, however, is potential problems associated with the alkali-carbonate reaction. ACR is described as a chemical reaction that takes place between free alkali from the cement and certain dolomitic limestones containing clay. As per ASTM C150, free alkali in cement is computed as percent of $Na_2O + 0.658K_2O$. This reaction is frequently

FIGURE 1 Typical map cracking caused by AAR, I-295, Burlington County, New Jersey.

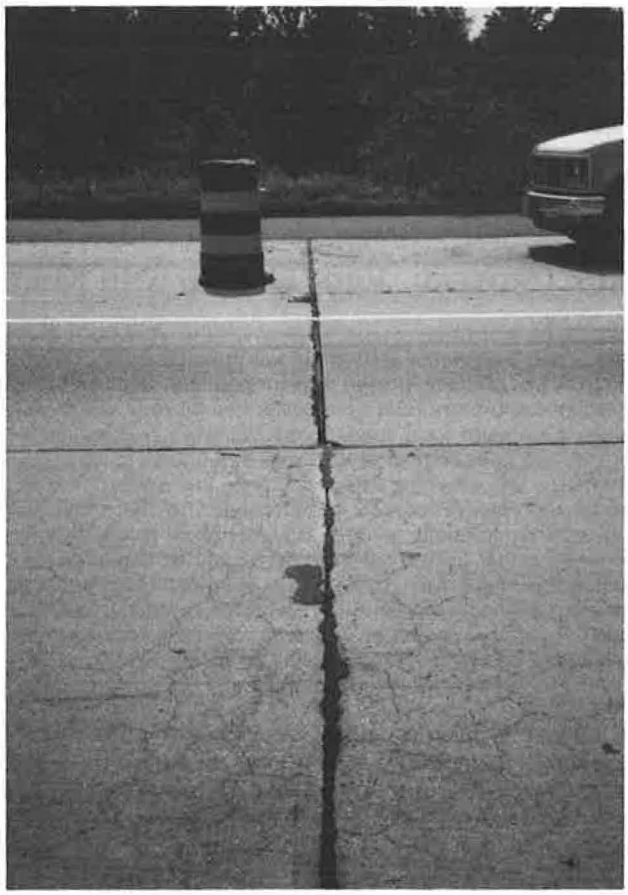

FIGURE 2 Full-width map cracking, I-295, Burlington County, New Jersey.

referred to as "dedolomitization." The series of chemical reactions that occurs in this process is expressed as follows (*2*):

$$Na_2O + H_2O \rightleftharpoons 2NaOH$$

$$K_2O + H_2O \rightleftharpoons 2KOH$$

$$CaMg(CO_3)_2 + 2NAOH \rightleftharpoons Mg(OH)_2 + CaCO_3 + Na_2CO_3$$

$$CaMg(Co_3)_2 + 2KOH \rightleftharpoons Mg(OH)_2 + CaCO_3 + K_2CO_3$$

(Dolomite) (Brucite)

As a result of the dedolomitization process, channels in the rock open, allowing water absorption on previously dry clay surfaces. The resultant swelling causes irreversible expansion of the rock, and subsequent cracking of the concrete. This process of progressive destruction takes from 3 to 15 years to produce detectable physical damage to the structure.

The destructive effects of the dedolomitization process can be further accelerated by two common highway maintenance practices. The first of these is the application of deicing salts, which increases the alkalinity of the concrete. The second is the use of cathodic protection systems. The latter systems, which are increasingly being used to prevent corrosion of bridge deck reinforcement, cause the entire reinforcing mat to serve as a negatively charged cathode. This negative charge attracts positively charged alkali ions to the rebars. These localized alkali concentrations can cause localized distress in a deck constructed with alkali-susceptible aggregates (*3*).

There are two basic ways to prevent AAR distress. First, avoid the use of susceptible aggregates. Second, reduce the free alkali content of the cement to a level below that required to initiate the reaction. (The latter approach is used in ASTM C150, which restricts the Na_2O equivalent alkali level to 0.6 percent.) Because the latter approach can be the most cost-effective under some conditions, both of the foregoing mitigation procedures were evaluated.

The alkali level of cement is primarily responsible for the alkali-aggregate reaction. The NJDOT's cement chemical analysis reports of the last 13 years (1976 to 1988) were reviewed to determine the average alkali levels of cement supplied during that period. As presented in Table 1, before the NJDOT's prohibition of the use of carbonate rock in 1983, only 3 out of 10 vendors consistently supplied high-alkali cement (alkali levels of 0.7 percent or higher). This number has increased dramatically in recent years. Currently, 7 out of 10 vendors consistently supply high-alkali cement. As shown in Figure 3, the weighted-average alkali level of cement supplied to the NJDOT has increased about 25 percent (from 0.57 to 0.73 percent) in recent years. This increase may be the result of environmental restrictions applied to the cement industry, which require recycling of high-alkali clinker and dust.

TABLE 1 AVERAGE ALKALI LEVELS OF CEMENT SUPPLIED TO NJDOT, 1976 TO 1988

	Carbonate Rock Allowed								Carbonate Rock Prohibited				
VENDOR	'76	'77	'78	'79	'80	'81	'82	'83	'84	'85	'86	'87	'88
A	1.0*	0.9*	---	1.0*	1.0*	1.0*	0.9*	0.9*	0.9*	0.9*	0.9*	0.9*	0.9*
B	0.5	0.5	0.6	0.1	0.1	0.1	0.7	0.7	0.5	---	0.6	0.7	0.7
C	0.4	0.3	0.3	0.3	0.4	---	0.3	---	---	---	---	---	---
D	---	---	---	---	---	---	---	---	---	0.8*	0.8*	0.7	---
E	---	---	---	---	---	---	---	---	---	1.0*	---	---	---
F	1.2*	---	---	1.0*	0.9*	0.9*	1.0*	1.0*	0.9*	0.8*	1.0*	0.9*	0.8*
G	0.7	0.9*	---	---	---	---	---	---	---	---	---	---	---
H	---	---	---	---	---	---	---	---	---	0.6	---	---	---
I	---	---	---	---	---	---	---	---	---	1.0*	---	---	---
J	0.7	0.5	0.6	0.7	0.7	0.7	0.8*	0.7	0.6	0.6	0.7	0.7	0.6
K	---	---	---	---	---	---	---	---	0.7	---	---	---	---
L	---	---	---	---	---	---	---	0.8*	0.8*	0.9*	0.9*	---	---
M	---	---	0.5	---	0.7	0.3	0.4	0.3	0.2	0.2	0.2	0.2	0.2
N	0.6	0.7	0.5	0.6	0.6	0.6	0.6	0.8*	0.8*	0.8*	0.8*	0.8*	0.7
O	0.1	0.1	0.1	0.1	0.1	0.1	0.1	---	---	---	---	---	---
P	0.8*	0.8*	0.8*	0.9*	0.9*	0.9*	1.0*	0.9*	---	---	0.9*	1.0*	0.9*
Q	0.2	0.1	0.2	0.2	0.1	0.2	0.2	1.0*	1.0*	0.9*	0.9*	0.9*	---

* Average Alkali Level exceeds 0.70 %

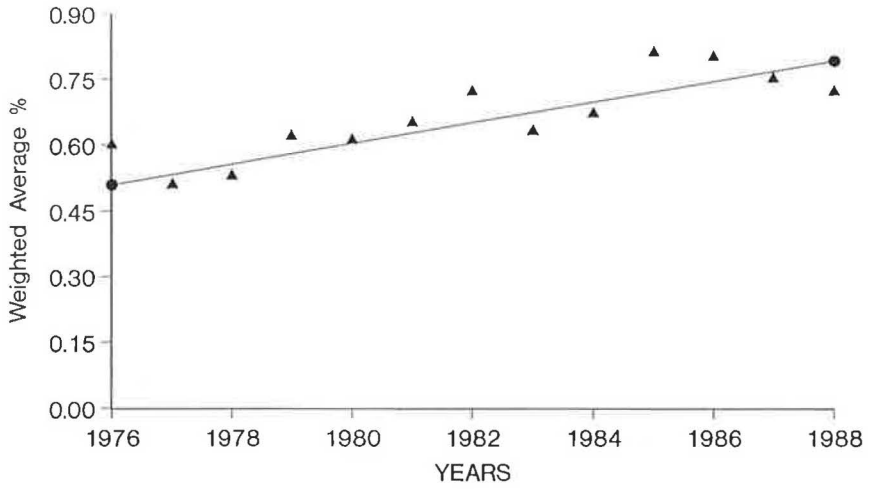

FIGURE 3 Cement alkali levels.

TEST METHODOLOGY

Sampling

More than 35 of the 150 NJDOT-approved aggregate sources are carbonate rock quarries. Of these, a representative group of eight was selected for tests on the basis of their geographic location and geologic type. The sampled quarries included the following local carbonate rock aggregate producers:

Name	*Location*
Eastern Industries	West Cocalico, Pa.
Keystone Portland Cement Co.	Bath, Pa.
A. G. Kurtz Co.	Denver, Pa.
New Enterprise Stone and Lime Co.	New Enteprise, Pa.
Huss Construction Co.	Andreas, Pa.
New Hope Crushed Stone Co.	New Hope, Pa.
Beaver Run Co.	Lafayette, N.J.
Carpentersville Sand and Gravel Co.	Carpentersville, N.J.

In order to provide a benchmark for gauging the sensitivity of the laboratory test procedures and the relative reactivity of the local carbonate aggregates, samples from three known reactive aggregate sources were also included in the testing program. These quarries were located in Kingston, Canada; Harrisonburg, Virginia; and Centerville, Tennessee.

Testing Procedure

Overview

The literature indicates that no single test can be relied on to consistently predict the reactive tendencies of carbonate rock. Rather, a battery of tests is required to determine potential reactivity.

The most commonly used combination of tests (the one adopted for use in this study) involves a petrographic examination (ASTM C295) and expansion tests performed on samples of the rock (ASTM C586) and concrete containing the carbonate aggregate (ASTM C1105). These procedures are outlined in the following subsections.

Petrographic Examination

The petrographic examination entails the use of an optical microscope to distinguish between nonreactive and potentially reactive carbonate rocks on the basis of their composition, texture, and grain size.

Using the optical microscope, the common features of expansive carbonate rocks can be identified as follows:

- Dolomitic with appreciable quantities of calcite,
- Presence of clay,
- Extremely fine-grained matrix, and
- Characteristic texture consisting of small isolated dolomite rhombs disseminated in a matrix of clay and finely divided calcite.

The petrographic examination is quick, but only identifies rock constituents that have the potential for reactivity. Additional testing is required to determine whether a given rock will, in fact, react in the presence of alkalies.

Rock Cylinder Test

Two to four ⅜-in. diameter, 1⅜-in.-long cores were drilled perpendicular to the bedding from each of the representative ledge rock samples at random locations. The ends of each rock cylinder core were ground to obtain smooth orthogonal faces.

The samples were initially conditioned by placing them in polypropylene bottles filled with distilled water for 30 h. The samples were dried, and the initial core length was measured with a micrometer and recorded. (All measurements taken at subsequent test ages were made using the same micrometer. The average of two or three readings taken independently by separate technicians was recorded as the final reading for each sample at each test age.)

For the remaining test period, the samples were stored at room temperature in NaOH solution. Length measurements were made after 1, 2, 3, 4, 8, 12, 16, 26, 39, and 52 weeks of conditioning.

At each test age, length change to the nearest 0.01 percent was calculated as

$$\text{Length change (percent)} = \frac{L_1 - L_0}{L_0} \times 100$$

where

L_1 = length at test age, and

L_0 = initial length.

The average length change reported at a given test age was the average of two or three readings.

Concrete Bar Test

General Each of the eight local aggregates and two of the three known reactive aggregates were used in separate batches of concrete made using a high-alkali cement (1.25 percent). In order to test the effect of lower alkali levels, two of the known reactive aggregates and one local source (Keystone) were also used in batches made with 0.74 percent alkali cement (see Table 2). Six concrete bars were cast from each batch. These bars were stored in the 100 percent humidity room. Length change measurements were made using the length comparator shown in Figure 4 at 1, 4, 12, 26, 39, and 52 weeks.

Mix Design The concrete mix was designed using ACI 211.1–74, *Standard Practice for Selecting Proportions for Normal, Heavy Weight, and Mass Concrete*. Approximately 200 lb of ledge rock from each source were crushed and graded to comply with AASHTO No. 57 size. Physical properties such as dry rodded weight, specific gravity, and percent absorption were determined for each batch. Table 2 presents mix proportions, and Table 3 presents details of physical properties.

A chemical analysis of the cement from Independent Cement Corporation, Catskill, N.Y., indicated that its total Na_2O equivalent alkali content (ASTM C150) was 0.74 percent. In

TABLE 2 MIX DESIGN DETAILS (PER CUBIC FOOT)

SAMPLE	CEMENT Lbs.	AGGR. Lbs.	SAND Lbs.	WATER Lbs.	NaOH Added	ALKALI %
Eastern Indus.	24.22	65.39	44.70	12.60	0.16	1.25
Keystone Co.(1)	22.72	66.15	48.46	11.85	0.16	1.25
Keystone Co.(2)	22.72	66.15	48.46	11.85	0.00	0.74
Keystone Co.(3)	22.72	66.15	48.46	11.85	0.00	0.74
Keystone Co.(4)	22.72	66.15	48.46	11.85	0.13	1.00
A.G.Kurtz Co.	22.72	66.78	50.51	11.85	0.16	1.25
New Enterprise Co.	22.72	64.26	52.72	11.85	0.16	1.25
Huss Const. Co.	22.72	62.37	52.11	11.85	0.16	1.25
Beaver Run Co.	22.72	64.89	51.60	11.85	0.16	1.25
Carpentersville Co.	22.72	64.26	52.75	11.85	0.16	1.25
New Hope Co.	22.72	64.26	50.52	11.85	0.16	1.25
Harrisonburg Va.(1)	22.72	64.26	50.51	11.85	0.16	1.25
Harrisonburg Va.(2)	22.72	64.26	50.15	11.85	0.00	0.74
Kingston,Canada.(1)	22.72	61.74	54.16	11.85	0.16	1.25
Kingston,Canada.(2)	22.72	61.74	54.16	11.85	0.00	0.74
Centerville,Tenn.	***	No Concrete Bars Made			***	

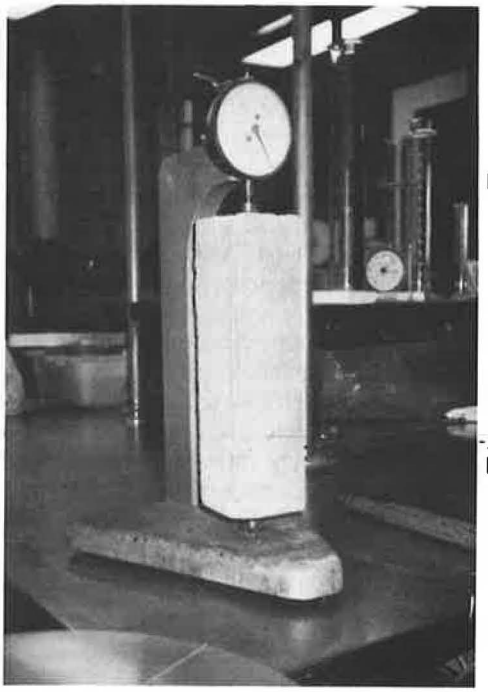

FIGURE 4 Length comparator with typical concrete bar sample.

TABLE 3 PHYSICAL PROPERTIES OF AGGREGATE SAMPLES

SAMPLE	BULK SP. GRAVITY	UNIT WT. (Lbs)	DRY RODDED WT. (Lbs)
Eastern Indus.	2.77	99.00	104.00
Keystone Co.	2.69	98.00	105.00
A.G.Kurtz Co.	2.80	97.00	106.00
New Enterprise Co.	2.79	96.00	102.00
Huss Constr. Co.	2.68	92.00	99.00
Beaver Run Co.	2.77	96.00	103.00
Carpentersville Co.	2.77	94.00	102.00
New Hope Co.	2.76	93.00	101.00
Harrisonburg,Va.	2.78	94.00	102.00
Kingston,Canada	2.74	91.00	98.00
Centerville,Tenn.	2.81	98.00	105.00

order to simulate severe in-service conditions (e.g., heavy application of deicing salts), the alkali level was raised to 1.25 percent by adding 0.16 lb of NaOH to the mixing water. Four batches were made with the alkali level at 0.74 percent (unchanged) to serve as a control.

Concrete Batching A total of 16 1-ft^3 batches of non-air-entrained concrete were made. From each batch, six 3 × 3 × 11 in. concrete bars were made for the length change test. These test bars were cast with stainless steel plugs at each end to act as reference points for length measurement using the length comparator equipment. The test bars were covered with plastic, cured at room temperature, and stripped on the following day. Each test bar was marked for identification and soaked in water for 30 min before initial length measurement.

Storage of Concrete Bar Samples After the initial measurement, the bars were stored in water for 28 days at room temperature. On completion of this 28-day period, test bars were stored in a 100 percent humidity room at 73°F for the entire test period of 1 year.

RESULTS AND ANALYSIS

Petrographic Examination

The results of the ASTM C295 petrographic examination are presented in Table 4. As indicated in the table, none of the local carbonate rocks were judged to be potentially reactive. Only one of the known reactive aggregates, that from Virginia, displayed the characteristic constituents of an AAR-susceptible aggregate. The potential activity of the Tennessee and Kingston, Canada, aggregates could not be determined by the petrographic examination.

Rock Cylinder Test

Evaluation Criteria

ASTM C586 states that an aggregate that expands more than 0.10 percent has undergone a detrimental chemical reaction, and should be further tested in concrete.

Results

The results of the rock cylinder test are presented in Table 5. Examination of this tabulation indicates that none of the local carbonate aggregates exceeded the ASTM C586 criteria. Only 2 of the 11 samples expanded appreciably during the 1-year test period.

The results for the known expansive aggregates are shown in Figure 5. Examination of this plot indicates that the Canadian aggregate failed the rock cylinder test in convincing fashion. After 1 month in test, this aggregate exceeded the failure criterion by a factor of eight (0.8 versus 0.1 percent); after a year, it expanded nearly 2 percent. The sample from another known expansive source in Harrisonburg, Virginia, expanded steadily over the entire test period and exceeded the failure criterion after 2 months in test. The aggregate from the third known expansive source in Centerville, Tennessee, shrank rather than expanded. This unexpected behavior might have been the result of sampling from the nonreactive strata of the quarry. (Because of a shortage of material, this sample could not be tested in concrete.)

Concrete Bar Test

Evaluation Criteria

Unlike the petrographic and rock cylinder test procedures, there is no established criteria for evaluating the results of the concrete bar test. Rather, as presented in Table 6, a

TABLE 4 RESULTS OF PETROGRAPHIC EXAMINATION

SAMPLE	PETROGRAPHIC DESCRIPTION	REACTIVE ?
Eastern Indus.	Limestone. No distinct Dolomite. No visible clay concntration. Fine grained.	No
Keystone Co.	Limestone. Elongated "eyes" of carbonate. Scattered quartz silt.	No
A.G.Kurtz Co.	Limestone. Fine grained. Large Dolomite crystals. No clay.	No
New Enterprise Co.	Limestone. Fine grained. Dolomite in small,local patches. Some quartz silt.	No
Huss Constr. Co.	Limestone. Fine grained. No Dolomite.	No
New Hope Stone Co.	Limestone. Fine grained. Significant quartz silt. No Dolomite.	No
Beaver Run Co.	Dolomite present. No clay concentration visible.	No
Carpentersville Co.	Dolomite present. No clay concentration visible.	No
Harrisonburg, Va.	Fine grained. Brittle. Clay present in significant amount.	Yes
Kingston, Canada.	Calcareous Argillite, fine grained. Significant amount of clay.	Undetermined
Centerville, Tenn.	Large amount of clay,quartz silt.	Undetermined

TABLE 5 ROCK CYLINDER TEST RESULTS (WITH LENGTH CHANGES EXPRESSED IN PERCENTAGES)

SAMPLE	TEST AGE				REACTIVE ?
	1 MO.	3 MO.	6 MO.	1 YR.	
Eastern Indus.	-0.05	-0.05	-0.05	-0.17	No
A.G.Kurtz Co.	0.00	0.00	-0.01	-0.04	No
Kingston,Canada	0.81*	1.56*	1.78*	1.86*	Yes
Carpentersville, NJ	-0.02	0.01	0.00	-0.01	No
Keystone Co.	0.03	0.00	0.02	0.03	No
New Enterprise Co.	-0.06	-0.06	-0.01	-0.04	No
Harrisonburg, Va.	0.05	0.19*	0.29*	0.52*	Yes
New Hope Co.	0.03	0.01	0.00	0.02	No
Beaver Run Co.	-0.08	-0.09	-0.04	-0.03	No
Huss Constr. Co.	-0.13	-0.12	-0.15	-0.14	No
Centerville, Tenn.	-0.06	-0.04	-0.02	-0.01	No

* Expansion exceeded the limit of 0.10 %

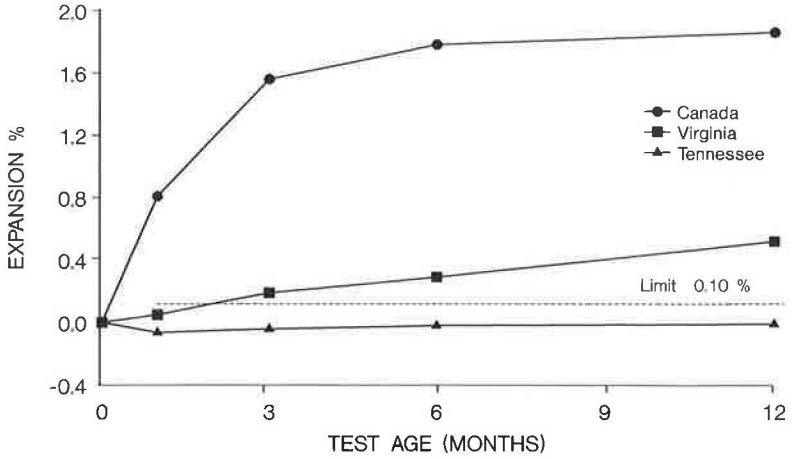

FIGURE 5 Rock cylinder test results for known reactive sources.

TABLE 6 SUGGESTED EVALUATION CRITERIA FOR CONCRETE BAR EXPANSION TEST

AUTHOR	% EXPANSION				
	3 mo.	6 mo.	1 yr.	3 yr.	5 yr.
Swenson & Gillot (HRB Record 45 pp 21-40 1964)	-----	0.02	-----	-----	-----
Smith (HRB Record 45 pp 126-133 1964)	0.02	-----	-----	-----	-----
Newlon (Va.HWY RES. Council 8 VHRC 71-R 41)	-----	-----	0.03	-----	0.05
Canadian Std. Assoc.	0.02	-----	-----	-----	-----
Walker (ASTM STP 1978 pp 772)	0.015	0.025	0.03	-----	-----
Ministry Of Trans. Canada	0.015	0.025	-----	-----	-----
ASTM Draft 10-81 (Com. C9)	0.015	0.025	0.03	-----	-----
NJDOT Research Suggestion	0.015	0.02	0.025	-----	-----

variety of threshold limits for expansion has been suggested by various agencies and authorities on the subject as being indicative of detrimental chemical reaction. The lowest of these test age suggested expansion limits are as follows: 0.015, 0.02, and 0.025 percent at 3, 6, and 12 months, respectively.

Results

The length changes presented in Table 7 represent the average measured on six samples. On the basis of the lowest threshold values, the known expansive source from Kingston (Canada) is identified as being an unacceptable concrete aggregate. It exceeded threshold values at all three test ages of 3 months, 6 months, and 1 year when concrete of 1.25 percent alkali level was used. Six additional concrete bars were made using the same Canadian source, but with a lower alkali level (0.74 percent). These bars also exceeded the threshold limits at all three test ages. These results indicate that this carbonate rock source is highly reactive. The second known expansive source from Harrisonburg, Virginia, expanded somewhat but never exceeded the threshold limit at any stage (see Figure 6). The third known expansive source from Centerville, Tennessee, could not be evaluated because of lack of material.

Two other sources, Eastern Industries (West Cocalico, Pennsylvania) and Keystone Portland Cement Co. (Bath, Pennsylvania), evidenced some expansion. The Eastern concrete bar sample exceeded the 3- and 6-month test age thresh-

TABLE 7 CONCRETE BAR TEST RESULTS (WITH LENGTH CHANGES EXPRESSED IN PERCENTAGES)

SAMPLE	TEST AGE			ALKALI
	3 MO.	6 MO.	1 YR.	%
Eastern Indus.	0.018*	0.020*	0.020	1.25
A.G.Kurtz Co.	0.010	0.002	0.017	1.25
Kingston,Canada (1)	0.025*	0.024*	0.040*	1.25
Carpentersville Co.	0.005	-0.002	0.007	1.25
Keystone Co. (1)	0.080*	0.112*	0.170*	1.25
New Enterprise Co.	0.005	0.010	0.008	1.25
Harrisonburg, Va.(1)	0.010	0.015	0.010	1.25
New Hope Co.	0.010	0.012	0.004	1.25
Beaver Run Co.	0.000	-0.002	-0.010	1.25
Huss Constr. Co.	-0.017	0.002	0.000	1.25
Kingston, Canada (2)	0.018*	0.027*	0.037*	0.74
Harrisonburg,Va.(2)	0.000	0.010	-0.002	0.74
Keystone Co.(2)	-0.010	-0.010	-0.010	0.74
Keystone Co. (3)	0.003	-0.002	0.005	0.74
Keystone Co. (4)	0.001	-0.002	0.002	1.00
Keystone Co. (5)	0.015*	0.012	0.020	1.25

* Expansion equalled or exceeded allowable limit. Limits shown below:

3 Months Test Age	0.015 %
6 Months Test Age	0.020 %
1 Year Test Age	0.025 %

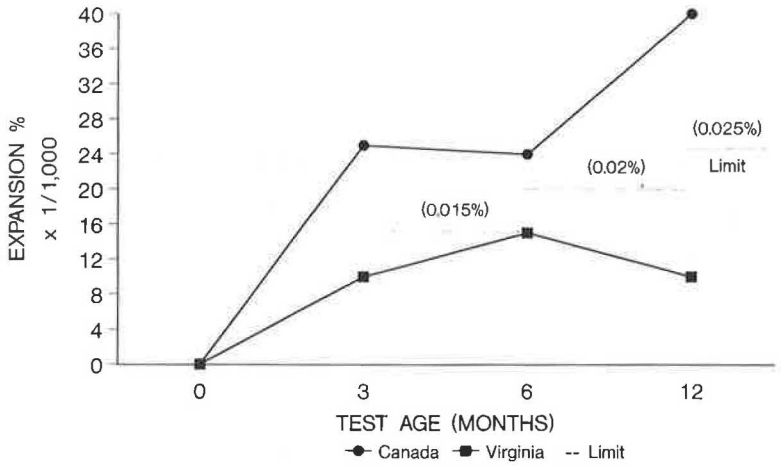

FIGURE 6 Concrete bar test for known reactive aggregate sources.

old criteria but did not exceed the 0.025 percent threshold limit for test specimens 1 year old. The sample from Keystone (Bath, Pennsylvania) far exceeded the threshold values at all test ages. Because this particular sample did not fail either the petrographic or the rock cylinder test, it was decided to retest using the same source. Three different alkali level concrete mixes identified in Table 7 as Keystone 3, 4, and 5 were batched using new material (AASHTO No. 57 stone) from the same source. The three alkali levels selected were 0.74, 1.0, and 1.25 percent.

As shown in Figure 7, the average expansion of the Keystone aggregate bars made at the 0.74 and 1.0 percent alkali

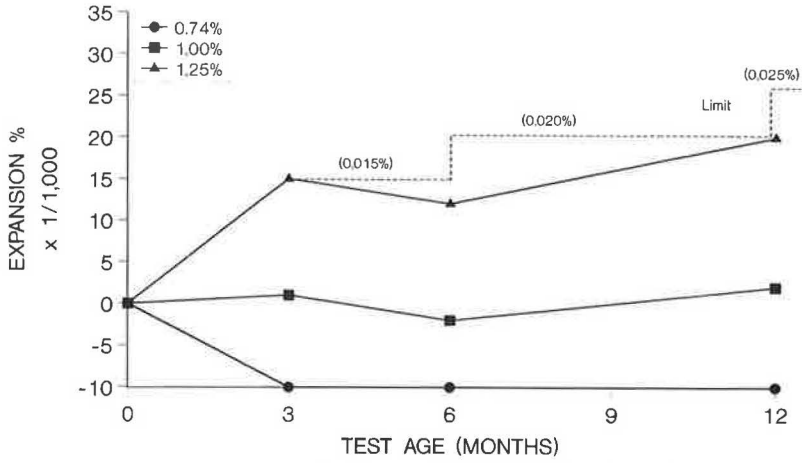

FIGURE 7 Concrete bar test for Keystone aggregate at various alkali levels.

levels was insignificant over the entire test period. The average expansion of the bars made at the 1.25 percent alkali level was significant, yet within allowable limits, indicating that the detrimental effects are indeed associated with the amount of alkali in the concrete mix.

The behavior of the Keystone aggregate may be akin to the experience noted with the Centerville, Tennessee, rock cylinder test. That is, the sampling procedure at the quarry apparently results in samples of varying rates of reactivity on the basis of the strata from which they are obtained.

CONCLUSIONS

The principal conclusions derived from this research study are as follows:

1. Application of the screening criteria will identify potentially reactive carbonate rock sources. The results suggest that the entire battery of tests—the petrographic examination and expansion tests on rock and concrete samples—should be performed. Passing any single test will not necessarily ensure that the aggregate is in fact nonreactive.
2. The careful selection of representative samples is critical, because the degree of reactivity may vary significantly within a given quarry.
3. The results of this study confirm that use of low-alkali cement is a viable means for reducing potential detrimental alkali-carbonate reactions. As a practical matter, selection of a limiting value defining a suitably low alkali level should take into account both the relative reactivity of the local aggregates and the prevailing level of alkali in the cement being supplied. For New Jersey conditions, it appears that a cement alkali level of 0.7 percent or less would provide a reasonable safeguard against destructive carbonate reactions. This 0.7 percent level should be attainable by local cement suppliers.
4. A satisfactory specification for carbonate aggregate can be based on a demonstrated nonreactivity under the battery of tests outlined here, coupled with the use of a low-alkali (0.7 percent or less) cement. The latter provision will help mitigate the effects of any failure to detect aggregate reactivity. Such a specification has been developed and is under consideration in New Jersey.

REFERENCES

1. G. Kauffman. Alkali Aggregate Reaction, I-295 MP 48.0 to 54.0, MP 56.5 to 57.0, Burlington County, N.J. New Jersey Department of Transportation Memorandum Report. Trenton, April 1988.
2. H. Woods. *Durability of Concrete Construction*. Iowa State University Press, Ames, Iowa, 1968.
3. K. Natesaiyer and K. C. Hoover. Investigation of Electrical Effects on the Alkali Aggregate Reaction. Noyes Publication, Park Ridge, N.J., 1987.

Publication of this paper sponsored by Committee on Mineral Aggregates.

Laboratory Tests for Predicting Coarse Aggregate Performance in Ontario

S. A. SENIOR AND C. A. ROGERS

Coarse aggregates used in granular base and asphaltic and portland cement concrete must be sound and capable of withstanding the prevailing environment. In Canada, aggregates must be frost resistant. Durability of coarse aggregate is normally evaluated in the sulfate soundness test and water absorption tests, and by measuring resistance to impact in the Los Angeles abrasion and impact test. These tests suffer from some disadvantages: poor precision and inadequate correlation with field performance. The Ministry of Transportation has been developing and evaluating new test procedures for a number of years. Some of the major findings are summarized. The likely performance of aggregates in granular base is best measured by the micro-Deval test and water absorption. The physical quality of portland cement concrete aggregates is best measured by the micro-Deval test, water absorption, and unconfined freezing and thawing. The quality of asphaltic concrete aggregates is best measured by the micro-Deval test, polished-stone value test, and unconfined freezing and thawing test. Petrographic examination is also an essential tool in the evaluation of aggregate quality.

The Ministry of Transportation uses aggregates in road construction for granular base, asphaltic concrete, and portland cement concrete. These aggregates must be sufficiently durable to withstand the effects of construction, weathering, and vehicle loads.

Temperature changes, seasonal and daily freezing and thawing cycles, and wetting and drying cycles contribute to the breakdown or weathering of the aggregates. Deicing salts also contribute to aggregate deterioration and have a marked accelerating effect on damage caused by freezing and thawing (*1*).

Increased traffic volumes and higher axle loads subject pavements and structures to higher stresses and more frequent loading cycles. High interparticle stresses lead to particle breakdown, reducing permeability and causing permanent deformations in granular base and asphaltic concrete. Abrasion of exposed aggregate by tires on asphalt and concrete surfaces can result in particle wear and polishing, thus reducing surface friction.

High-quality aggregates may not always be available at a reasonable price. Competition for land use from urbanization or other uses such as agriculture, forests, and wetlands has diminished the availability of some aggregate resources in areas of high demand. Compromises in material quality must be made where marginal or lower-quality aggregates are more readily available than good ones. The decision to accept marginal aggregates has hidden costs if they perform below expectations and reduce pavement life.

Engineering Materials Office, Ministry of Transportation, 1201 Wilson Avenue, Downsview, Ontario M3M 1J8.

Aggregates must be carefully selected if they are to perform satisfactorily in highways. The selection process is made by subjecting aggregates to a series of quality tests designed to measure their physical properties, or to apply an appropriate simulation of the field conditions the aggregates will be exposed to and measure the response. By using appropriate tests, the risk of acceptance of marginal aggregates is reduced.

The physical requirements of coarse aggregates used for road construction in Ontario are currently measured using the following tests: Los Angeles impact and abrasion test (MTO LS-603, ASTM C131); magnesium sulfate soundness test (MTO LS-606, ASTM C88); 24-hr water absorption test (MTO LS-604, ASTM C127); and petrographic evaluation leading to a petrographic number, or PN (MTO LS-609).

The acceptance of aggregates is dependent on the material meeting all of the minimum requirements as outlined in specifications. However, poor performance of a suitable aggregate in an inappropriate test may prevent it from being used. For example, a quarried sandy dolostone (sandy dolomite) from eastern Ontario typically gives losses in the magnesium sulfate test up to 17 percent (considerably outside the specification for asphalt aggregate), yet it is not a frost-sensitive material. It has excellent frictional properties and is used as a premium-quality asphalt wearing course aggregate.

Although the four tests can help distinguish between an excellent aggregate and a poor one, they are not as good at predicting material behavior where borderline or marginal aggregates are concerned. In particular, the use of the sulfate soundness test for aggregate soundness and the Los Angeles test for aggregate abrasion resistance both have demonstrated poor correlation with field performance. These tests do not reflect the conditions of the weathering environment, or the construction and in-service pavement conditions.

AGGREGATE QUALITY AND SOUNDNESS

Aggregate quality is assessed mainly with respect to physical parameters, that is, processes that cause particle fragmentation without any associated mineralogical alteration. Much of this type of degradation occurs during the construction processes of material processing or manufacture, transportation, mixing, placement, and compaction. Sudden impact and short-lived dynamic loads are imparted to the aggregates at this time.

Long-term aggregate breakdown occurs when the material is in service and undergoes ongoing stresses of loading and unloading. Numerous weathering factors are involved in the physical changes that occur to aggregates, including temper-

ature and moisture fluctuations. A comprehensive review of in situ physical weathering of materials in engineering applications is given by Fookes et al. (*2*).

Measurement of aggregate resistance to impact and abrasion in Ontario has relied exclusively on the Los Angeles test. This test uses a large, horizontally mounted steel drum into which 5000 g of sample are placed along with a specified number of steel spheres 45 mm in diameter. The drum is rotated 500 times at 33 rpm. A steel plate attached to the inside of the drum picks up the steel spheres, which then fall directly onto the test sample. After the test, the sample is screened on the 1.70-mm (No. 12) sieve with the material passing indicated as a percent loss of the original mass.

The Los Angeles test is not always appropriate because the steel balls impart a severe impact loading on the test sample, overshadowing any interparticle abrasion, which is the predominant process in pavement subject to traffic stress. Coarse-grained crystalline materials, particularly brittle granites and gneisses, yield high losses in this test yet perform well in service. However, high losses (>45 percent) indicate a potential breakdown problem during the construction process. In contrast, fine-grained, soft-rock aggregates, such as argillaceous carbonates or shales, tend to absorb the impact energy of the steel balls resulting in low test values, well within normal acceptance limits. These materials are usually susceptible to slaking and particle degradation when wet, which results in poor pavement performance.

The test conditions of the Los Angeles test do not simulate the in-service pavement conditions because only oven-dried aggregates may be properly and easily tested in the apparatus. When aggregates are tested in a moist or saturated condition, fines adhere to the side of the drum, altering the test conditions and making it difficult to retrieve them for analysis (*3*). This consideration is important because the moisture condition of an aggregate may significantly alter its behavior. Pintner (*4*) reported in a study of fines production in a shaker test that the loss was increased nine times for an aggregate sample with 5 percent moisture, as contrasted with the same material in a dry state.

Soundness is a synonym for the long-term durability of an aggregate as a result of the material's ability to resist weathering forces. In a highway pavement environment, the weathering of aggregates varies greatly according to their exposure. Granular base courses are the least protected from the effects of weathering. Wetting and drying cycles are most likely to affect these materials. Asphalt aggregates are only slightly better protected from moisture by a coating of asphalt cement. Concrete aggregates are the most protected by the dense microporous cement paste. All aggregates are within the upper 1 m of the road surface and are exposed to thermal cycling. In the presence of moisture, this becomes much more severe freeze-thaw cycling.

The Ontario Ministry of Transportation, like many highway agencies in North America, has relied on the sulfate soundness test as a simulation of the weathering environment. The crystallization of soluble salt in rock pores bears little resemblance to the environmental conditions found in Ontario. The sulfate soundness test also subjects the aggregate to thermal expansion and contraction cycles as well as wet-dry cycling. Salt crystallization is used to simulate ice crystallization, a model that may have been acceptable when the test was originally developed, but is no longer so. Equipment is now available to accurately recreate freezing and thawing conditions in the laboratory (*1*).

ALTERNATIVE TEST METHODS

The objective has been to investigate alternative methods of measuring the performance of coarse aggregates using tests that are relatively quick and simple to perform, yet give repeatable and reproducible results. The goal has been to select tests that are better indicators of aggregate quality than those currently used. The expected benefits are that the test results would be more effective in selecting or rejecting marginal aggregates. Selection criteria require that each test demonstrates good correlation with field performance and has excellent reproducibility of results within, and between, laboratories. Ideally, new test procedures should be reliable, precise, quick, and cheap compared to the standard tests. In order to attain these objectives, tests that simulated the field environment as nearly as possible were used because it was likely that they would be more inclined to correlate with field performance. It was also desired that these tests used, as far as possible, simple and inexpensive equipment.

The tests under investigation have either been developed within the Ministry or adopted from other agencies. Although a number of tests have been studied (*5*), only the following tests are discussed in this report:

1. Unconfined freeze-thaw test for coarse aggregate (MTO LS-614),
2. Micro-Deval abrasion test (BNQ 2560–070/82),
3. Aggregate impact value test (BS 812),
4. Polished stone value test (BS 812), and
5. Aggregate abrasion value test (BS 812).

The evaluation of the conventional and the alternative tests has been conducted using a suite of over 100 coarse aggregate samples collected from across Ontario. These samples represented a wide cross section of rock types and aggregate sources.

Ontario aggregates are composed of either a mixture of rock types from glaciofluvial deposits, or quarried Paleozoic sedimentary or Precambrian igneous and metamorphic rock types. Most of the sources had previously been used by the Ministry so that their field performance in various environments and value ratings could be applied. Evaluation criteria used for the ratings are presented in Table 1.

Unconfined Freeze-Thaw Test

This test has been under development at the University of Windsor and the Ministry of Transportation over the last 10 years. It is designed to measure the frost resistance of aggregates by simulating the conditions of freeze-thaw cycling in the presence of moisture and deicing salts. The results of this investigative work and a copy of the procedure have been published by the Ministry of Transportation (*1*,*6*).

The unconfined freeze-thaw test is conducted by placing three fractions of an aggregate (Table 2) into separate 1-L jars. The samples are soaked for 24 hr in a 3 percent NaCl

TABLE 1 FIELD PERFORMANCE EVALUATION CRITERIA OF AGGREGATES TESTED IN THIS STUDY

Evaluation	Description
GOOD	• used for many years with no reported failures, popouts, or other signs of poor durability
FAIR	• used at least once where popouts or some reduced service life had resulted, but pavement or structure life extended for over 10 years
POOR	• used once with noticeable disintegration of pavement after one winter, severely restricting pavement life

TABLE 2 GRADATION AND MASS OF FREEZE-THAW TEST SAMPLE

PASSING	RETAINED	MASS (g)
19.0 mm	13.2 mm	1250
13.2 mm	9.5 mm	1000
9.5 mm	4.75 mm	500

solution, drained, sealed, and cycled five times, frozen for 16 hr at −18°C, and thawed at room temperature for 8 hr. Following the test, the material is drained, dried, and resieved on the original sieves. A weighted average loss is determined from the "as received" coarse aggregate gradation (percent retained) and the percent loss from all three fractions.

The equipment and procedure of this test are calibrated by testing a control material (slightly shaley dolomitic limestone with an average freeze-thaw loss of 24.5 percent) along with any samples under investigation.

Micro-Deval Abrasion Test

This test was developed in France during the 1960's (*7*) and is based on equipment used in the grinding industry. This test is currently being used in the province of Quebec and the procedure has been adopted from its standards (*8*). An aggregate sample (consisting of 250 g retained on the 13.2-mm sieve, and 250 g retained on the 9.5-mm sieve) is initially soaked for 24 hr and then placed in a jar mill with 2.5 L of water and an abrasive charge consisting of 5 kg of steel balls of 9.5-mm diameter. The jar, aggregate, water, and charge are revolved at 100 rpm for 2 hr. The sample is then washed and oven-dried. The loss is the amount of material passing the 1.18 mm (No. 16) sieve expressed as a percent by mass of the original sample. Comparison with the magnesium sulfate test indicates similarity of test results but with a greater amount of precision. Linear regression analysis gives a correlation coefficient of 0.85 for 106 samples (Figure 1). A comparison of the standard deviation of test results from the micro-Deval abrasion test and the magnesium sulfate soundness test is shown in Figure 2. The precision of the micro-Deval test, especially for materials with high losses, is greater than the precision measured by the soundness test.

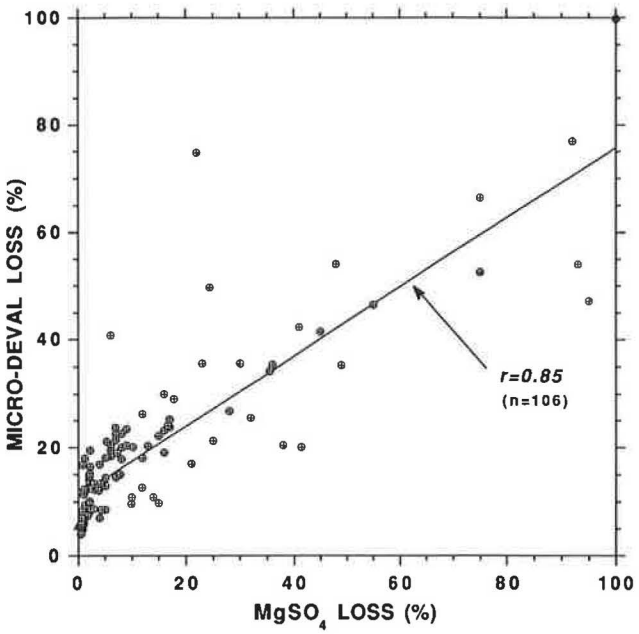

FIGURE 1 Correlation of micro-Deval abrasion against magnesium sulfate soundness.

Aggregate Impact Value Test

This procedure assesses aggregates passing the 13.2-mm sieve and retained on the 9.5-mm sieve (*9*). It measures fines production by the repeated impact of a falling weight (13.5 to 14.0 kg) onto a small confined sample (300 to 350 g). The percent fines is calculated as the mass of material passing the 2.36-mm (No. 8) sieve as a ratio to the original mass. Two samples are tested and the resulting average is known as the aggregate impact value (AIV). This test has demonstrated good correlation with the Los Angeles impact and abrasion test, which is shown in Figure 3. Linear regression analysis of the two data sets illustrates a significant similarity between the two tests. This test has the advantage over the Los Angeles impact test in that the equipment is inexpensive and portable, uses less material than the Los Angeles test and can easily test samples in a moist or saturated condition if desired, thus better simulating field conditions.

Polished-Stone Value Test

This test is a laboratory simulation of polishing of aggregate by vehicle tires (*9*). Selected aggregate particles are placed and cemented in a mould so that an aggregate surface is exposed for study in a tablet. The tablet is placed on the outside of a steel wheel that brings the sample into contact with a rubber tire. The samples are subjected to wear by a coarse and a fine emery abrasive powder under the rubber tire for 3 hr each. Water is continually added to the aggregate surface. The resulting microtexture, or polish, of the sample is measured by evaluating the resistance of a rubber testing

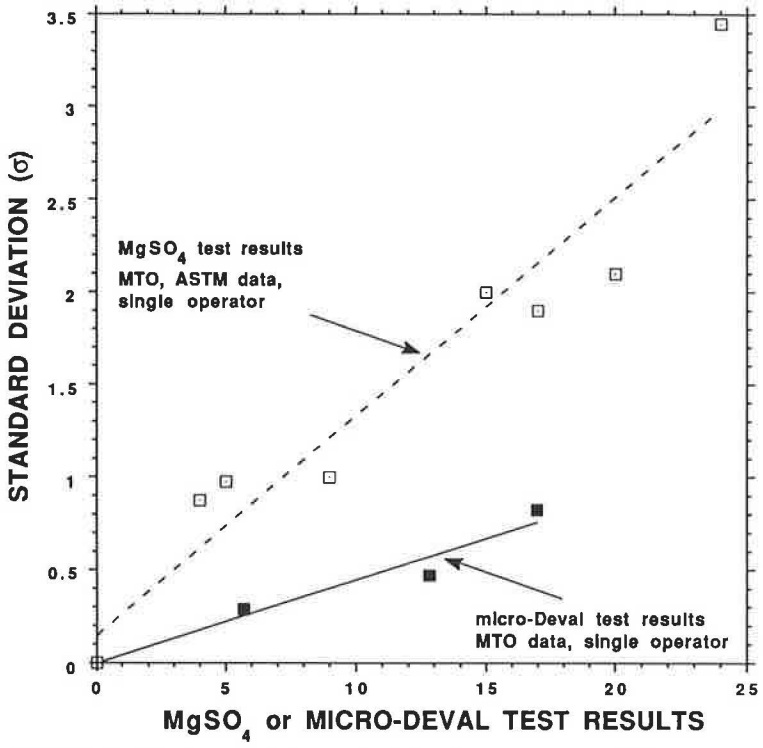

FIGURE 2 Standard deviation against loss in magnesium sulfate soundness or micro-Deval abrasion test.

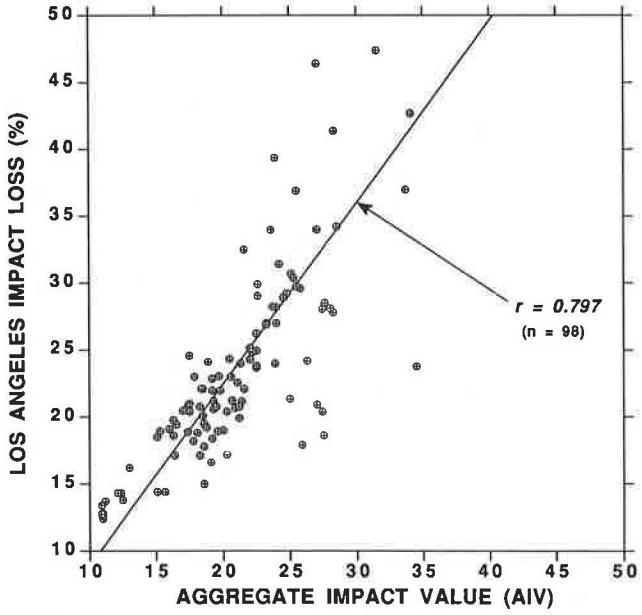

FIGURE 3 Relationship between Los Angeles impact and aggregate impact value.

pad at the end of a free-swinging pendulum arm across the aggregate surface. The travel of the pendulum arm after the pad has contacted the aggregate surface is measured by a calibrated scale and the resulting number is known as the polished stone value (PSV). Rough surfaces offer more resistance to the rubber pad and give higher values, whereas highly polished surfaces, offering little resistance, give low values.

A good correlation of PSV with friction levels of asphalt pavements has been demonstrated for different coarse aggregates, used in similar asphalt mixtures, on the same section of highway (*10*). In other words, everything else being equal, a material with a high PSV will provide higher friction than a material with a low PSV.

Aggregate Abrasion Test

This test evaluates overall wear resistance of aggregate, measuring both mineral hardness and bonding between individual grains, by abrasion (*9*). Aggregate particles are held in a mould and an exposed test surface is placed on a flat, rotating steel plate. A standard weight is placed on the mould to bring the exposed aggregate surface into direct contact with the plate, while silica sand is metered onto the plate surface as it rotates and is used to abrade the aggregate. No water is added to the sample and all abrasion is done dry. The sample mass is taken before and after the test. The resulting percentage loss, normalized for density of the aggregates, is the aggregate abrasion value (AAV). Wear-resistant aggregates yield low values and soft aggregates yield high values.

RESULTS AND DISCUSSION

Granular Base

Current granular base design in Ontario is a matrix-supported system. Most granular base failures have been caused by low permeability as a result of the presence of plastic fines or the

presence of platy pore-blocking minerals such as chlorite and biotite mica derived from high-grade metamorphic rock. During service, granular bases are subjected to loading, freeze-thaw, and wet-dry cycling.

The Los Angeles test indicates little correlation with field performance when the loss is less than 50 percent (Figure 4). The aggregate impact value has a similar lack of relationship to field performance. During construction, aggregate handling of granular base materials is minimal. Any resulting aggregate breakdown is easily accommodated within the wide gradation band that is acceptable for these materials. Stone with losses in excess of about 45 percent may be susceptible to excessive breakdown during handling, although gneissic materials with losses up to 60 percent can still be used provided they do not contain excessive amounts of mica.

Petrographic examination is useful in predicting performance of granular base aggregates (Figure 4). This test examines individual particles retained on standard sieve sizes (about 200 particles from each fraction), starting with the coarsest fraction until a minimum of 70 percent of the material is examined. The particles are separated into quality categories of good, fair, poor, or deleterious using a variety of techniques and criteria. The percent weight of each category is multiplied by a factor of 1, 3, 6, or 10, respectively, and summed. The resulting number is the PN value (*11*). For example, an aggregate sample consisting of material determined to be 75 percent good, 15 percent fair, 8 percent poor, and 2 percent deleterious would have a PN of 188 [(75 × 1) + (15 × 3) + (8 × 6) + (2 × 10)]. Aggregates that have yielded poor performance in granular base courses generally have a PN value greater than 200, whereas satisfactorily performing aggregates have PN values much less than this. Marginal aggregates are not easily separated using petrographic and impact tests together.

The micro-Deval test is useful for separating good- from poor-quality aggregates (Figure 5). Material with a micro-Deval loss less than 40 percent generally has performed well in granular base, whereas losses greater than this value identify shaley material that is marginal or poor. Figure 6 also shows how the micro-Deval test can distinguish between good and fair-to-poor performing aggregates that are not identified by water absorption values.

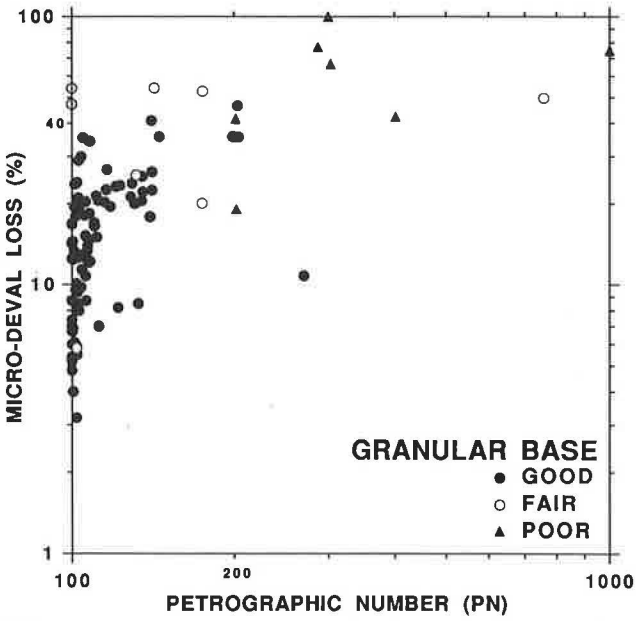

FIGURE 5 Field performance ratings for granular base: relation between micro-Deval abrasion and PN value.

The micro-Deval test demonstrates considerable promise as a relative indicator of coarse aggregate performance in granular base, particularly when used with petrographic number. The PN is not invariably capable of separating out poor performers, but the micro-Deval test is able to identify poor aggregates. Not all marginal or poor performing base course

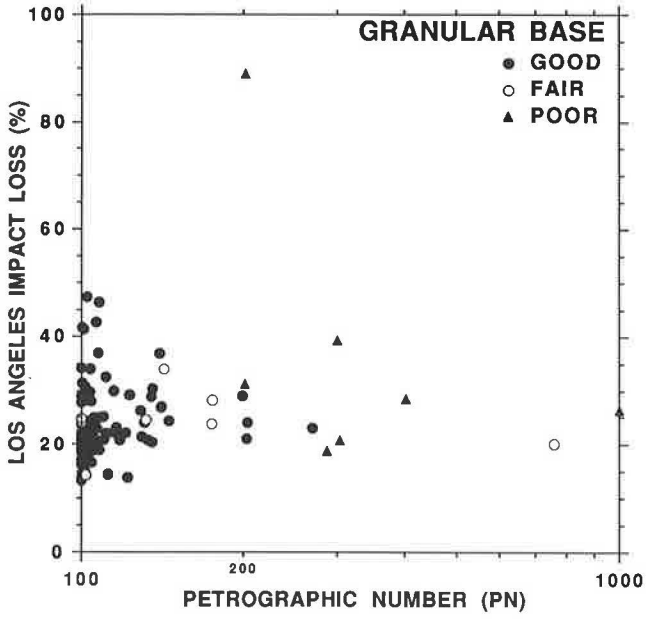

FIGURE 4 Field performance for granular base: relation between Los Angeles impact and PN value.

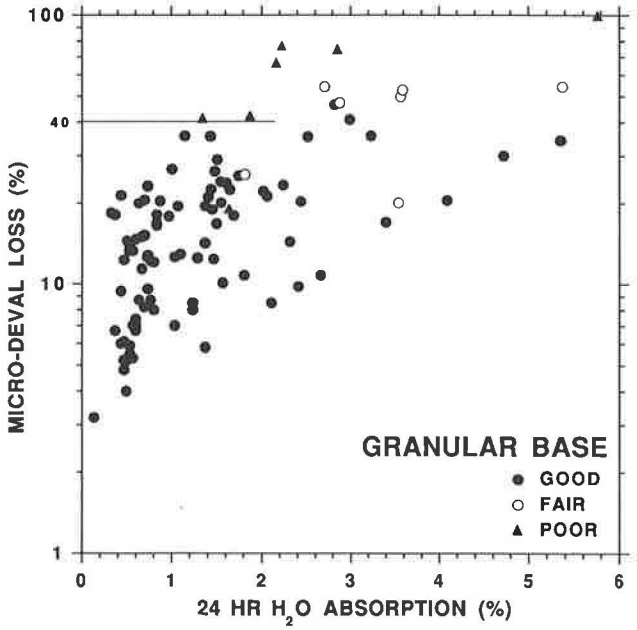

FIGURE 6 Field performance ratings for granular base: relation between micro-Deval abrasion and water absorption.

aggregates are identified by this test alone, because failures of these materials are often caused by unsatisfactory properties of the sand-sized fraction. More work needs to be done on fine aggregate properties in this regard, and a modification of the micro-Deval test for fine aggregate demonstrates promise (*12*).

Concrete

Current tests for concrete aggregates include the magnesium sulfate test, the Los Angeles abrasion test, water absorption, and petrographic evaluation in addition to tests for chemical stability.

The impact tests conducted on aggregates used in concrete have demonstrated little relation to their field performance behavior. Impact tests do not reflect the in-service, or the construction environment, of portland cement concrete. Although it is important to identify weak and weathered materials, it may be done more effectively by petrographic examination.

Figure 7 shows the relationship of field performance to test results of petrographic examination and micro-Deval loss for concrete aggregates. Poor-quality materials are indicated with a micro-Deval loss of greater than 20 percent and a PN value greater than 160. A number of marginal aggregates yield test values less than these but they are usually aggregates that contain shale or chert particles that produce objectionable popouts and are more readily recognized by a petrographic examination.

Figure 8 shows similar fields when micro-Deval loss is plotted against water absorption. Water absorption is perhaps to be preferred to petrographic examination because it is less subjective, although there are some aggregates with high absorption values that still perform satisfactorily.

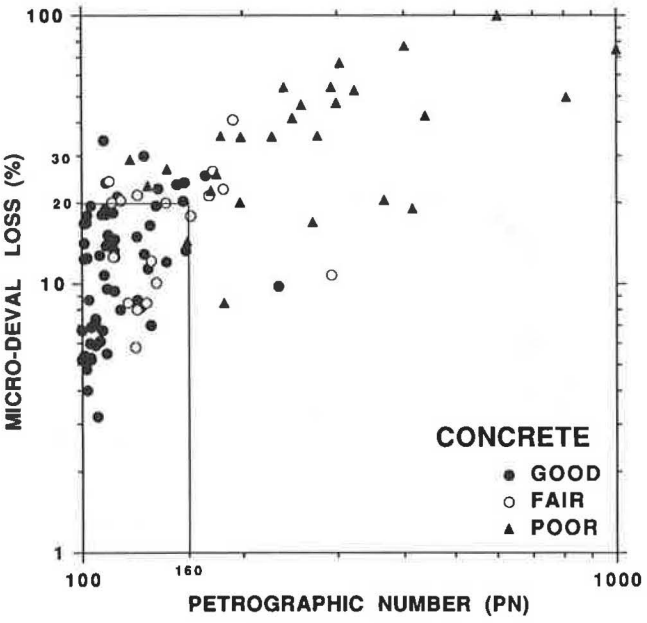

FIGURE 7 Field performance ratings for concrete: relation between micro-Deval abrasion and PN value.

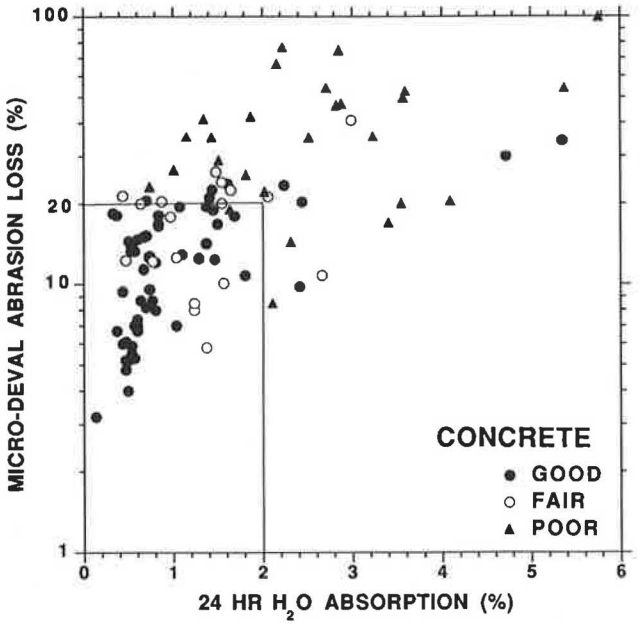

FIGURE 8 Field performance ratings for concrete: relation between micro-Deval abrasion and water absorption.

Figure 9 shows freeze-thaw test results plotted against water absorption. The freeze-thaw test can identify marginal aggregates (those of fair performance), separating them from poor and good performers. Materials with unconfined freeze-thaw losses of less than 6 percent and water absorption less than 1.5 percent are mostly aggregates exhibiting good field performance, with some marginal materials plotting in the higher water absorption portion of this range (water absorption between 1.0 and 1.5 percent). Marginal aggregates are further separated in the range of unconfined freeze-thaw losses be-

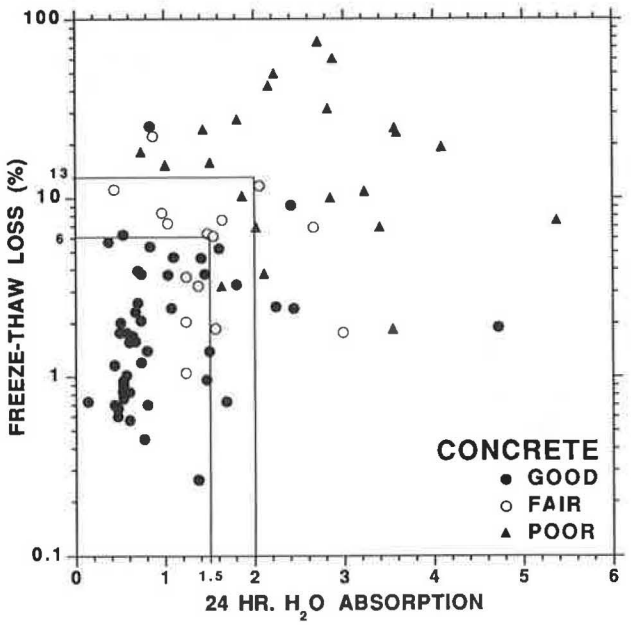

FIGURE 9 Field performance ratings for concrete: relation between unconfined freeze-thaw and water absorption.

tween 6 and 13 percent and water absorption between 1 and 2 percent. Freeze-thaw losses in excess of 13 percent and water absorption greater than 2 percent are usually, but not always, associated with poor-performing aggregates. Figure 10 combines both the unconfined freeze-thaw and the micro-Deval test results. On this plot, poor and marginal aggregates are identified with freeze-thaw losses greater than 6 percent and micro-Deval losses greater than 10 percent. Aggregate performance decreases as test results increase for these two tests.

No test procedure by itself is totally reliable for separating good, fair, and poor aggregate performance in concrete. If two tests are chosen, then micro-Deval combined with unconfined freeze-thaw seems the most reliable. The micro-Deval simulates the construction environment that includes wet mixing and abrasion, and the environment of the unconfined freeze-thaw test simulates low-temperature thermal cycling in the presence of moisture and road salts. The petrographic evaluation and water absorption have also been useful in predicting the performance of concrete aggregates (*12*).

Asphalt Surface

Asphalt surface or wearing course is the layer of asphaltic concrete exposed to traffic. It resides in a severe environment where, in addition to maximum temperature and moisture fluctuations, it is subject to the abrasion and polishing of vehicle tires, shear forces, and impact loads. Aggregate for this application on high-volume roads is normally of the highest quality. Such tough materials as trap rock and other hard indurated rock or slags are typically used. The aggregates, in addition to being unaffected by thermal cycles, wetting and drying, and impact loads, must also have the ability to resist abrasion and polishing action.

Asphalt paving aggregates are normally tested with the Los Angeles impact and abrasion, magnesium sulfate soundness, and water absorption tests, and petrographic examination. They have the most stringent requirements of all aggregates tested in Ontario.

Figure 11 shows that the performance of these aggregates is not related to water absorption. Those with high sulfate soundness loss (>15 percent) usually are poor performers. There are, however, a number of fair and poor performers with sulfate soundness losses less than 10 percent. Figure 12 shows that PN value is also useful in separating out poor material but not a totally reliable indicator of likely perfor-

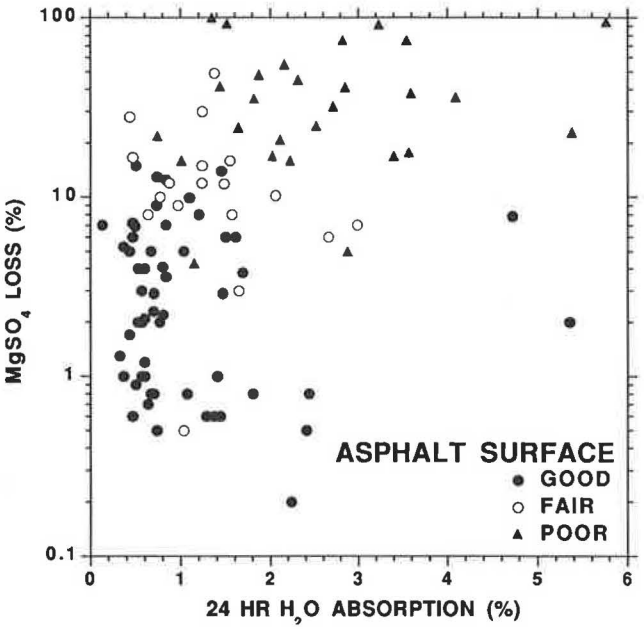

FIGURE 11 Field performance ratings for asphalt surface: relation between magnesium sulfate loss and water absorption.

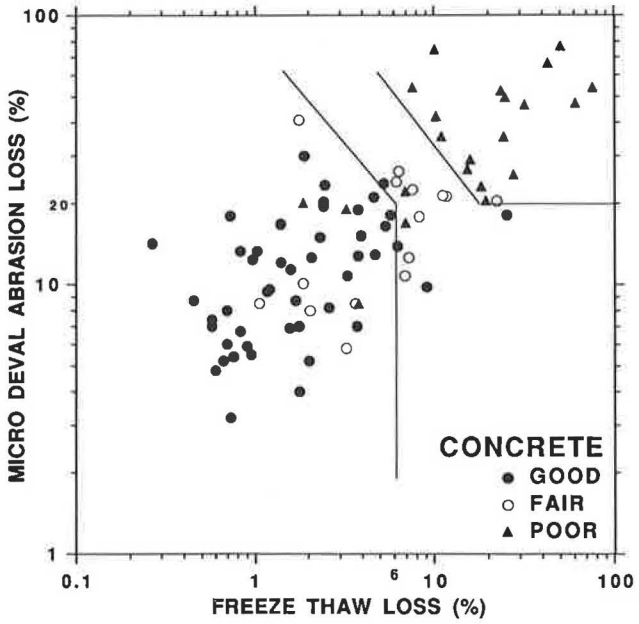

FIGURE 10 Field performance ratings for concrete: relation between micro-Deval abrasion and unconfined freeze-thaw.

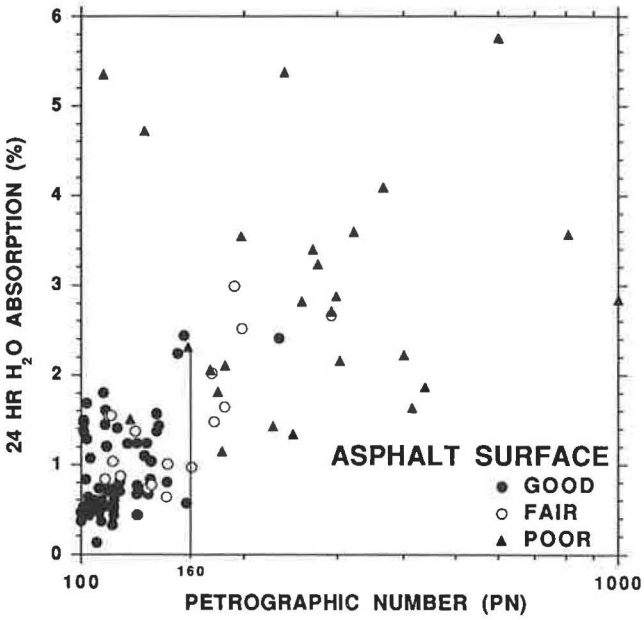

FIGURE 12 Field performance ratings for asphalt surface: relation between water absorption and PN value.

mance. The combination of magnesium sulfate loss and petrographic number shows a fairly good separation (Figure 13). The unconfined freeze-thaw test (Figure 14) is to be preferred because it shows better discrimination than the sulfate test and is more precise.

Wear resistance of noncarbonate aggregates is not related to material loss in impact tests, but there is a relationship within the carbonate group. The lower the wear resistance as measured by the AAV, the higher the Los Angeles impact loss for carbonate rocks (*10*). The results of these tests, when applied to poor-quality carbonates, are good indicators of materials that do not develop sufficient macrotexture and may cause problems related to frictional properties.

At the present time, for surfaces with high traffic volume, it is desirable to have an AAV of about 6 or less. For lower-volume roadways, the AAV may be as high as 18. Above this value, no good-quality aggregates were found. Figure 15 shows that the micro-Deval is also related to AAV, at least for values less than 20 percent. This is to be expected because the test environments both expose the aggregate to abrasive deterioration except that the aggregate abrasion test is done dry and the micro-Deval is done in the presence of water. In the test results shown (Figure 15), good performance of aggregates in asphalt surface course is identified, with one exception, by a micro-Deval loss less than 10 percent and AAV less than 6 percent. For micro-Deval abrasion losses greater than 15 percent, performance is generally worse and the AAV can vary from low to high. The AAV test is a more expensive, time-consuming procedure than the micro-Deval test. The micro-Deval test is preferable as a quicker method of assessing resistance of aggregates to traffic wear.

Another desirable aggregate property is an adequate, long-term surface microtexture that provides adhesion of tires to the road surface. Microtexture is measured by the PSV test. Figure 16 shows the association between PSV and AAV in which there is no obvious relationship. This independence is to be expected because each test measures complementary aggregate properties. High-polished stone values of poor-performing aggregates are caused by their generally soft and friable nature. Because this test is done in the presence of water, material is lost from the surface, so that little polishing takes place, resulting in high frictional values for shaley materials. A high-polished stone value is desirable provided that the aggregate is durable. The lower target for roadway surfaces of high traffic volume is a PSV of approximately 50.

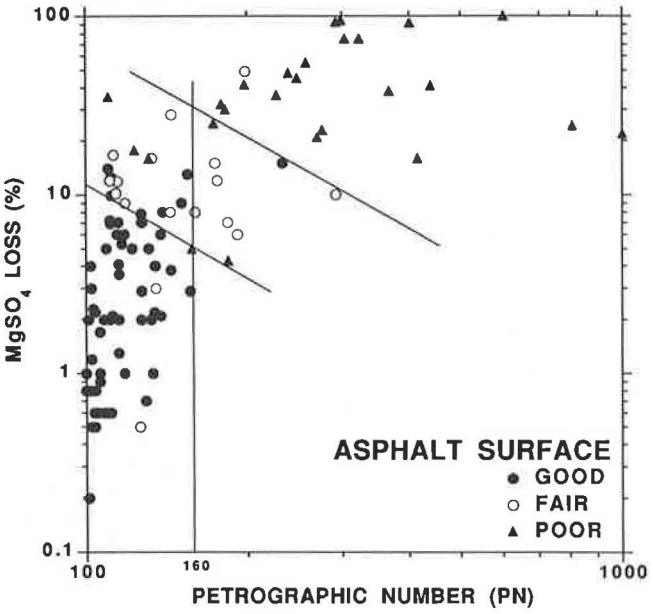

FIGURE 13 Field performance ratings for asphalt surface: relation between magnesium sulfate loss and PN value.

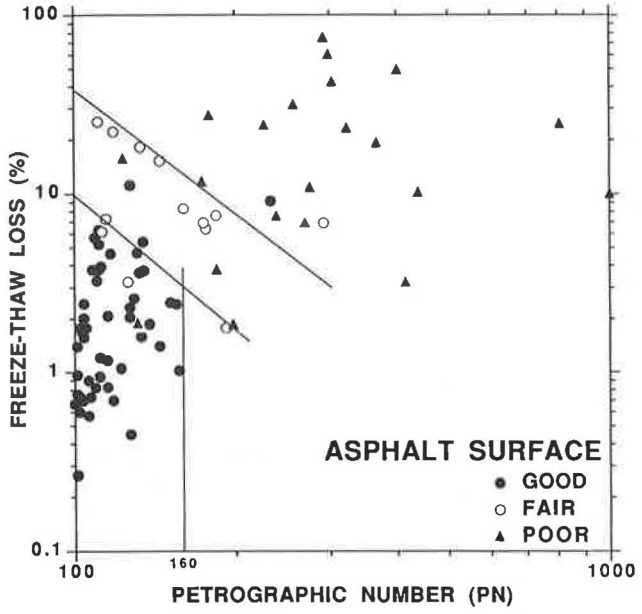

FIGURE 14 Field performance ratings for asphalt surface: relation between unconfined freeze-thaw and PN value.

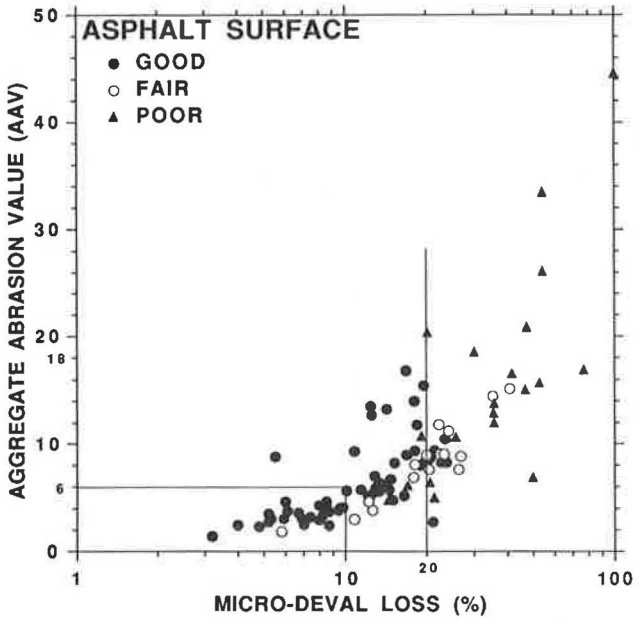

FIGURE 15 Field performance ratings for asphalt surface: relation between AAV and micro-Deval abrasion loss.

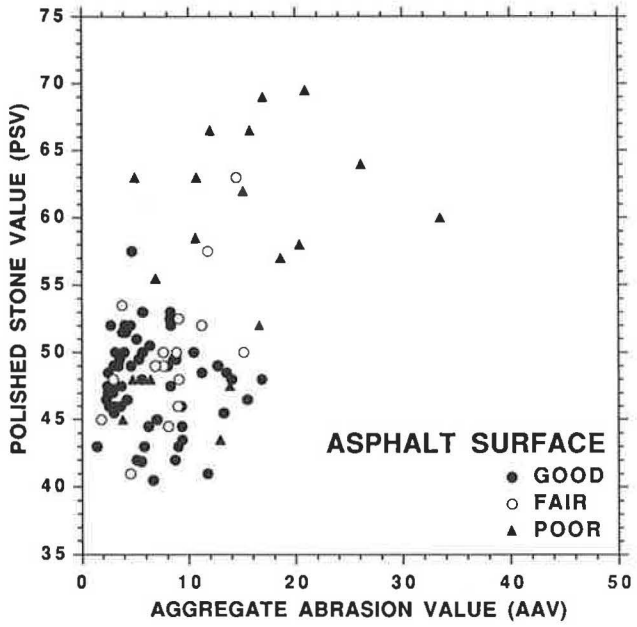

FIGURE 16 Field performance ratings for asphalt surface: relation between PSV and AAV.

For other uses, a PSV of greater than 40 may be adequate. No materials tested in this study had values less than 40.

Figure 17 shows PSV versus micro-Deval abrasion loss. The micro-Deval test separates durable and nondurable aggregates well. For high-volume roads, acceptable aggregates would have a micro-Deval loss of less than 10 percent and a PSV of 50 or better. Additional selection criteria shown in Figures 14 and 18 require that these aggregates also have PN values of less than 160 and freeze-thaw losses of less than 6 percent.

For lower-volume roads, a PSV of greater than 40 combined with a micro-Deval loss of less than 20 percent and a freeze-thaw loss of less than 30 percent would be acceptable (Figures 17 and 18). A petrographic number of less than 160 would still be required. This range includes aggregates of fair performance. Materials outside this range may occasionally be used but only after a thorough examination, including actual field performance evaluations of test sections, has been completed.

CONCLUSIONS

In addition to the standard quality tests for coarse aggregate, several alternative tests have been under investigation by the Ministry of Transportation that provide reasonable simulations of the field environment of aggregates used in granular base courses, portland cement concrete, and asphaltic concrete.

The aggregate impact value test is seen as a practical substitute for the Los Angeles impact test for determining the extent of material breakdown caused by processing and construction handling. Both of these tests measure aggregate degradation by direct impact energy. Comparison of test results with field performance indicate that both of these tests have limited capability in predicting in-service behavior. The AVI test, however, may be done using simple, portable equipment.

The unconfined freeze-thaw test and the micro-Deval abrasion test are two tests that approximate the deterioration of materials in the weathering environment. These tests have shown a fair correlation with the sulfate soundness test but, when used in conjunction with the 24-hr water absorption and petrographic examination tests, are better at predicting field performance for marginal aggregates. The micro-Deval test has proved to be the more precise of the two tests and can be completed in a fraction of the time required to conduct a sulfate soundness test. The unconfined freeze-thaw test is a better simulation of the weathering environment experi-

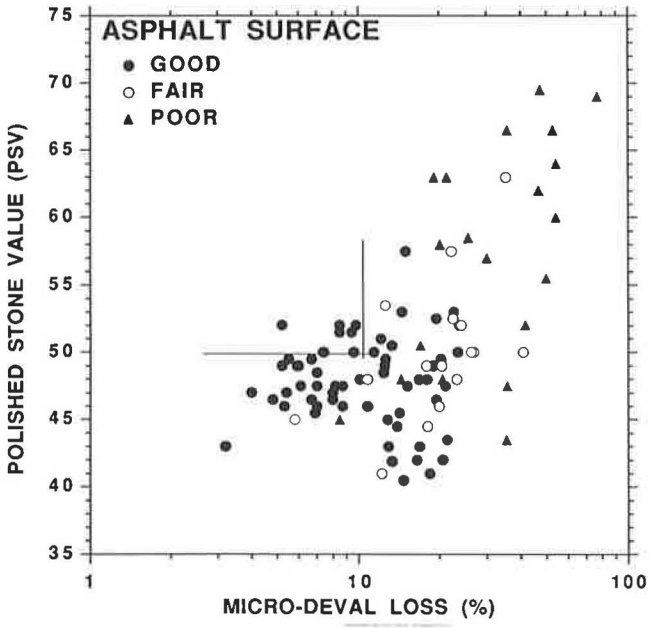

FIGURE 17 Field performance ratings for asphalt surface: relation between PSV and micro-Deval abrasion.

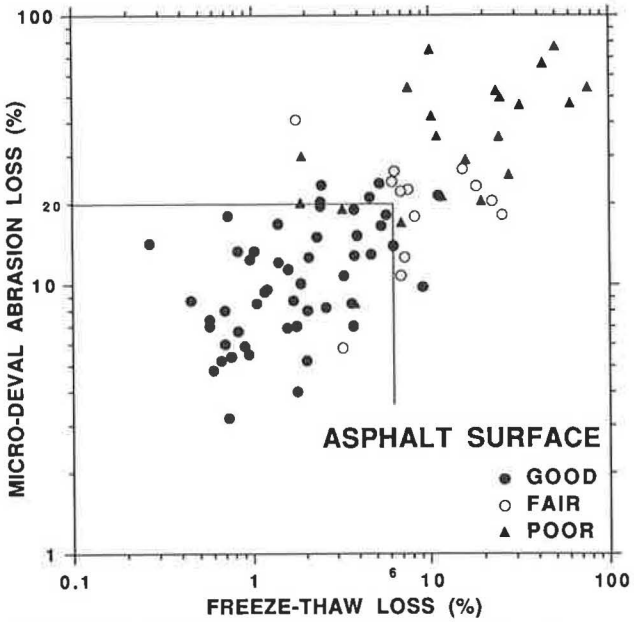

FIGURE 18 Field performance raings for asphalt surface: relation between micro-Deval abrasion and unconfined freeze-thaw.

enced by aggregates in Ontario's highways. Both the micro-Deval and the freeze-thaw tests have good multilaboratory precision.

Performance of aggregates in granular base course is best identified using the micro-Deval abrasion test and petrographic examination. The micro-Deval test is reasonably able to separate marginal aggregates from good ones. Petrographic examination, although not able to consistently separate marginal aggregates from good ones, is useful in separating poor aggregates from both good and fair aggregates. The water absorption test is useful in identifying poor aggregates when used in conjunction with the micro-Deval test.

The unconfined freeze-thaw test and the micro-Deval abrasion test have shown that they are useful in differentiating marginal and poor-quality aggregates for use in portland cement concrete. Water absorption has also been shown to be useful in identifying potentially poor-quality aggregates when used with either one of these tests.

Aggregates for use in surface course asphaltic cement concrete are best identified by the freeze-thaw test, which is shown to be marginally better than the magnesium sulfate test when used with petrographic examination. The AAV test is a good measure of wear resistance. An association has been shown between this test and the micro-Deval abrasion test where high-quality aggregates are concerned. The micro-Deval test is preferred as it is the simpler of the two tests to complete. The PSV test is valuable in differentiating potentially good aggregates when used in conjunction with the micro-Deval test.

No single test or set of tests can adequately identify the weathering stability of an aggregate source. By using more appropriate simulations of the weathering and construction environment with simple, rapid tests, this potential may be better realized.

ACKNOWLEDGMENTS

The test results presented in this paper are the outcome of a combined effort by the dedicated and diligent technical staff of the Soils and Aggregates Section. Their interest and enthusiasm in this work is thoroughly appreciated. We wish to thank the following people for their contributions: V. Bartoletti, E. Betts, P. Corsaro, G. Gage, D. Hanna, P. Hannas, D. Howard, K. Junor, B. Price, M. Scomparin, and B. Smith.

REFERENCES

1. C. A. Rogers, S. A. Senior, and D. Boothe. Development of an Unconfined Freeze-Thaw Test for Coarse Aggregates. Report EM-87. Ministry of Transportation, Ontario, July 1989, 21 pp.
2. P. G. Fookes, C. S. Gourley, and C. Ohikere. Rock Weathering in Engineering Time. *Quarterly Journal of Engineering Geology*, Vol. 21, 1988, pp. 33–57.
3. T. R. West, R. B. Johnson, and N. M. Smith. *NCHRP Report 98: Tests for Evaluating Degradation of Base Course Aggregates.* HRB, National Research Council, Washington, D.C., 1970, 92 pp.
4. R. M. Pintner, T. S. Vinson, and E. G. Johnson. Quantity of Fines Produced During Crushing, Handling, and Placement of Roadway Aggregates. *Geotechnical Testing Journal*, Vol. 10, No. 4, Dec. 1987, pp. 165–172.
5. P. P. Hudec. Aggregate Tests—Their Relationship and Significance. *Durability of Building Materials*, Vol. 1, 1983, pp. 275–300.
6. *MTO Laboratory Test Manual, Vol. II, Aggregates.* Engineering Materials Office, Highway Engineering Division, Ministry of Transportation, Downsview, Ontario.
7. C. Tourenq. L'Essai Micro-Deval. *Bulletin Liason Laboratoire Routières Ponts et Chausées*, Paris, France, No. 50, 1971, pp. 69–76.
8. *Détermination du Coefficient d'Usure par Attrition à l'Aide de l'Appareil Micro-Deval.* BNQ-2560-070. Bureau de Normalisation du Québec, Ministère de L'Industrie, du Commerce, et du Tourisme, Québec, Canada.
9. *Mechanical Properties: Methods for Sampling and Testing of Mineral Aggregates, Sands, and Fillers.* BS 812, Part 3. British Standards Institute, London.
10. C. A. Rogers. Search for Skid Resistant Aggregates in Ontario. Miscellaneous Paper 114. In *Proc., 19th Forum on the Geology of Industrial Minerals*, Ontario Geological Survey, 1983, pp. 185–205.
11. C. A. Rogers. Petrographic Examination of Aggregate and Concrete in Ontario. In *Petrography Applied to Concrete and Concrete Aggregates*, ASTM STP 1061, Bernard Erlin and David Stark, eds., ASTM, Philadelphia, Pa., 1990, pp. 5–31.
12. C. A. Rogers, M. L. Bailey, and B. Price. *Micro-Deval Test for Evaluating the Quality of Fine Aggregate for Concrete and Asphalt.* Report EM-96. Ministry of Transportation, Downsview, Ontario, 1991, 21 pp.

Publication of this paper sponsored by Committee on Mineral Aggregates.

Measurement of Aggregate Shape, Surface Area, and Roughness

RICHARD D. BARKSDALE, MICHAEL A. KEMP, WILLIAM J. SHEFFIELD, AND JAMES L. HUBBARD

The physical characteristics of aggregates have an important influence on the behavior not only of unstabilized bases but also of asphalt concrete and portland cement concrete mixes. Experimental techniques using modern data acquisition methods for measuring and analyzing aggregate characteristics are described. A Pencept Penpad digitizer accurate to 0.0015 in. together with an IBM-XT microcomputer was used to collect and analyze the necessary data for measuring aggregate shape, surface area, and roughness. Measured coordinates of critical points were stored in an Autocad DXF file. The data were edited using a Basic program and then transferred to Lotus 1–2–3 with which they were analyzed and presented in the form of graphs, tables, and histograms. All data transfer and manipulation were performed electronically. Methods for shape and surface area measurement, classification, and interpretation were reviewed. Two different techniques for measurement of aggregate surface area were compared and demonstrated to yield reasonably similar results. A special shadow technique for studying the characteristics of particles smaller than the No. 8 sieve was described. In addition, the accuracy of the digitizer procedure for measuring surface roughness was assessed.

Asphalt mix designs are based on many factors including the type and amount of asphalt, air voids, aggregate characteristics, aggregate gradation, and mineral filler. In order to investigate the effects of aggregate characteristics, which are usually not fully considered, the Georgia Department of Transportation (DOT) initiated, through the Georgia Institute of Technology, a comprehensive research program. In the final phase of the study, the effects of these variables will be evaluated on the rutting performance of Georgia DOT asphalt mix designs. This paper describes the measurement of aggregate shape, surface area, and roughness using modern digitizing techniques taking advantage of a microcomputer.

PARTICLE SHAPE

Introduction

The shape of the aggregate influences the gradation curve obtained by sieving (*1*). Flaky particles tend to diagonally pass sieves having square holes. Also, the shape of the particle has a significant influence on the volume of particles retained on a specific sieve. For material retained on a given sieve size, Lees (*1*) has shown that rod-shaped particles are about 2.5 times the size of disc-shaped particles. This difference in size affects the ability of the particles to properly fill voids of coarser size aggregate.

R. D. Barksdale, School of Civil Engineering, Georgia Institute of Technology, Atlanta, Ga. 30332. M. A. Kemp, Atlanta Testing and Engineering, 11420 Johns Creek Parkway, Duluth, Ga. 30136. W. J. Sheffield, Law Engineering Testing Company, 396 Plasters Avenue, Atlanta, Ga. 30324. J. L. Hubbard, Research Institute, Georgia Institute of Technology, Atlanta, Ga. 30332.

Simple Classification Systems

The shapes of fine- and coarse-aggregate particles can be divided into the following four general shape categories (*1*,*2*): (a) flaky, (b) cuboidal, (c) blade, and (d) rod. Although British Standard BS 812 (*2*) separates the aggregate into these four rather broad categories, the method does not define the exact location of an aggregate within each category. A special, simple gauge is used to measure the two indices required for shape classification.

ASTM (*3*) and the Corps of Engineers (*4*) also have test methods similar to BS 812 (*2*) for evaluating flat and elongated coarse particles in aggregates to be used in concrete. These methods use a specially designed caliper to determine particle shape ratios. Measurements are performed by hand to determine if particles have certain length-to-thickness or width-to-thickness ratios; specific particle dimensions are not measured. Although simple, these methods are just classification schemes and do not permit determination of surface area. Different ratios separating aggregate classes have been proposed for describing aggregate particles (*1*,*5*).

The four broad categories defined by these methods allow a large range of particle shape characteristics within each classification. For research purposes, these methods might give misleading results, affecting aggregate performance. Also, these classification tests are not suitable for measuring the shape of particles much finer than about the No. 12 sieve, and surface area cannot be determined using the results. Classification systems that use just one aspect ratio are not suitable for defining particle shape.

Generalized Classification Systems

Both fine and coarse aggregate particle shape can be determined by measuring the flatness ratio and elongation ratio (*1*). The flatness ratio (p) is the ratio of the shortest length (c) divided by the intermediate length (b), and the elongation ratio (q) is the ratio of intermediate length (b) divided by the greatest length (a). By determining the actual flatness and

elongation ratios, a continuously varying classification can be developed. This approach also permits defining a shape factor $F = p/q$ and sphericity ψ. Sphericity ψ is the ratio of surface area of a sphere of the same volume as the particle divided by the surface area of the particle (*1*). The proposed method is considerably more flexible for research purposes than the Corps or British classification schemes. The British and Corps classifications can be quickly obtained from the general flatness and elongation ratio method described by Lees.

Also, the surface area and sphericity of the aggregate can be determined using the more general shape classification method. The generalized shape classification concept is a method of tridimensional shape analysis where each grain is approximated by a tetrakaidecahedron (*2,6*). Three mutually perpendicular particle dimensions (length, width, and thickness) are measured and used to calculate the ratio of surface area of the particle compared to that of an equivalent sphere, or else surface area is directly calculated.

Particle Shape Using a Digitizer

For shape classification, the aggregates studied in this investigation were divided by sieving into the following four size ranges: ½ to ⅜ in., Nos. 4 to 8, Nos. 8 to 120, and smaller than the No. 120 sieve. These size ranges were selected by a panel of engineers as being appropriate. For the two larger size aggregate ranges (the ½ to ⅜ in. and Nos. 4 to 8 sizes), an aggregate sample consisted of 150 particles of each size, with the number of particles being counted visually. In the smaller size ranges, microphotographs and special techniques were used to measure the aggregate shape. The number of particles in each sample of smaller particles varied from 50 to 150, on the basis of the number of particles captured in each photograph. At least three different samples were measured for each aggregate type. This approach resulted in the use of a minimum of 450 particles for each of the coarser two sizes studied and a minimum of 150 particles for each of the finer two particle sizes studied; usually 250 or more particles were included. The use of more than 150 particles was desirable but was too expensive to achieve in all cases for the microscopic particles.

Aggregate shape was determined and numerous plots and tables produced without a human hand ever working with the data. The procedure developed for particle analysis is completely automated and uses a relatively inexpensive digitizer that automatically feeds data into an IBM–XT microcomputer.

Aggregate Greater Than No. 8 Sieve in Size

For the aggregate greater in size than the No. 8 sieve, photocopies were made of the flattest profile of the particles. A Savin 7350 copying machine was used to provide images of 50 particles at a time, which were placed in a small box. The box had a clear plastic bottom and dividers so as to give five rows of 10 aggregates each. The copy machine was found not to distort the photocopied image of the aggregate. By providing a profile view of the aggregates, the length and width were easily digitized directly from the photocopy using a Penpad digitizing tablet manufactured by Pencept, Inc. The digitizer had an accuracy of 0.0015 in., which was sufficient, particularly considering the relatively large observed variation in aggregate shape and dimensions. The length was digitized as the longest dimension of the aggregate, and the width as the average dimension, in the plane of the photocopied image, perpendicular to the length. The coordinates (x,y) of each point representing one end of a dimension were digitized, and the actual dimension was later calculated. If the original ordering of length, width, and thickness was to correct, a computer program later automatically reordered the dimensions correctly.

Shadows were created when trying to photocopy the profile of the aggregate to measure its thickness. Therefore, aggregate thickness was not digitized directly from a photocopy. Instead, vernier calipers were used to measure the average thickness directly from the aggregate. The calipers, open to the proper width, were then laid on the digitizing pad, and the tips of the calipers, representing thickness of the aggregate, were digitized. A pen-type digitizer, as opposed to one with cross-hairs, was used, enabling digitizing of the vernier caliper measurements.

This method of measuring the dimensions proved to be efficient. With experience, an operator can digitize the three dimensions of 150 aggregates in approximately 30 to 45 min. After digitizing the three perpendicular dimensions for all aggregates, the data are saved as an Autocad DXF file in ASCII code.

Aggregate Smaller Than No. 8 Sieve in Size

Aggregates less than the No. 8 sieve in size require the use of specially prepared optical microphotographs. Similar to the large aggregate, aggregate length was digitized directly from the photograph as the longest dimension and the width as the average dimension, in the plane of the photograph, perpendicular to the length.

Because these particles are small, the height cannot be measured directly using calipers. Therefore, a special technique was used relating a shadow length on the photograph to particle height. As the particles were prepared for the microscope, uniform reference spheres were added to establish the scale for vertical height. A thin film of metal was evaporated onto the surface at an angle to the substrate on which the particles set to create a shadow (*7*). Because the evaporation source is a relatively long distance away, the angles at which it strikes the particles and reference spheres are approximately equal. Therefore, by geometry, a unique ratio exists between the shadow lengths of the reference spheres and the aggregate particles and their heights. A special technique, described subsequently, was used to capture the shadow on the photograph.

Similar to the large aggregate, all digitized dimensions were saved as an Autocad DXF file in ASCII code. A set of microphotograph data can be digitized in 25 to 50 min depending on the number of aggregates in a sample.

Manipulation of Data Using Autocad and Lotus 1–2–3

After digitization, all dimensions were stored in an Autocad DXF file. An Autocad DXF file contains all the formatting,

scaling, size, and other information that Autocad uses when displaying and working with a drawing. A Basic program called DFXTRACT was used to remove all the unwanted formatting information and extract only the coordinates of the ends of lines defining the dimensions of the aggregates. This program then saved the data in a form that Lotus 1–2–3, or other spreadsheets. was able to use readily.

Once the endpoints of the lines representing the dimensions of the aggregates were extracted and stored in the Lotus 1–2–3 PRN file, the PRN file was imported into a Lotus 1–2–3 worksheet using the Lotus 1–2–3 import command. The lengths of the dimensions were then calculated using the coordinates of the end points and stored in a Lotus 1–2–3 worksheet file named "WK1."

The conversion of endpoints to lengths defining the dimensions of the aggregate can be performed faster using Basic as a part of the DFXTRACT program. Using the Basic program requires about 30 sec on an IBM–XT computer, compared with 3 min for the Lotus 1–2–3 macro. However, errors, such as adding a stray line or extra point, are sometimes made using the digitizer and Autocad. The Lotus 1–2–3 worksheet approach allows examination of the data; in most cases the error can be corrected even after general processing of the data has been finished. A Basic program would probably blow up or give useless results in the same situation. Typical results demonstrating how the resulting shape measurement data can be readily presented using a spreadsheet are shown in Figures 1 and 2.

Three-Dimensional Measurements of Very Fine Aggregate Samples

The fine aggregate samples studied (smaller than the No. 8 sieve in size) have a broad size range that requires the use both of low- and of high-magnification techniques, which cannot be accomplished using only one instrument. As a result, aggregate varying in size from the No. 8 to the No. 120 sieve was treated differently than aggregate smaller than the 120 sieve. The larger fraction particle size (Nos. 8 to 120 sieve size) is large enough to present difficulties in direct optical measurements and especially in macrophotography because of the limited depth of field of optical techniques. If measurement of the thickness of these particles is required, a unique sample preparation problem exists.

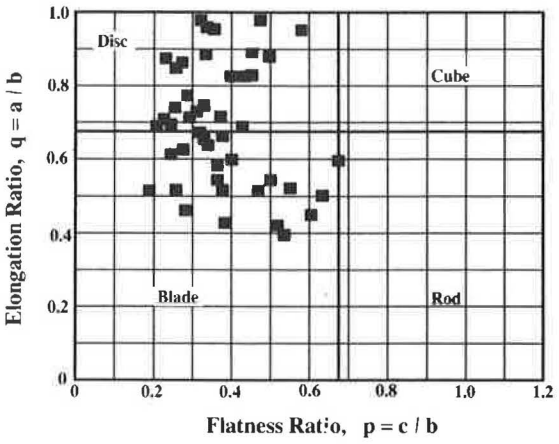

FIGURE 1 Typical shape classification scatter diagram for a selected Georgia specimen.

Large Fraction—Particles of Nos. 8 to 120 Sieve Size

Sample Dispersion The solution for measuring aggregate shape of small particles is to look not at the particles themselves but to create flat silhouette representations of the particles from which measurements can be taken. If a shadow is added to the silhouette directly related to a particle's height, the three dimensions of length, width, and height can easily be measured in one flat plane. The technique of vacuum evaporation of thin metal films, such as that used in the preparation of samples for transmission electron microscopy (TEM), was used to prepare these flat, two-dimensional representations of three-dimensional samples (*7*). In order to prepare fine aggregates so that silhouettes could be obtained, aluminum was used instead of platinum (which is used in TEM preparation because of its ease of evaporation).

First, a glass microscope slide was cleaned with soap and water to ensure good adherence of the evaporated film. A good dispersion of the sample particles was placed on this slide. Care was exercised to ensure that the particle spacing was sufficient to allow for a shadow between the particles, and that the dispersion was representative of the true size distribution. Obtaining good sample dispersion is perhaps the hardest but most important part of the sample preparatior. A wide variety of dispersion techniques can be used depending on the nature of the particulate material being studied.

For the particles used in this study, the dispersion was prepared in the following manner. Each sample was placed in a plastic bag. The sample was then mixed by shaking the bag back and forth while turning it (*8*). Shaking was carried out for a sufficiently long period of time to thoroughly mix the sample. A number of small subsamples were taken from different areas of the bag and mixed to further ensure a representative sample. Because the mica consisted of relatively large flakes, an antistatic spray was not required to prevent sticking of these particles to the sides of the bag. A number of cleaned glass slides were placed on a flat surface and the extracted sample allowed to drop onto the slides from a height of about 1 ft. This technique was performed in an area that had no air movement. A small quantity of uniform glass spheres was also dropped onto the slides. The size of the spheres was later determined by measuring their diameters on the photograph and calculating sizes knowing the scale of the photograph. One of the slides that visually appeared to have the best dispersion was selected for further processing.

Evaporation of Aluminum The slide having the best dispersion of particles was placed in a vaccum evaporation unit in which two filaments had been set up for evaporation of aluminum. One filament was located directly above the slide while the other was placed off to the side at an angle of about 30° to the slide surface. The unit was evacuated to a pressure of at least 10^{-4} mm of mercury and the aluminum evaporated. The proper amount of aluminum evaporated was determined experimentally to give the best contrast both for shadow and

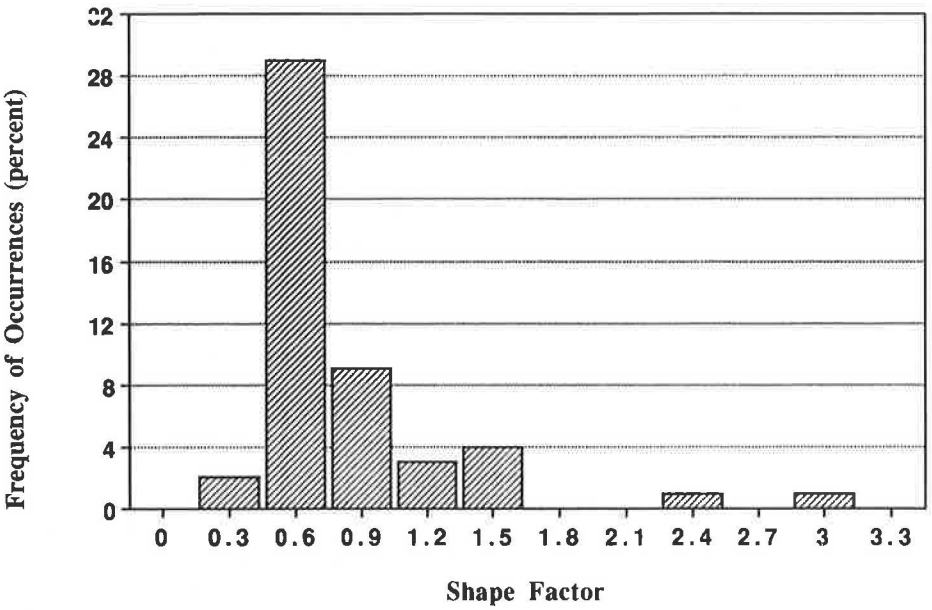

FIGURE 2 Typical shape factor histogram for a selected Georgia aggregate.

silhouette. For a single particle, two areas are present on the slide that may be coated by only one layer of aluminum, the shadow area and an area opposite the shadow if the particle is not square with the surface.

The slide is removed from the coating unit, and the particles are then removed from the slide by blowing them off with air. If the fine particles resist removal by blowing, the slide is placed in a beaker of water containing a small amount of wetting agent and then treated in an ultrasonic bath for a few seconds.

Fine Fraction Smaller Than No. 120 Sieve Size

Particle size measurements of the fine fraction less than the No. 120 sieve in size were made from micrographs taken using the scanning electron microscope (SEM). The particles were dispersed on a plastic substrate and the preparation coated with carbon by evaporation to prevent charging the SEM. The dispersion was then shadowed with aluminum as previously described. The paricles were left in place on the slide because depth of field is not a problem in the SEM. The micrographs were taken using the backscatter signal, which is sensitive to elemental differences. Good contrast was obtained using this technique between the particle, shadow, and background. Uniform glass or latex spheres were included in the dispersion for shadow and thickness determinations.

Estimation of Particle Thickness

After following the previously given procedures for sample preparation, all of the particle information is now represented in the single plane of the slide, which can be photographed at any magnification or viewed on a projection screen where direct measurements can be made. Figure 3 shows the shadowed silhouette of a single particle; A is the particle length, B the width, and C the shadow length. The shadow length of the spheres can be used to convert shadow length of the particles to thickness using the formula

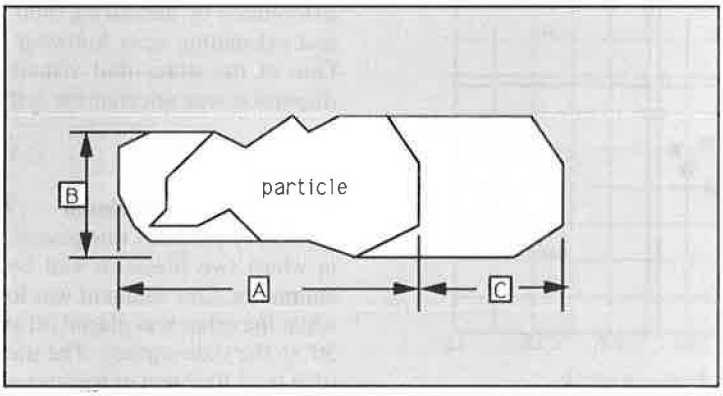

FIGURE 3 Optical presentation of coated and shadowed slide with particle removed.

$$T = \mathrm{Sh}_p\{\tan[2(\arctan r_{ap})/(\mathrm{Sh}_{ap} + r_{ap})]\} \quad (1)$$

where

T = particle thickness
Sh_p = particle shadow length,
r_{ap} = sphere radius, and
Sh_{ap} = sphere shadow length.

For low shadowing angles, the simpler formula

$$T = \mathrm{Sh}_p\,[2r_{ap}/(\mathrm{Sh}_{ap} + r_{ap})] \quad (2)$$

can be used as a close approximation.

SURFACE AREA

Introduction

The surface area of the aggregate for a given quantity of asphalt has a significant effect on the asphalt film thickness and as a result can influence mix performance. Surface area can be determined by a number of methods including (a) the tridimensional approximation described by Aschenbrenner (*6*), (b) quantitative stereology (*9*), (c) surface coatings including wax and paint (*1*,*5*), (d) air and mercury permeability (*10*), and (e) gas adsorption. The tridimensional method described by Aschenbrenner (*6*) has been previously summarized. In addition to this approach, the quantitative stereology and the gas (usually nitrogen) adsorption methods probably offer the best techniques for determining surface area. The gas adsorption method, however, indirectly measures the external surface area of the particle and also any pores greater in size than about 4 Å. This method requires several ideal assumptions to calculate surface area using thermodynamic principles.

Quantitative Stereology

Fundamentals

An interesting method for measuring surface area of aggregates is by using quantitative stereology (*9*). Quantitative stereology is a direct measurement method and consists of preparing a random sample of N aggregates placed in a container of known volume. The aggregates are encased in a cementing agent such as an expoxy to form a solid block. The solid block is then sawed into several random pieces with the cuts oriented in different directions. A number of circles of radius R are inscribed on each saw cut surface, and the number (P) of times each circle intersects an aggregate boundary is counted. Now let P_L equal

$$P_L = P/2\pi R \quad (3)$$

where R is the radius of the circle and P is the number of intersections. Next, calculate the average value of P_L (i.e., $\overline{P}_L$) for all the circles drawn on all sections. The average surface area S of the particles inside the block of aggregate is then equal to

$$S = 2\overline{P}_L V_0/N \quad (4)$$

where

S = surface area,
$\overline{P}_L$ = average number of particle intersections per circle,
V_0 = volume of the sample, and
N = total number of particles in the sample.

The quantitative stereology approach makes no geometric assumptions concerning aggregate shape (*9*). This method is statistically exact provided a sufficient number of measurements are performed. However, the sample must be statistically representative of the aggregate, and a sufficient number of circles must be drawn on the cut faces. The best results are obtained if the particles are randomly positioned in the container, with the distribution being homogeneous. If a random distribution does not exist, more sampling planes cutting through the block of aggregates at different angles are required, or more sampling circles must be drawn on the cut faces or both. Even if the aggregates are not randomly oriented, the correct surface area can be obtained if a sufficient number of circles and sections are used together with a sufficiently large number of particles.

Sample Preparation

The procedure used for the quantitative stereology method is considerably more labor intensive than the computer method used to obtain aggregate shape and surface area. Approximately 500 aggregates from the ½- to ⅜-in. sieve size were counted for each sample from each of the seven selected quarries for which surface area was measured using this technique. Of these 500 aggregates, 100 were digitized in this study into the computer for analysis by the Aschenbrenner method to compare results. After digitizing was complete, these 100 aggregates were combined with the remaining 400 particles and later placed in a cylinder.

A two-part epoxy glue, which was quick drying and strong, was used to bind the aggregates together. Plastic cylinders 5.25 in. high and 3 in. in diameter were used as molds. This size is convenient to work with and handle, and provides a sufficient volume to produce a representative sample of the size of aggregate studied.

After mixing, a small amount of epoxy was poured into the bottom of the mold. Several aggregates were then dropped into the mold. The mold was tapped for several minutes with a metal rod to move the aggregates into a dense packing and to drive any air bubbles present to the surface. When most of the air bubbles were out, more epoxy and more aggregates were added and the tapping was repeated. This preparation cycle was continued until all the aggregates were placed in the mold. Extra epoxy was also added to top off the mold and to act as a handle to hold the sample when it was cut. The mold was then placed in a warm location and allowed to harden for approximately 24 hr.

The mold was stripped away from the sample after hardening. The sample was then labeled with a permanent marker. Measurements were then taken of the height of the aggregate-epoxy specimen; the total height of the epoxy cylinder was not measured because the volume of actual aggregate is used in the formulas for calculating surface area. Next, the lower

portion of the epoxy-aggregate sample from the bottom up was cut into disks approximately ½ to 1 in. thick. The remaining cylindrical-shaped sample was split down the center, forming two long, semicircular sections. One side of each of the three disks and one of the flat semicircular sides was photocopied. The data were taken from the photocopies and reduced to preserve the integrity of the original samples.

Measurements

Five circles were drawn on each cross section that was photocopied. The long flat side of the semicircular section had 12 circles drawn on it. The number of intersections each circle made with the edges of aggregates was recorded. This large number of circles, 27 in all, was used to achieve a representative sample of the aggregates. The number of intersections per circle was then averaged and entered into Equations 3 and 4 to calculate the surface area. The epoxy cylinder radius, volume of epoxy cylinder containing aggregate, and the total number of aggregates in the sample are also required. Either three or five aggregate-filled specimens were studied from each quarry.

Comparison of Results

Table 1 presents the results of the quantitative stereology method for evaluating surface area with the one described by Aschenbrenner. For the stereology technique, the average standard deviation of the aggregate from the seven granite quarries included in this portion of the study is 0.030 in.^{2}, which is 4.3 percent of the average measured value of 0.700 in.^{2} per aggregate. For the Aschenbrenner approach, the average standard deviation is 0.050 in.^{2}, which is 6.7 percent of the average measured value of 0.749 in.^{2} per aggregate. The percent differences in average results vary for individual quarries from -10.7 to $+9.2$ percent. The algebraic average difference in surface area between the two methods for the seven quarries is 2.2 percent. These results appear to indicate that the Aschenbrenner model is probably sufficiently accurate for at least most purposes, particularly considering its simplicity.

SURFACE ROUGHNESS MEASUREMENT

Definition of Surface Roughness

Quantifying surface roughness is not easy, particularly for aggregates that have curved surfaces. Further, the value of surface roughness depends on the magnification at which roughness is examined. Numerous definitions of surface roughness have been proposed (*11–13*). For this study, the definition developed for surface roughness (R) is as follows:

$$R = L_T/L_p \tag{5}$$

where

L_T = true length of the segment of surface being analyzed, and
L_p = length of the line of best fit for the segment of surface.

This definition, which is slightly different than that used for flat surfaces, was developed because using the line of best fit appears to contribute to the reduction of error caused by the curvature of an aggregate. Coupling this definition with evaluating small sections of the particle, the problems caused by curvature are minimized.

Methods of Measuring Surface Roughness

Most work in measuring microtexture has involved the roughness of flat metal surfaces. Techniques for measuring surface roughness of aggregates include the following (*11,12*):

1. Stylus. A pen stylus is drawn over the aggregate surface. Optical, mechanical, or electronic magnification is usually used to enhance the profile and process the results.
2. Cut Section. The cut profile surface can be measured of an aggregate embedded in an epoxy. The block of epoxy and aggregate is cut, polished, and photographed at the desired level of magnification such as 15× to 125×. The surface profile is then directly measured by automatic measuring techniques.
3. Casting. A casting of the surface is made. The magnified image of the casting is then examined to determine the profile.
4. Oblique Lighting. Illuminating the surface by oblique lighting produces a shadow. A projection microscope is used to observe the shadow.

Stylus-type equipment, which appears at first to be ideal, is made to measure surface roughness along a flat surface; deviation from this plane can cause measurement errors and even instrument damage. Also, a stylus-type instrument cannot follow indentations less than the radius of the stylus and cannot measure roughness where overhangs occur. Flat surfaces on an aggregate particle where measurement is possible are often limited.

Roughness Measurement

The cut section method, previously described, was used to measure surface roughness. Data were collected automatically with the same Pencept Penpad and IBM–XT computer that was used to measure aggregate shape and surface area.

Specimen Preparation

A representative, random sample of 30 aggregate particles was taken from each source. The aggregate sample was then placed in a small plastic cylinder 6 in. high and 1½ in. in diameter. A two-part epoxy was used to bind the aggregate together within the cylinders. Magnolia Plastics Epoxy Compound 2014 and Curing agent 346 were chosen because of their ability to hold the aggregate particles in place while cutting, their good polishing characteristics, and their ability to harden within 24 hr.

Thirty particles ⅜ to ½ in. in size were dropped one at a time into the cylinder, which was one-half full of epoxy. This

TABLE 1 COMPARISON OF SURFACE AREA BY QUANTITATIVE STEREOLOGY AND COMPUTER SURFACE AREA ANALYSIS FOR SELECTED QUARRIES

Quarry	Sample	Aggregate Type	SA by Stereology[1] ($in.^2$)	Mean	Std. Deviation	SA by Computer[1] ($in.^2$)	Mean	Std. Deviation
Dixie Sand	CA1	Alluvial	0.636					
Chatt., TN	CA2	Alluvial	0.641	0.636	0.005	0.580	0.580	-
	CA3	Alluvial	0.632					
Florida Rock	EA1-1	Granite	0.767			0.752		
Mt. View, GA	EA1-2	Granite				0.715		
	EA2	Granite	0.843	0.816	0.042	0.733	0.738	0.015
	EA3-1	Granite	0.837			0.747		
	EA3-2	Granite				0.745		
Florida Rock	GA1-1	Granite	0.713			0.891		
Tyrone, GA	GA1-2	Granite				0.833		
	GA2	Granite	0.801	0.767	0.048	0.841	0.850	0.025
	GA3-1	Granite	0.788			0.830		
	GA3-2	Granite				0.853		
GA. Marble	IA1	Granite	0.809			0.823		
Buford, GA	IA2	Granite	0.827	0.821	0.010	0.747	0.759	0.059
	IA3	Granite	0.827			0.707		
GA. Marble	JA1	Granite	0.677			0.700		
Cumming, GA	JA2	Granite	0.737	0.733	0.054	0.935	0.762	0.152
	JA3	Granite	0.784			0.651		
Vulcan Materials	RA1	Granite	0.815			0.763		
Kennesaw, GA	RA2	Granite	0.774	0.813	0.038	0.825	0.789	0.032
	RA3	Granite	0.849			0.780		
Vulcan Materials	UA1	Granite	0.759			0.770		
	UA2	Granite	0.781	0.774	0.013	0.742	0.763	0.019
	UA3	Granite	0.782			0.777		

Note 1: The surface area (SA) is given for one aggregate.

technique was found to allow settlement of the particles to the bottom minimizing the number of air bubbles trapped during particle placement in the cylinder. No tapping of the cylinder was needed because the samples were small. After curing for 24 hr in a warm location, two to three rock saw cuts across the diameter were performed on each cylinder, giving three or four cut aggregate surfaces suitable for measuring roughness on.

Surface Polishing

Numbers 120, 300, and 600 polishing grits were used to obtain a smooth aggregate surface and sharp contrast between the aggregate surface profile and epoxy. The No. 120 coarse grit was used to take out most of the unevenness caused by the saw cut; at the same time it placed small grooves in the sample. The No. 300 grit was used to polish out the grooves placed by the coarse No. 120 grit. Finally, the No. 600 grit polished out any remaining tiny marks or grooves to provide a smooth, finished surface. The sample was polished a minimum of 5 min with each grit. The samples were washed between grit changes to prevent any contamination of the finer grit with the coarser ones.

Surface Photography

A photograph of the aggregate surface gives the surface profile in a form suitable for digitizing. A scale was also photographed to accurately quantify the level of magnification used. For the purposes of this study, a magnification of approximately 20 × was selected for the photomicrograph as being suitable for defining the surface roughness characteristics (Figure 4). The photographs were later blown up 50 percent using a photocopier. This procedure gave a 30 × magnification of the surface and resulted in significant savings on printing costs compared with those for blowing the negative up to 30 × during printing.

The use of other magnification levels of the surface would be expected to yield different values of surface roughness. Wright, for example, suggested using 125 ×, which perhaps is too much magnification to evaluate surface roughness of the gross surface. The appropriate value of magnification to use certainly deserves further study.

Kodak PX–125 black-and-white film was used for the photographs. Three aggregate particles from each quarry were evaluated for surface roughness. Pictures were taken of two different locations on the surface of each of the three particles, resulting in six photographs per quarry. In determining surface roughness, each photograph was broken into three smaller segments to minimize the curvature effects of the aggregates. This procedure resulted in 18 values of surface roughness from each quarry.

Digitization

A similar scheme of manipulating the data as used for shape analysis was also used for roughness. A macro routine within Lotus 1–2–3 arranged the digitized points, calculated the true length of the digitized surface, and calculated the line of best fit of the data. The macro routine also adjusted the length for magnification, calculated the surface roughness, and then created a graph of the real surface and the line of best fit or projected surface. Both the graph and the worksheet were saved on disk.

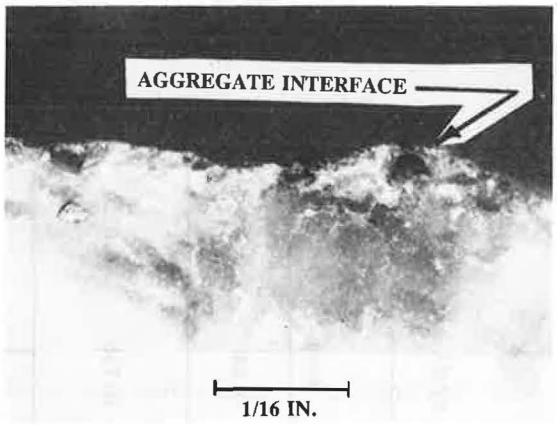

FIGURE 4 Photograph of polished aggregate at surface after 20 × magnification.

Calibration of Digitization Procedure

Several calibrations were performed to find any errors, problems, or limitations of the overall digitization methodology used to evaluate surface roughness. Calibrations were obtained from a simple comparison of measured surface roughness with the calculated surface roughness of surfaces having simple, easily defined shapes. The first surface used consisted of two semicircles connected together as shown in Figure 5. For all calibrations, points on the surface were digitized at distances on the photographs varying from 0.01 to 0.1 in.

Figure 5 shows that an optimum spacing of digitized points of about 0.05 in. exists, which gives the minimum error for a surface consisting of two semicircles. A closer spacing of digitization points, which intuitively would be thought to be more

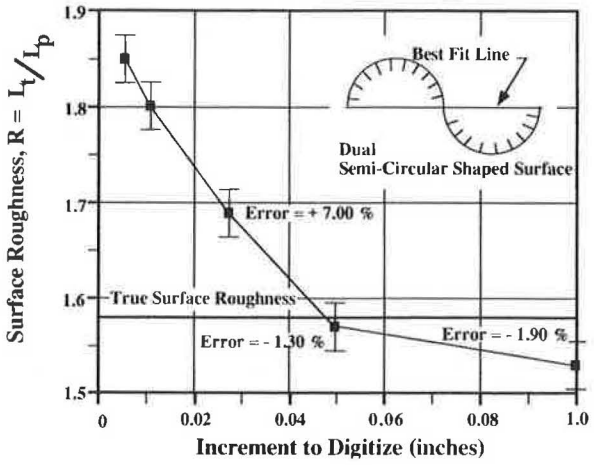

FIGURE 5 Calibration of surface roughness digitization using a sine wave surface.

accurate, was actually found to be less desirable. The loss in accuracy was apparently caused by small levels of shaking of the hand (referred to as hand vibrations). A surface with sawtooth shape was also used for calibration. The optimum digitization spacing was found to be 0.04 in., which was close to that found for the circular surface.

The calibration studies indicated that a digitization increment of 0.05 in. yielded good results. An average correction factor of +2.0 percent was used to correct calculated surface roughness to increase the accuracy on the basis of the calibration studies.

Reproducibility of roughness measurements on aggregate surfaces obtained by a single experienced operator was found to be good. In comparing the results from three digitizer operations (only one having a high level of experience), the standard deviation of roughness was found to be 0.023 for three quarries in a supplementary study. This study indicated that the operator should become experienced using the digitizer on reference surfaces such as the one shown in Figure 5.

Results

As presented in Table 2 and found by Wright (*11*), surface roughness varies greatly both over the surface of a single particle and from one particle to another for the same quarry. Therefore, only general trends of surface roughness should be considered and as many measurements as practical should be performed. Observed variations in surface roughness were as follows: 1.16 to 1.26 for 15 granite gneiss quarries; 1.13 to 1.15 for 3 limestone quarries; 1.16 for an injection quartz; and 1.13 for an alluvial gravel.

CONCLUSIONS

The use of modern data acquisition procedures, which include a relatively low-cost digitizer and microcomputer, makes possible the accurate and rapid acquisition of large quantities of data. These devices were used together with Autocad and Lotus 1–2–3 spreadsheet, to acquire and process large quan-

TABLE 2 ROUGHNESS DATA ILLUSTRATING VARIABILITY FOR A STREAM DEPOSIT—DIGITIZATION INCREMENT OF 0.05 in., AGGREGATE ⅜ TO ½ in.

SAMPLE	ROUGHNESS PER SAMPLE	CORRECTED ROUGHNESS	AVG. RGH PER GROUP	AVG. RGH PER AGG.	AVG. RGH PER QUARRY
CA1051	1.16	1.18			
2	1.10	1.12	1.14		
3	1.09	1.11		1.12	
CA2051	1.09	1.11			
2	1.07	1.09	1.10		
3	1.07	1.09			
CA3051	1.07	1.09			
2	1.12	1.14	1.12		
3	1.09	1.11		1.15	1.13
CA4051	1.23	1.25			
2	1.08	1.10	1.18		
3	1.16	1.18			
CA5051	1.10	1.12			
2	1.10	1.12	1.11		
3	1.06	1.08		1.13	
CA6051	1.20	1.22			
2	1.10	1.12	1.16		
3	1.10	1.12			
Mean -	1.13	Standard Deviation -		0.50	

Roughness per Sample - True Length/Projected Length

Corrected Roughness - (1.0199) + Roughness per Sample

Avg. Rgh. per Group - Average roughness of samples from same picture

Avg. Rgh. per Agg. - Average roughness of 2 groups (pictures) taken from same aggregate

Avg. Rgh. per Quarry - Average roughness of 3 agg. from each quarry sample, A or B

tities of data without ever touching the data after digitization. The use of a spreadshseet makes possible easy interpretation and presentation of the data. Sample preparation and data acquisition have been described for shape, surface area, and roughness of aggregates. These techniques can, however, also be applied to many other materials applications.

ACKNOWLEDGMENTS

The results of this study were primarily sponsord by the Georgia DOT in cooperation with the FHWA under the HPR Program. The fine technical support given by Pete Malphurs, State Materials Engineer, and others of the Georgia DOT's Office of Materials and Research is gratefully acknowledged.

REFERENCES

1. G. Lees. The Measurement of Particle Shape and Its Influence in Engineering Materials. *Journal, British Granite and Whinstone Federation*, Vol. 4, No. 2, 1964, pp. 1–22.
2. British Standards Institute. *Flakiness Index Test.* BS 812. United Kingdom, 1984.
3. Standard Test Method for Flat or Elongated Particles in Coarse Aggregate. ASTM D-4791-89. *Annual Book of ASTM Standards, Vol. 04.03*, ASTM, Philadelphia, Pa., 1990.
4. A Method of Test for Flat and Elongated Particles in Coarse Aggregates. CRD-C119-53. *Handbook for Concrete and Cement, Corps of Engineers*, U.S. Army Waterways Experiment Station, Vicksburg, Miss.
5. B. Mather. Significance of Tests and Properties of Concrete and Concrete-Making Materials. ASTM STP 169-A. *Shape, Surface Texture, and Coatings*, 1966, pp. 415–431.
6. B. C. Aschenbrenner. A New Method for Expressing Particle Sphericity. *Journal of Sedimentary Petrology*, Vol. 26, No. 1, 1957, pp. 15–31.
7. D. Kay. *Techniques for Electron Microscopy*. 2nd ed., F. A. Davis Co., Philadelphia, Pa., 1965, pp. 136–144.
8. J. L. Hubbard. Microscopy and Image Analysis. *Metals Handbook*, 9th ed., Vol. 7, American Society for Metals, Metals Park, Ohio, 1984, pp. 225–230.
9. E. E. Underwood. *Quantitative Sterology* Ch. 2. Addison-Wesley, Reading, Mass., 1974.
10. P. C. Carman. Determination of the Specific Surface of Powders. *Transactions*, Institute of Chemical Engineers, Vol. 57, 1938, p. 225.
11. P. J. F. Wright. A Method of Measuring the Surface Texture of Aggregate. *Magazine of Concrete Research*, Vol. 7, No. 21, 1995, pp. 151–160.
12. E. E. Underwood and K. Banerji. Quantitative Fractography. *Metals Handbook* 9th ed., Vol. 12, Metals Park, Ohio, pp. 199–210.
13. J. I. McCool. Relating Profile Instrument Measurements to Functional Performance of Rough Surfaces. *Journal of Tribology*, Vol. 109, April 1987, p. 264–270.

Publication of this paper sponsored by Committee on Mineral Aggregates.

Physical Characteristics of Polish Resistance of Selected Aggregates

BARBARA J. SMITH AND GLENN A. FAGER

The British polishing wheel and the British pendulum tester were used to provide polish values similar to skid resistance information on several construction aggregates potentially usable in bituminous pavements. The aggregates included light-weight aggregates (expanded shales), industrial slags, trap rock, chert, siliceous gravel, and carbonate aggregates. Ranked from good to poor polish values, the aggregates are expanded shale; soft carbonates with high acid-insoluble residue contents, some limestones and dolomites; sandstone; boiler slag; trap rock; hard limestones with low acid-insoluble residue contents; steel slag; siliceous gravels; and chert. Petrographic studies of the aggregates demonstrate the trend of soft or surface-renewing rock providing the best results, grading to harder, or more finely crystalline, aggregates yielding the poorest results within similar lithologic types. More research is needed to determine the potential for better use of several aggregates not currently or commonly used in Kansas bituminous pavements. Future research should include field studies of aggregates that have good potential in the laboratory tests but are not now being used.

The testing of a variety of available coarse aggregates, both natural and industrially produced, could provide information for determining appropriate aggregate types for skid resistance in bituminous pavements. The researchers sought to evaluate frictional characteristics of individual aggregates rather than of the mixes. It was the first time coarse stone aggregate had been so characterized in Kansas. The methods followed were ASTM-D3319 and ASTM-E303. Eight different kinds of aggregates were tested on 21 sample sets.

BACKGROUND

Kansas researchers have evaluated aggregates for skid resistance in bituminous pavements since the 1970s (*1–3*). The design of skid-resistant pavements is a safety problem for any pavement designer. Strength and durability too often hold the primary concern of the designer, especially in bituminous construction. Even though the pavements may retain serviceable strength and durability, the frictional characteristics of some pavements deteriorate faster than others, posing a potential safety hazard. Because the previous evaluations have been field tests of pavements under traffic, some pavements being much older than others, a faster method to find skid resistance characteristics had to be found. Kansas Department of Transportation (KDOT) field data of the aggregates for evaluation are sparse or nonexistent because they had not been used or the information on projects using the limestones had been difficult to find. By polishing the several kinds of aggregates on the British polishing wheel, the time for obtaining a terminal polish on the aggregates could be cut to hours in the laboratory instead of years in the field. This saving was demonstrated by the Texas Highway Department (*4*) and was reported more recently by the New Jersey Department of Transportation (NJDOT) (*5,6*).

Kansas Department of Transportation, Topeka, Kans. 66611.

TESTING

The eight kinds of aggregates tested were steel slag; siliceous gravel consisting of quartz, feldspar and other igneous rocks, both crushed and uncrushed; carbonate-cemented sandstone; chat (crushed chert as a by-product of lead and zinc mining in southeast Kansas); boiler slag; trap rock; lightweight aggregate (expanded shale), in this report known as expanded shale, from two sources; and 12 carbonate aggregates including limestones, dolomitic limestone, and dolomite. One limestone was used as the reference stone on the polishing wheel. Altogether, 21 samples were polished and then tested with the pendulum. All are available as potential construction materials in Kansas. The procedure for polishing was ASTM-D3319 using the British polishing wheel. Each sample was run with the reference limestone. Because the methods were unfamiliar, some time was spent in checking procedures and accuracy.

Each aggregate selected for testing was supplied in a sample passing the ½ in. but retained on the ⅜ in. screen. From this sample, a set of molded samples was prepared using a polymer compound. The molded samples fit around the outer circumference of the larger wheel on the polishing machine. Each aggregate sample was run with the reference limestone. A weighted rubber-tired wheel continuously supplied with grit and water revolved in contact with the exposed aggregate surfaces of the samples. This process supplied the wear for comparative testing. At planned intervals, the wheel was stopped and the molded samples were removed for testing with the pendulum tester.

The ASTM-E303 method was used to measure the surface frictional properties with the British pendulum tester. Most of the aggregates began at an initial high polish value (PV), then quickly lost PV as the test proceeded. After several kinds of aggregates had been run for 26 and 52 hr, it was clear that the surface friction values obtained changed little after 10 hr. Thereinafter, the samples were run for times of only 10.5 hr (Figures 1–6). The wheel revolved at 320 rpm; testing was stopped at 200,000 revolutions and final PV was obtained. The higher the PV obtained at the 10.4-hr testing the better the skid resistance of the aggregate.

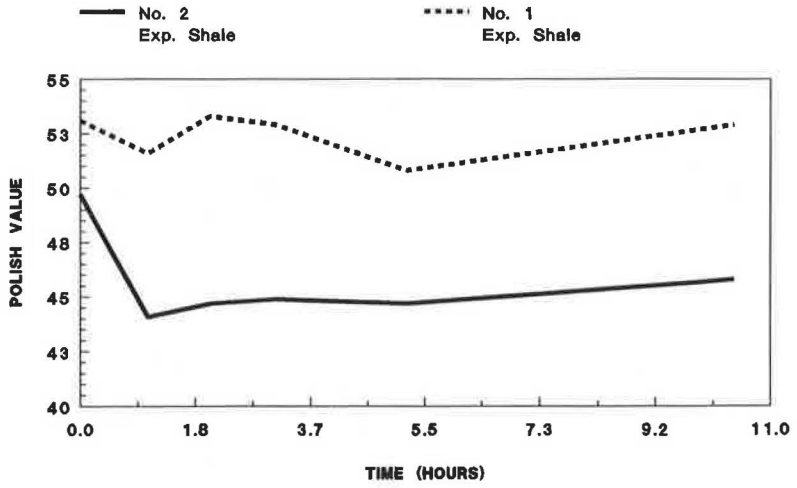

FIGURE 1 PVs of two expanded shales during more than 10 hr of testing.

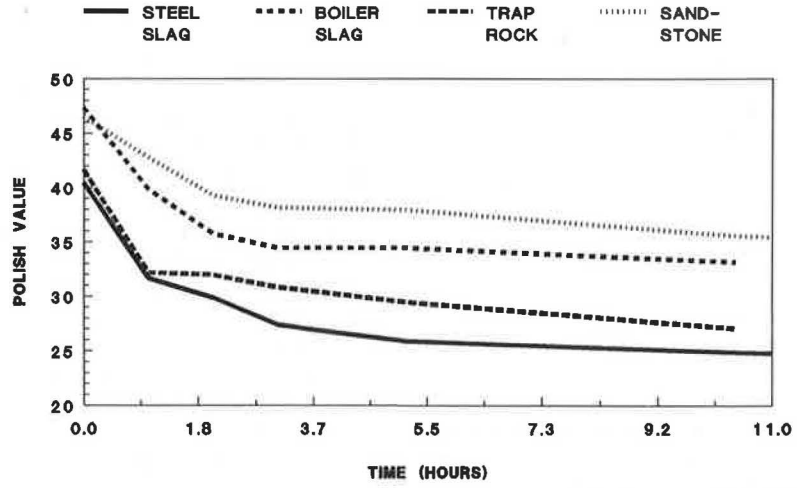

FIGURE 2 PVs of two slags, trap rock and sandstone, during more than 10 hr of testing.

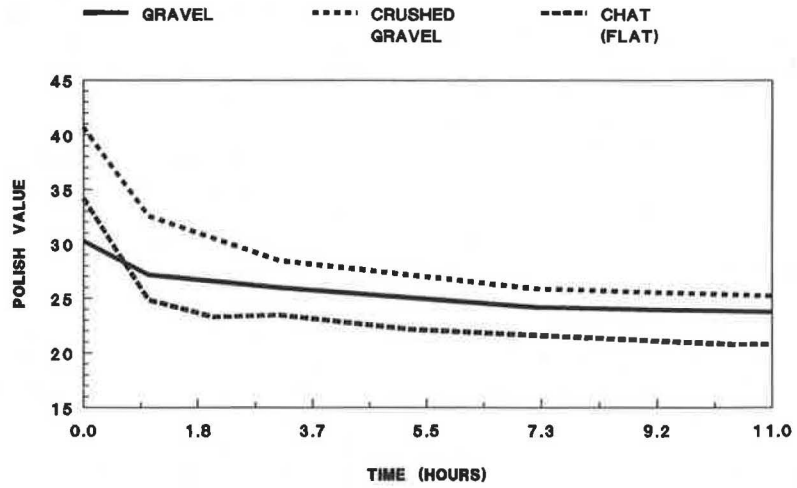

FIGURE 3 PVs of natural gravel, the same gravel crushed, and chat in a flat orientation during 11 hr of testing.

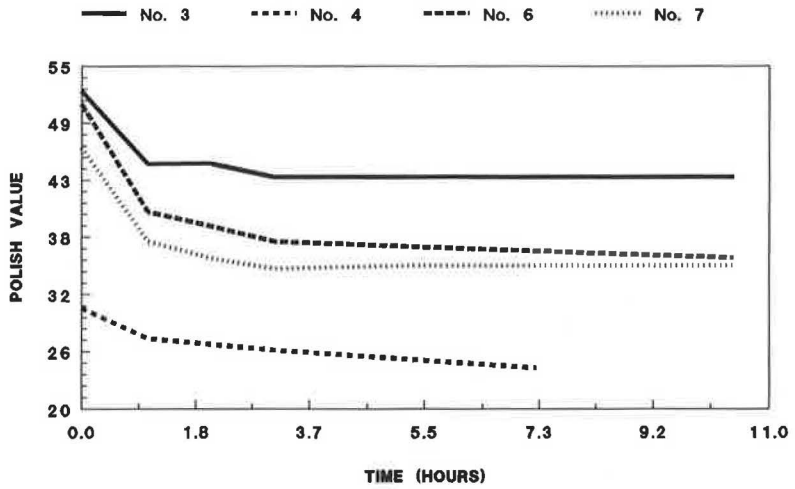

FIGURE 4 PVs of carbonate aggregates identified by rank as being in the top third of 21 aggregates tested.

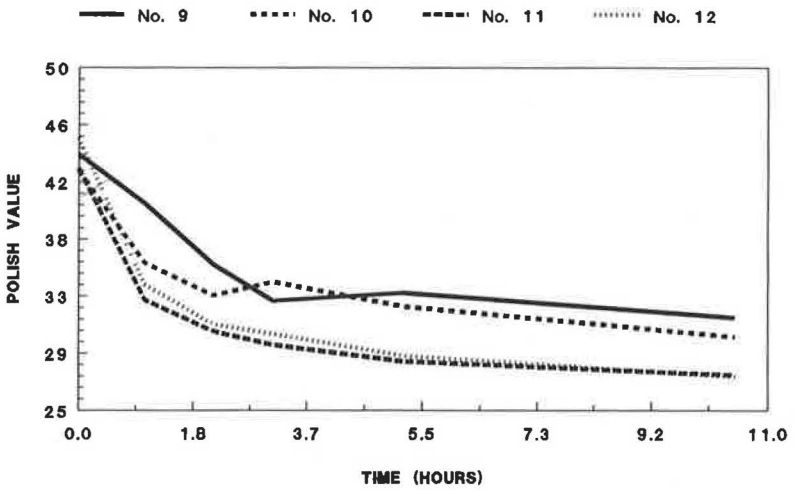

FIGURE 5 PVs of carbonate aggregates identified by rank as being in the middle portion of 21 aggregates tested.

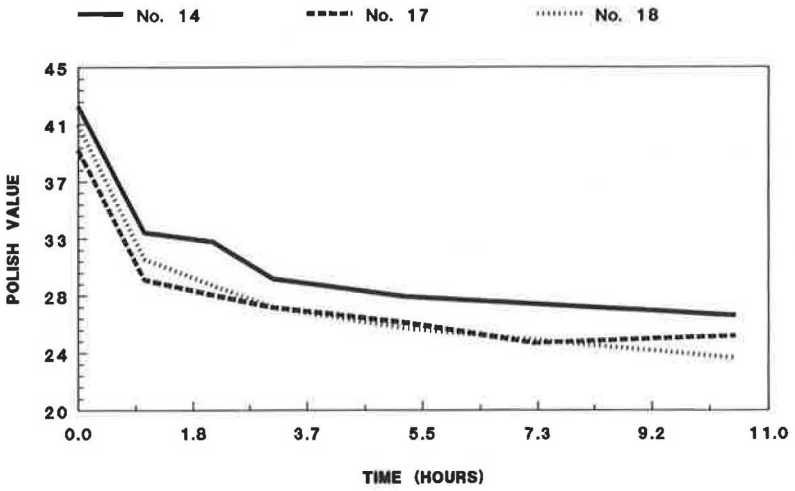

FIGURE 6 PVs of carbonate aggregates identified by rank as being in the lowest third of 21 aggregates tested.

Comparisons of some pendulum values were made with New Jersey test results (Table 1). Many of the rock samples in the comparisons are not included in the study reported here and this table has no other relevance except to demonstrate similarity of values obtained. The samples were run on different wheels for various amounts of time. Then they were tested by both KDOT and NJDOT. These comparisons were reasonable. One variable found was the age of the pad on the pendulum. Results of old pads (those used but still meeting ASTM specifications) were compared with newly conditioned pads. Changing to newly conditioned pads before testing each new aggregate sample and using them for the duration of tests on that sample resulted in better reproducibility of test numbers (Figures 7 and 8). The correlation coefficient increased from 0.62 to 0.78 for the comparison readings. For reading consistency, the swing of the pendulum had to be in the same direction as the wear of the polishing wheel tire.

A reference aggregate was established and run with each tested aggregate. This reference aggregate ensured that the tests were all comparable. Although the reference aggregate was always the same, the results of each run varied as would be expected. An average of the reference aggregate values is reported as the value for that aggregate (Figure 9).

In order to compare the aggregate test results with a bituminous mix result, several samples of KDOT BM–1 gradations were prepared using only the reference limestone. Two molded samples of each selected percent of asphalt were run. This was the first time a mix had been run on the polishing wheel and it was not known whether the molded samples would hold up. Some ran almost 10 hr; others failed earlier (Table 2). Comparisons of these values with those for the reference limestone indicated that the BM–1 had not obtained the same level of polishing as the aggregate alone, the BM–1 having higher PV than the limestone. Although no field tests could be run on the test aggregates, this finding may have relevance in trying to correlate field and test data at a later time. The test of aggregates alone may be more predictive of performance of aggregates in seal coats or friction courses than that in mixes. Because of the early failure, there has been no further attempt to correlate the mix results either with limestone results or field measurements.

DISCUSSION OF RESULTS

After the completion of the tests, the results were ranked from highest to lowest PV (Table 3). The value used for ranking was the curve-fitted final PV point at 10.4 hr of wheel wear for each sample. This value was chosen rather than the actual data point because not all samples had been tested at exactly 200,000 revolutions in the beginning of the study. More discussion of this curve fitting was given by Fager and Smith (*7*).

Of the noncarbonate aggregates tested, the expanded shales and the slags had vesicular structures consisting of tiny to larger rounded cavities throughout the resultant aggregate. The sandstone was carbonate-cemented quartz. The trap rock was generally dark igneous and metamorphic fragments with hematite and sulfides such as galena and pyrite. The gravels were igneous rocks and minerals such as granite, quartz, and feldspars with some sandstones and limestones. Chat was a cryptocrystalline quartz variety of chalcedony or chert, produced as a by-product in southeast Kansas. The trend that could be seen in this group was that the vesicular aggregates and sandstone tested better than the crystalline igneous or metamorphic rock aggregates. The cryptocrystalline variety of quartz polished easily. The vesicular aggregates possibly wore by breaking and renewing the wearing surface with a fresh edge, the more edges available the better the skid-resistant characteristics. Always having an unpolished surface best explains the lack of decrease in PV as in the other aggregates tested (Figure 1). The sandstone had a soft cement that wore faster than the harder sand particles, bringing into relief the sand and therefore always renewing at the surface. It also could renew by breaking through the cement. Of the noncarbonate aggregates tested, vesicular and sandstone aggregates produced better PV values.

The two expanded shales tested proved to have the best polish resistance characteristics of the aggregates tested. Although these were in limited use in Kansas for bituminous mixes, more use might be made especially on critical pavements, i.e., those with large traffic volumes. In early field testing of expanded shale in open-graded mixes or as sprinkle treatment (*8*,*9*), the surfaces retained ice and snow and were unsuitable for driving in Kansas winters. Because these results were the same for other aggregates in the field trials as well, the expanded shale should be tested in other pavement designs. One characteristic that could limit the use of expanded shale is its low resistance to freeze-thaw damage, thus possibly lowering the pavement design life. Field tests need to be run to separate assumptions from actual limits in use.

Chat has been used for many years in Kansas for bituminous design. It seems to have good skid resistance in the field that was not shown by the present tests. This limitation of the polishing tests was clearest with chat but it could also be biasing other aggregate results in less obvious ways. In order to make the small molded samples run on the wheel, individual aggregate pieces had to be selected from the sample and placed in the mold. These pieces stayed in place while the full mold set was selected. Ottawa sand was then used to fill the lower small spaces of the mold before placing the polymer over the exposed aggregate. After the polymer cured for 1 hr and the mold forms were removed, the aggregate surfaces that were on the bottom of the mold were then the exposed aggregate surfaces, having been protected from polymer penetration by the sand.

Chat is usually platy, bladed or elongated in shape, seldom compact. The pieces that best made into acceptable test molds were bladed, elongated, or compact, and the exposed surfaces were always rather smooth on the finished molded sample. This assortment was chosen as rather a random orientation of pieces in the mold. One set of samples was made with the narrow edges exposed for testing. Upon turning on the wheel to begin the test, it was apparent that the knife-like edges were wearing the test wheel excessively. Also, the wheel began to bounce rather than rolling smoothly. This test was not completed.

In the field, the chat would not have all flat surfaces or all knife-edged surfaces exposed but would be a mixture of both with pieces overlapping at angles to each other. It is probable that the narrow-edged surfaces exposed would chip off, leaving a new sharp edge under traffic, and thus would compen-

TABLE 1 NJDOT/KDOT PV COMPARISONS

No.	Description	New Jersey	KDOT[a]	KDOT[b]
1	Limestone	30	27.6	
2	Limestone	29	26.0	
3	Limestone	31	31.7	
4	Chat	20	22.6	23.3
5	Chat	19	22.3	24.4
6	Chat	22	22.9	24.0
7	Gneiss	33.4	27.0	32.0
8	Argille	28.2	23.0	27
9	Trap Rock	25.2	20.6	24.3
10	Carbonate Rock	21.0	19	22.7
11	Crushed Gravel	31.2	23	26.4
12	Steel Slag	26	19.6	22.6
13	Limestone	30	33	35.4
14	Limestone	33	27.9	32.6
15	Steel Slag	25	22.1	23.7
16	Limestone	32	28	33.0
17	Limestone	35	30	33.9
18	Limestone	30	27.3	31.7
19	Limestone	30	28.9	32.6
20	Limestone	30	23.4	27
21	Limestone	26	22.4	26.6
22	Limestone	26	23	24.7
23	Limestone	27	26.6	27.4
24	Limestone	26	27.4	31.3
25	Limestone	40	32.6	34
26	Limestone	35	25.4	32
27	Limestone	31	24.4	27.3
28	Limestone	30	23	26.0
29	Trap Rock/Fanwood	30	30	30
30	Trap Rock/Tilcon	29	28	29
31	Carb.Rock/Berks,Oley	20	24	24
32	Crush.Grav./Warner	34	34	36
33	Crush.Grav./Warner	34	33	34
34	Kingston Argillite	27	25	26
35	Carb Rock/Glasgow	21	25	24
36	Gneiss/DeVault	28	26	27
37	Trap Rock/Stavela	26	28	28
38	Gneiss/Riverdale	27	27	33
39	Gneiss/Hopatcong	27	33	26

[a] - Measured using a pad passing ASTM standards.

[b] - Measured using a newly conditioned pad.

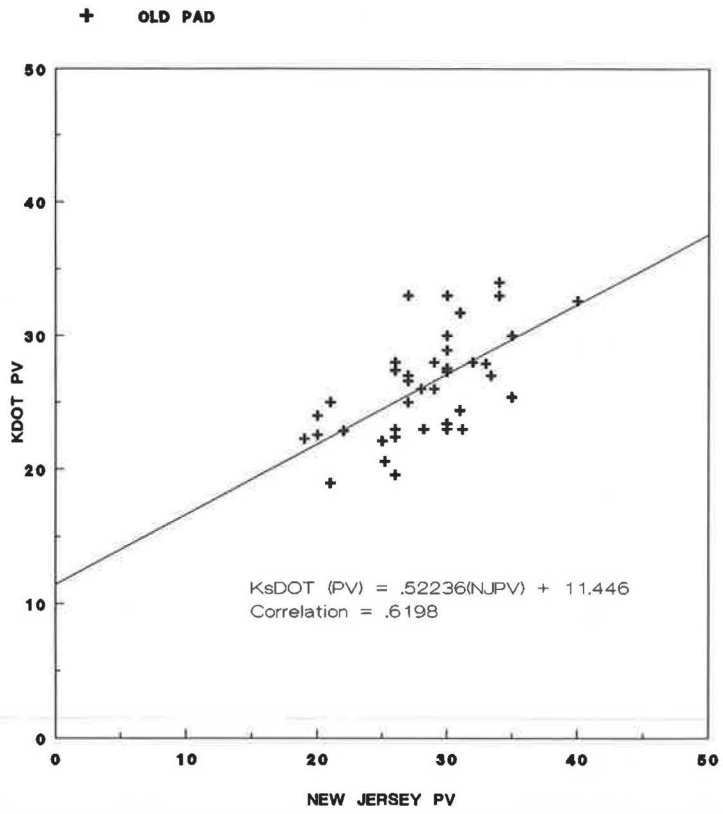

FIGURE 7 Test values recorded using the same older test pad by two agencies.

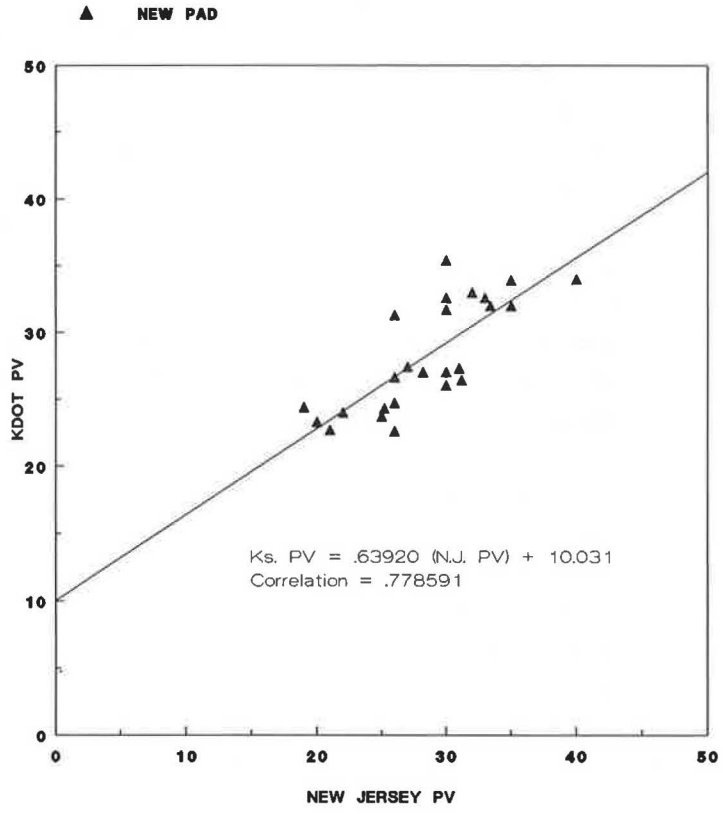

FIGURE 8 Test values recorded using a new test pad by two agencies.

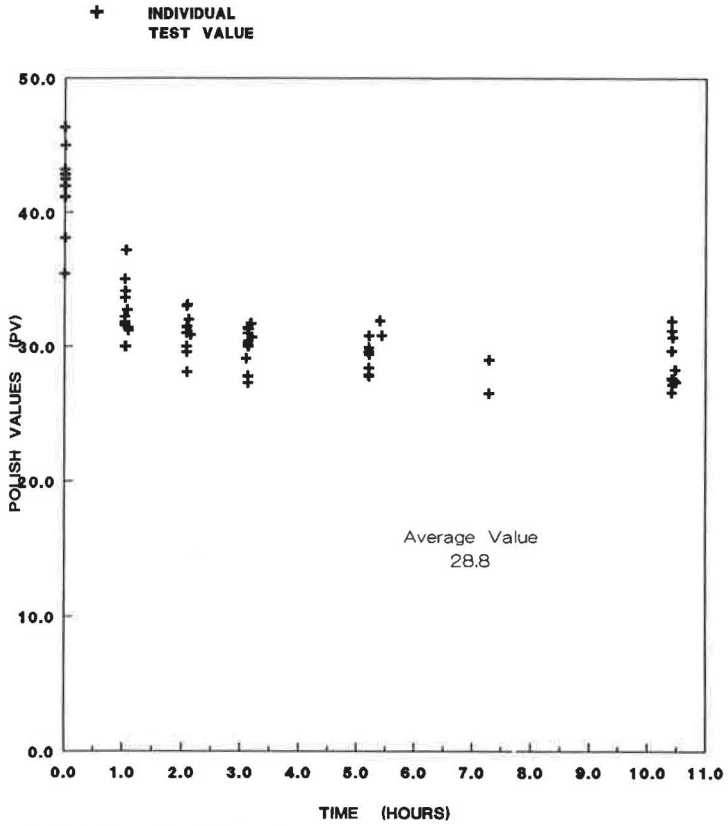

FIGURE 9 PVs of the reference aggregate during many test runs of nearly 11 hr each.

sate for those flatter, smoother surfaces th.. were polishing. The shapes of the aggregate in the molded samples tested were not randomly placed. This defect biased the results of the test. Other aggregates with variations in lithology that might be reflected in shape such as the carbonates (see Table 4) could be biased similarly by the process of choosing, although the results might not be as pronounced as with the chat test. They would depend on the variability within the aggregate sample.

The number of carbonate aggregates studied was limited relative to the many carbonate rock sources in the state. For 12 samples, carbonate aggregates tested included a dolomite and a dolomitic limestone as well as the usual limestone aggregates. The very light-colored limestones as well as the very dark aggregates do not usually make the best concrete for use in Kansas. Light-to-medium colors usually perform best in the concrete suitability tests and in the field. A range of colors was picked in choosing the aggregates for this study. Some of the aggregates were suitable for use in concrete and others were not. A representative sample from each aggregate was split into describable lithologies; information listed included crystallinity, luster, color using the Munsell color charts, shape, edge, and side characteristics. Tables 4 and 5 summarize some of the aggregate descriptive characteristics as well as physical test results.

While studying the characteristics of only the carbonate aggregates ranked by the research test results, several interesting relations come forth. The carbonate aggregate results overlapped the noncarbonate aggregate results. The 12 aggregates were listed by rank using the final PV results of all the aggregates tested (Tables 3–5). As an aid in generalizing the characteristics of the carbonates only, the top four, the middle four, and the bottom four by rank were grouped. The top four were ranked 3rd, 4th, 6th, and 7th, respectively, of the 21 samples. The middle four were ranked 9th, 10th, 11th, and 12th, respectively. The lowest four carbonates were ranked 13th, 15th, 16th, and 20th out of the field of 21 aggregates. These 12 aggregates have been numbered as Samples 1 through 12 for Tables 3–5, their rank in the group of 21 given in the column labeled "rank" in Table 4.

The top performers in the first group were mostly very soft limestones with dull, even chalky, luster. The softness was also evidenced by the generally rounded edges of the rock and the high Los Angeles (LA) wear numbers. Also the absorptions were high. Three had very light colors designated in Table 4 by high percentage *L*. Only one had a large acid insoluble residue (AIR), but it also had a lower absorption and wear number and darker coloration. One was a dolomite. The dolomite rock in Kansas that passed for concrete use was usually of light-to-medium color.

In the middle group, the aggregates appeared to be harder as evidenced by angular edges; straight, smooth sides; and generally lower LA wear numbers. They also were less absorptive. The luster was less dull, but the one that did exhibit a dull luster was a dolomitic limestone. This group contained the aggregates of light-to-medium color.

In the lowest grouping, all exhibited angular edges (indicating harder rock) and lower absorptive values. This group also included the aggregates having the lowest contents of acid-insoluble minerals and medium (M) to darker (D) colors.

TABLE 2 PVs OF A BM-1 ASPHALT MIX

Table 2. Polish Values (PV) of a BM-1 Asphalt Mix.							
Asphalt %	Initial PV	PV Readings at Intervals 1 hr	2 hrs	3.5hrs	5.5hrs	9.75hrs	
5.75	46.8	36.7	39.1	failed			
6.25	49.3	36.0	37.5	35.7	35.9	34.7	failed
6.75	47.1	36.3	35.8	34.3	35.5	failed	
7.25	47.9	36.3	37.5	34.3	34.6	33.7	failed
7.75	42.6	33.3	33.9	34.5	35.0	failed	
8.25	31.5	33.9	34.1	34.7	33.1	failed	
8.75	32.1	32.8	33.1	32.0	34.1	32.3	failed

TABLE 3 PVs OF TESTED AGGREGATES

Rank	PV	Aggregate and Laboratory Number	
1	50.7	Expanded Shale	
2	44.0	Expanded Shale	
3	43.6	Limestone	83-1430-5
4	41.3	Limestone	83-2171-1
5	35.4	Sandstone	
6	35.3	Limestone	83-1659-1
7	34.2	Limestone	81-931-4
8	33.1	Boiler Slag	
9	31.7	Limestone	88-105-4
10	30.3	Limestone	81-749-2
11	28.7	Limestone	86-4527 Reference
12	27.5	Limestone	81-750-1
13	27.4	Limestone	81-83-13
14	27.0	Trap Rock	87-3134
15	26.8	Limestone	82-2990-2R
16	25.3	Limestone	83-2531-5
17	24.8	Steel Slag	
18	24.3	Crushed Gravel	
19	23.1	Gravel	
20	21.9	Limestone	81-945-1
21	20.7	Chat (flat)	

There was less earthy luster. From higher to lower PV, the acid-insoluble contents and absorptions tended to smaller values and the rocks tended from softer to harder. The softness of the higher-ranked carbonates probably produced higher PV by wearing away rather than by polishing, similar to the vesicular aggregates discussed.

Questions for further study center on possibilities for more research on expanded shales and dolomite or dolomitic limestones for bituminous pavements. Are there dolomites and dolomitic limestones that do not qualify for concrete aggregate but have characteristics that should be tested for bituminous pavements? If pretreated, can the softer, more absorptive carbonates be durable enough to make long-lasting, skid-resistant pavements without excessive wear ruts occurring? Are there limestones in Kansas that have reactive quartz varieties excluding them from use in concrete, but that contain enough quartz as acid-insoluble residue fraction to add abrasiveness, thereby raising the polishing value of the aggregate? How well do expanded shales weather during Kansas winters?

TABLE 4 LIMESTONE DESCRIPTIONS

Sample	Rock	Rank	Luster	Color[s]	Mineral	Shape	Edge	Sides
1	Ls[a]	3	e[d]	$L^{t}_{10}{}^{w}$		b[g]	sr[k]	p[o]
2	Ls	4	e	$L_7M_3{}^{u}$		c[h],p[i]	sr,r[l]	i[p]
3	Dol[b]	6	e	L_4M_6	Dol	p,c	r,a[m]	sm[q],p
4	Ls	7	e,cx[e]	L_3M_7		p,b,e[j]	a,sa[n],sr	sm,r[r]
5	Dol.Ls[c]	9	e	$M_3D_7{}^{v}$	Dol	p,b,c	a	sm,r
6	Ls	10	cx,fx[f]	L_6M_4		b,p	a, sr	sm,r
7	Ls	11	e,fx	L_5M_5		c,p,e	a,sa, rd	r,sm
8	Ls	12	fx	M_{10}		c,p	a	sm,r
9	Ls	13	fx,e	L_5M_5	ch.,sh[x]	c,e,p	a,sa	sm,r
10	Ls	15	e,cx	L_7M_3		c,p	sa,a	r,i
11	Ls	16	fx	M_2D_8		c,p	a,sa	sm,r
12	Ls	20	fx	M_4D_6		c,p	a,sa	sm,r

a limestone
b dolomite
c dolomitic limestone
d earthy
e coarsely crystalline
f finely crystalline
g bladed
h compact
i platy
j elongated
k subrounded
l rounded
m angular
n subangular
o pitted, vuggy
p irregular
q smooth
r rough
s Munsell Color Charts used for obtaining value of color, lightness or darkness.
t light colored, values of 7.5 or higher.
u medium colored, values of 6 to 7.
v dark colored, values of 5.5 or darker.
w subscript times 10 gives percent of aggregate with value characteristic
x cherty, shaly

TABLE 5 LIMESTONE TEST RESULTS

Sample	Rock	A.I.R.[d]	Class	Bit	Absorption[j]	L.A.[k]
1	Ls[a]	3.94	1	NA	9.94	33
2	Ls	6.97	1	No	7.24	46
3	dol[b]	3.05	1[f]	NA	5.7	39
4	Ls	13.46	0[g]	NA	2.84	22
5	dol.Ls[c]	NA[e]	0	NA	4.72	14
6	Ls	2.29	1	Yes[h]	3.18	29
7	Ls	NA	NA	NA	2.1	29
8	Ls	7.97	0	No[i]	1.72	27
9	Ls	8.19	0	No	3.05	27
10	Ls	1.15	1	NA	2.16	35
11	Ls	1.77	0	Yes	1.49	NA
12	Ls	7.84	1	Yes	1.09	19

a - limestone
b - dolomite
c - dolomitic limestone
d - acid insoluble residue, determination of total
e - not available
f - usable in concrete
g - not usable in concrete
h - usable in bituminous pavement
i - not usable in bituminous pavement
j - Kansas Test Method KT-6
k - Los Angeles Wear Test AASHTO T96

CONCLUSIONS

Several tests of the procedure for accuracy and reproducibility were performed and comparisons with other agencies were made. The results of the study have enabled ranking of 21 different aggregates. Most of the aggregates had a rapid decrease in PV to a lower value, and then the PV leveled out. The general trend was for vesicular or softer rock to polish less than crystalline rock, and very finely crystalline rock to polish exceedingly well. The two expanded shales and the one sandstone tested gave excellent to good results. Boiler slag and trap rock performed better than similar-looking steel slag and siliceous gravel materials tested. Chat performed poorly in the flatter orientation tested. Carbonate aggregates overlapped the upper through the lower PVs. Dolomite content and the higher acid-insoluble residue contents in softer limestones of the tested aggregates characterized the better-performing aggregates. Further research should be done with these. Expanded shales warrant testing for use in critical pavements having higher traffic volumes.

ACKNOWLEDGMENTS

This research was conducted by the Kansas Department of Transportation and was coordinated by FHWA. John Knickerbocker accomplished almost all of the laboratory testing. The typing of the report was completed by V. Freeman.

REFERENCES

1. H. E. Worley, T. M. Metheny, and F. W. Stratton. *Pavement Surface Dynamics Friction Measurement and Analysis in Kansas*. Report FHWA-KS-RD 73-3. Planning and Development Department, Research Section, Kansas Department of Transportation, Topeka, June 1976.
2. W. H. Parcells, Jr., T. M. Metheny, and R. G. Maag. Design Prediction of Pavement Skid Resistance from Laboratory Tests. Report FHWA-KS-80-1. Planning and Development Department, Research Section, Kansas Department of Transportation. Topeka, Aug. 1980, 27 pp.
3. W. H. Parcells, Jr., T. M. Metheny, and R. G. Maag. Predicting Surface Friction from Laboratory Tests. In *Transportation Research Record 843*, TRB, National Research Council, Washington, D.C., 1982, pp. 33–40.
4. T. S. Patty. Accelerated Polish Test For Coarse Aggregate. Presented at the 24th Annual Highway Geology Symposium, Sheridan, Wyo., Aug. 1973.
5. K. T. Diringer. *Polish Resistance of Selected New Jersey Aggregates*. Report FHWA/NJ 86-016-7711. Division of Research and Demonstration, New Jersey Department of Transportation, Trenton, Feb. 1987.
6. K. T. Diringer. *Aggregates and Skid Resistance*. Report FHWA/NJ 89-008-7110. Division of Research and Demonstration, New Jersey Department of Transportation, Trenton, March 1989.
7. G. A. Fager and B. J. Smith. *Polish Resistance of Selected Kansas Aggregates*. FHWA-KS-90/2. Bureau of Materials and Research, Research Section, Kansas Department of Transportation, Topeka, 1990.
8. W. H. Parcells, Jr. *Open Graded Asphalt Friction Courses*. Final Report, Dec. 1986, 2 pp.
9. W. H. Parcells, Jr., and R. G. Maag. Sprinkle Treatment. FHWA-KS-84-2. Sept. 1984, 14 pp.

Publication of this paper sponsored by Committee on Mineral Aggregates.

Rapid, Accurate Method for the Determination of Sulfur Trioxide in Hydraulic Cement

S. W. BISHARA

A method for determining sulfur trioxide (SO_3) content of hydraulic cement is described. The method depends on heating the sample with the least possible amount of nitric acid. After filtration, the filtrate is diluted to a given volume and an aliquot passed through a cation exchange resin (hydrogen form) to separate all cations present. The eluant is diluted to volume, and an aliquot titrated against standard barium perchlorate solution using dimethylsulfonazo III (DMSA III) as visual indicator. Acetone helps detection of the equivalence point that is characterized by a color change from purple to sky blue. Seven Standard Reference Material portland cements and three commercially available cements were analyzed. Each cement sample was analyzed six times. The average absolute error for 60 determinations amounted to ±0.041 percent, and the pooled standard deviation, s_p, for the 10 samples is 0.031 percent, for 50 degrees of freedom. All of the samples analyzed passed the t test at the 99 percent level. One sample determination consumes about 2 hr. The method requires no equipment other than a pH meter and ordinary glassware.

The significance of the sulfur trioxide (SO_3) content of cement cannot be overemphasized. The amount of SO_3 present in portland cement affects the creep as well as other physical properties of concrete (*1*). The behavior of portland cement mortars (*2*) is also influenced by the SO_3 content.

A sulfate environment, as well, can be detrimental. Sodium sulfate in the ground moisture subjects concrete to corrosion and destruction (*3*). Asbestos cement pipes are vulnerable to sulfate attack if sulfate salts exist in the vicinity (*4*). Ouyang et al. (*5*) discussed the sulfate attack resistance of portland cement mixtures containing phosphogypsum.

The ASTM C114-85 describes a gravimetric method for determination of the SO_3 content in hydraulic cement (*6*). In that method, sulfate is precipitated as barium sulfate ($BaSO_4$); after digestion for 12 to 24 hr, the precipitate is ignited at 800°C to 900°C for several hours. After cooling to room temperature, the weight of $BaSO_4$ is used to calculate the SO_3 equivalent. For rapid determinations, the digestion time may be cut to 3 hr, but rejection of a cement for violation of the specification requirement must be based only on the 12- to 24-hr digestion period.

A visual titrimetric finish can offer both the high degree of accuracy and the level of precision usually associated with gravimetry, but in a much shorter time, provided a suitable indicator is available. Sulfate ion (either as inorganic sulfate, or as obtained after oxidative combustion of organic sulfur) can be determined titrimetrically against barium ion solution using thorin (*7,8*), tetrahydroxyquinone (*9*), carboxyarsenazo (*10*), sulfonazo III (*11*), arsenazo III (*12*), or chlorphosphonazo III (*13*) as visual indicator. But there seems to be some difficulty in detecting the equivalence point with most of these indicators (*11,14,15*). Budesinsky and Krumlova (*16*) carried out a comparative study on the titrimetric determination of sulfur and sulfate, against barium ion solution using six different indicators: thorin, carboxyarsenazo, sulfonazo III, dinitrosulfonazo III (*17*), dimethylsulfonazo III (DMSA III) (*18*), and dibromosulfonazo III (*18*). The authors (*16*) noted that DMSA III is the best indicator, and that this is true both for the visual and the photometric titrations. Reijnders et al. (*19*) reported the superiority of DMSA III to other indicators, e.g., thorin, for determination of sulfate in real environmental water samples. Not surprisingly, a titrimetric procedure (*20*) applying DMSA III as the indicator has been recommended by the Association of Official Analytical Chemists (AOAC), for titration of sulfate against barium perchlorate solution.

In the present method, DMSA III is used as visual indicator of the equivalence point for the sulfate versus barium titration. The amount of sulfate involved and the cement matrix, however, did introduce difficulties, and pretreatment of the sample is deemed necessary.

EXPERIMENTAL

Apparatus

Orion pH meter, model 601A, digital Ionalyzer, capable of reading the pH value to 0.01 of a pH unit.

Reagents and Materials

- Potassium sulfate (ACS), powdered and dried;
- Dowex 50W, cation exchange resin, hydrogen form, 8 percent cross-linked, dry-mesh 50–100;
- Barium perchlorate standard solution, 0.01 M. Dissolve about 3.4 g of the anhydrous salt in 1 L of distilled water and adjust the pH value of the solution to 3.0 with 0.5 N HCl. Standardize as follows. Weigh, by difference, 5 to 10 mg (weighed to the nearest 0.01 mg) of freshly dried potassium sulfate.

Materials and Research Center, Kansas Department of Transportation, 2300 Van Buren, Topeka, Kans. 66611.

Introduce the sample into a 200-ml tall-form graduated beaker. Add 50 ml of distilled water, and stir to dissolve. Adjust the pH value of the solution to 3.0 ± 0.2 by addition of 0.5 N HCl. Add 50 ml of acetone, followed by 0.3 ml of DMSA III indicator solution. Titrate as described later under procedure. Correct the titration by making a blank determination under the same conditions but without sulfate. Calculate the exact molarity of the barium perchlorate solution.

- Dimethylsulfonazo III indicator solution, 0.1 percent. Dissolve 100 mg of DMSA III in 30 ml of distilled water. Elute the solution through a column of Dowex 50 ion exchange resin (pretreated with HCl). Dilute the eluent to 100 ml with distilled water.
- Ammonium hydroxide, 1:1, and 0.5 N solutions.
- Acetone, reagent grade.
- Nitric acid, 70 percent solution.

Procedure

Weigh, by difference, 0.5 g of cement to the nearest 0.01 mg. Introduce the sample into a 250-ml beaker. Add 25 ml of distilled water, then 1.2 ml of concentrated nitric acid solution. Grind the material with a glass rod, and add 25 ml more of distilled water. Digest for 10 min on a hot plate at a temperature just below boiling, then boil gently for 5 min. Filter to separate undissolved matter, and transfer the filtrate quantitatively to a 100-ml volumetric flask. Complete to volume with distilled water. Pipet 50 ml of the solution into a separatory funnel mounted at the top of a 100-ml buret filled with the ion-exchange resin. Elute the sample solution through the column at a flow rate of 3 to 4 ml/min. Rinse the column with three 50-ml portions of distilled water. Collect the eluant and washings in a 250-ml volumetric flask, and add distilled water up to the mark.

Pipet 50 ml in a 200-ml tall-form graduated beaker. Immerse a combined glass electrode in solution and introduce a few drops of 1:1 ammonium hydroxide solution until the pH value of solution is about 2.0. Adjust the pH value to 3.0 ± 0.2 with 0.5 N ammonium hydroxide solution. Add 50 ml of acetone, then 0.3 ml of DMSA III solution. Stirring vigorously, titrate slowly with 0.01 M barium perchlorate solution to a sky-blue color that persists while stirring for at least 30 sec.

Carry out a reagent blank under exactly the same conditions except for the cement sample.

The ion exchange resin (*21*) is regenerated as follows. At a high flow rate, elute 1 L of 1 N HCl solution through the column. Rinse the regenerant with 100 ml of distilled water. After every three or four sample runs, backwash the resin bed to eliminate resin compaction and to wash off insoluble contaminants.

Calculate the SO_3 percentage as follows:

$$SO_3, \% = \frac{80.06 \times [\text{ml } Ba(ClO_4)_2 - \text{Reagent Blank}] \times F \times 100}{V \times W} \quad (1)$$

where

80.06 = atomic weight of SO_3, mg;
F = dilution factor (F = 10 for the given volumes);
V = volume of barium perchlorate solution that contains 1 mM of barium ion, ml; and
W = sample weight, mg.

RESULTS AND DISCUSSION

In the present method, sulfate is removed from solution as barium sulfate; complete removal is manifested by appearance of the blue color of the stable barium-DMSA III complex. The use of barium as titrant offers the advantage that its sulfate salt has the lowest solubility product (1.1×10^{-10}) among the insoluble sulfates (*22*).

Pretreatment of Sample

For DMSA III to detect the equivalence point of the precipitation titration of sulfate versus barium, the reaction medium has to have a pH value of 3.0 ± 0.2. Under this condition, metal ions such as iron, aluminum, and calcium known to be present in cement will precipitate and render detection of the end point difficult. Elimination of iron and aluminum through precipitation as hydroxides by addition of 1:1 ammonium hydroxide solution, and removal of calcium as calcium oxalate by addition of solid ammonium oxalate, then removing the excessive oxalate (which would otherwise precipitate barium) by boiling with HCl solution was tried, but, the color change of the indicator was not very sharp, and the repeated steps of boiling, precipitation, filtration, and washing render the procedure more susceptible to error.

To eliminate metal ions from sample solution, at the same time avoiding the introduction of foreign ions in the reaction medium, an alternative approach is to use a cation exchange resin in the H^+ form.

The color change of DMSA III proved to be much sharper in dilute solutions. In order to have a minimum ionic concentration in the reaction medium, 1.2 ml of nitric acid solution is used to dissolve the cement sample, instead of the 5 ml of hydrochloric acid solution used in the reference method (*6*). To effect dissolution, a 10-min digestion period is necessary. Subsequent boiling of the acidic sample solution for 5 min ensures decomposition of any carbonate present to avoid formation of barium carbonate precipitate (*22*) during the subsequent titration.

After eluting the sample solution through the resin bed, the eluant volume is increased to 250 ml. For each titration, 50 ml is used. Such a design has two advantages: (a) it keeps the ionic concentration at a low level, and (b) it allows three or four titrations from each sample solution. The volume of titrant consumed per titration is not too small and is in the vicinity of 2 ml for most of the samples analyzed.

In order to test the effect of time on the treated sample solution, a part of an eluant was titrated 24 hr after elution. Comparing the results with those obtained immediately after elution reveals practically no variation in the volume of titrant consumed. Thus, the treated sample solution may be left to stand overnight before titration, if necessary.

Barium-DMSA III Complex

In the precipitation titration of sulfate against barium, the poorest reversibility of the indicator color change occurs at the beginning of the titration, because of the precipitation mechanisn of the titration; the proper course of the titration requires the formation of precipitation centers in solution (*16*). Therefore, the first three or four drops of titrant should be added slowly. The reversibility of the color change improves rapidly as the titration continues and is satisfactory at the equivalence point. Budesinsky et al. (*23*) reported an experimental value of 3.8×10^4 for the effective stability constant of the barium-DMSA III complex.

Accuracy, Precision, and *t*-Test for Sample Averages

Analysis of seven Standard Reference Material (SRM) portland cements, obtained from the National Institute for Standard Technology, and three commercially available cements reveals high accuracy of the proposed method (Table 1). For 60 sample runs, the average absolute error amounted to ± 0.041 percent. The precision, as calculated by the sample standard deviation, s, ranged between 0.009 and 0.043 percent for the 10 samples analyzed; for each estimate of s, the degrees of freedom (df) was equal to 5. However, the pooled standard deviation, s_p, would be based on the sum of the df values for each of the standard deviation estimates, in this case $(n - 1)$

TABLE 1 ANALYSIS OF STANDARD AND COMMERCIAL CEMENT SAMPLES FOR THEIR SO_3 CONTENT

Sample	Sample Weight (mg)	SO_3 (%) Expected	Found	Error	Standard Deviation, s
SRM 633	–	2.20	–	–	0.043
	452.23		2.19	−0.01	
			2.17	−0.03	
			2.15	−0.05	
	532.46		2.11	−0.09	
			2.09	−0.11	
			2.09	−0.11	
SRM 634	–	2.21	–	–	0.036
	480.45		2.22	+0.01	
			2.20	−0.01	
			2.14	−0.07	
	487.82		2.24	+0.03	
			2.18	−0.03	
			2.17	−0.04	
SRM 635	–	7.07	–	–	0.036
	481.34		6.96	−0.11	
			7.01	−0.06	
			6.99	−0.08	
	483.59		7.03	−0.04	
			7.06	−0.01	
			7.04	−0.03	
SRM 636	–	2.31	–	–	0.009
	482.86		2.36	+0.05	
			2.36	+0.05	
			2.34	+0.03	
	503.16		2.28	−0.03	
			2.27	−0.04	
			2.27	−0.04	
SRM 637	–	2.38	–	–	0.036
	506.32		2.45	+0.07	
			2.43	+0.05	
			2.38	0.00	
	456.90		2.41	+0.03	
			2.41	+0.03	
			2.35	−0.03	
SRM 638	–	2.34	–	–	0.018
	529.38		2.33	−0.01	
			2.36	+0.02	
			2.36	+0.02	
	482.56		2.40	+0.06	
			2.38	+0.04	
			2.31	−0.03	
SRM 1880	–	3.37	–	–	0.033
	463.36		3.27	−0.10	
			3.29	−0.08	
			3.36	−0.01	
	458.06		3.33	−0.04	
			3.34	−0.03	
			3.31	−0.06	

(*continued on next page*)

TABLE 1 (*continued*)

Sample	Sample Weight (mg)	SO_3 (%) Expected	Found	Error	Standard Deviation, *s*
Missouri Portland Type III	–	2.95	–	–	0.027
	556.82		3.02	+0.07	
			3.02	+0.07	
			2.99	+0.04	
	455.00		2.95	0.00	
			2.98	+0.03	
			3.00	+0.05	
Monarch Type II	–	2.45	–	–	0.014
	498.13		2.42	−0.03	
			2.46	+0.01	
			2.46	+0.01	
	553.06		2.42	−0.03	
			2.41	−0.04	
			2.41	−0.04	
Monarch Type III	–	2.85	–	–	0.042
	464.61		2.89	+0.04	
			2.87	+0.02	
			2.83	−0.02	
	485.45		2.77	−0.08	
			2.83	−0.02	
			2.86	+0.01	

(0.10) = 50, where n is the number of determinations carried out for each sample, and 10 is the number of standard deviations involved. The pooled standard deviation is calculated from the following expression (*24*):

$$s_p = \left[\frac{(s_1^2 \times df_1) + (s_2^2 \times df_2) + \ldots (s_n^2 \times df_n)}{df_1 + df_2 + \ldots df_n}\right]^{1/2} \quad (2)$$

where s_1^2, s_2^2, s_n^2 = variance for first, second, and nth sample data, respectively, and df_1, df_2, df_n = degrees of freedom for first, second, and nth sample, respectively. The pooled standard deviation = 0.031 percent, for 50 df.

Because the population standard deviation, σ, is not known, a test of significance should use the t statistic (*25*).

$$t = \frac{\bar{x} - \mu}{s/(n)^{1/2}} \quad (3)$$

where $\bar{x}$ is the average SO_3 percentage found, and μ is the expected value.

The t test was first used to find out whether the calculated statistic of sample average, $\bar{x}$, found for each of the seven SRM cement samples agrees with the expected value (the population average, μ). The t test was then applied to judge whether the calculated sample average, $\bar{x}$, found for each of the commercially available cement samples agrees with the value reported by the Materials Unit Laboratories of the Kansas Department of Transportation (KDOT) using ASTM C114 (*6*) for the SO_3 content. Table 2 indicates that the null hypothesis (H_0: $\mu = \mu_0$) is correct for all of the samples analyzed. That is, for the seven SRM cements, the sample average, $\bar{x}$, found practically agrees with the population average, μ, reported by the SRM certificate; for the commercial cements, $\bar{x}$ agrees with the SO_3 content reported by the Materials Unit, KDOT.

For SRM 634, the t statistic is

$$t = \frac{2.19 - 2.21}{0.036/(6)^{1/2}} = -1.333$$

From the t distribution critical values table, across from df = 5, a t value equal to 1.333 (the sign is not significant) has a P-value between 0.10 and 0.15. Because the alternate hypothesis, H_a is double-sided, the P-value should be doubled and is between 0.20 and 0.30. At the 99 percent level, α equals 0.01, and $p = \alpha/2$ or 0.005. A comparison between the value of p (0.005) and the P-value of 0.20 to 0.30 indicates that the standardized difference between the sample average obtained (2.19 percent) and the SRM certificate value of 2.21 percent is not statistically significant, and is caused by the expected sampling distribution. For a commercial cement, t is calculated similarly except that the SO_3 content reported by the Materials Unit Laboratories is substituted for μ in the previous equation.

Under the specified experimental conditions, the proposed method can detect as little as 0.1 percent of SO_3 in cement.

SO_3 Content of Fly Ash

As for cement, the SO_3 content of fly ash is of interest. The present method has been tested, without modification, on fly ash. The results of testing a limited number of samples agree favorably with those obtained by the ASTM C311-77 (*26*),

TABLE 2 APPLICATION OF THE *t* TEST FOR THE AVERAGE SO_3 CONTENT OF THE CEMENT SAMPLES ANALYZED

Sample	Average SO_3 %, $\bar{x}$	Null Hypothesis	Alternate Hypothesis*	t**	P-Value (range)	Decision §
SRM 633	2.13	H_o:μ=2.20	H_a:$\mu\neq$2.20	-3.889	0.010-0.020	a
SRM 634	2.19	H_o:μ=2.21	H_a:$\mu\neq$2.21	-1.333	0.200-0.300	a
SRM 635	7.01	H_o:μ=7.07	H_a:$\mu\neq$7.07	-4.000	0.010-0.020	a
SRM 636	2.31	H_o:μ=2.31	H_a:$\mu\neq$2.31	0.0	>0.50	a
SRM 637	2.41	H_o:μ=2.38	H_a:$\mu\neq$2.38	2.000	0.100-0.200	a
SRM 638	2.36	H_o:μ=2.34	H_a:$\mu\neq$2.34	2.857	0.020-0.040	a
SRM 1880	3.32	H_o:μ=3.37	H_a:$\mu\neq$3.37	-3.846	0.010-0.020	a
Missouri Portland Type II	2.99	H_o:μ=2.95	H_a:$\mu\neq$2.95	3.636	0.010-0.020	a
Monarch Type II	2.43	H_o:μ=2.45	H_a:$\mu\neq$2.45	-3.333	0.020-0.040	a
Monarch Type III	2.84	H_o:μ=2.85	H_a:$\mu\neq$2.85	-0.588	>0.50	a

* Double-sided test.
** df = 5 for each estimate.
§ At the 99% confidence level, with p equal to 0.005.
a = H_o is correct.

but the time required for analysis is much shorter than for the reference method. Details from testing an adequate set of standard and samples will be published in the future.

CONCLUSIONS

The proposed method is characterized by having high precision and accuracy. The maximum difference between replicates, as well as the maximum difference of the average of replicates from seven SRM certificate values, are within the limits specified by the ASTM C114-85 method (*6*). Furthermore, the time required for one determination is about 2 hr. This time compares favorably with the ASTM C114-85 method (*6*) used at KDOT, which requires a period of 9 hr, as a minimum for routine testing, and 18 hr for check testing. The present method is recommended as a reference method for determination of the SO_3 content of hydraulic cement.

ACKNOWLEDGMENTS

This work was accomplished in cooperation with the FHWA under the line item "Implementation of Research and Development" in the annual work program. There is no doubt that the FHWA Region 7 and Kansas Division's flexibility on administration of this line item has contributed significantly to the rapid and successful completion of this research. The author would like to thank Richard L. McReynolds for his continuous interest and support of this work. Thanks are also owed to Will Entz of the Materials Unit, KDOT.

REFERENCES

1. K. M. Alexander, J. Wardlaw, and I. Ivanusec. The Influence of Sulfur Trioxide Content of Portland Cement on the Creep and Other Physical Properties of Concrete. *Cement and Concrete Research*, Vol. 9, 1979, pp. 451–459.
2. D. W. Hobbs. The Influence of SO_3 Content on the Behaviour of Portland Cement Mortars. *World Cement Technology*, Vol. 8, 1977, pp. 75–85.
3. L. H. Tuthill. Lasting Concrete in a Sulfate Environment. *Concrete International: Design and Construction*, Vol. 10, 1988, pp. 85–86.
4. M. A. Matti and A. Al-Adeeb. Sulfate Attack on Asbestos Cement Pipes. *International Journal of Cement Composites and Lightweight Concrete*, Vol. 7, 1985, pp. 169–176.
5. C. Ouyang, A. Nanni, and W. Chang. Sulfate Attack Resistance of Portland Cement Mixtures Containing Phosphogypsum. Katherine and Bryant Mather International Conference, Atlanta, Ga., 1987.
6. *Standard Methods for Chemical Analysis of Hydraulic Cement*. ASTM C114-85. ASTM, Philadelphia, Pa., 1985, pp. 120–121.
7. H. Wagner. Microdetermination of Sulfur in Organic Substances. *Mikrochimica Acta*, 1957, p. 19.
8. A. F. Colson. The Removal of Phosphate in the Barium Perchlorate Titration of Sulfate. Application of the Method to the Oxygen Flask Combustion Technique. *Analyst*, Vol. 88, 1963, pp. 26–29.

9. A. Steyermark, E. A. Bass, C. C. Johnston, and J. C. Dell. Microdetermination of Sulfur in Organic Compounds Utilizing the Schoeniger Combustion. *Microchemical Journal*, Vol. 4, 1960, pp. 55–58.
10. K. F. Novikova, N. N. Basargin, and M. F. Tsyganova. Microdetermination of Sulfur in Organic Substances by Using Carboxyarsenazo for Titration of Sulfate Ions. *Zhurnal Analiticheskoi Khimii*, Vol. 16, 1961, pp. 348–351.
11. B. Budesinsky. Modification of Flask Method of Sulfur Determination. *Analytical Chemistry*, Vol. 37, 1965, p. 1159.
12. K. Hozumi and K. Umemoto. Modified Microdetermination of Sulfate Ion: Application to Flask Combustion for Organic Sulfur. *Microchemical Journal*, Vol. 12, 1967, pp. 46–54.
13. A. M. Lukin and T. V. Chernysheva. Titrimetric Determination of Sulfates with Chlorophosphonazo III. *Zavodskaya Laboratoriya*, Vol. 34, 1968, pp. 1054–1056.
14. A. M. G. Macdonald. The Oxygen Flask Method. A Review. *Analyst*, Vol. 86, 1961, pp. 3–12.
15. S. W. Bishara, M. E. Attia, and H. N. A. Hassan. Microdetermination of Organic Sulfur or Inorganic Sulfate. *Revue Roumaine Chimie*, Vol. 19, 1974, pp. 1099–1105.
16. B. Budesinsky and L. Krumlova. Microdetermination of Sulfur and Sulfate by Titration with Barium Perchlorate. *Analytica Chimica Acta*, Vol. 39, 1967, pp. 375–381.
17. V. I. Kuznetsov and N. N. Basargin. Indicator for Barium During a Volumetric Determination of Sulfates in the Presence of Phosphates and Arsenates. *Zavodskaya Laboratoriya*, Vol. 31, 1965, pp. 538–541.
18. B. Budesinsky and D. Vrzalova. Determination of Organic Sulfur and Sulfates with Dibromosulfonazo III and Dimethylsulfonazo III. *Chemist Analyst*, Vol. 55, 1966, p. 110.
19. H. F. R. Reijnders, J. J. van Staden, and B. Griepink. Flow-Through Determination of Sulfate in Water Using Different Methods: A Comparison. *Fresinius Zuitschrift fur Analytische Chemie*, Vol. 300, 1980, pp. 273–276.
20. T. S. Ma and R. C. Rittner. *Modern Organic Elemental Analysis*. Marcel Dekker, Inc., New York, 1979.
21. *A Laboratory Manual on Ion Exchange*. The Dow Chemical Company, 1982.
22. W. C. Pierce and E. L. Haenisch. *Quantitative Analysis*, 3rd ed. John Wiley, London, 1953.
23. B. Budesinsky, D. Vrzalova, and A. Bezdekova. Spectrophotometric Determination of Barium and Strontium with Dimethylsulfonazo III and Related Compounds. *Acta Chim. Academy of Sciences of Hungary*, Vol. 52, 1967, pp. 37–47.
24. R. L. Anderson. *Practical Statistics for Analytical Chemists*. Van Nostrand Reinhold Co., New York, 1987.
25. D. S. Moore and G. P. McCabe. *Introduction to the Practice of Statistics*. W. H. Freeman Co., New York, 1989, pp. 509–520.
26. *Standard Methods of Sampling and Testing Fly Ash or Natural Pozzolans for Use as a Mineral Admixture in Portland Cement Concrete*. ASTM C311-77, ASTM, Philadelphia, Pa., 1977 p. 223.

Publication of this paper sponsored by Committee on Basic Research Pertaining to Portland Cement and Concrete.

Chloride Content of Portland Cement Concrete Powder by a Method Using Flocculation

K. RAMAMURTI AND G. P. JAYAPRAKASH

A simple and rapid method of determining chloride in portland cement concrete powder is described. This method can be used under field conditions in a portable laboratory. An organic flocculant is used to flocculate the insoluble portion from a portland cement concrete powder suspension in hot water. The clear decant is analyzed for chloride content using a chloride ion-selective electrode.

The minimum quantity of chloride required to initiate the corrosion of steel in concrete is called the chloride content corrosion threshold. Although this concept has been well received, an agreed-upon corrosion threshold has not found wide acceptance. Lewis (*1*) reported that the water-soluble chloride threshold is 0.15 percent by weight of cement. The American Concrete Institute (ACI) Committee 222 Report 222 R-85(89) (*2*) cites the work of Lewis (*1*). It also cites later studies by FHWA (*3*), California (*4*), and New York (*5*) that also demonstrate that a water-soluble chloride content as low as 0.15 percent (or 0.20 percent acid-soluble chloride) is sufficient to initiate corrosion of embedded steel in concrete exposed to chlorides in service. Hence, ACI Committee 222 recommended that the acid-soluble chloride content limit not exceed 0.20 percent (*2*).

Many bridge design engineers, however, are more interested in the more readily available water-soluble chlorides of in-service concrete structures, that is, the chloride fraction that is most likely to be involved in current or near-future corrosion of bridge-reinforcing steel. Hence, the determination of chloride content of concrete structures is important in relation to corrosion potential, and a simple procedure that could be used in field studies is of much value.

BACKGROUND

In concrete, chloride is present both in water-soluble and insoluble forms. During the last 20 years, methods have been developed to determine the chloride content of concrete. Berman (*6*) developed a wet-chemical method for determination of the total chloride content of concrete. This method involves the boiling of powdered concrete with acidified water, vacuum filtration, and titration with silver nitrate using a solid state chloride ion-specific electrode.

For the field determination of chloride in portland cement concrete (PCC), Rhodes et al. (*7*) developed a neutron gamma ray method capable of providing a rapid and nondestructive survey of total chloride content of concrete bridge deck at the depth of the uppermost mat of reinforcing steel. However, the inordinate high cost of the equipment, together with the periodic maintenance costs and the need for skilled scientific personnel for operating the assembly, limits the use of this procedure.

For the corrosion of steel in concrete, it is the water-soluble segment that is most important. Therefore, modifying Berman's wet-chemical method (*6*), Morrison et al. (*8*) have reported a method to determine the water soluble chloride content of PCC. Their method, hereinafter referred to as the water-soluble chloride method, extracts the water-soluble chloride in powdered concrete with boiling water. This step is followed by vacuum filtration, acidification of the filtrate, and final titration with silver nitrate solution using a chloride ion-specific electrode. The values obtained by the water-soluble chloride method are lower than those obtained by the Berman method. The FHWA laboratories report water-soluble chloride content in concrete powder samples as 75 to 80 percent of the total chloride in concrete (*9*). This fraction agrees with the findings of Morrison et al. (*8*).

Another available method is the rapid in situ determination of water-soluble chloride ion in PCC developed in Kansas by Morrison et al. (*8*). This method involves drilling a 19-mm-diameter clean hole to the desired depth downward from concrete surface, using a vacuum drilling method developed in Kansas (*10*).

The Kansas vacuum drilling technique consists of a vacuum drill system that allows the preparation of a uniform size and depth hole that is free of pulverized concrete. A vacuum swivel chuck that is fitted into a standard Jacobs chuck is used. A vacuum hose from a shop vacuum is attached to the swivel outlet and removes the powder produced by drilling. The drill is used with a hollow 19-mm-diameter carbide-tipped bit, and a drill stop that can be adjusted on the bit shank to provide a uniform predetermined hole depth. The drill stop is designated to contact the bridge surface away from the hole to minimize the chance of high-chloride surface chips falling into the drilled hole. An in-line filter for the drill vacuum system is constructed. This collector fits between the drill chuck vacuum connection and the hose from vacuum cleaner. Glass fiber filter paper (Whatman, GF/A) of 11-cm diameter,

K. Ramamurti, Bureau of Materials and Research, Kansas Department of Transportation, Topeka, Kans. 66611. Current address: 678 Tiffany Court, Sunnyvale, Calif. 94087. G. P. Jayaprakash, Bureau of Materials and Research, Kansas Department of Transportation, Topeka, Kans. 66611. Current affiliation: Transportation Research Board, 2001 Wisconsin Avenue, N.W., Washington, D.C., 20007.

chloride-free, high-volume, which retains particles greater than 1 μm in diameter, retains essentially 100 percent of the sample that is removed from the hole. The powder and the filter paper are then transferred to a sample bottle and returned to the laboratory for chloride analysis.

In the clean hole, a measured amount of borax buffer (pH 9) is introduced. A chloride ion-sensitive electrode attached to a stirring mechanism is directly inserted and stirred. After 90 sec, the potential across the electrode is measured and the values are converted to chloride values using a calibration curve. The average estimation time per sample is 5 min, which includes the time involved in moving the equipment to a new sample site. Although the rapid in situ method is used in locations where a hole can be drilled vertically down from a concrete bridge deck, it cannot be used in situations where vertical holes cannot be drilled downward (i.e., in structural members such as piers, abutments, and parapet walls). Hence, for many situations concrete samples for chloride analysis must be obtained by suitable procedure. In the late 1980s, further simplification of the Kansas water-soluble chloride method was explored by the Kansas Department of Transportation (KDOT) by using organic flocculants. A simple method for chloride analysis of such samples is described in this report.

The use of flocculants to sediment phosphate suspensions has been reported by LaMer et al. (*11*). Magnifloc 834A, an organic flocculant, has been successfully used in the determination of nitrite in powder samples of PCC (*12*). The flocculant method should improve the quality of the decanted liquid for chloride testing. Magnifloc 834A is a white powder, having anionic characteristics and a specific gravity of 628 to 720 kg/m^3 with a relative molecular mass between 8 to 10 million. Magnifloc 834A, while sedimenting PCC powder slime, also caused the formation of firm flocs by decantation.

EXPERIMENTAL

In order to determine the effect of the presence of Magnifloc 834A on the results of chloride content determinations, experiments were conducted with standard sodium chloride solutions of different concentrations. The results indicated that inclusion of several levels of the flocculant had no effect on the determined chloride values. The next step was directed towards using the flocculant (Magnifloc 834A) in determining the chloride content in sodium chloride-doped concrete.

Several sodium chloride-doped concrete beams were prepared with a chloride content that ranged from 0.35 to 1.42 kg/m^3. Dry-powder samples of concrete was obtained from these beams using the Kansas vacuum drilling technique (*10*). A total of 252 samples, representing seven locations on each beam and three levels at each location, was obtained from 12 beams. Each of the 252 samples was split to provide two sets of samples. The chloride content of one set of samples was determined according to the water-soluble method. The second set of samples was used to evaluate the flocculant method.

In the flocculant method, 5 g of the powdered PCC sample weighed to the nearest milligram were quantitatively transferred to a 125-ml Erlenmeyer flask. After the addition of 75 ml of boiling water to the powdered material, the flask was continuously swirled to obtain a uniform suspension. To this suspension, 1 ml of flocculant (Magnifloc 834A, 100 ppm) was added, swirled for 15 sec, and allowed to stand for 2 min. Soon after, the clear supernatant was decanted into a clean 250-ml beaker. The extraction was repeated with 0.5 ml of flocculant. Then the clear supernatant was decanted and combined with the first extract in the 250-ml beaker. During the initial trails, the third extraction proved to be of no benefit. Hence only two extractions of each sample were made in this study. The combined extracts were acidified with 2 ml of nitric acid and chloride content was determined using a chloride ion-sensitive electrode as in Gran end point determination procedure. The results of the flocculant method are presented in Table 1 along with those of the water-soluble method. Although the chloride values presented in Table 1 are an average of 21 determinations, calculation of the standard deviation was not considered, because the 21 chloride values obtained for each beam by each method were identical.

Data presented in Table 1 indicate that there is no significant difference between the values obtained by the water-soluble chloride and flocculant methods. The chloride contents determined by the flocculant method were 99.6 to 100 percent of those obtained with the water-soluble chloride method. The foregoing results indicated that the accuracy of the flocculant method was equal to that of the water-soluble chloride method. Because of thorough mixing, the distribution of salt in laboratory samples was relatively homogeneous.

FIELD SAMPLES

Chloride distribution in field concrete is nonhomogeneous. Therefore, other salt-contaminated samples were analyzed by both methods. Initially, samples from two concrete slabs that were exposed to outdoor salting during the work related to another KDOT project (*13*) were used. Each sample was split into two and the duplicates were analyzed by both methods. The range of water-soluble chloride contents in these samples was from 0.24 to 4.77 kg/m^3. Values of chloride content ob-

TABLE 1 CHLORIDE DETERMINATIONS OF NaCl-DOPED CONCRETE BEAMS

Beam No.	Cl^- Expressed as kg/m^3		
	Actual Addition	Water-Soluble Method[a]	Flocculant Method[a,b]
613	0.350	0.404	0.404
614	0.350	0.402	0.402
615	0.350	0.404	0.402
621	0.710	0.727	0.726
623	0.710	0.727	0.727
625	0.710	0.727	0.725
631	1.062	1.051	1.047
634	1.062	1.051	1.047
635	1.062	1.051	1.047
640	1.416	1.374	1.368
643	1.416	1.374	1.368
645	1.416	1.374	1.368

NOTE: The data for each method represent 252 chloride determinations, and a total of 504 determinations for the two methods.
[a]Chloride contents indicated represent average of 21 samples from each beam. Little or no variation was found in the values of the 21 samples.
[b]Data are for duplicate samples.

tained by the flocculant method were 73 to 100 percent of those obtained by the water-soluble chloride method. A plot of Cl^- contents determined using water-soluble chloride method, against those of the flocculant method is shown in Figure 1. Linear regression analysis of the data indicates a correlation coefficient of 0.997. Again, this value indicates that the accuracy of the flocculant method is equal to that of the water-soluble chloride method.

The two factors that are of most concern that might have been responsible for the observed differences in the determined chloride values are differences in the two analytical methods and differences in the sample locations. In order to investigate the effect on the results caused by differences in methods, the data shown in Figure 1 were reexamined. The percent of sample pairs out of the total number of pairs analysed by both the water-soluble and the flocculant methods was determined. The findings are presented in Table 2. Almost 28 percent of the sample pairs did not have any difference and none of the sample pairs had a difference in chloride value of more than 0.59 kg/m³. The range of chloride content in these samples was from 0.24 to 4.77 kg/m³.

In order to determine the variation of chloride content caused by sample location, 27 cores of 2-in. (50.8-mm) diameter from concrete bridge decks, subjected to winter salting, were used. Each core was longitudinally split into two halves and each half was sliced into ¾-in. (19-mm) layers

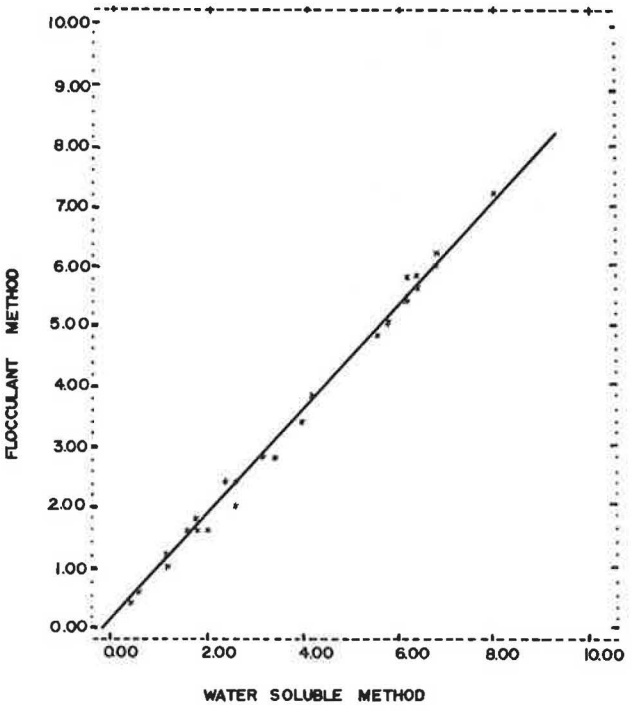

VARIABLE X: WATER SOLUBLE — VARIABLE Y: FLOCCULANT

MEAN OF X	= 2.79616	MEAN OF Y	= 2.50825
S.D. OF X	= 2.09307	S.D. OF Y	= 1.8519
MAXIMUM X	= 8.08	MAXIMUM Y	= 7.27
MINIMUM X	= .41	MINIMUM Y	= .41

NUMBER OF PAIRS (N) = 44
CORRELATION COEFFICIENT (R) = .997
DEGREE OF FREEDOM (DF) = 42
SLOPE (M) OF REGRESSION LINE = .881711
Y INTERCEPT (B) FOR THE LINE = .0428471

FIGURE 1 Plot of Cl^- values by water-soluble chloride method versus flocculant method (1 unit = 0.59 kg/m³).

TABLE 2 VARIATIONS IN CHLORIDE CONTENT OF CONCRETE—ANALYTICAL METHOD

Differences in Cl^- Content, kg/m³	Observed Differences in Cl^- due to Analytical Method[a]	
	Samples (%)	Cumulative (%)
>0.59	0	0
0.44–0.59	14	14
0.29–0.44	18.6	32.6
0.15–0.29	25.6	58.2
0–0.15	14	72.2
0	27.8	100

[a]Duplicate samples of salt-contaminated outdoor exposure slabs analyzed using the water soluble and flocculant methods. Range of the salt content was 0.24 to 4.76 kg/m³ (Cl^-).

(Figure 2). Chloride content of each of the layers of the two core halves was determined using only the water-soluble chloride method. The results are presented in Table 3. The data indicate that 26 percent of the sample pairs had no difference in their chloride content and almost 15 percent of the sample pairs had a difference in chloride content of 0.59 kg/m³. The range of chloride content in these samples was from 0.04 to 4.31 kg/m³, which was comparable to that of samples used for comparing the variation in results caused by differences in the two analytical methods.

The investigation of field samples indicated that the variations in salt content of adjacent samples caused by location was greater than that caused by differences in the two methods. The nonhomogeneity of concrete indicated that the salt data obtained using relatively simple methods were equal in significance to those of more sophisticated analyses.

SUMMARY AND CONCLUSION

Knowledge of chloride content, particularly the water-soluble fraction, of reinforced-concrete structures is believed to be important in regard to corrosion of steel and hence the durability of the structures. A new method that uses an organic flocculant in the determination of chloride content of powdered concrete was developed. Laboratory and field samples

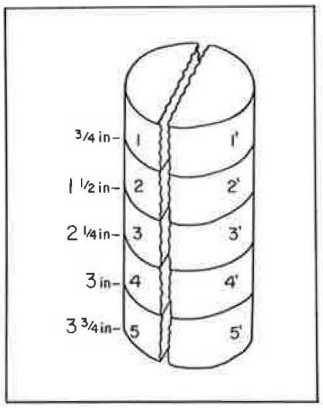

FIGURE 2 Two halves of a 2-in.-diameter bridge deck concrete core, each split into ¾-in. layer, that provided adjacent salt samples for Cl^- analysis.

TABLE 3 VARIATIONS IN CHLORIDE CONTENT OF CONCRETE—SAMPLE LOCATIONS

Differences in Cl^- Content, kg/m³	Observed Differences in Cl^- due to Sample Locations[a]	
	Samples (%)	Cumulative (%)
>0.59	14.8	14.8
0.44–0.59	3.7	18.5
0.29–0.44	3.7	22.2
0.15–0.29	18.5	40.7
0–0.15	33.3	74.0
0	26	100

[a]Two adjacent core halves of bridge deck salt samples (see Figure 2) analyzed using the water soluble method only. Range of the salt content was Cl^- = 0.04 to 4.31 kg/m³.

were analysed by the water-soluble and the flocculant methods. The variation in chloride content of juxtaposing concrete samples was greater than that caused by differences in these two methods. It is concluded that the flocculant method has the same level of accuracy and provides results as rapidly as the water-soluble chloride method. Therefore, the flocculant method is presented as an alternative method for the existing methods to determine the water-soluble chloride content of powdered concrete samples.

ACKNOWLEDGMENT

The authors thank Carl F. Crumpton, Kansas Department of Transportation, for his encouragement and support for this work.

REFERENCES

1. D. A. Lewis. Some Aspects of the Corrosion of Steel in Concrete. *Proc. 1st International Congress on Metallic Corrosion*, London, 1962, pp. 547–555.
2. Corrosion of Metals in Concrete. ACI 222R–85(89). ACI Committee 222 Report, American Concrete Institute, Detroit, Mich., 1985, 1989.
3. K. C. Clear. *Time-to Corrosion of Reinforcing Steel in Concrete Slabs. Vol. 3. Performance After 830 Daily Salt Applications.* Report FHWA-RD-76-70. FHWA, 1976.
4. R. F. Strattful, W. J. Jurkowitch, and D. L. Spellman. Corrosion Testing of Bridge Decks. In *Transportation Research Record 539*, TRB, National Research Council, Washington, D.C., pp. 50–59.
5. W. P. Chamberlain, R. J. Irwin, and D. E. Ansler. *Waterproofing Membranes for Bridge Deck Application.* Research Report 52 (FHWA-NY-77-59-1). New York State Department of Transportation, Albany, 43 pp.
6. H. A. Berman. *Determination of Chloride in Hardened Portland Cement Paste, Mortar, and Concrete.* Report FHWA-RD-72-12, FHWA, U.S. Department of Transportation, 1972.
7. J. R. Rhodes, J. A. Stout, R. D. Sieberg, and J. S. Schindler. *In Situ Determination of the Chloride Content of Portland Cement Concrete Bridge Decks.* Report FHWA/RD-80/030. Final Report, FHWA, U.S. Department of Transportation, 1980.
8. G. L. Morrison, P. V. Yash, K. Ramamurti, and W. J. Gilliland. *Rapid In Situ Determination of Chloride Ion in Portlant Cement Concrete Bridge Decks.* Final Report, Report FHWA-KS-RD-75-2. Kansas Department of Transportation, Topeka, 1976.
9. *NCHRP Synthesis Report 57: Durability of Concrete Bridge Decks.* TRB, National Research Council, Washington, D.C., 1979.
10. F. W. Stratton and B. F. McCollum. *Repair of Hollow or Softened Areas in Bridge Decks by Rebonding with Injected Epoxy Resin or Other Polymers.* Report K-F-72-5. Kansas Department of Transportation, Topeka, 1974.
11. V. K. LaMer, R. H. Smellie, Jr., P. K. Lee, and K. Ramamurti. *The Preparation and Evaluation of Superior Flocculating Agents for Phosphate Slimes.* Progress Report NYO-7403. United States Atomic Energy Commission, Columbia University, New York, 1956.
12. K. Ramamurti. Method for Determination of Water Soluble Nitrite in Concrete. Appendix C in *Electro-Osmotic Techniques for Removal of Chloride from Concrete and for Emplacement of Concrete Sealants.* Kansas Department of Transportation, Topeka, 1982.
13. G. P. Jayaprakash, J. E. Bukovatz, K. Ramamurti, and W. J. Gilliland. *Electro-Osmotic Techniques for Removal of Chloride from Concrete and for Emplacement of Concrete Sealants.* Final Report, Report FHWA-KS-82-2, Kansas Department of Transportation, Topeka, 1982.

Publication of this paper sponsored by Committee on Basic Research Pertaining to Portland Cement and Concrete.

Abridgment

Visualization of Chloride Distribution in Concrete

J. W. JANG AND I. IWASAKI

Chloride contents of concrete are usually measured by dry drilling and chemical analysis of the drilled samples. However, the conventional method does not provide any information on chloride distribution. A visualization technique involving color mapping was developed for the determination of chloride ion distribution and concentration near the reinforcement in concrete.

Localized corrosion of reinforcements in concrete is caused by the impurities of the reinforcement material, deformation of the reinforcement surfaces, concentration difference of chloride ion near the reinforcement, and the complex interactions of the preceding factors (*1,2*). Deformed or defective surfaces of reinforcements could be the corrosion initiation sites even under very low chloride ion concentrations because of their thermodynamic instabilities, whereas no corrosion may be found on the deformation-free or defect-free surfaces, respectively, under relatively high chloride ion concentrations. Galvanic interactions between corroding and noncorroding areas accelerate the localized corrosion at the surfaces of reinforcements.

Similarly, the concentration differences of chloride ion near reinforcements create galvanic cells between the high- and low- or no-chloride concentration surfaces of the reinforcements (*2*). Areas of high chloride concentration become the anode, and areas of low or no chloride concentration the cathode. Corrosion rates increase as the chloride concentration difference increases.

Chloride contents of concrete are usually measured by dry drilling and chemical analysis of the drilled samples. However, the conventional method does not provide any information on chloride distribution near the reinforcement in concrete, particularly along hairline cracks. Such information would be essential in understanding the localized corrosion mechanisms and kinetics.

A visualization technique is in use for the determination of chloride ion distribution and concentration near the reinforcements in concrete, as described in the following sections.

EXPERIMENTAL

Concrete blocks containing reinforcements were collected in the field, cut, and ground to expose flat, smooth surfaces. The concrete surfaces were finished with 320 grit silicon carbide abrasive papers. A crack was intentionally made from one edge of the concrete block to the reinforcement, as shown in Figure 1a. A solution of 10 percent $CaCl_2$ was applied repeatedly to the crack to simulate the chloride penetration through the crack.

The indicator solutions used for detection and determination of chloride ion on the surface of the concrete block were 0.025 percent mercuric nitrate in 0.008 M nitric acid, and 0.25 percent diphenylcarbazone in methanol. A filter paper was wetted by the mercuric nitrate solution uniformly. The filter paper was placed over the flat, smooth concrete block and pressed firmly for about 5 min. Then, the filter paper was peeled off and the diphenylcarbazone solution was sprayed over it and air-dried. For the purpose of calibration, 0, 0.01, 0.1, 1, and 10 percent $CaCl_2$ solutions were also applied to filter papers, and the color was developed as before.

RESULTS AND DISCUSSION

Chloride ion concentrations in aqueous solutions can be determined by titration with mercuric nitrate in the presence of diphenylcarbazone as an indicator (*3*). This method was adapted to this investigation. Chloride ion on the concrete block surface reacted with mercuric ion to form insoluble mercuric chloride. Excess mercuric ion produced violet color when the diphenylcarbazone solution was sprayed over the filter paper as follows:

$$Hg^{++} + 2Cl^{-} \rightarrow HgCl_2$$

$$\text{Excess } Hg^{++} + \text{diphenylcarbazone} \rightarrow \text{violet color}$$

The color map of Figure 1b shows the chloride ion distribution and concentration in the concrete. The light area indicates where chloride ion is present, and the different shades of purple represent chloride ion concentrations that may be estimated from the calibration strips shown in Figure 1c. This technique for the determination of chloride ion concentration and its distribution in concrete is simple and rapid.

ACKNOWLEDGMENT

The authors express appreciation to the Center for Transportation Studies at the University of Minnesota for support of this research.

Mineral Resources Research Center, University of Minnesota, Minneapolis, Minn. 55455.

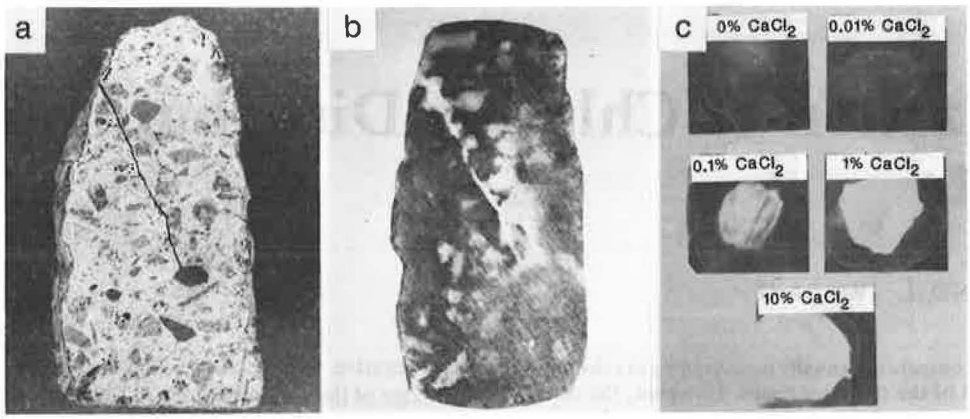

FIGURE 1 Visualization results for chloride ion distribution and concentration in concrete: *a*, concrete sample with rebar; *b*, color map; and *c*, calibration strips.

REFERENCES

1. G. P. Ray and R. A. Jarman. Effect of Non-Metallic Inclusions on the Corrosion Fatigue of Mild Steel. *British Corrosion Journal*, Vol. 15, 1980, pp. 226–227.
2. J. W. Jang and I. Iwasaki. Rebar Corrosion Under Simulated Concrete Conditions Using Galvanic Current Measurement, *Corrosion*. (In press.)
3. D. F. Boltz and J. A. Howell. *Colorimetric Determination of Nonmetals*, 2nd ed., John Wiley, New York, 1978, pp. 92–97.

Publication of this paper sponsored by Committee on Basic Research Pertaining to Portland Cement and Concrete.

Roller-Compacted Concrete Slabs Using Phosphogypsum

N. GHAFOORI AND W. F. CHANG

The use of phosphogypsum, a phosphate mining solid waste, was investigated as an aggregate in construction of various roller-compacted concrete (RCC) slabs. Several phosphogypsum-based concrete mixtures were prepared in three different mixing procedures and were compacted using a self-propelled vibratory roller. The results of three projects are described: (a) small slabs of various compositions, (b) a parking lot ramp, and (c) large-scale construction of driveways (including service drive) and parking areas. Field results of all projects were compared with their equivalent laboratory samples to evaluate the performance of the tested mixtures under a less-controlled environment. A thickness design procedure for phosphogypsum concrete pavement was also suggested. The demonstration projects indicate that phosphogypsum-based RCC is suitable for pavement construction application. Phosphogypsum provides additional fineness for better compactibility and surface finishability of final products. It also compensates for some of the dry shrinkage to limit the extent of cracking and retards setting time so that continuity at the cold joints is ensured. When tricalcium aluminate is less than 7 percent of cement, the presence of calcium sulfate does not adversely affect the sulfate resistance durability of concrete slabs.

The development and application of compaction concrete, particularly in the form of roller-compacted concrete (RCC) for water-retaining structures and pavements, has progressed rapidly in the last few years (*1*). Although not without problems, roller compaction is an attractive placement technique because it offers a fast and simple method for handling and placing concrete. Moreover, compaction concrete is economically advantageous because strength properties can be attained with a cement content lower than that of conventional concrete. The use of low cement content and its subsequent low water-cement ratio should result in less shrinkage cracking.

In recent years, the use of industrial and mining wastes in structural concrete, consolidated by compaction, has received increasing attention (*2*). The presence of such fine materials in compaction concrete provides better workability and finishability, improves the engineering properties of the mix in the hardened state, and brings about economic benefits by using a by-product that could otherwise go to waste. Clearly, application of RCC in pavement construction can be one of the most promising approaches in use of the large quantities of already abundant waste materials.

Phosphogypsum is a by-product of the phosphoric acid industry, which is involved in the production of phosphate fertilizers. With worldwide phosphogypsum production of 120 to 150 million metric tons per year (*3*), providers of fertilizer throughout the world are becoming increasingly concerned about the proper disposal and possible use of this waste material. Currently, nearly 86 percent of the world's phosphogypsum is discarded in land or sea, causing environmental pollution, adverse aesthetic appearance, and growing economic concerns.

Extensive laboratory research over the past few years indicates that the raw phosphogypsum, subjected to proper compaction force, can be transformed into a strong solid of valuable strength. Cylinder compressive strength of over 700 psi (4.82 MPa) can be readily obtained using the modified Proctor compaction energy (*4*). These unique properties have encouraged the use of this waste product as a viable construction material and have promoted the development of compacted phosphogypsum-based concrete. Additional laboratory tests have also revealed that up to 50 percent increase in compressive strength of concrete can be achieved by replacing a portion of fine aggregate with phosphogypsum in the mixtures of low cement content (*5*). The improvement of strength under compaction is attributed to the phosphogypsum's self-adhesive nature, its extremely fine gradation, and the reduced amount of mixing water required by compaction consolidation.

This study was intended to investigate the feasibility of using phosphogypsum in RCC pavement construction. Data presentation and discussion are with regard to strength properties, strength development, durability in terms of internal sulfate attack, abrasion resistance, drying shrinkage, mixing techniques, and pavement design recommendation. Field and laboratory results both encourage the application of phosphogypsum-based concrete in construction of RCC pavements.

MATERIALS

Phosphogypsum

Phosphoric acid is an important raw material for the production of fertilizers (88 percent), detergents (6 percent), and other agricultural products (*6*). World manufacturing consists of approximately 25 million tons per year of phosphoric acid. The most common industrial process is the wet process operation (95 percent), which includes at least four technologies characterized by different operations and qualities of by-product residues. In all processes, ground phosphate rock is

N. Ghafoori, Department of Civil Engineering and Mechanics, Southern Illinois University, Carbondale, Ill. 62901–6603. W. F. Chang, Phosphogypsum Institute of Research, University of Miami, Coral Gables, Fla. 33124.

TABLE 1 TYPICAL COMPOSITION ANALYSIS OF RAW PHOSPHOGYPSUM (*11*).

Gypsum (%)	85.0-93.0
Phosphate (%)	0.2- 1.7
Fluoride (%)	0.4- 1.3
Sand (%)	1.4- 8.4
Soluble Salt (%)	0.1- 5.3
PH	3.1- 5.3
Radium-226 (pci/g)	17.0-25.0

combined with sulfuric acid in a series of mixing tanks (*7*). The phosphoric acid and phosphogypsum produced are pumped into a filter to separate the phosphoric acid. Finally, phosphogypsum is either slurried with water and pumped to sedimentation ponds (wet stacking) or transported to large stockpiles by trucks or belt conveyors (dry stacking) (*8*). For each ton of wet phosphoric acid, approximately 5 tons of phosphogypsum are produced (*9*). An increasing demand for phosphate fertilizers has subsequently increased phosphogypsum stockpiles throughout the world. Currently, in the state of Florida alone, the phosphoric acid industry generates 33 million tons of gypsum each year. In addition, over 400 million tons of this material has been stacked in huge retaining ponds on the ground in central Florida. It is expected that by the year 2000, over a billion tons of phosphogypsum will be stockpiled in the state of Florida (*10*).

Depending on the nature of the phosphate rock and industrial operations, the chemical composition of phosphogypsum may vary (*11*). A typical chemical analysis, as presented in Table 1, indicates that phosphogypsum primarily consists of calcium sulfate, up to 93 percent. The remainder is a combination of impurities such as sand, phosphate, fluoride, and organic constituents. Crystals of calcium sulfate can exist in at least three forms: dihydrate ($CaSO_4 \cdot 2H_2O$), hemihydrate ($CaSO_4 \cdot \frac{1}{2}H_2O$), and anhydrate ($CaSO_4$) (*12*). The phosphate industry generates most phosphogypsum in dihydrate form (84 percent), the type used throughout this investigation.

The pH values of phosphogypsum range from 3.1 to 5.5. However, when it is mixed with portland cement-based material, the alkalinity level of cementitious matrix remains at the level required to prevent the corrosion of steel reinforcement. Measurements of pH by Nanni (*13*) in accordance with ASTM G51-77, for cement-phosphogypsum mixes having cement contents of 10, 20, and 30 percent, have yielded values ranging from 12.05 to 12.35. Passivation of steel normally occurs in alkaline environments with pH above 11.

The grain size of phosphogypsum depends on the process and degree of grinding of the rock used. Typical phosphogypsum particles are approximately 0.02 to 0.50 mm, with the coarser size mostly consisting of silica sand and unprocessed phosphate. The grain size distribution curve of dihydrate phosphogypsum used throughout this investigation is shown in Figure 1. According to the AASHTO classification system, raw dihydrate phosphogypsum can be classified as an A–4 soil.

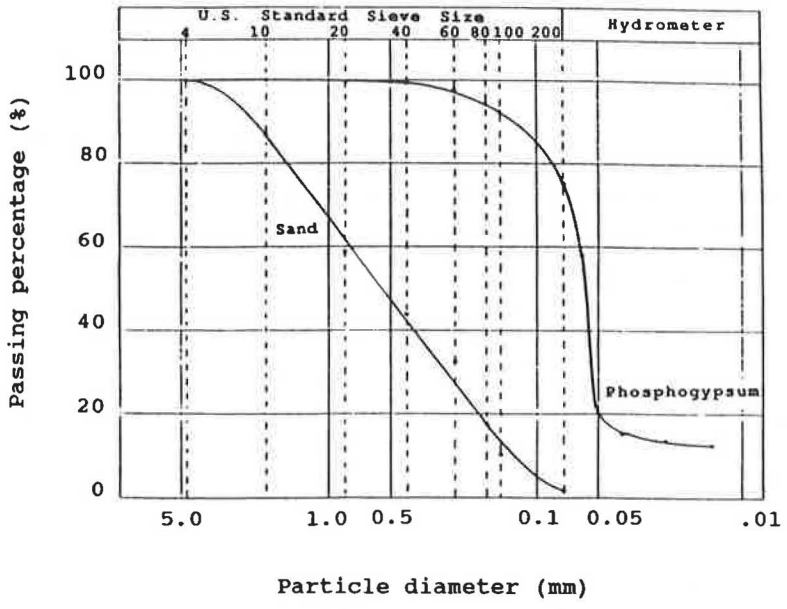

FIGURE 1 Phosphogypsum and sand grading.

Fine Aggregate

Sand used during this investigation was finely crushed limestone. Southern Florida was the source of sand for Projects 1 and 2. It had an averaged specific gravity of 2.70 and fineness modulus of 2.60. Grain size distribution, as shown in Figure 1, indicates that this sand is a well-graded fine aggregate. In Project 3, a well-graded sand with an averaged specific gravity of 2.50 was obtained from a central Florida quarry.

Coarse Aggregate

A uniform-graded limestone coarse aggregate, obtained from a Southern Florida quarry, was used for Projects 1 and 2. It had a maximum nominal size of ⅜ in. and specific gravity of 2.70. Coarse aggregate used in Project 3, obtained from central Florida, was also uniform-graded limestone. Its averaged specific gravity was 2.50 with a maximum nominal size of ¾ in.

Cement

Unless otherwise stated, portland cement type I (ASTM-150) was used throughout this experimental program.

RESULTS AND OBSERVATIONS

Strength Characteristics

In Project 1, six mixtures, produced at their optimum moisture content, were used in the preparation of small slab sections (3 ft × 3 ft × 6 in. thick) built at the campus of the University of Miami. Seven and one-half inches of loose materials was compacted over an existing limerock base into a nearly 6-in. final lift in one single layer with 10 passes using a field vibratory roller. The slabs were constructed next to each other with no joint treatment or load transfer device between them. They were seal-cured for a period of nearly 2 weeks before sample extraction and tested for 28-day strength. Field-collected cores, of similar size to the laboratory samples (3 in. in diameter and 6 in. in height), were tested for compression and split-tension strength (ASTM C39 and C496). Beams of dimensions 3 × 3 × 14 in. were also saw-cut and tested in flexure using third-point loading. All laboratory specimens were seal-cured for a period of 4 weeks before testing (ASTM C171).

The test results of the initial dry-density, unconfined compression, splitting tension, flexural tensile capacity, and modulus of elasticity are presented in Table 2. Field values were found to compare reasonably well with laboratory results. In fact, the initial dry density and strength of the field-

TABLE 2 TWENTY-EIGHT-DAY STRENGTH PROPERTIES OF PHOSPHOGYPSUM-BASED CONCRETE SLABS FOR PROJECT 1

Proportion by Dry Weight (Percent) (lb/yd³)	Sample Type	Initial Moisture Content (%)	Initial Dry Density (lb/ft³)	28-day Strength (psi)			
				Compression	Split-Tension	Flexure	Modulus of Elasticity
7.5 20 20 52.5 230 614 614 1610	Field	14.5	113.61	1495	227	383	------
7.5 20 20 52.5	Lab	13.5(M) 14.0(S)	112.56(M) 107.51(S)	1642(M) 1028(S)	245(M) 121(S)	402(M) 277(S)	$1.2*10^6$
7.5 0 40 52.5 231 0 1231 1616	Field	13.25	114.0	1609	247	370	------
7.5 0 40 52.5	Lab	12.50(M) 13.10(S)	113.26(M) 108.46(S)	1852(M) 1311(S)	252(M) 164(S)	396(M) 260(S)	$1.3*10^6$
15 20 20 45.0 495 660 660 1734	Field	12.80	122.3	3378	424	643	------
15 20 20 45.0	Lab	12.10(M) 12.65(S)	120.85(M) 113.56(S)	3530(M) 2876(S)	437(M) 343(S)	655(M) 608(S)	$2.0*10^6$

C= Cement SA= Sand GA= Gravel PG=Phosphogypsum

M= Modified Proctor Compaction S= Standard Proctor Compaction

TABLE 3 PROPERTIES OF FIELD AND LABORATORY MIXES FOR THE PARKING LOT RAMP OF PROJECT 2

Mix*	Initial Moisture Content (%)	Initial Dry Density (lb/ft^3)	Compressive Strength 28-Day (psi)	One-Year (psi)	Two-Year (psi)	28-day Split-Tensile Strength (psi)	28-day Modulus of Rupture (psi)	28-day Modulus of Elasticity (psi)
Field	12	129.23	3801	3682	3532	441	---	---
Lab	11	132.37	4563	----	----	558	902	2.64x10^6

*Cement=350 lb/yd^3 Phosphogypsum=698 lb/yd^3
Fine Aggregate=1396 lb/yd^3 Coarse Aggregate=1047 lb/yd^3

compacted samples can be considered equivalent to the values obtained in the laboratory with the modified Proctor method (ASTM D-1557, energy input of 56,250 lb-ft/ft^3). Results of this project confirmed that, under a less-controlled environment, strength characteristics of laboratory samples can be properly attained in the field. Additional laboratory test results (not given here) indicated that reaching a compressive strength level of 3,000 psi with cement content of 10 percent or less (by weight of total dry solids) required a smaller percentage of phosphogypsum. This finding was incorporated in the selection of the matrix constituents chosen for Project 2.

Project 2 involved the construction of a parking lot ramp using a phosphogypsum-based concrete mixture built on the campus of the University of Miami. The ramp measured 24 ft wide and 14 ft long with a slope of approximately 4 percent. The matrix constituents consisted of 20 percent (698 lb/yd^3) phosphogypsum, 40 percent (1,396 lb/yd^3) fine-crushed limestone aggregate, 30 percent (1,047 lb/yd^3) limestone coarse aggregate and 10 percent (350 lb/yd^3) Type I cement with tricalcium aluminate (C_3A) content of 12 percent. Moisture content at the time of mixing was 12 percent of the total dry weight. The 7½ in. of loose material was compacted into final thickness of 6 in. using a road construction vibratory roller (1 layer and 10 passes). The ramp was seal-cured for a period of nearly 2 weeks before it was opened to traffic. The dimensions both of field and laboratory specimens were identical to those used in Project 1.

Table 3 presents the engineering properties both of field- and laboratory-collected samples. The field specimens exhibited excellent strength properties when compared to those of laboratory specimens fabricated in accordance with the modified Proctor method. During its 4-year service, the ramp was subjected to traffic loads consisting mostly of automobiles and occasional trucks. The ramp remained crack-free and in excellent condition. The successful construction of the parking lot ramp demonstrated the potential application of phosphogypsum-based concrete in highway surface course and encouraged the construction of a larger-scale RCC pavement project.

Project 3 included the construction of driveways and parking areas. They were built at the Florida Institute of Phosphate Research by a local contractor. The paved area was approximately 2,000 yd^2. Because the locally mined limestone aggregate, which was selected for economic reasons, had limited strength-producing properties, target mix design compressive strength was limited to 2,500 psi, which is at the low end of what is currently used for RCC pavement applications.

The proportions of the matrix constituents are presented in Table 4. Fine and coarse crushed limestone aggregates were initially blended at the ratio of 1:1 and then added to phosphogypsum to obtain a combined grading that was well within grading limits proposed by the Corps of Engineers specifications. The combined aggregate was fed through the pugmill mixer and then stockpiled at the site of the mixing plant until the time of mixing with cement. Moisture content of the combined aggregate was such that no water had to be added during mixing. The reported moisture content of 8.5 percent (by dry weight) resulted from natural moisture both in phosphogyp-

TABLE 4 FIELD MIX PROPORTIONS FOR PROJECT 3

Constituents	Proportions by Dry Weight: Percent	Proportions by Dry Weight: lb/yd^3	SSD Specific Gravity
Type II Cement	14.0	496	---
Fine and Coarse Aggregate	73	2584	2.50
Phosphogypsum	13	460	2.42
Total Water	8.5	301	---

TABLE 5 PROPERTIES OF FIELD AND LABORATORY MIXES FOR PROJECT 3

Mix	Sample Type	Initial Moisture Content (%)	Initial Dry Density (lb/ft^3)	Compressive Strength		Modulus of Elasticity (psi)	Split-Tensile Strength (psi)
				28-day (psi)	90-day (psi)	28-day	28-day
P13-14	Field	8.5	131.1	3174	3539	2.26* 10^6	318
P13-14	Lab	8.0	132.7	2767	----	-----	---
P13-0	Lab	8.0	132.3	3024	----	-----	---

sum and aggregate. The mix optimum moisture content obtained in accordance with the modified Proctor method (ASTM D1557) was 8.0 percent.

The mix was then loaded into the dump truck and hauled to the construction site located less than 2 mi from the plant. Finally, RCC mixture was dumped into a heavy-duty double-tamping screened paver and placed over the 7-in. base course of phosphogypsum (equivalent to 4 in. of cement-stabilized base). The subgrade course consisted of silty sand with modulus of subgrade reaction (K) of 200 lb/in.^{3}. The final value of K was calculated to be 220 lb/in.^{3}. The design index (DI) of 1, in accordance with TM 5-822-6, was used. The measured final pavement thickness was 6 in. According to the design chart (U.S. Army Corps of Engineers document ETL 1110-141), the required pavement thickness (using f_r = 420 psi, K = 220 lb/in.^{3}, and DI = 1) was 5.4 in., which was smaller than the pavement thickness provided. After completion of the paving operation, lateral edges were sloped and consolidated with a plate-type hand compactor. A curing compound was sprayed on the pavement surface to maintain sufficient moisture content for the hydration of cement. Construction that started at midafternoon was interrupted in the early evening and completed the morning after. Because of the set-retarding effect of phosphogypsum, it was evident by visual inspection that continuity was ensured at the construction joints. No contraction joint was provided.

Mechanical properties of field-collected cores and laboratory-fabricated cylinders of identical dimensions are presented in Table 5. Two different mixes were used to prepare the laboratory samples. Mix P13–14 had similar proportion to that used in field mix, whereas phosphogypsum was entirely replaced with limestone screening in mix P13–0. Laboratory samples were fabricated in a 4.0 × 4.5 in. mold according to the modified Proctor method, which simulated the paver compaction effort. Test results in Table 5 indicate that the field cores have excellent compressive strength when compared to laboratory samples and that the presence of phosphogypsum is not detrimental to strength characteristics. Observations of the compressive failure mode consistently demonstrated the crushing of the limestone aggregates produced in central Florida. The values of split-tensile strength and modulus of elasticity were found to be within the expected ranges.

Higher-strength results, obtained from the previously built phosphogypsum-based RCC ramp (Project 2), were a consequence of the use of good-quality limestone aggregate produced in southern Florida.

Strength Development

The numerical data presented in Table 6 indicate that the continuity at construction joints was ensured by the retarded setting of concrete mix due to presence of phosphogypsum. Laboratory specimens of the same gradation and proportion used in Project 3, but of higher-quality aggregate obtained in southern Florida, were fabricated according to the modified Proctor method. Eight hours after mixing, specimens C13–14 (i.e., 13 percent cement and 14 percent phosphogypsum) possessed very low compressive strength compared with that of the reference specimens C13–0 (i.e., 13 percent cement and no phosphogypsum). The strength of specimens C13–14 at 18 hr is equivalent to that of reference specimens C13–0 at 4 hr. After 74 hr, the difference in strength of the two specimens is of the order of 14 percent.

TABLE 6 COMPRESSIVE STRENGTH DEVELOPMENT

Time (hrs.)	Strength (psi)	
	C13-14	C13-0
4	29	72
8	38	349
18	92	1175
74	2809	3207
168	3343	3772

Abrasion

The 28-day field-collected cores of Project 3 were subjected to abrasion tests according to the ball-bearing method (ASTM C779, Procedure C). The top 3-in. portion of each field core was saw-cut and both top (pavement surface) and bottom (saw-cut) surfaces were tested under wear with averaged results shown in Figure 2. It was evident that the abrasion resistance of the exposed top surface, composed of a thin layer of fine particles (i.e., cement paste and fine), was better than that of the saw-cut surface, which was mainly composed of limestone coarse aggregate. The wear resistance of top and bottom surfaces of field cores was compared with that of two concrete mixes made with higher-quality limestone aggregate obtained from a southern Florida quarry. The composition of mix 15–10 was 15 percent cement and 10 percent phosphogypsum, whereas mix 15–15 contained 15 percent cement and 15 percent phosphogypsum. Results shown in Figure 2 indicate that the quality of the limestone aggregate greatly affects the abrasion performance.

Sulfate Resistance Durability

Research studies of the past several decades have suggested that the chemical reaction between C_3A of portland cement and sulfate ions obtained from a sulfate-rich environment can cause excess expansion in concrete (*14*). As a consequence, crack formation and strength reduction become unavoidable. Today, such chemical reaction is commonly referred to as "external" sulfate attack.

The sulfate attack in cement-based mixtures resulting from the use of phosphogypsum, which primarily consists of calcium sulfate, has different characteristics from the external sulfate attack. In external sulfate attack, sulfate ions must penetrate into the matrix to instigate chemical reaction. Expansion may then cause matrix cracking, which in turn accelerates the penetration of new sulfate ions. On the other hand, in the internal sulfate attack, SO_3 ions exist inside the matrix from the time of mixing. The number of sulfate ions decreases as the chemical reactions proceed and the rate of sulfate attack tends to slow down with the aging of the matrix.

Extensive laboratory investigation has indicated that the sulfate resistance of phosphogypsum-based concrete is not impaired when C_3A content of cement is less than 7 percent (*15*). This restriction is independent of the amount of phosphogypsum content in the mixture and is only applicable when the matrix remains continuously submerged in water. In practical applications such as pavement construction, where the matrix is always exposed to periods of rain and dryness, the completion of chemical reaction between C_3A and SO_3 ions does not fully take place. As a consequence, the subsequent crack and strength reduction are expected to be smaller than those of laboratory specimens tested under continuously soaked conditions.

Expansion and compressive strength of four mortar mixes at 10 and 15 percent cement content and with 0 or 16 percent phosphogypsum are shown in Figure 3 as functions of time. The amount of C_3A in the cement was 7 percent, and specimens in the forms of bar and cylinder were consolidated by rodding or compaction hammer. Testing for bar expansion was conducted using ASTM C452. Figure 3 indicates that the expansion of continuously submerged specimens is higher when phosphogypsum is used and the compressive strength does not decrease with time. The results of the field-collected samples extracted from two pavement sections containing cement with 6.7 and 12 percent C_3A, along with their equivalent laboratory samples, are shown in Figure 4. For the mixture containing cement with C_3A of 6.7 percent, the averaged compressive strength both of field and laboratory samples increased with their age. The laboratory samples of concrete matrix with 12 percent C_3A had 41 percent loss in strength after a period of 1 year of continuously being placed in water. On the other hand, field specimens of similar C_3A content had 4.8 percent gain in strength after 1 year of exposure to prevailing weather conditions. Core samples extracted from the phosphogypsum concrete ramp after 2 years of service have demonstrated less than 7 percent reduction in compressive strength. This deviation is attributed to the core specimens being taken from different pavement locations and also

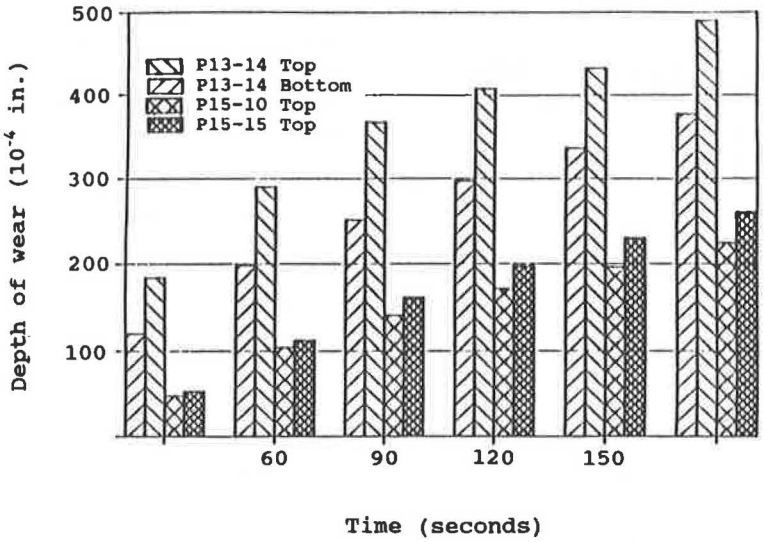

FIGURE 2 Comparative abrasion resistance.

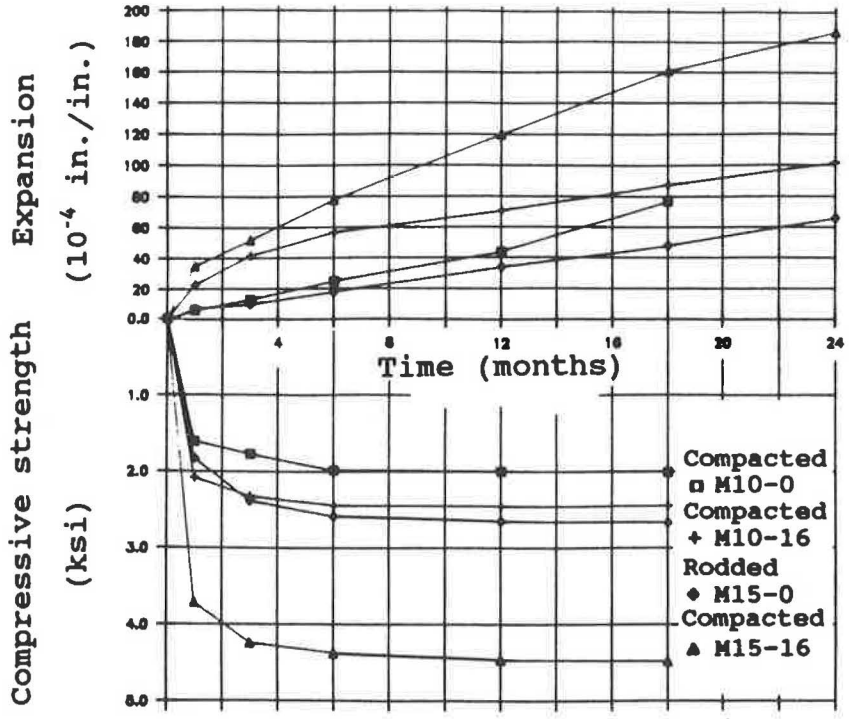

FIGURE 3 Mortar expansion and strength versus time.

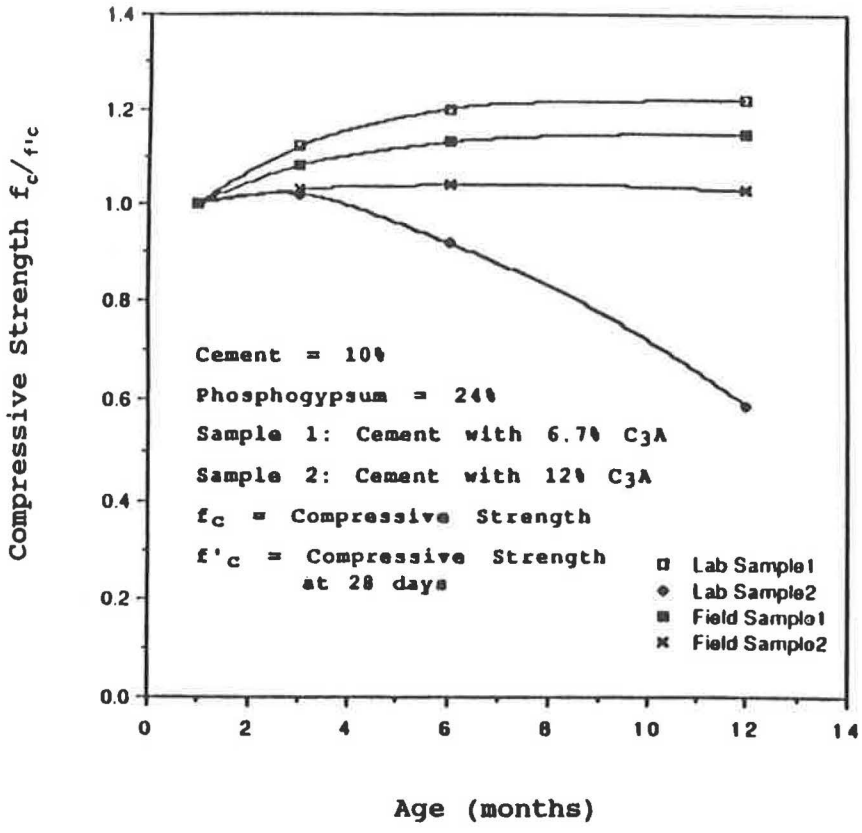

FIGURE 4 Strength of field and laboratory samples versus time.

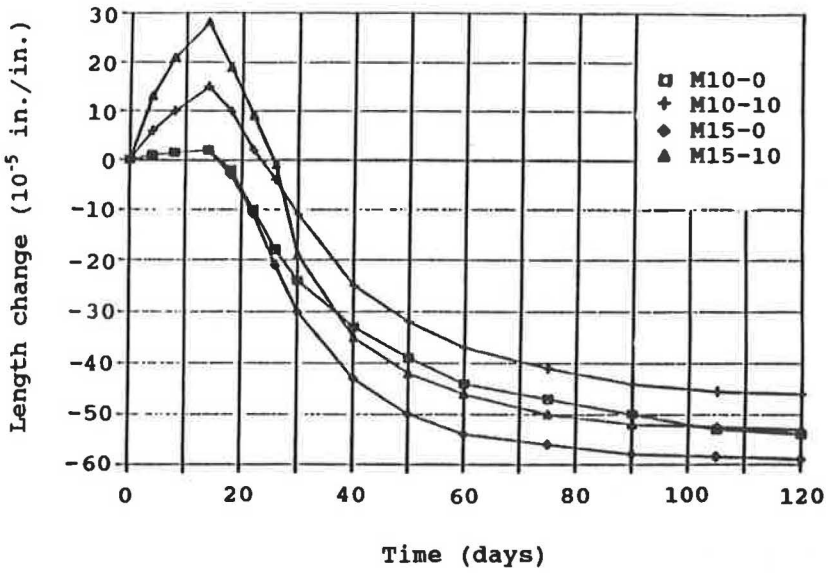

FIGURE 5 Mortar bar length change.

to the heterogeneous nature of the matrix. After 4 years of parking lot traffic, the phosphogypsum-based concrete ramp of Project 2 remained crack-free and in good condition.

Shrinkage Compensation

The RCC phosphogypsum ramp and pavement, built for Projects 2 and 3, respectively, were inspected on many occasions after construction. No natural joint has yet opened and no crack has yet been observed. A possible reason for this performance may be in the reduced drying shrinkage of a matrix containing phosphogypsum. In Figure 5, the length change of laboratory specimens tested according to ASTM C806 indicated that addition of 10 percent phosphogypsum reduced the drying shrinkage of the mortars compared with those without phosphogypsum (i.e., mixes M10–0 and M15–0). In field applications, the repeated moisture fluctuations should further reduce drying shrinkage of phosphogypsum-based concrete mixtures.

Effect of Mixing Procedure

Raw phosphogypsum, as available from stockpiles, consists of mostly small particles bound together in lumps, varying in

TABLE 7 EFFECT OF DIFFERENT MIXING PROCEDURES ON STRENGTH PROPERTIES

Mixing Procedure	Compression (psi)	Split-Tension (psi)	Modulus of Rupture (psi)
Pan-Mix	1495 (1.0)	227 (1.0)	383 (1.0)
Drum-Mix	962 (0.643)	152 (0.669)	233 (0.608)
Hand-Mix	689 (0.461)	81 (0.3610)	148 (0.390)
Cement: 7.5% Sand: 20% Gravel: 20% Phosphogypsum: 52.5%			
Pan-Mix	1609 (1.0)	247 (1.0)	370 (1.0)
Drum-Mix	1029 (0.640)	157 (0.636)	211 (0.567)
Cement: 7.5% Gravel: 40% Phosphogypsum: 52.5%			

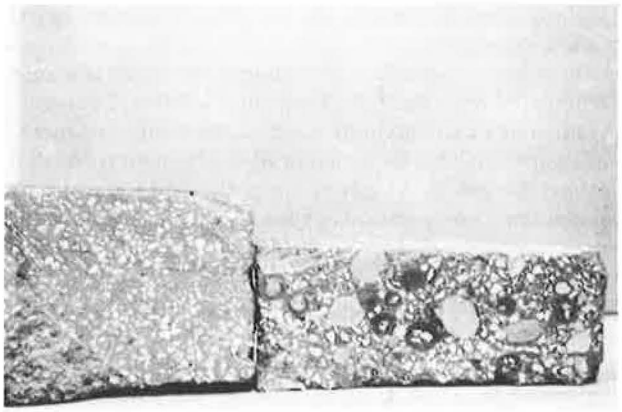

FIGURE 6 Cross section of concrete slabs mixed with pan mixer (*left*) and drum mixer (*right*). Note lumps of phosphogypsum in specimen mixed with drum mixer.

size from fractions of one to several inches. When phosphogypsum is included in a concrete matrix, the extent to which these lumps are crushed affects the homogeneity of the mix and, therefore, the product properties in the hardened state.

The strength characteristics of samples obtained from the field-compacted concrete slabs of Project 1, using three different mixing procedures, are presented in Table 7. Clearly, results indicate that the highest strength is obtained when using the pan mixer with grinding wheels. As shown in Figure 6, the drum mixer is not capable of crushing phosphogypsum lumps and, in addition, increases the tendency of the fine constituents to ball. As a result, strength drops to approximately one-third of that of the corresponding mixes prepared with the pan mixer. Finally, hand-mixing directly on the ground yields the lowest results, which are approximately half of the maximum values. The significance of these findings can be important for road construction application where for the selected mixing technique, design considerations should allow for appropriate strength parameters.

Pavement Design Consideration

A mix design that possessed the desired characteristics was used for the thickness design evaluation of the phosphogypsum-based concrete pavements. The engineering properties and traffic loadings are presented in Table 8. Two conventional rigid-pavement design procedures recommended by AASHTO and the Portland Cement Association were used. Additionally, a finite-element computer program for rigid pavement design termed "ILLI-SLAB" (*16*) was used to predict the

TABLE 8 RIGID PAVEMENT DESIGN PARAMETERS

1. Matrix Constituent Proportion:
(percentage by weight of total dry solid)

Cement	Sand	Gravel	Phosphogypsum	Water
10%	40%	30%	20%	11%

2. Engineering Properties:

Unconfined Compressive Strength:	4563 psi
Split-Tensile Strength:	558 psi
Third-Point Flexural Strength:	901 psi
Modulus of Elasticity:	$2.64 \times 10^{+6}$ psi
Poisson's Ratio:	0.195
Flexural Fatigue:	75-80% after 10^{+6} load applications

3. Traffic Loading:

Total Average Daily Traffic:	1600
Passenger Car:	80%
Truck:	20%
Average Gross Load:	31.5 kips
Average Axle Load:	14 kips
Traffic Growth:	5% per year
Design Life:	20 years

Axle Distribution:

Single Axle		Tandem Axle	
Wt. (kips)	% Axle	Wt. (kips)	% Axle
2- 6	15%	6-10	10%
6-10	25%	16-20	10%
16-20	20%	20-24	5%
20-24	5%		

Present Serviceability Index (PSI): 2.5

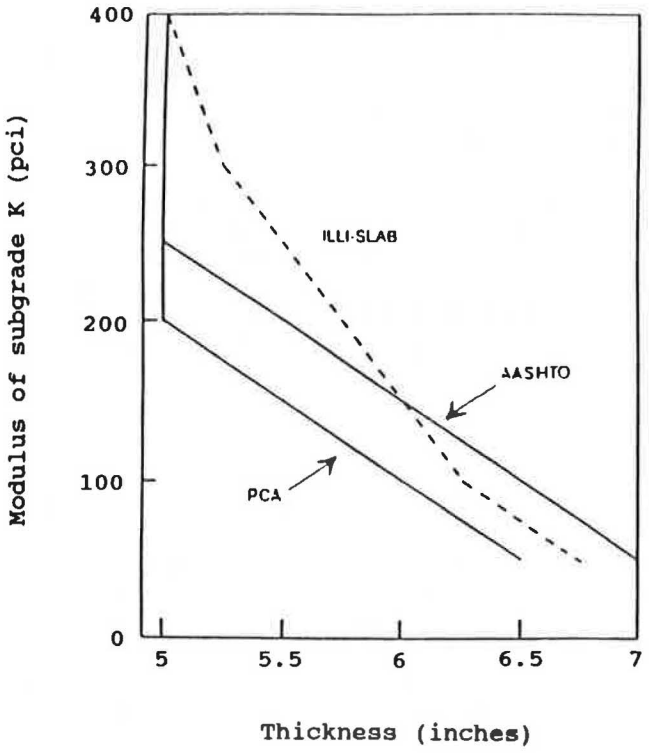

FIGURE 7 Subgrade modulus versus slab thickness.

phosphogypsum concrete rigid pavement's exact response to loadings. ILLI-SLAB uses stress and deformation analysis based on Westgard theory.

The required rigid pavement thickness obtained from the two conventional design methods and the computer-aided design are shown in Figure 7 as a function of subgrade modulus, *K*. The three design methods provided approximately similar results for the required slab thickness. The ILLI-SLAB finite-element program demonstrated satisfactory results compared with those of conventional design procedures. Moreover, results indicated that traditional methods of design available for concrete rigid pavement can be properly used for the concrete slab containing phosphogypsum.

CONCLUSIONS

Data assembled during the course of this investigation lead to the following conclusions:

1. The three demonstration projects indicated that phosphogypsum-based mixtures are suitable for the construction of RCC pavements. Because of its fine gradation, phosphogypsum provides additional workability, compactibility, and surface finishability for the mix. In addition, it contributes to set retardation for a better bond at construction joints, and drying shrinkage compensation to limit the occurrence of cracking when saw-cut joints are not provided.
2. The mixing procedure affects the strength capacity of the final product. Grinding of the phosphogypsum lumps ensures the desired homogeneity of the mix. The use of pan mixing with grinding wheels, over other mixing methods, results in the highest strength capacity for the phosphogypsum-based concrete mixtures.
3. The sulfate resistance of phosphogypsum-based concrete is not impaired when the C_3A of cement is less than 7 percent.
4. In lieu of a more accurate method, the traditional methods of design available for concrete rigid pavement (provided by AASHTO and PCA) can be properly used for concrete pavements containing phosphogypsum.

ACKNOWLEDGMENT

This research was funded by a grant from the Florida Institute of Phosphate Research, Bartow, Florida. The authors would like to express their gratitude to the Institute for its financial support.

REFERENCES

1. E. K. Schrader. World's First All-Rollcrete Dam. *Civil Engineering—ASCE*, Vol. 53, No. 4, April 1982, pp. 45–48.
2. W. Gutt. Aggregate from Waste Materials. *Chemistry and Industry*, 1972, pp. 439–447.
3. J. B. Charmichael. Worldwide Production and Utilization of Phosphogypsum. *Proc., 2nd International Symposium on Phosphogypsum*, Miami, Fl., Dec. 1986.
4. K. T. Lin. *Strength of Stabilized Phosphogypsum*. Master's thesis, University of Miami, Miami, Fla., May 1984.
5. N. Ghafoori and W. F. Chang. Engineering Characteristics of Phosphogypsum-Based Concrete. *Proc., 3rd Workshop on By-Product of Phosphate Industries*, Tampa, Fla., Dec. 1985.
6. Symposium on Phosphogypsum. *Proc., 2nd Workshop on By-Product of Phosphate Industries*, Miami, Fla., May 1984.
7. F. Wirching. Drying and Agglomeration of Flue Gas Gypsum. ASTM STP 861. *Proc., ASTM Symposium on Technology of Gypsum and Gypsum Products*, Sept. 1984, pp. 160–172.
8. G. F. Palm. *Overview of Florida Phosphate Industry Materials*. RCRA Report, 1980, pp. 1–9.
9. *Proc., 1st International Symposium on Phosphogypsum*, Vol. 1. Florida Institute of Phosphate Research, Bartow, Fla., 1980.
10. J. W. Sweeney and A. May. Assessment of Environmental Impacts Associated with Phosphogypsum in Florida. *Proc., International Symposium on Phosphogypsum*, Vol. II, Florida Institute of Phosphate Research, Bartow, Fla., p. 481.
11. J. W. Palmer and A. P. Kouloheris. Slime Waste Solidification with Hydra-table Calcium Sulfate. *Proc., 2nd Workshop on By-Products of Phosphate Industries*, Florida Institute of Phosphate Research, Bartow, Fla., May 1985, pp. 267–295.
12. C. A. Gregory, D. Saylack, and W. B. Ledbetter. The Use of By-Product Phosphogypsum for Road Bases and Subbases. In *Transportation Research Record 998*, TRB, National Research Council, Washington, D.C., 1984, pp. 47–52.
13. A. Nanni. *Phosphogypsum as a Building Material: Strength Characteristics and Housing Application*. Ph.D. dissertation, University of Miami, Miami, Fla., May 1985.
14. P. K. Mehta and H. H. Haynes. Durability of Concrete in Seawater. *Journal of the Structural Division, ASCE*, Vol. 101, 1975, pp. 1679–1686.
15. C. Oyang, A. Nanni, and W. F. Chang. Sulfate Attack Resistance of Portland Cement Mixtures Containing Phosphogypsum. *Concrete Durability, Vol. II*, SP-100, American Concrete Institute, Detroit, Mich., 1987, pp. 1007–1016.
16. A. Tabatabaie and E. Barenberg. Structural Analysis of Concrete Pavement Systems. *Proc., American Society of Civil Engineers*, ASCE Transportation Division, Vol. 106, No. TE5, Sept. 1980.

Publication of this paper sponsored by Committee on Performance of Concrete.

Effect of Fly Ash on Alkali-Silica Reactivity in Concrete

PETER G. SNOW

Improvements in the properties of portland cement concrete can be achieved through the use of mineral admixtures such as coal fly ash. One such improvement is the potential reduction of alkali-silica reactivity (ASR), which causes an expansive reaction in certain aggregates and can lead to deterioration of the concrete. In sufficient amounts, fly ash may be used to inhibit ASR.

The availability of fly ash and its lower cost relative to portland cement make it the most commonly used mineral admixture for concrete. One of the several beneficial attributes of mineral admixtures such as fly ash when added to concrete mixtures is the potential for reduction of deleterious expansions of hardened concrete caused by alkali-silica reactivity (ASR). This laboratory investigation concerned the influence of the constituents of portland cement, aggregates, and mineral admixtures on ASR in concrete.

One nonreactive aggregate and two reactive aggregates were used. Pyrex glass served as a control aggregate for the tests, as required by ASTM C441. In order to distinguish between the two naturally reactive aggregates, they were referred to as the "highly reactive" aggregate and the "moderately reactive" aggregate.

Four Type I cements and one Type IP cement were used, as presented in Table 1. The two Type I cements reflect the range of available alkali content (0.43 to 0.66 percent) of cement produced in Texas. Another Type I cement, from a source outside Texas, had a 1.03 percent total available alkali content. A local Type I cement with an available alkali content of 0.53 percent was used both directly and to produce a Type IP cement with a Class F fly ash that had an available alkali content of 0.50 percent.

This investigation included fly ash from nine different sources. Five fly ashes were Class C and four were Class F as defined by ASTM C618. These fly ashes are presented in Table 2. Seven fly ash sources were selected on the basis of their classification and alkali content, so a wide range of available alkali contents could be studied for both Classes C and F. Also, because chemicals are sometimes added to fly ash to enhance the effectiveness of the collection process, one Class C fly ash treated with such an agent (No. 7 in Table 2) was obtained for testing along with another Class C fly ash of similar alkali content (No. 6 in Table 2) that had not been treated. When such chemical agents are used, the fly ash may contain an objectionable amount of available alkalies.

During the third year of the research study, fly ash Nos. 4, 7, 8, and 9 were sampled again and tested to investigate the effect of fineness of fly ash in reducing ASR. The different levels of fineness, expressed in terms of amount retained on a 45-μm sieve, were obtained by grinding of the fly ash using a laboratory ball mill. Although the fly ashes were sampled from the same sources, the difference in time of sampling accounted for a slight difference in available alkali content reported. Their available alkali content and the fineness to which they were ground are presented in Table 3.

PGS Associates, Inc., 733 Hummingbird Way, North Palm Beach, Fla. 33408.

EXPERIMENTAL

Primary guidance for the work in this study was from ASTM C227, *Standard Test Method for Potential Alkali Reactivity of Cement-Aggregate Combinations (Mortar-Bar Method)*, which contains requirements for facilities and equipment, test procedures, and interpretation of results.

DISCUSSION OF TEST RESULTS

Test results indicated that the 0.60 percent limit on available alkalies in ASTM C150 was not a reliable guideline. The mixtures containing the two reactive aggregates and the cement having an available alkali content of 0.66 percent, with no fly ash replacement, did not exceed the 180-day expansion limit, even after 900 days of exposure testing, as shown in Figure 1. On the other hand, the mixture containing the control aggregate and the cement having an available alkali content of 0.43 percent, with no fly ash replacement, exceeded expansion limits at those test ages.

The use of the cement having an available alkali content of 1.03 percent resulted in a significant increase in expansion, as shown in Figure 2.

ASTM C618, *Standard Specification for Fly Ash and Raw or Calcined Natural Pozzolan for Use as a Mineral Admixture in Portland Cement Concrete*, includes an optional chemical requirement that limits available alkalies to 1.5 percent for fly ashes to be used with potentially reactive cement-aggregate combinations. Test results from this study, shown in Figure 3, indicated that when sufficient amounts of fly ash were used, expansions were reduced below the ASTM limits at 180 days for all cement-aggregate combinations, even when available alkalies in the fly ash exceeded the 1.5 percent limit. On the basis of these results, the limit of 1.5 percent available alkalies in fly ash does not appear to be an appropriate guideline.

Figure 4 shows the results obtained for the fly ash treated with a chemical precipitating agent. No conclusive data were collected because of the difficulties in determining the amount

TABLE 1 CEMENTS USED IN STUDY

Identification No. of Cements	ASTM Type	Total Available Alkali Content, %
1	C 150 - I	0.43
2	C 150 - I	0.66
3	C 150 - I	1.03
4	C 150 - I	0.53
5	C 595 - IP	0.50

TABLE 2 FLY ASHES USED IN STUDY

Identification No. of Fly Ash	Class per ASTM C 618	Coal Rank	Total Available Alkali Content, %
1	F	Lig.	0.31 *
2	F	Lig.	0.57
3	F	Lig.	1.38
4	C	Sub.	1.67
5	F	Bit.	1.76
6	C	Sub.	2.04 **
7	C	Sub.	2.35 ***
8	C	Sub.	3.75
9	C	Sub.	4.35

Notes: * Used in Type IP cement tested in this program.
** Similar to fly ash #7 but not treated.
*** Fly ash treated with alkaline precipitating agent

TABLE 3 EFFECT OF GRINDING ON FLY ASH FINENESS

Identification No. of Fly Ash	% Ret. on 45-Micron Sieve Initial	Level #1	Level #2	Total Available Alkali Content, %	
4	18.3	6.7	0.9	0.96	(1.67)*
7	16.4	7.3	1.2	1.90	(2.35)*
8	11.3	5.9	1.4	3.73	(3.75)*
9	13.3	6.7	0.9	4.35	(4.35)*

Note: * Alkali content in parentheses is from original ash sample tested in year one of this study (see Table 2).

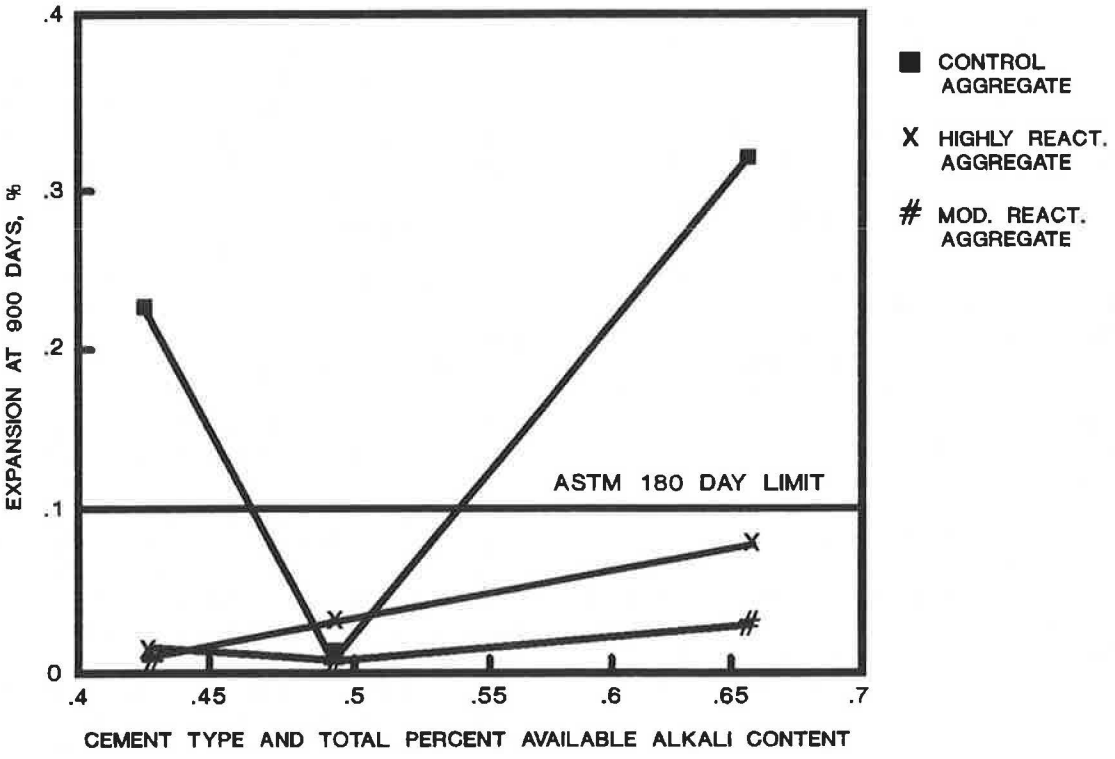

FIGURE 1 Influence of available alkali content of cement on expansion.

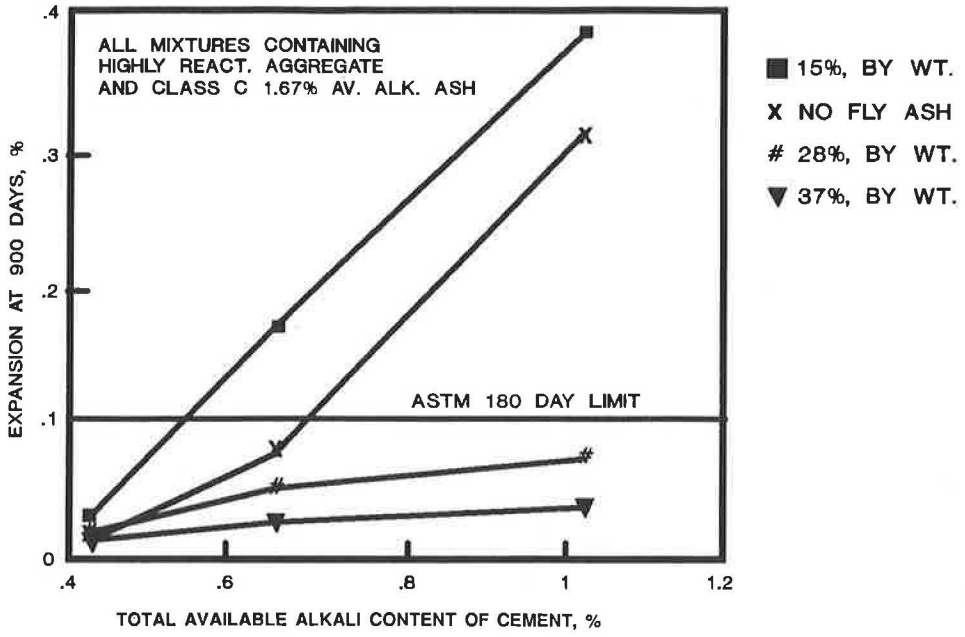

FIGURE 2 Influence of available alkali of cement and fly ash on expansion.

of alkalies added to the fly ash by the precipitating agent, or the availability of these alkalies to participate in deleterious reactions. Further research is needed to determine the quantity of alkalies added to fly ash by these agents and their effect on ASR.

Eight different fly ashes were tested in mixtures containing highly reactive aggregate and two cements with 0.43 and 0.66 percent alkali contents. Figure 5 shows the effect of the alkali content of these fly ashes on the expansion of these mixtures. Figure 5 indicates that expansions generally became greater as the alkali content of the fly ash increased. Expansions tended to increase sharply for alkali contents exceeding 2.0 percent. However, the replacement of 17.5 percent, by volume (15 percent, by mass), of cement with Class C fly ash caused expansions much greater than those of corresponding mixtures without fly ash, whereas cement replacements

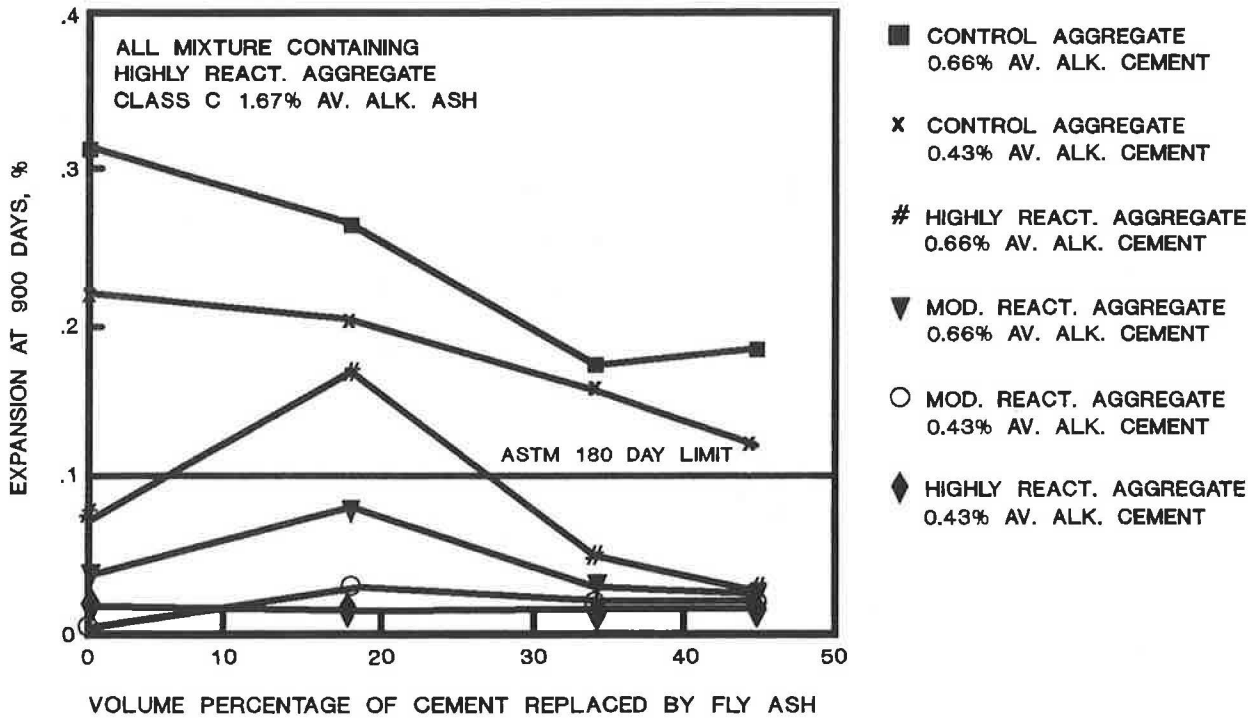

FIGURE 3 Influence of cement and fly ash replacement on expansion.

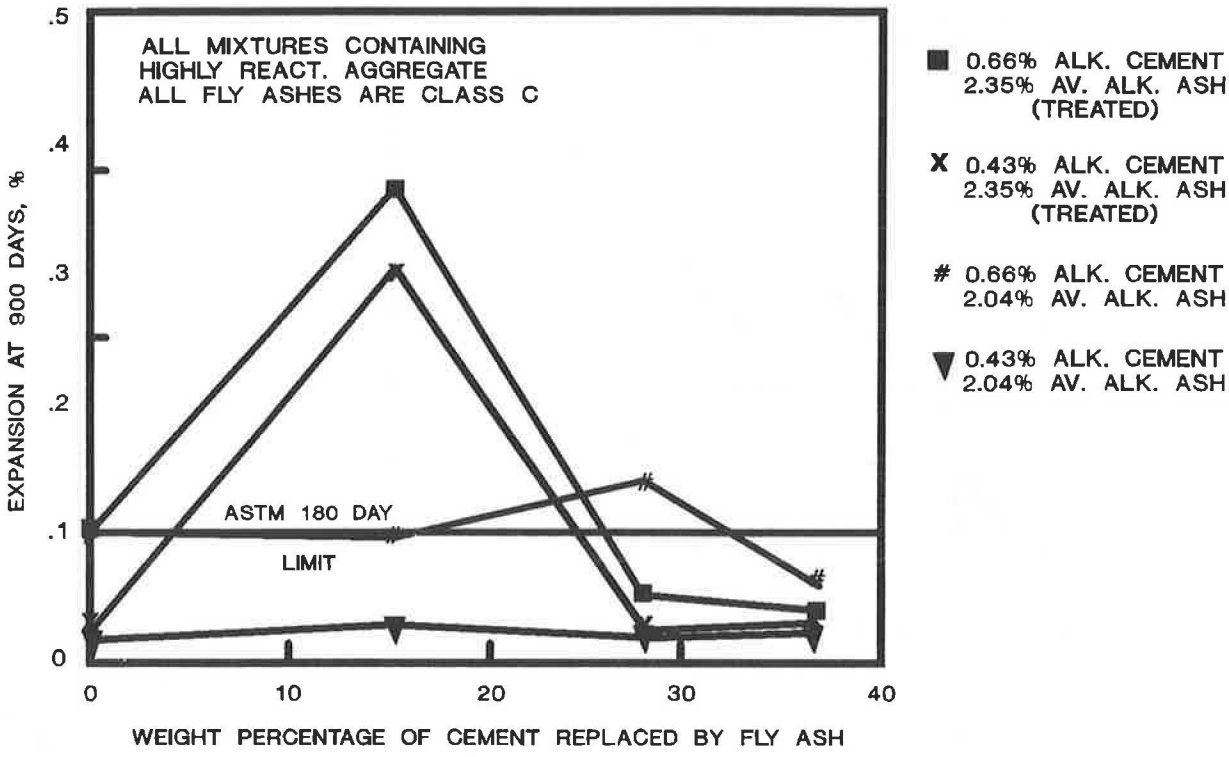

FIGURE 4 Fly ash treated with a precipitating agent.

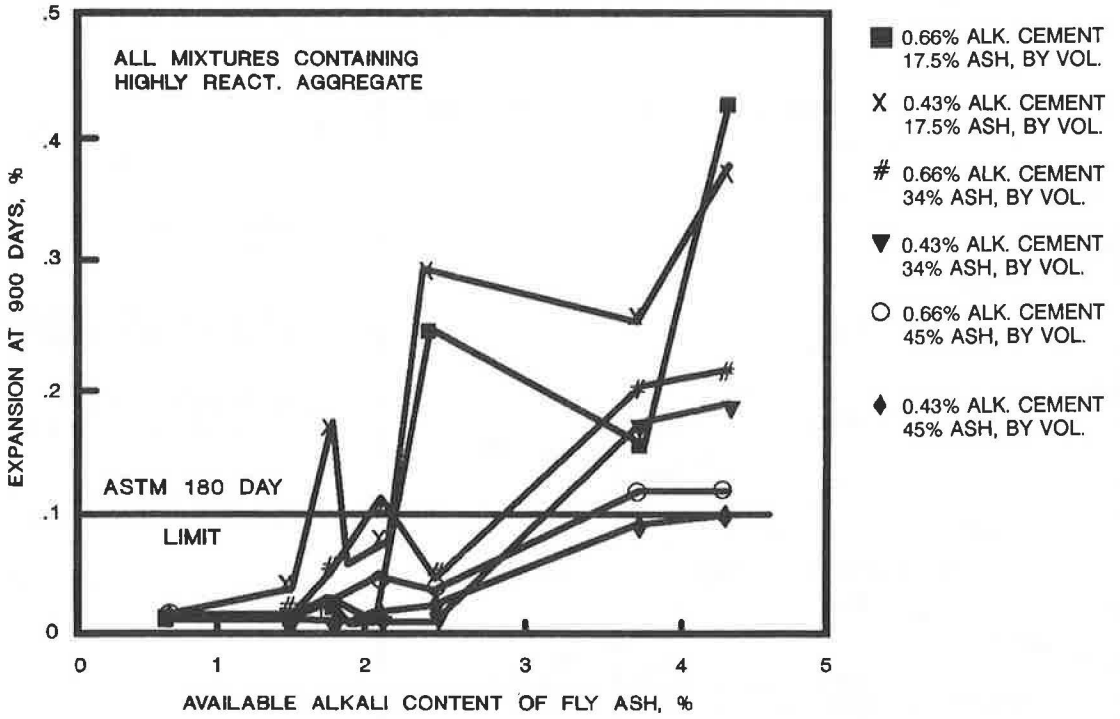

FIGURE 5 Available alkali content of fly ashes.

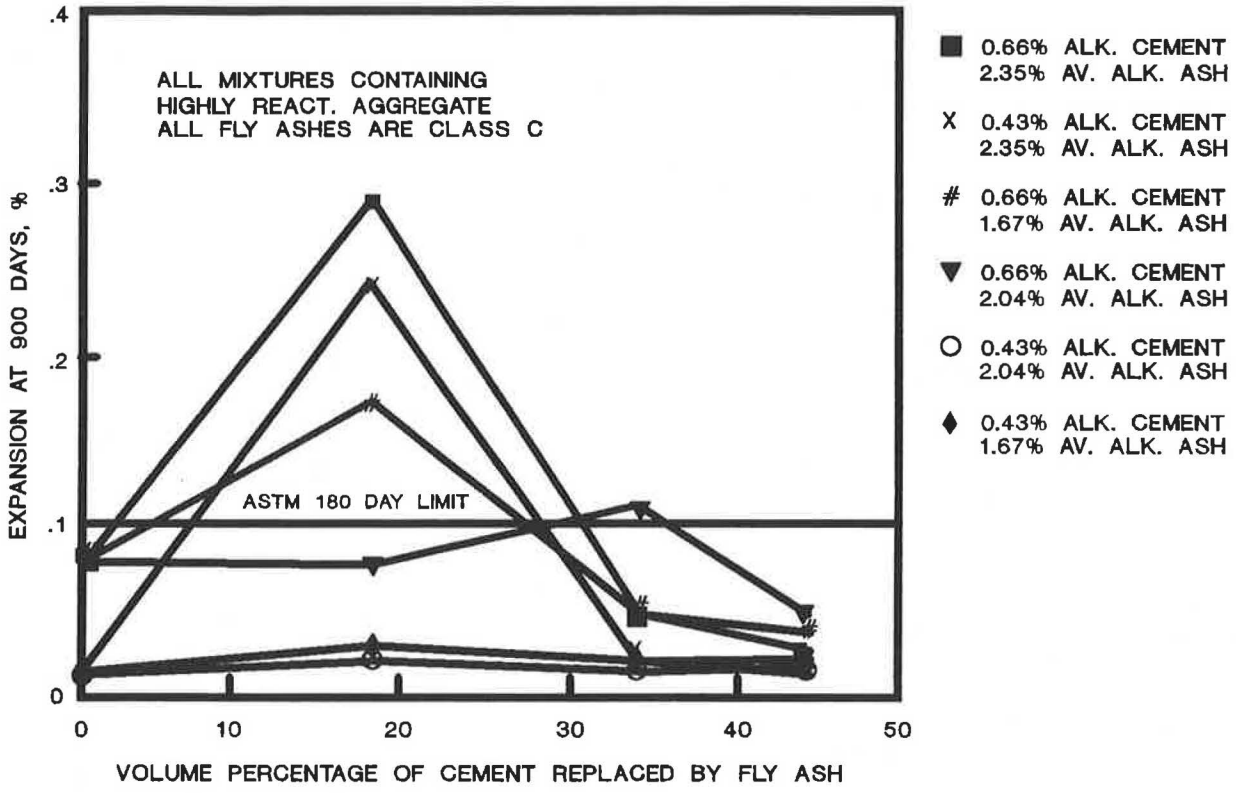

FIGURE 6 Pessimum effect of several Class C fly ashes.

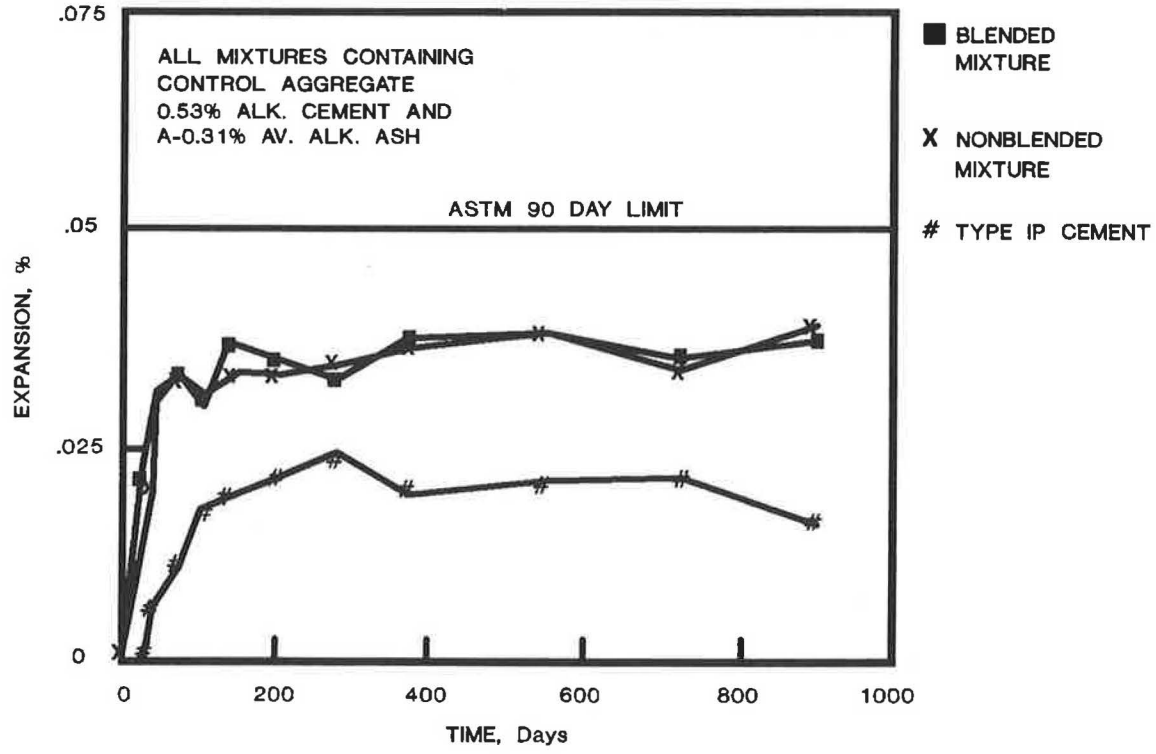

FIGURE 7 Fineness and preblending of fly ash and cement used in Type IP cement.

of 34.3 percent with Class C fly ash caused reductions in expansion.

Additional results, shown in Figure 6, indicated that volume replacements of 26 percent were comparable to the 34.3 percent replacement level in effectiveness. Subsequent increases in volume replacement beyond 34.3 percent had much less effect on concrete expansions. On the basis of these results, increasing the cement replacement as little as 10 volume percentage points beyond the so-called "pessimum" value may be sufficient to obtain satisfactory results.

The Type IP cement used in this study proved to be much more effective in inhibiting concrete expansions than the other cement-fly ash combinations tested. Therefore, two mixtures were made with the same cement and fly ash used to produce the Type IP cement. The cement and fly ash used in one mixture were mechanically blended before batching to simulate the blending of the Type IP cement during its manufacture. The intent was to determine what factors associated with the Type IP cement were responsible for its superior performance.

The results shown in Figure 7 indicated that the two cement-fly ash mixtures behaved similarly, and that they expanded more than the Type IP cement mixtures. The increased fineness of the fly ash in the Type IP cement, because of fly ash-clinker intergrinding, appeared to be the factor that enhanced the effectiveness of IP cement in inhibiting expansion. In order to investigate this factor, four Class C fly ashes were ground to two fineness levels and then added to the mortar as mineral admixtures. The first fineness level was approximately 50 percent of the original fineness, measured as the percentage retained on a 45-μm sieve. At the second fineness level, approximately 1 percent fly ash was retained on a 45-μm sieve. All mixtures contained the highly reactive aggregate and the cement with available alkalies of 1.03 percent. The available alkali contents and fineness of the fly ashes are presented in Table 3.

No consistent relationship was found between the percentage of weight retained on a 45-μm sieve and concrete expansions.

CONCLUSIONS

This study has shown that the 0.6 percent limit in ASTM C150 for the available alkali content of cement and the 1.5 percent maximum available alkali content designated by ASTM C618 for fly ash are not sufficient requirements to control deterioration of concrete caused by ASR. However, it is clear from test results in this study that the degree of ASR in concrete mixtures increases when the available alkali content of the cement increases.

The results also demonstrated that replacement of a portion of cement with fly ash is an effective means for reducing expansion in concrete caused by ASR. However, as the available alkali content of fly ash increases, there is a percentage of cement replaced by fly ash, defined as the pessimum limit, at which fly ash causes expansions larger than those of a mixture without fly ash, and above which fly ash reduces expansions.

The finer size of fly ash in Type IP cement appears to be the factor that enhances its performance in reducing ASR by comparison to similar cement-fly ash combinations. However, no correlation was found between Class C fly ash fineness and mortar bar expansion.

Publication of this paper sponsored by Committee on Chemical Additions and Admixtures for Concrete.

Lignite Fly Ash Concrete Highway Pavement—A 15-Year Performance History

DANIEL M. VRUNO, MAUREEN B. DOWNS, AND STEVEN S. SMITH

A research study was conducted at Twin City Testing Corporation in 1973, in cooperation with the North Dakota State Highway Department and the FHWA. The purpose of the study was to determine the effect on properties and performance of paving concrete with lignite fly ash substituted for various percentages of portland cement. The test program included both laboratory and field evaluations of compressive and flexural strength and freeze-thaw durability. The good performance of this concrete after 15 years of field exposure supports the original laboratory findings. The fly ashes used in this study do not conform to certain chemical and physical requirements of the current version of ASTM C618, the national consensus specification generally used as guidance for fly ash procurement; however, the nonspecification fly ash was used in pavement construction only after laboratory testing indicated its potential for providing satisfactory performance.

In 1973, the cost of lignite fly ash in North Dakota was about half the cost of portland cement. A savings of approximately $0.80 per cubic yard of concrete, or $0.20 per square yard of 9-in. concrete pavement, could be realized by replacing 15 percent of the portland cement with fly ash. However, there had been reluctance to use fly ash in paving concrete because of uncertainty concerning the effect of fly ash on the scaling resistance of such concrete when subjected to freeze-thaw cycles in the presence of deicing salts. Phase 1 of this study comprised laboratory testing to determine the effect on fresh and hardened concrete properties of lignite fly ash substituted for various percentages of portland cement; Phase 2 comprised laboratory and field testing of paving concrete installations for a freeway ramp in the fall of 1973, and a 10-mi section of I-29 south of Fargo, North Dakota, in 1974; and Phase 3 comprised an analysis to relate the performance of the paving concrete placed in Phase 2, after 15 years of exposure, to laboratory data compiled in Phases 1 and 2.

PROCEDURE

Phase 1: Laboratory Concrete

The laboratory test program included testing of control mixtures containing 5.5 bags of portland cement per cubic yard of concrete, and mixtures in which 15, 25, and 35 percent, by mass, of the portland cement was replaced with lignite fly ash from each of two sources. Compressive and flexural strengths were determined, and the air-void systems were analyzed. Resistance to rapid freeze-thaw and to deicer scaling was determined for all mixtures.

The fly ashes used in this study were supplied from two major lignite coal-fired power plants in Minnesota (Source 1) and North Dakota (Source 2). The following tables present the chemical (Table 1) and physical (Table 2) analyses of these fly ashes, together with pertinent ASTM C618 specifications for fly ash to be used as a mineral admixture in portland cement concrete.

As presented in Tables 1 and 2, the fly ashes used in this study did not conform to certain chemical and physical requirements of ASTM C618, the national consensus specification generally used as guidance for fly ash procurement; however, the nonspecification fly ash was used in pavement construction only after laboratory testing indicated its potential for providing satisfactory performance. It was found in Phase 3 that good performance of this paving concrete after 15 years of field exposure supports the original positive laboratory findings from Phase 1.

Specimens from each mixture were tested for compressive and flexural strength at ages of 3, 7, 28, and 90 days, and 1 year following laboratory moist curing. Additional specimens from each mixture were examined to determine air-void characteristics, and tests for resistance to freeze-thaw (ASTM C666) and deicer scaling (ASTM C672) were also performed for all mixtures. A description of materials used in the concrete mixtures is presented in Table 3.

Typical mixture proportions for the control concrete (0 percent fly ash) and the fly ash concretes (15, 25, and 35 percent, by mass, of the total cementitious material) are presented in Table 4. The approximate ratio, by mass, of water to cementitious material was 0.52 for all of the concrete mixtures. The average slump, air content, and unit weight of the fresh concrete mixtures are presented in Table 5.

The compressive and flexural strength test results for all concrete mixtures are presented in Tables 6 and 7, respectively.

The air contents measured in the fresh concrete mixtures are presented in Table 8. The microscopical determination of air-void content and parameters of the air-void system in hardened concrete is presented in Table 9 for each concrete mixture. The results of freeze-thaw tests are presented in Table 10.

The scaling resistance of concrete surfaces exposed to deicing chemicals is expressed in terms of visual rating numbers

D. M. Vruno and M. B. Downs, Twin City Testing Corp., 662 Cromwell Avenue, St. Paul, Minn. 55114. S. S. Smith, North Dakota State Highway Department, 300 Airport Road, Bismarck, N.Dak. 58504.

TABLE 1 CHEMICAL CHARACTERISTICS OF LIGNITE FLY ASHES

Characteristic	Source #1	Source #2	ASTM C 618
Silicon Dioxide (SiO_2)	22.17	36.86	
Aluminum Oxide (Al_2O_3)	17.57	11.87	
Iron Oxide (Fe_2O_3)	9.69	14.15	
Total Oxides (above)	49.43	62.88	50.0 Min
Sulfur Trioxide (SO^3)	7.20	2.90	5.0 Max
Calcium Oxide (CaO)	35.44	27.35	
Magnesium Oxide (MgO)	6.68	5.54	
Loss on Ignition	0.65	0.20	12.0 Max
Available Alkalies	3.48	2.56	1.5 Max

TABLE 2 PHYSICAL CHARACTERISTICS OF LIGNITE FLY ASHES

Characteristic	Source #1	Source #2	ASTM C 618
Fineness			
Blaine Sq cm/cu cm	7660	4330	6500 Min
Specific Gravity	2.66	2.59	5% Max Var
Compressive Strength of Mortar Cubes			
Ratio to Control at			
7 days, %	157	148	
28 days, %	120	111	
Pozzolanic Activity Index			
With Port. Cement, psi	3140	2990	
Ratio to Control at 28 days, %	58.2	55.4	85 Min
With Lime at 7 days, psi	1150	504	800 Min
Water Requirement, % of Control	95.0	93.0	105 Max
Increase in Drying Shrinking of Mortar Bars at 28 Days, %	-0.01	-0.01	+0.03 Max
Amount of Air Entraining Agent Needed in Mortar to Produce 18% Air, ml	0.40	0.39	20% Max Var

TABLE 3 DESCRIPTION OF CONCRETE MATERIALS

Material	Description
Fly Ash:	
Source #1	Ottertail Power Company - Fergus Falls, Minnesota
Source #2	Basin Electric Power Company - Stanton, North Dakota
Portland Cement	Universal Atlas - Duluth, Minnesota; ASTM C 150, Type I.
Air Entraining Agent	Protex Industries - Denver, Colorado; ASTM C 260.
Fine Aggregate	Downer Pit - Clay County, Minnesota; ASTM C 33.
Coarse Aggregate (Gravel)	Ten Acre Pit - Clay County, Minnesota; ASTM C 33.

TABLE 4 TYPICAL MIXTURE PROPORTIONS FOR CONTROL AND FLY ASH CONCRETES

Material	Amount per cubic yard
Total cementitious material	521 lb (cement plus fly ash)
Air Entraining Admixture	As required.
Fly Ash Range	0%, 15%, 25% and 35%, by mass.
Fine Aggregate	1242 lb
Coarse Aggregate (1 1/2 - 3/4")	875 lb
Coarse Aggregate (3/4" - #4)	1069 lb
Coarse Aggregate - Total	1944 lb
Water, Net	269 lb

TABLE 5 FRESH CONCRETE CHARACTERISTICS

Characteristic	Average
Slump	3 7/8 inches
Air Content	5.7 %
Unit Weight	146.3 lb/cu ft

TABLE 6 COMPRESSIVE STRENGTHS (ASTM C39)

	Average Compressive Strength Test Results, psi				
Mixture	3-day	7-day	28-day	90-day	1-year
Control	2450	3340	4530	5340	6160
15% Source #1	2470	3270	4930	5290	6050
25% Source #1	2520	3350	4330	5110	5660
35% Source #1	2410	3140	3110	4680	5320
15% Source #2	2290	3230	4440	5070	6070
25% Source #2	2180	3030	4390	4870	5860
35% Source #2	1840	2580	3500	4350	5680

TABLE 7 FLEXURAL STRENGTHS (ASTM C78)

	Average Flexural Strength Test Results, psi				
Mixture	3-day	7-day	28-day	90-day	1-year
Control	480	630	760	820	730
15% Source #1	470	605	745	745	750
25% Source #1	295	670	775	790	725
35% Source #1	450	570	740	825	780
15% Source #2	450	555	700	795	735
25% Source #2	460	525	690	795	835
35% Source #2	450	460	680	630	845

TABLE 8 AIR CONTENT OF FRESH CONCRETE

Mixture	Air Content, %
Control	5.4
15% Source #1	5.6
25% Source #1	5.6
35% Source #1	6.0
15% Source #2	5.6
25% Source #2	5.3
35% Source #2	5.7

TABLE 9 AIR-VOID CHARACTERISTICS OF HARDENED CONCRETE (ASTM C457)

Mixture	Avg Chord Intercept	Avg No. Sections	Air Void Content %	Specific Surface in^2/in^3	Spacing Factor
Control	0.0075	4.6	3.4	552.6	0.010
15% Source #1	0.0066	4.5	2.9	646.8	0.009
25% Source #1	0.0068	5.5	3.4	642.3	0.009
35% Source #1	0.0059	9.5	5.6	711.1	0.006
15% Source #2	0.0071	7.6	5.4	573.6	0.008
25% Source #2	0.0060	9.7	5.8	675.3	0.006
35% Source #2	0.0055	12.1	6.5	730.0	0.006

TABLE 10 FREEZE-THAW TEST RESULTS (ASTM C666)

Mixture	Relative Dynamic E After 300 Cycles, %	Average Weight Loss After 300 Cycles, %
Control	96	0.6
Source #1	95	0.4
Source #1	90	1.3
Source #1	89	2.3
Control	99	1.3
Source #2	98	0.7
Source #2	90	2.0
Source #2	91	1.8

as defined in ASTM C672, as presented in Table 11. The results of deicer scaling tests are presented in Table 12.

The use of lignite fly ashes from Sources 1 and 2 as various percentages of the total cementitious material in paving concrete mixtures was demonstrated by test results from Phase 1 to produce strong, durable concrete.

Phase 2: Field Concrete

Typical field test results for air content and slump are presented in Table 13. Field-cast cylinders were cured in the laboratory and tested at ages of 7 and 28 days, with strength results as presented in Table 14.

Phase 3: Pavement Evaluation at 15 Years

The majority of the paving concrete in I-29 south of Fargo, North Dakota, was placed in 1974 with lignite fly ash as 15 percent of the cementitious material, thus providing a site for direct comparison of concretes with and without fly ash. The pavement had been subjected to 15 years of traffic, deicers, plowing, and temperature extremes that ranged from −33°F to +106°F. This service history provided an excellent opportunity to observe on site the durability of concrete containing portland cement and lignite fly ash.

A general condition survey was performed on the subject paving concrete 15 years after construction and there existed no visual differences between the concretes with and without fly ash.

Four specific locations were chosen, on the basis of the availability of strength and other data for these locations from Phase 2, for extraction of core samples for determinations of field strength at an age of 15 years. The 15-year strengths are presented in Table 15 along with the compressive strengths from 7 and 28 days (Phase 2, Table 14) for comparison.

CONCLUSIONS

The use of lignite fly ashes as 15 percent, by mass, of the total cementitious material in paving concrete resulted in a strong,

TABLE 11 RATING SYSTEM FOR RESISTANCE TO DEICER SCALING (ASTM C672)

Rating	Condition of Surface
0	No scaling
1	Very slight scaling (1/8 in. depth, max, no coarse aggregate visible)
2	Slight to moderate scaling
3	Moderate scaling (some coarse aggregate visible)
4	Moderate to severe scaling
5	Severe scaling (coarse aggregate visible over entire surface)

TABLE 12 TEST RESULTS, RESISTANCE TO DEICER SCALING (ASTM C672)

Mixture	75 cycles	150 cycles	225 cycles	300 cycles
Control	0	1	2	3
Source #1	0	1	2	2
Source #1	0	0	1	2
Source #1	0	0	1	1
Source #2	0	1	2	2
Source #2	0	1	1	2
Source #2	0	1	1	2

TABLE 13 FIELD TESTS, AIR AND SLUMP

Pavement Station	Lane Direction	Fly Ash	Air Content, %	Slump, inches
872+34	North Bound	15%	2.2	1
900+15	North Bound	15%	5.5	1 1/2
926+30	North Bound	0%	5.6	1 1/4
2+62	South Ramp	15%	5.5	2

TABLE 14 LABORATORY STRENGTH OF FIELD CONCRETE

Pavement Station	Lane Direction	Fly Ash	Compressive Strength, psi 7-day	28-day
872+34	North Bound	15%	3930	4560
900+15	North Bound	15%	3380	4020
926+30	North Bound	0%	3990	4600
2+62	South Ramp	15%	3900	4600

TABLE 15 COMPARISON OF COMPRESSIVE STRENGTH

			Strength, psi Phase 2		Phase 3
Pavement Station	Lane Direction	Fly Ash	7-day	28-day	15-year
872+34	North Bound	15%	3930	4560	7620
900+15	North Bound	15%	3380	4020	7100
926+30	North Bound	0%	3990	4600	6880
2+62	South Ramp	15%	3900	4600	6050

durable concrete pavement for I-29 south of Fargo, North Dakota, after 15 years of exposure under field conditions.

The good performance of this concrete after 15 years of field exposure supports the original laboratory findings. The fly ashes used in this study do not conform to certain chemical and physical requirements of the current version of ASTM C618, the national consensus specification generally used as guidance for fly ash procurement; however, the nonspecification fly ash was used in pavement construction only after laboratory testing indicated its potential for providing satisfactory performance.

Publication of this paper sponsored by Committee on Chemical Additions and Admixtures for Concrete.